To the Graduate Council

I am submitting herewith a thesis written by George Alexander Barclay entitled "Behavior of Structural Clay Tile Infilled Steel Frames Subjected to In-Plane Loading." I have examined the final copy of this thesis for form and content and recommend that it be accepted in partial fulfillment for the degree of Master of Science, with a major in Civil Engineering.

Richard M. Bennett

Dr. Richard M. Bennett, Major Professor

We have read this thesis and recommend its acceptance:

W. Goodpasture

Edwin G. Burdette

Accepted for the Council:

Lewis Nikel

Associate Vice Chancellor
and Dean of The Graduate School

STATEMENT OF PERMISSION TO USE

In presenting this thesis in partial fulfillment of the requirements for a Master of Science degree at The University of Tennessee, Knoxville, I agree that the Library shall make it available to borrowers under rules of the Library. Brief quotations from this thesis are allowable without special permission, provided that accurate acknowledgment of the source is made.

Permission for extensive quotation from or reproduction of this thesis may be granted by my major professor, or in his absence, by the Head of Interlibrary Services when, in the opinion of either, the proposed use of the material is for scholarly purposes. Any copying or use of the material in this thesis for financial gain shall not be allowed without my written permission.

Signature Nancy Barcelon

Date 4/22/93

Behavior of Structural Clay Tile Infilled Steel Frames Subjected to In-Plane Loading

A Thesis

Presented for the

Master of Science

Degree

The University of Tennessee, Knoxville

George Alexander Barclay

May, 1993

DEDICATION

This thesis is dedicated to my wife Terri and to my parents, Dr. and Mrs. Lee Roy Barclay for all of the love and support they have given me during this experience.

ACKNOWLEDGMENTS

I would like to thank my major professor, Dr. Richard Bennett, for his invaluable guidance and patience during the past several years. This thesis would not have been possible without his direction and unique input. I would also like to thank the other committee members, Dr. Edwin Burdette and Dr. David Goodpasture, for their comments and assistance during this process. I would like to express my thanks to my wife, Terri, for her understanding and extreme patience during the past four years. If it were not for her, I would not be writing this acknowledgement now. I would like to thank Roger Flanagan and Martin Marietta Energy Systems, who provided the opportunity for this research. Lastly, but certainly not least, I would also like to thank the lab crew, Jim Bernardi, Kurt Boyd, Chris Columber, and Joele Fowler. Their hard work and persistence has helped make the project possible. Their unique and well-timed humor also helped make it bearable when the pressure began to rise.

ABSTRACT

The behavior of two one-bay, one-story structural clay tile infilled structural steel frames subjected to horizontal in-plane racking loads applied at roof level is investigated. The steel frames had W10 x 30 wide flange columns bent about the weak axis and a W12 x 35 beam. Eight inch by twelve inch by twelve inch structural clay tile masonry was placed into the frames using Type N mortar. The tile was placed with the cells horizontal using full bed joints and face shell bedding in the head joints. The two specimens varied only in the aspect ratio of the frames. One frame had an aspect ratio of 1:1, with nominal dimensions of eight feet by eight feet. The second frame had an aspect ratio of 1.5:1, with nominal dimensions of twelve feet long by eight feet high.

The loading of the specimens was cyclic in nature with each specimen being loaded both in compression and tension to a predetermined set of deflection increments. Each specimen was loaded to failure, with failure being defined as increasing deflection with no increase in load. The specimens were instrumented in such a manner that frame displacements, panel-frame relative displacements and frame member forces were obtained through a computerized data collection system. The load-deflection relationships and infilled frame behavior are the primary interest of this study.

TABLE OF CONTENTS

CHAPTER		PAGE
Chapter 1:	**INTRODUCTION**	1
1.1	General	1
1.2	Problem Statement	1
1.3	Objectives	2
1.4	Scope	2
Chapter 2:	**LITERATURE SURVEY**	4
2.1	Introduction	4
2.2	Review of Previous Experimental Programs	4
2.2.1	Early Experimental Programs	4
2.2.2	The New Brunswick Research	9
2.3	Analytical Methods	18
2.4	Summary	23
Chapter 3:	TEST SETUP	24
3.1	Introduction	24
3.2	Reaction Frame Design	24
3.3	Specimen Frame Design	26
3.4	Out-of-Plane Bracing	31
3.5	Laboratory Setup	35
3.6	Instrumentation	36

3.7 Testing Procedure 40
3.7.1 Pre-Testing Requirements 40
3.7.2 Testing 43
3.7.3 Post-Testing Activities 46

Chapter 4: **GENERAL SYSTEM BEHAVIOR** 47
4.1 Introduction 47
4.2 Envelope behavior 52
4.2.1 Stiffness and softening of the system 52
4.2.2 Ultimate load and post-ultimate behavior 58
4.2.3 Bare Frame Envelope Behavior 60
4.3 Hysteretic Behavior 62
4.3.1 Frame 2 Hysteresis 62
4.3.2 Frame 17 Hysteresis 71
4.4 System Energy Absorption 78
4.5 Bare Frame Hysteresis 79
4.6 Frame Comparison and Summary 82

Chapter 5: **PANEL BEHAVIOR** 90
5.1 Introduction 90
5.2 Load-Strain Relationships 90
5.3 Stress-Strain Relationships 102
5.4 Panel Hysteretic Behavior 104
5.4.1 Frame #2; Panel Hysteresis 106
5.4.2 Frame #17; Panel Hysteresis 110

Chapter 6: **FRAME-PANEL RELATIVE MOVEMENT** 118

6.1 Introduction 118

6.2 Relative hysteresis 118

6.2.1 Frame 2 Relative Hysteresis 119

6.2.2 Frame 17 Relative Hysteresis 137

6.3 Relative-Frame Displacement Comparisons . . . 153

Chapter 7: **SUMMARY, CONCLUSIONS, AND RECOMMENDATIONS** . 174

7.1 Research Summary 174

7.2 Conclusions 174

7.2.1 General System Behavior 175

7.2.2 Panel Behavior 176

7.2.3 Frame-Panel Relative Displacements . . 176

7.3 Recommendations For Further Study 178

LIST OF REFERENCES 180

APPENDIX 184

VITA 189

LIST OF FIGURES

FIGURE		PAGE
Figure 2.1:	Testing Apparatus	10
Figure 2.2:	Specimen Summary	11
Figure 2.3:	Results Summary	14
Figure 3.1:	Typical Test Setup	25
Figure 3.2:	Specimen frame plan	27
Figure 3.3:	Specimen section	28
Figure 3.4:	Connection Detail	30
Figure 3.5:	Base Plate	31
Figure 3.6:	Out-of-plane reaction frame	32
Figure 3.7:	Specimen bracing; plan	33
Figure 3.8:	Specimen bracing; section	34
Figure 3.9:	Bracing detail	35
Figure 3.10:	Partial lab floor plan	37
Figure 3.11:	LVDT placement	38
Figure 3.12:	Panel LVDT placement	38
Figure 3.13:	Strain gage locations	39
Figure 3.14:	Instrumentation Schematic	41
Figure 3.15:	Ram and Load cell configuration	44
Figure 4.1:	Lvdt numbering scheme	48
Figure 4.2:	Frame 2 hysteresis	49
Figure 4.3:	Frame 17 hysteresis	50

Figure 4.4: Selected deflection cycles 51

Figure 4.5: Load-deflection envelope 53

Figure 4.6: Initial stiffness 54

Figure 4.7: Third cycle stiffness 56

Figure 4.8: Bare frame load-deflection envelopes . . . 61

Figure 4.9: Frame #2; Loop #1 63

Figure 4.10: Frame #2; Loop #2 64

Figure 4.11: Frame #2; Loop #3 65

Figure 4.12: Frame #2; Loop #4 66

Figure 4.13: Frame #2; Loop #5 67

Figure 4.14: Frame #2; Loop #6 68

Figure 4.15: Frame #17; Loop #1 72

Figure 4.16: Frame #17; Loop #2 73

Figure 4.17: Frame #17; Loop #3 74

Figure 4.18: Frame #17; Loop #4 75

Figure 4.19: Frame #17; Loop #5 76

Figure 4.20: Frame #17; Loop #6 77

Figure 4.21: Energy absorption 80

Figure 4.22: Bare frame hysteresis 81

Figure 4.23: Bare frame energy absorption 83

Figure 4.24: Stiffness degradation 86

Figure 4.25: Composite - bare frame comparison; Frame 2 88

Figure 4.26: Composite - bare frame comparison; Frame 17 89

Figure 5.1: Load-strain, Compressive diagonal 91

Figure 5.2: Frame #2; Compressive diagonal strain . . 92

Figure 5.3: Frame #17; Compressive diagonal strain . . 93

Figure 5.4: Load-strain envelope; tension diagonal . . 95

Figure 5.5: Load-strain envelope, panel vertical . . . 97

Figure 5.6: Horizontal load-strain; both frames . . . 99

Figure 5.7: Frame #2; Vertical and horizontal load-strain 100

Figure 5.8: Frame #17; Vertical and horizontal load-strain 101

Figure 5.9: Compressive strut; Stress-strain envelopes 103

Figure 5.10: Prism stress-strain curve (after Boyd, 1993) 105

Figure 5.11: Frame #2; LVDT #27 hysteresis 107

Figure 5.12: Frame 2; LVDT #28 hysteresis 108

Figure 5.13: Frame #2; Panel horizontal hysteresis . . 111

Figure 5.14: Frame #2; Panel vertical hysteresis . . . 112

Figure 5.15: Frame #17; LVDT #27 hysteresis 113

Figure 5.16: Frame 17; LVDT #28 hysteresis 114

Figure 5.17: Frame 17; Panel horizontal hysteresis . . 116

Figure 5.18: Frame 17; Panel vertical hysteresis . . . 117

Figure 6.1: Frame 2; LVDT 12 hysteresis 120

Figure 6.2: Frame 2; LVDT 13 hysteresis 121

Figure 6.3: Frame 2; LVDT 14 hysteresis 122

Figure 6.4: Frame 2; LVDT 20 hysteresis 123

Figure 6.5: Frame 2; LVDT 21 hysteresis 124

Figure 6.6: Frame 2; LVDT 22 hysteresis 125

Figure 6.7: Frame 2; LVDT 23 hysteresis 126

Figure 6.8: Frame 2; LVDT 24 hysteresis 127

Figure 6.9: Frame 2; LVDT 15 hysteresis 128

Figure 6.10: Frame 2; LVDT 12 vs. Beam CL deflection . 130

Figure 6.11: Frame 2; LVDT 13 vs. Beam CL deflection . 131

Figure 6.12: Frame 2; LVDT 20 vs. Beam CL deflection . 133

Figure 6.13: Frame 2; LVDT 21 vs. Beam CL deflection . 135

Figure 6.14: Frame 17; LVDT 12 hysteresis 138

Figure 6.15: Frame 17; LVDT 13 hysteresis 139

Figure 6.16: Frame 17; LVDT 14 hysteresis 140

Figure 6.17: Frame 17; LVDT 20 hysteresis 141

Figure 6.18: Frame 17; LVDT 21 hysteresis 142

Figure 6.19: Frame 17; LVDT 22 hysteresis 143

Figure 6.20: Frame 17; LVDT 23 hysteresis 144

Figure 6.21: Frame 17; LVDT 24 hysteresis 145

Figure 6.22: Frame 17; LVDT 15 hysteresis 146

Figure 6.23: Frame 17; LVDT 12 vs. Beam CL deflection 147

Figure 6.24: Frame 17; LVDT 13 vs. Beam CL deflection 149

Figure 6.25: Frame 17; LVDT 20 vs. Beam CL deflection 150

Figure 6.26: Frame 17; LVDT 21 vs. Beam CL deflection 152

Figure 6.27: Frame 2; Relative & frame displacement vs. load (LVDT 12 & 9; Loops 1 & 2) 154

Figure 6.28: Frame 2; Relative & frame displacement vs. load (LVDT 12 & 9; Loops 3 & 4) 155

Figure 6.29: Frame 2; Relative & frame displacement vs. load (LVDT 13 & 10; Loops 1 & 2) 156

Figure 6.30: Frame 2; Relative & frame displacement vs. load (LVDT 13 & 10; Loops 3 & 4) 157

Figure 6.31: Frame 2; Relative & frame displacement vs. load (LVDT 20 & 1; Loops 1 & 2) 158

Figure 6.32: Frame 2; Relative & frame displacement vs. load (LVDT 20 & 1; Loops 3 & 4) 159

Figure 6.33: Frame 2; Relative & frame displacement vs. load (LVDT 21 & 18; Loops 1 & 2) 160

Figure 6.34: Frame 2; Relative & frame displacement vs. load (LVDT 21 & 18; Loops 3 & 4) 161

Figure 6.35: Frame 17; Relative & frame displacement vs load (LVDT 12 & 9; Loops 1 & 2) 162

Figure 6.36: Frame 17; Relative & frame displacement vs load (LVDT 12 & 9; Loops 3 & 4) 163

Figure 6.37: Frame 17; Relative & frame displacement vs load (LVDT 13 & 10; Loops 1 & 2) 164

Figure 6.38: Frame 17; Relative & frame displacement vs load (LVDT 13 & 10; Loops 3 & 4) 165

Figure 6.39: Frame 17; Relative & frame displacement vs load (LVDT 20 & 1; Loops 1 & 2) 166

Figure 6.40: Frame 17; Relative & frame displacement vs load (LVDT 20 & 1; Loops 3 & 4) 167

Figure 6.41: Frame 17; Relative & frame displacement vs load (LVDT 21 & 18; Loops 1 & 2) 168

Figure 6.42: Frame 17; Relative & frame displacement vs load (LVDT 21 & 18; Loops 3 & 4) 169

Figure 6.43: Leeward column-panel displacements . . . 172

Figure 6.44: Leeward column-panel displacements . . . 173

Figure A.1: Frame 2 prior to testing 185

Figure A.2: Frame 17 prior to testing 186

Figure A.3: Frame 2; Corner crushing 187

Figure A.4: Frame 2 after testing 188

Chapter 1: INTRODUCTION

1.1 General

An infilled system typically consists of a structural steel frame infilled with concrete or masonry. Masonry infill panels are often considered as non-structural components. However, the masonry infill can greatly increase the stiffness and ultimate strength of structural steel frames when subjected to racking loads. A steel frame alone is a very ductile system that can undergo large lateral deflections while maintaining its strength. A masonry panel, however, is a very stiff and non-ductile system that can withstand little deformation before cracking, which greatly reduces its strength. The two systems combined have obvious advantages in that the panel adds significantly to the stiffness of the over-all system and the steel frame provides ductility and confinement of the brittle masonry.

1.2 Problem Statement

Perhaps one of the main reasons that masonry element of infilled steel frame assemblages have not been included in the structural design of the system is the difficulty in quantifying the behavior of the composite system. Unlike steel, the properties of masonry and mortar are highly variable. Variations in construction practices and boundary

conditions also add to the degree of design and analysis difficulty. With the masonry panels, there are also a number of failure modes that depend on the boundary conditions, steel frame stiffness and nature of the applied load.

1.3 Objectives

The main objectives of this study are:

1) To introduce a test program to study the behavior of full scale structural clay tile infilled structural steel frames when subjected to cyclic horizontal racking loads. This study includes two different frames varying only in the aspect ratio of the frame.
2) To conduct a detailed literature survey in order to acquire analytical techniques that may be applicable to the current research.
3) To compare previous analytical methods to the current research data to determine their effectiveness in quantifying the behavior of similar systems.

1.4 Scope

A literature survey of previous similar research is presented in chapter 2. Chapter 3 delineates the activities leading up to the current program and also outlines the testing procedures of the program. Chapters 4 through 6 are devoted to the analysis of the resulting data. The focus of this study is on the load deflection relationships of the

system under statically applied cyclic loading. Chapter 4 entails a detailed study of the over-all load-deflection characteristics of the system. Chapter 5 is a study of the panel deformations and stress-strain relationships and chapter 6 investigates the panel-frame relative movements. Chapter 7 presents conclusions and recommendations for future studies.

Chapter 2: LITERATURE SURVEY

2.1 Introduction

This review considers pertinent research in the field of masonry infilled frames subjected to in-plane loading. The current research is focusing on clay tile infilled frames; however, the scope of this review includes general masonry infills. The literature review is divided into a discussion of previous experimental programs and results and techniques for the analysis of masonry infilled steel frames.

2.2 Review of Previous Experimental Programs

There has been a substantial amount of research done in the area of infilled frames during the past 45 years. For years, masonry infills were considered to be nothing more than part of the dead weight for which the load bearing structure had to be designed. In the late 1940's, it was recognized that masonry panels had some structural value. Since that time, there have been a number of experimental programs attempting to quantify that structural value.

2.2.1 Early Experimental Programs

Some of the earliest documented research in the area of masonry infilled frames subjected to horizontal racking loads was performed by Polyakov (1956) in the U.S.S.R. from 1948 to

1953. Polyakov tested 65 different panels using two different steel frame member sizes with pinned connections. Thirty-three of the specimens were 4′-4″ by 4′-4″ and the other 32 were 9′-10″ long by 6′-7″ high. Polyakov studied the effects of varying masonry unit type, mortar mix type, loading patterns, and the presence of openings in the masonry panels.

During this initial research, Polyakov noted that masonry infilled frames pass through three distinct stages when subjected to racking loads. During the first stage, when the masonry panel and the members of the confining frame are acting as a monolithic unit, shear and normal stresses are present along the panel-infill interface because there is no separation of the two during this stage. The first stage ends with the formation of peripheral cracks. These peripheral cracks extend around the perimeter of the masonry panel except where compressive stresses are transmitted from the frame to the panel.

The second stage is distinguished by a shortening of the compression diagonal and a lengthening of the tension diagonal of the masonry panel. At this point in the loading, the strains along the tension diagonal of the infill are much smaller than the strains of the frame. The second stage ends with the development of cracking along the compression diagonal. This cracking usually follows the mortar joints in a stair stepping pattern along the diagonal.

During the third stage, the structure will continue to resist an increasing load. As the load increases, the diagonal cracking continues to widen and increase in length. The cracking usually stops at the loaded corners due to the biaxial stress that exists in the loaded corner. Biaxial compression results in increased strength of the brickwork (Richardson, 1986). Although the panel will continue to resist a slightly increased load, the structure has lost most of it's practical value at this point.

Polyakov discovered that variation in the mortar type had very little effect on the load carrying capabilities of the system. However, the presence of openings greatly affected the load capacity and stiffness of the assemblage. With the presence of an opening, the stiffness of the system was significantly reduced as the size of the opening was increased. Repeated loading in one direction and cyclic load reversals also notably reduced the stiffness of the system.

In an ensuing paper Polyakov (1966) researched the effects of racking loads on a multi-story half scale model. The model consisted of 9 panels in 3 rows of 3 panels each. Polyakov wished to determine, during horizontal loading, if each of the panels behaved as individual diagonal bracing, or if the system acted monolithically with the beams and columns of the frame acting as reinforcement for the masonry.

Up to a load of 46 kips, the 9 panels behaved as a monolithic unit. At this point, boundary cracks appeared in

all of the panels and load was transmitted only in those portions where contact still existed between frame and masonry, which was along the diagonal zone subjected to compression during the shearing distortion of the panel (Polyakov, 1966). From this information and the individual panel deformation patterns, Polyakov surmised that the panels acted individually after initial cracking and each of the masonry panels behaved as diagonal a strut to its respective frame.

Holmes (1961, 1963) tested frames infilled with both concrete and masonry. He derived empirical formulae for the ultimate racking load and the accompanying horizontal deflection. These relationships were based on the crushing strength of the infill along the compression diagonal and the strain of the infill at the time of failure. Holmes concluded from his research that the effective width of the equivalent diagonal strut was approximately equal to the one-third of the length of the panel diagonal. Holmes also inferred from his testing that the ultimate horizontal load a brick masonry infilled frame can withstand was as much as twice that of the frame alone.

Stafford-Smith (1962, 1966, 1967, 1968) has written several papers on the strength and stiffness of infilled frames subjected to racking loads. In Stafford-Smith's earliest work (1962), he investigated the lateral stiffness of infilled frames using the equivalent diagonal strut theory. He found

that the length of contact between the infill and the frame was largely dependent on the relative stiffness of the infill and frame.

Stafford-Smith and Carter (1969) further investigated the diagonal strut theory and relative stiffness. They also researched various failure modes and ultimate racking loads of infilled frames. For a masonry infill, Stafford-Smith and Carter found that the infill fails either by shear cracking in the mortar joints, tension cracking in the mortar joints, or local crushing of the mortar or masonry in the loaded corners of the panel.

Stafford-Smith and Carter (1969) determined that the equivalent width of the diagonal strut, length of contact between frame and infill, and frame-infill relative stiffness were all interrelated. The equivalent width of the diagonal strut is dependant on the length of contact at the loaded corners and the value of the diagonal load. Therefore, the width of the equivalent strut constantly changes during the loading history of the panel. The length of contact at the loaded corners was shown to be dependent on the relative stiffness of the frame and infill. Relative stiffness is a non-dimensional parameter that is dependent on the geometric and material properties of the frame and the infill.

Klingner and Bertero (1978) tested a one-third scale model of an 11 story structure. As with the current research, this model was subjected to cyclic load reversals. The panels were

concrete block masonry units with horizontal and vertical joint reinforcement. The hollow cores of the block were filled with grout. From their research, Klingner and Bertero noted that after the formation of cracks along the boundary between the frame and infills, the subassemblages behaved essentially as a frame braced by equivalent diagonal compression struts. They also noted that repeated load reversals on the structure eventually reduces the stiffness of the system from the frame and infill acting together to that of the bare frame.

Bertero and Brokken (1983) continued a similar research program using, among other materials, hollow clay tile block for the frame infill. This research yielded the same conclusions as Klingner and Bertero (1978).

2.2.2 The New Brunswick Research

In the mid 1980's at the University of New Brunswick, there was a research program taking place similar to the current one. Yong (1984), McBride (1984), Amos (1985), and Richardson (1986) all performed racking load tests on assemblages consisting of structural steel frames infilled with concrete masonry block. Figure 2.1 illustrates the apparatus used to test all panel assemblages and figure 2.2 is a summary of the varying parameters used for the different frames. The first letter of the specimen designation number, A, B, C, or D, are the works of Yong, McBride, Amos, and Richardson respectively.

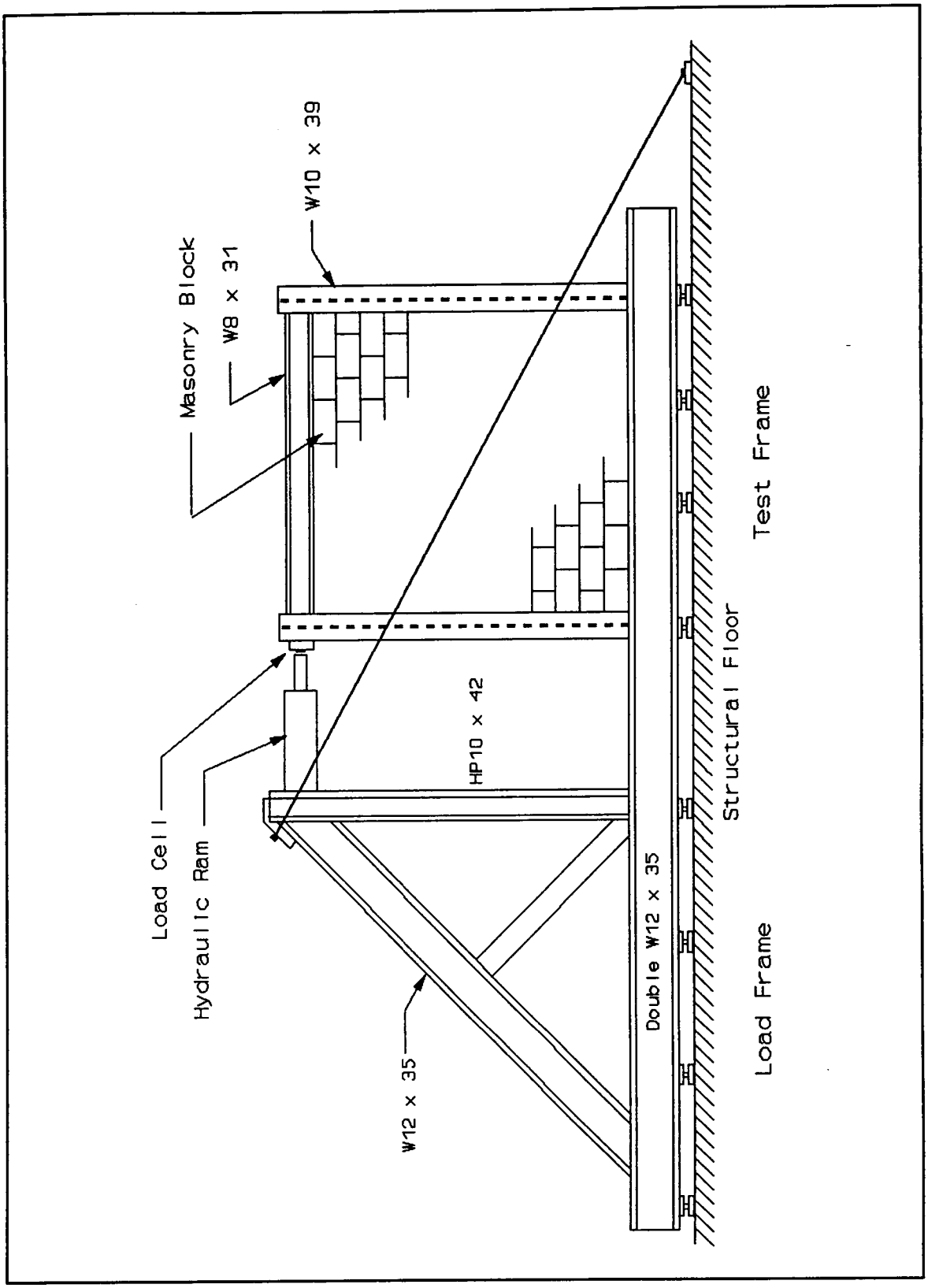


Figure 2.1: Testing Apparatus

Specimen Number	Joint Reinforcement	Mortar between Flanges	Tie System	Bond Beam	Air Space @ Beam	Openings	Loading History
A1	YES	YES	NO	NO	NO	NO	MONO. (COMP.)
A2	YES	NO	NO	NO	NO	NO	MONO. (COMP.)
A3	YES	NO	NO	NO	NO	NO	MONO. (COMP.)
A4	YES	NO	NO	NO	YES	NO	MONO. (COMP.)
A5	YES	NO	YES	NO	YES	NO	MONO. (COMP.)
A6	YES	NO	YES	NO	NO	NO	MONO. (COMP.)
B1	YES	YES	NO	NO	NO	NO	MONO. (COMP.)
B2	YES	NO	NO	NO	NO	NO	MONO. (COMP.)
B3	YES	NO	NO	NO	NO	NO	MONO. (COMP.)
B4	NO	NO	NO	NO	NO	NO	MONO. (COMP.)
B5	YES	NO	YES	NO	NO	NO	MONO. (COMP.)
B6	YES	NO	YES	YES	NO	NO	MONO. (COMP.)
C1	YES	NO	NO	NO	NO	NO	MONO. (COMP.)
C2	YES	NO	NO	NO	NO	NO	MONO. (COMP.)
C3	YES	NO	NO	YES	NO	YES	MONO. (COMP.)
C4	YES	NO	NO	YES	NO	YES	MONO. (COMP.)
C5	YES	NO	NO	YES	NO	YES	MONO. (COMP.)
C6	YES	NO	NO	YES	NO	YES	CYCLIC
C7	NO	NO	NO	NO	NO	NO	CYCLIC
C8	YES	NO	NO	NO	NO	NO	CYCLIC (COMP & TEN)
C9	YES	NO	NO	NO	NO	NO	CYCLIC (COMP & TEN)
C10	YES	NO	NO	NO	NO	NO	CYCLIC (COMP & TEN)
D1	YES	NO	NO	NO	NO	NO	CYCLIC (COMP & TEN)
D2	YES	NO	NO	NO	NO	NO	CYCLIC (COMP & TEN)
D3	YES	NO	NO	NO	NO	NO	CYCLIC (COMP & TEN)
D4	YES	NO	NO	NO	NO	NO	CYCLIC (COMP & TEN)
D5	YES	NO	NO	YES	NO	YES	CYCLIC (COMP & TEN)
D6	YES	NO	NO	NO	NO	NO	CYCLIC (COMP & TEN)
D7	YES	NO	NO	NO	NO	NO	MONO. (COMP.)
D8	YES	NO	NO	NO	NO	NO	MONO. (COMP & TEN)
D9	YES	NO	NO	NO	NO	NO	MONO. (COMP & TEN)
D10	YES	NO	NO	NO	NO	NO	MONO. (COMP & TEN)
D11	NO	NO	NO	NO	YES	NO	MONO. (COMP & TEN)
D12	NO	NO	NO	YES	NO	YES	MONO. (COMP & TEN)

Figure 2.2: Specimen Summary

Throughout all of the New Brunswick testing, the masonry panel sizes were consistently 11′-10″ long by 9′-2″ long. Type S mortar was used in constructing the masonry panels. All but four of the panels included horizontal joint reinforcement in alternating courses. The confining frames consisted of two W10 x 39 columns and a W8 x 31 beam. For most of the tests, the frame connections were semi-rigid moment connections. Richardson's (1986) testing utilized moment connections for the first seven tests and simple hinge connections at all four corners of the frame for the latter five tests.

The test frames were instrumented with linear variable displacement transducers (LVDTs) on the frame at the beam centerline in order to obtain deflection data for the frame as a whole. Dial gages were placed at the frame-infill interface to obtain relative displacements between the frame and infill. Strain gages were placed on the frame members and along the diagonal of the infill. Inclinometers were also used at the frame connection points to register joint rotation.

The load for each frame was applied statically in five kip increments. For the first 17 tests, the load was applied monotonically in one direction. For this type of loading, the specimen was loaded until reaching a maximum deflection of 0.984″ (25 mm). All frames attained an ultimate load before reaching this deflection. There were three other types of loading. Two specimens were loaded cyclically between zero

and a percentage of their expected ultimate load. The following nine specimens were loaded cyclically, alternating sign from tension to compression. The five remaining frames were loaded monotonically in compression and then in tension.

From the results of all experimental programs of masonry infilled steel frames, the conclusion has been drawn that the masonry panel greatly increases the in-plane strength and stiffness of the system. Figure 2.3 is a summary of the test results from the test programs of Yong, McBride, Amos and Richardson. The table includes first cracking load, ultimate load and initial stiffness of the system for all 34 tests. The initial stiffness given in the table was taken from the straight line portion of the load-deflection curve.

Dawe and Seah (1988) summarized the New Brunswick testing. For the purposes of behavior description, a standard specimen is defined as one which has a solid panel with standard horizontal joint reinforcement, no openings or ties, and is mortar-fitted snugly to the frame but is not mortared in between the column flanges. At approximately 10 kips, peripheral cracks began to form at the bottom and at the loaded column-panel interface. This corresponded to roughly 10% of the ultimate load. Cracking along the top two mortar joints occurred at about 30 kips, approximately 28% of the maximum load. At 72 kips, the first major cracking along the compression diagonal occurred. This coincided with 68% of the ultimate load of 106 kips. Ultimate load was defined as the

SPECIMEN NUMBER	1st CRACK LOAD (kN)	1st CRACK LOAD (KIPS)	ULTIMATE LOAD (kN)	ULTIMATE LOAD (KIPS)	INITIAL STIFF. (kN/mm)	INITIAL STIFF. (KIPS/in)
WA1	342	76.88	471	105.88	73	416.83
WA2	356	80.03	440	98.91	82	468.22
WA3	200	44.96	463	104.08	74	422.54
WA4	211	47.43	476	107.00	63	359.73
WA5	334	75.08	445	100.04	113	645.23
WA6	483	108.58	489	109.93	87	496.77
WB1	245	55.08	449	100.94	72	411.12
WB2	307	69.01	456	102.51	74	422.54
WB3	413	92.84	538	120.94	67	382.57
WB4	169	37.99	209	46.98	27	154.17
WB5	200	44.96	231	51.93	34	194.14
WB6	311	69.91	423	95.09	73	416.83
WC1	270	60.70	420	94.42	41	234.11
WC2	155	34.84	310	69.69	46	262.66
WC3	55	12.36	285	64.07	34	194.14
WC4	64	14.39	335	75.31	34	194.14
WC5	90	20.23	245	55.08	39	222.69
WC6	67	15.06	365	82.05	50	285.50
WC7	310	69.69	534	120.04	64	365.44
WC8	387	87.00	445	100.04	65	371.15
	-356	-80.03	-420	-94.42	-62	-354.02
WC9	267	60.02	400	89.92	54	308.34
	-200	-44.96	-374	-84.08	-6	-34.26
WC10	302	67.89	458	102.96	68	388.28
	-178	-40.01	-423	-95.09	-9	-51.39
WD1	307	69.01	378	84.97	55	314.05
	-156	-35.07	-374	-84.08	-9	-51.39
WD2	200	44.96	445	100.04	63	359.73
	-133	-29.90	-378	-84.97	-12	-68.52
WD3	267	60.02	356	80.03	110	628.10
	-133	-29.90	-356	-80.03	-7	-39.97
WD4	287	64.52	467	104.98	73	416.83
	-187	-42.04	-378	-84.97	-15	-85.65
WD5	67	15.06	334	75.08	55	314.05
	-45	-10.12	-334	-75.08	-15	-85.65
WD6	454	102.06	623	140.05	110	628.10
	-448	-100.71	-548	-123.19	-7	-39.97
WD7	356	80.03	494	111.05	123	702.33
WD8	62	13.94	200	44.96	17	97.07
	-133	-29.90	-156	-35.07	-13	-74.23
WD9	267	60.02	267	60.02	55	314.05
	-227	-51.03	-237	-53.28	-13	-74.23
WD10	178	40.01	278	62.49	55	314.05
	-100	-22.48	-245	-55.08	-8	-45.68
WD11	156	35.07	167	37.54	14	79.94
		0.00	-105	-23.60	-3	-17.13
WD12	44	9.89	196	44.06	20	114.20
	-22	-4.95	169	37.99	-5	-28.55

(-) Denotes compression; (+) Denotes tension

Figure 2.3: Results Summary

load beyond which the frame experienced increasing deflection without a significantly increased load. As previously discussed, all specimens had realized their ultimate load before reaching the preset maximum deflection of 0.984". All tests were halted at this point with the exception of specimen WD7. Specimen WD7 was loaded to a complete destruction of the system in order to verify the ultimate load for the other specimens. After reaching the criterion of an ultimate load, 111 kips for this panel, the load continued to drop with further increase of deflection. This particular experiment also illustrated the equivalent diagonal strut behavior of the panel. The crack pattern at ultimate load for WD7 clearly indicated the formation of a compression diagonal bounded by two major diagonal cracks (Dawe, 1988).

Dawe, Yong, McBride, Amos, and Richardson examined the effects of varying several different parameters throughout their testing. McBride (1984) noted that the variation of mortar strength did not significantly affect initial cracking load, initial stiffness, or ultimate strength of the system. Dawe (1988) and Yong (1984) stated that the integrating of the panel to the confining frame, either with column ties or the packing of mortar in between the column flanges, results in a lower in-plane shear strength. When panels were tied or mortared in between the column flanges, there was extensive randomized cracking. This random cracking prevented the compression diagonal from being fully developed (Dawe, 1988).

Most of the test specimens included horizontal joint reinforcement in alternating courses of the panel. Dawe (1988), along with several others, noted that the inclusion of the joint reinforcement had very little impact on the ultimate load of the system. However, the one specimen that did not include joint reinforcement did have the lowest stiffness. The lack of joint reinforcement also appeared to introduce more random cracking.

There were several specimens that were constructed with an air gap between the top course and the beam of the confining frame. In all of these cases, it was concluded that this condition results in lower initial stiffnesses and reduced ultimate loads of the panels. The effect of openings in the panels, simulating doorways, was also studied in several specimens. Dawe (1988) concluded that the presence of an opening may reduce the initial cracking load of the panel; however, the ultimate load did not appear to be seriously affected. Dawe also noted that if the opening were placed closer to the loaded side of the panel, the ultimate load was affected even less significantly.

When horizontal bond beams were included in the panels, the initial stiffness and initial crack load were increased. Amos (1985) expressed a concern that with the initiation of major cracking very near to the maximum load, there is little warning of approaching failure.

Yong (1984), in a parametric analytical study, experimented with varying the aspect ratio of the panels. The height of the frame remained 9′-2″ while the length of the panel was increased. It was surmised that as the aspect ratio (length/height) is increased, the stiffness of the system was also increased.

Cyclic loading of the specimens is perhaps the most relevant aspect of the Canadian research with respect to the current research. Amos (1985) and Richardson (1986) experimented with loading several specimens in a cyclic manner. Richardson (1986) loaded several specimens up to first crack load in the compressive direction and then in the opposite direction. These frames exhibited an almost equal stiffness in the second direction as the first load. Some specimens were loaded beyond the first crack load in the compressive direction and then the load was reversed and the frame was loaded through zero in the second direction. These specimens displayed a significantly reduced stiffness in the second direction.

Richardson (1986) experimented with repetitive reversed loadings above and below the first crack loading of the frame. He noted that a large number of low magnitude load cycles affects the infilled frames as adversely as a smaller number of cycles of load of a higher magnitude. In both cases, after a large number of load cycles, the system gradually reduces toward the bare frame response (Richardson, 1986).

2.3 Analytical Methods

This section discusses analytical techniques that have been established by past investigators of masonry infilled frames. There have been several techniques developed to quantify different aspects of the behavior of masonry infilled frame behavior subjected to horizontal loads. Polyakov (1956) was the first to suggest the use of an equivalent diagonal strut for analysis of the panel. Since that time, several researchers have incorporated this concept into their analyses.

Holmes (1961) proposed a procedure for predicting the ultimate horizontal racking load of an infilled frame by using the diagonal strut theory. The following equation is based on the value of strain along the compressive diagonal that will cause failure of the infill material:

$$H = \frac{24EI\varepsilon d}{h^3\left(1+\frac{I}{I_o}\cot\theta\right)\cos\theta} + Af_c\cos\theta \qquad \textbf{EQ. 2.1}$$

Where: H = ultimate horizontal load

EI = flexural rigidity of the columns

ε = strain in the infill at failure

d = length of the panel diagonal

h = height of the panel

I_o = moment of inertia of the columns

I = moment of inertia of beam

θ = angle diagonal makes with the horizontal

A = area of the equivalent diagonal strut

f_c = crushing strength of the infill

The area of the equivalent diagonal strut was taken by Holmes as being equal to td/3, where t is the thickness of the infill. The first term in the equation is the force that is carried by the steel alone and the second term is the horizontal component that the diagonal strut will carry with Af_c being the compressive force in the strut. In the same paper, Holmes (1961) derived an equation for the horizontal deflection at the point of the applied load:

$$S_H = S_{BD}\cos\theta = \varepsilon d(\cos\theta) \qquad \textbf{EQ. 2.2}$$

Stafford-Smith and Carter (1969) found that the strength and stiffness of a frame is dependent on the length of contact between the frame and the infill. The length of contact, in turn, is dependent on the relative stiffness, given by:

$$\lambda h = \sqrt[4]{\frac{E_i t \sin 2\theta}{4EI_o l}} \qquad \textbf{EQ 2.3}$$

where the terms are defined the same as for equation 2.1 and 2.2; where l is the length of the infill; and E_i is the modulus of elasticity of the infill. The length of contact, α, of the infill at the loaded corners is given by:

$$\frac{\alpha}{h} = \frac{\pi}{2\lambda h} \qquad \text{EQ. 2.4}$$

The length of contact equation was developed from an equation for length of contact of a free beam on an elastic foundation.

Jamal suggested that Stafford-Smith and Carter's relative stiffness parameter over-estimated the actual stiffness of the system due to neglecting the steel-infill slippage. Baura (1977) suggested equation 2.5 for estimating the initial stiffness of the system. Jamal (1993) also suggested a

$$\frac{S}{Et} = \frac{0.2234}{\sqrt{\lambda I}} \qquad \text{EQ. 2.5}$$

modified equation for the equivalent strut width, α_c, which is shown in equation 2.6.

$$\alpha_c = C_1 C_2 \frac{\pi}{2\lambda} \qquad \text{EQ. 2.6}$$

Where: C_1 = 1.0 for initial stiffness

0.66 for 50% secant stiffness

0.39 for ultimate stiffness

and C_2 = 1.0 for rigid frames

0.71 for hinged frames

Liauw and Kwan (1982, 1983) presented several papers on multi-story infilled frames using plastic theory and a finite element approach. The finite element program considers the non-linear behavior of the infill material (Liauw and Kwan, 1982). In a subsequent paper, Liauw and Kwan (1983) considered interface shear due to friction as a part of the program. Several other investigators have utilized finite element programs to study the behavior of infilled frames. Barua and Mallick (1977) presented a finite element program that takes into account the axial deformations of the columns, length of contact, interface shear and interface slip. Stafford-Smith and Riddington (1975) produced a finite element model that considers failure by shear, diagonal tension, or corner compression.

Yong (1984) developed a finite element program that considers interface shear and slippage. Yong's program can be adjusted to include such parameters as bond beams, column-infill tie systems and joint horizontal reinforcement. The input data consists of frame data, panel data, and reinforcement data. The program output includes

displacements, rotations, moments, and forces at each node in the frame and panel displacements and element stresses and reactions for the infill.

A comparison of Yong's theoretical data from the finite element program is made to his experimental data (Yong, 1984). The load-deflection curves demonstrated fairly good agreement. The theoretical curves maintained slightly higher values than experimental for all comparisons. Predicted length of contact did not show good correlation with experimental values; however, the measured values of length of contact may not have been very accurate due to the laboratory equipment available (Yong, 1984). Principal stress contours and resulting predicted crack patterns displayed good correlation for both reinforced and unreinforced joints.

McBride (1984) compared several methods of predicting ultimate loads, initial stiffness, and mode of failure with his experimental data. He found that Holmes' method does not recognize the various possible modes of failure and results in substantially higher values than observed (McBride, 1984). The ultimate load prediction method by Stafford-Smith and Carter did not show good correlation for the value of the load; however, the method did correctly predict the mode of failure for all specimens. Stafford-Smith and Carter's theoretical relative stiffness displayed good agreement with the initial stiffness of the experimental specimens.

2.4 Summary

Research into masonry infilled frames behavior is still ongoing. There have been many experimental programs in the past 45 years; therefore, most methods of analysis have been empirical ones. Theoretical investigations into the subject have been lacking due to the nature of the masonry infill material. The availability of research material on structural clay tile infills is even less than that of general masonry infills. The behavior of infilled frames under cyclic loading and load reversals also has relatively little literature available. There have been some fairly accurate empirical methods for behavior prediction published. There is a need for a deeper theoretical investigation into the behavior of the infill, perhaps from a fundamental material behavior point of view.

Chapter 3: TEST SETUP

3.1 Introduction

This chapter describes the preparations that proceeded the experimental program. These preparations included the design and construction of the reaction frame, and design of the specimen frame connections. Frame instrumentation methods were also considered in the preliminary stages. Figure 3.1 illustrates a typical test setup. All steel was type A36.

3.2 Reaction Frame Design

The reaction frame consisted of wide flange shapes in a triangular configuration welded to two 5′-3½″ by 3′-0″ by 1½″ base plates. The frame was fastened to a structural floor with 1¼″ threaded rods. Structural tube sections were used at each end of the base plates to provide additional restraint. The design load for the reaction frame was 150 kips. This value was deemed to be in excess of the ultimate load for any given panel in the scope of the testing. This load is also the upper limit of the ram and load cell used during testing.

The direct stiffness method was used in analyzing the reaction frame. The criteria used in sizing the members were the combined stress standards in chapter H of the ninth edition AISC Allowable Stress Design Manual (AISC, 1989). The reaction frame connections were designed as end plate moment

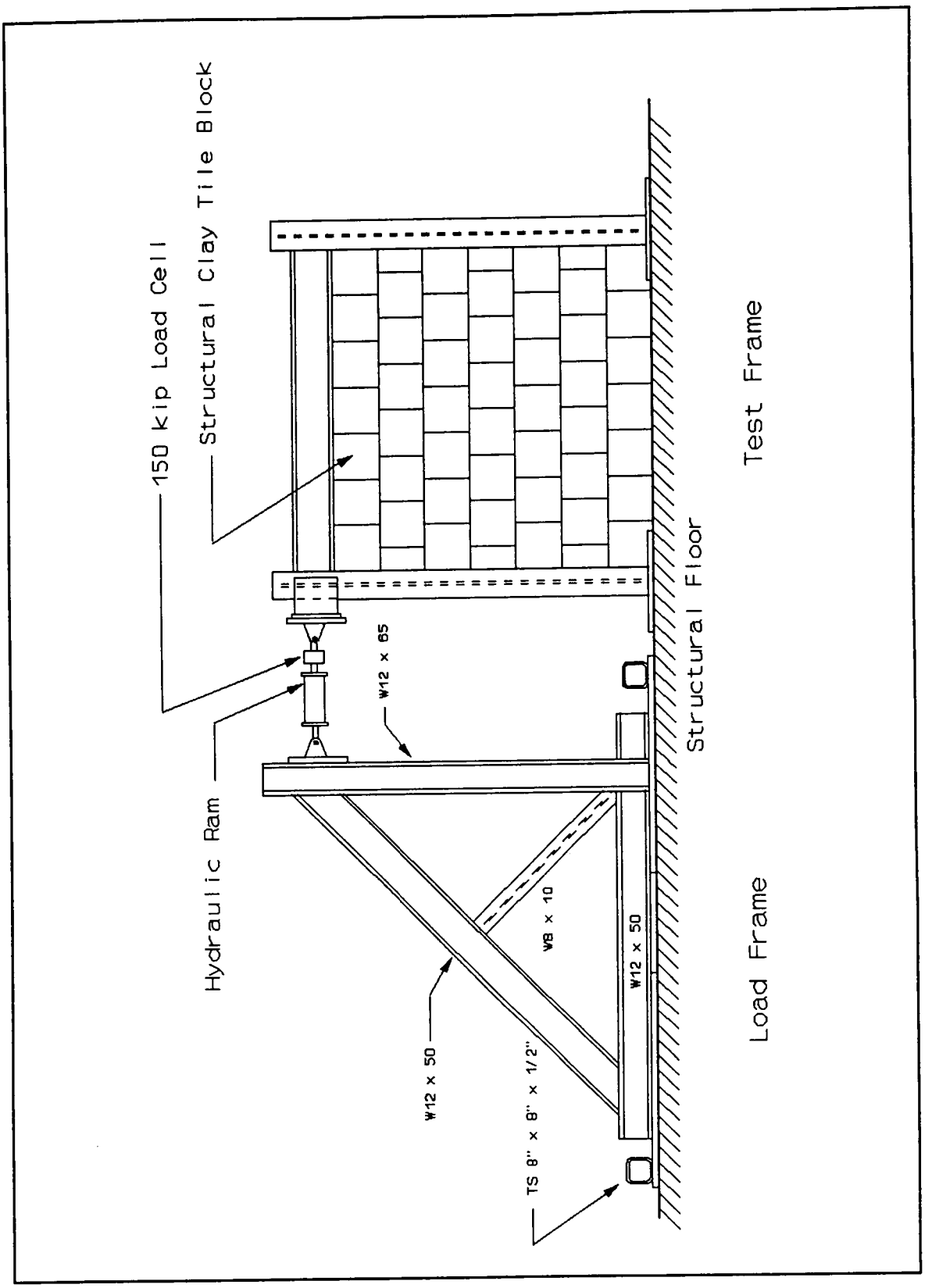


Figure 3.1: Typical Test Setup

connections with the exception of the W12 x 50 beam to the W12 x 65 column connection. This was a simple double clip angle connection.

In figure 3.1, the W12 x 50 beam was welded to the back base plate and the W12 x 65 column was welded to the front plate. The connection between these two parts of the reaction frame was made with the clip angle connection. Stiffeners were provided at the point of loading and at the diagonal to beam connection to prevent web crippling. Additional stiffness was added to the base plate by welding a 1′-0″ section of a W12 x 50 at the base of the column.

3.3 Specimen Frame Design

The specimen frame shown in figure 3.1., which is depicted in plan in figure 3.2, also consisted of wide flange shapes. Both of the frames consisted of W10 x 30 columns and a W12 x 35 wide flange beam. The member sizes were selected in order to replicate in-situ conditions at the Y-12 plant in Oak Ridge and also to accommodate the dimensions of the structural clay tile. The specimen frame columns were oriented for bending about the weak axis. The panel for frame 2 was approximately 7′-4″ long by 7′-4″ high. Panel 17 measured 11′-4″ long by 7′-4″ high. Figure 3.3 illustrates a wall section of the specimen frame construction.

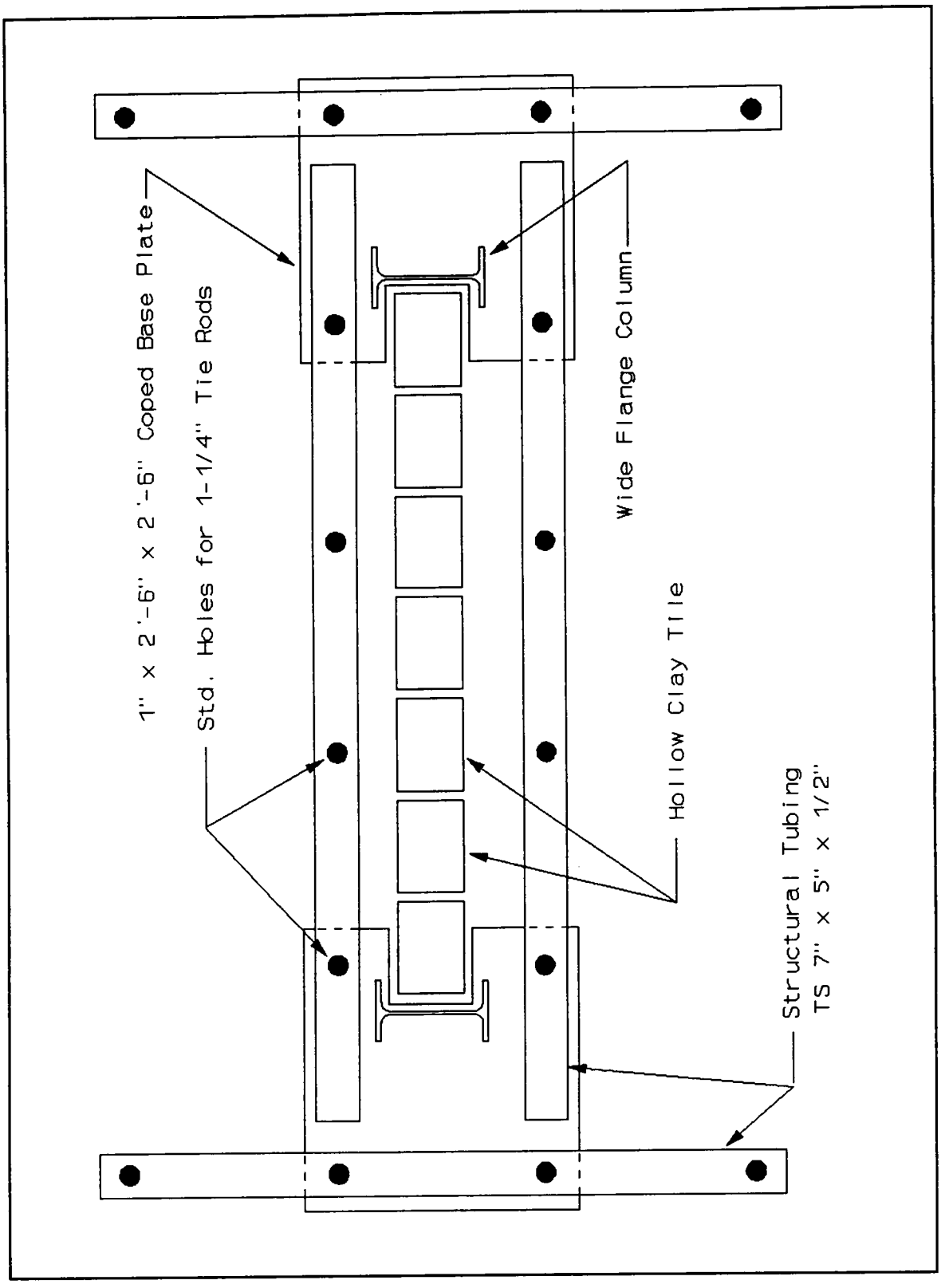


Figure 3.2: Specimen frame plan

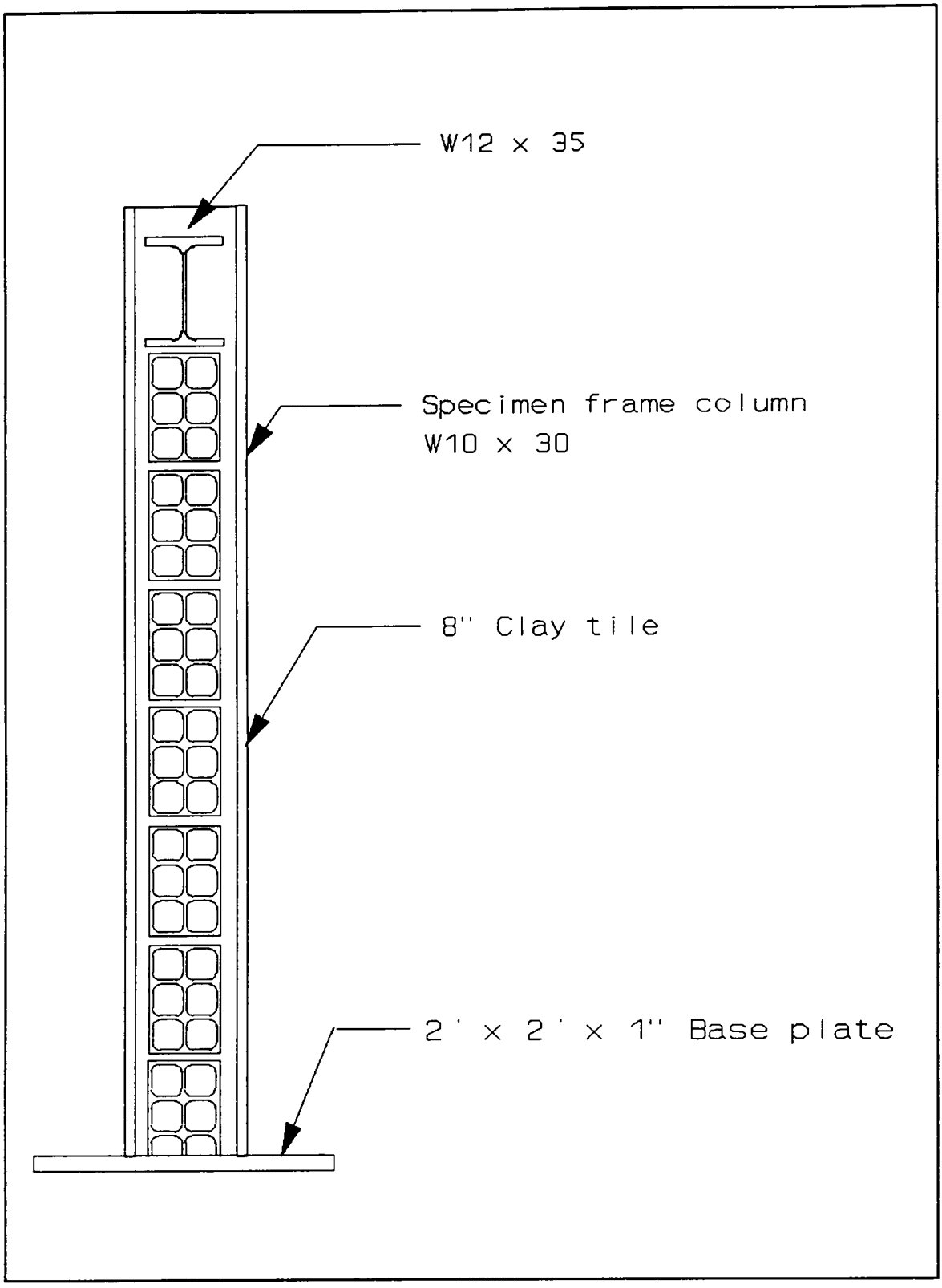


Figure 3.3: Specimen section

The simple beam to column connections of the confining frame were double clip angle connections. The clip angles were designed to transmit the lateral tension load without significant prying action. The bolts were sized according to double shear criteria for the beam to angle connection and for pure tension for the column to angle connection. Bearing on the beam webs typically governed for shear design. There was therefore adequate resistance to block shear in the beam webs. Figure 3.4 illustrates the beam to column connection used for both frames. The required angle thickness to prevent prying action of the angles was ⅞". This thickness was not available and the 1" thick angles were substituted. The non-standard angle size, 6" x 4" x 1", was fabricated by clipping a larger angle.

The base plates of the specimen frames were designed for bending stress at a critical section of the plate. The analysis yielded a 1½" base plate to provide an adequate section modulus. In order to reduce the size of the specimen base plates, structural tubes were added on all four sides of the specimen to provide additional constraint and reduce the bending stress in the base plates. This can be seen in figure 3.2. The column of each specimen frame was attached with an "all around" ¼" fillet weld. An 8½" by 10⅝" cope cut in each plate provided access for the clay tile block to be laid against the column web and have the full area of the block

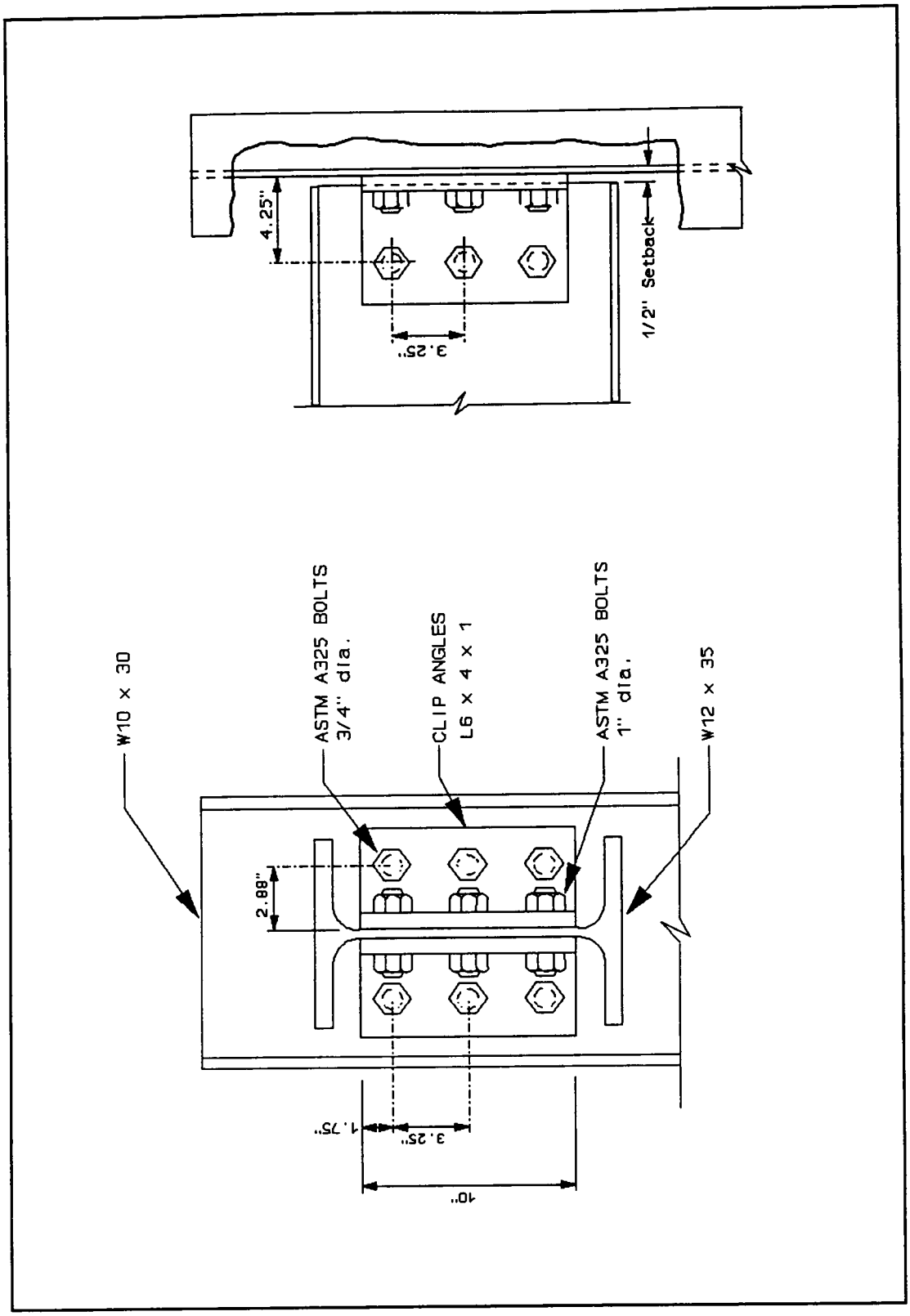


Figure 3.4: Connection Detail

interface with the floor. Figure 3.5 represents a typical base plate detail.

3.4 Out-of-Plane Bracing

The restriction of out-of-plane movement of the specimen frame was of concern during the design stages of the testing program. A reaction frame had to be designed for out-of-plane loading, which is beyond the scope of this thesis. Once this frame was designed, it was modified to double as an out-of-plane bracing frame. Figure 3.6 depicts the cantilevered beam used as the out-of-plane loading frame.

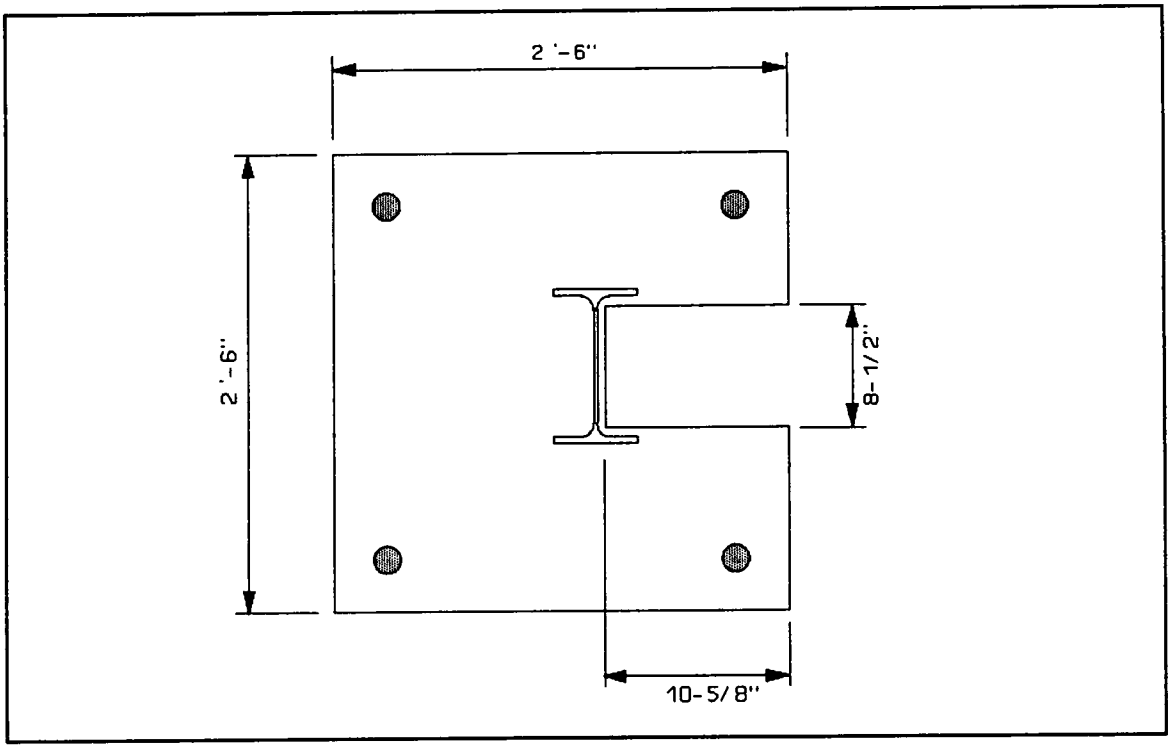


Figure 3.5: Base Plate

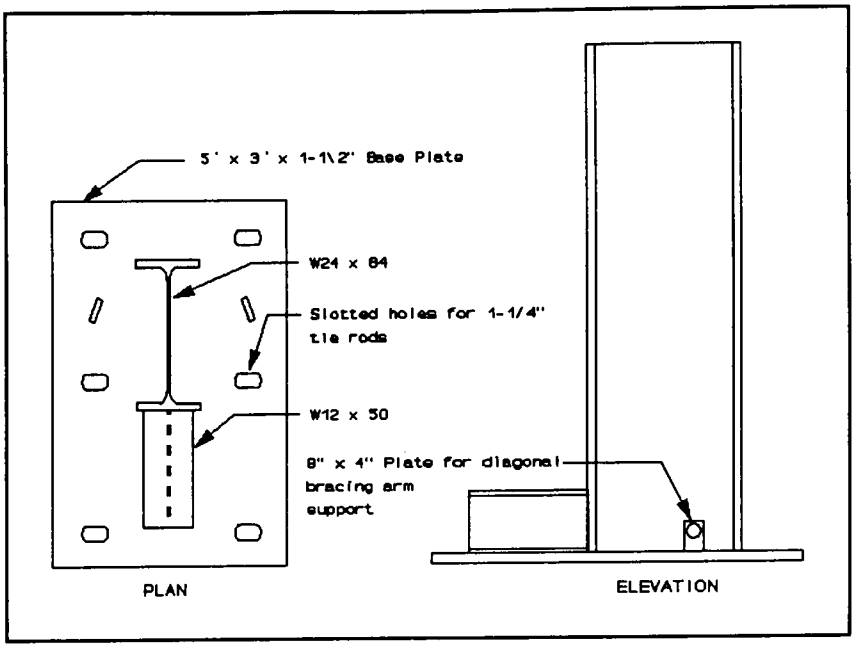


Figure 3.6: Out-of-plane reaction frame

Figures 3.7 and 3.8 illustrate the modifications made to this frame in order for it to restrict any movement of the specimen orthogonal to the plane of loading. The "connection" of the bracing arms to the beam of the specimen frame allow unrestricted in-plane movement of the specimen frame. Figure 3.9 illustrates the bracing arm connection to the specimen frame beam. The 2″ x 2″ x ⅜″ angles welded to the W4 x 13 bracing arm nor the bracing arm itself makes contact with the confining frame beam, thus allowing the necessary in-plane movement. The specimen frame is braced at the two points indicated in figure 3.7.

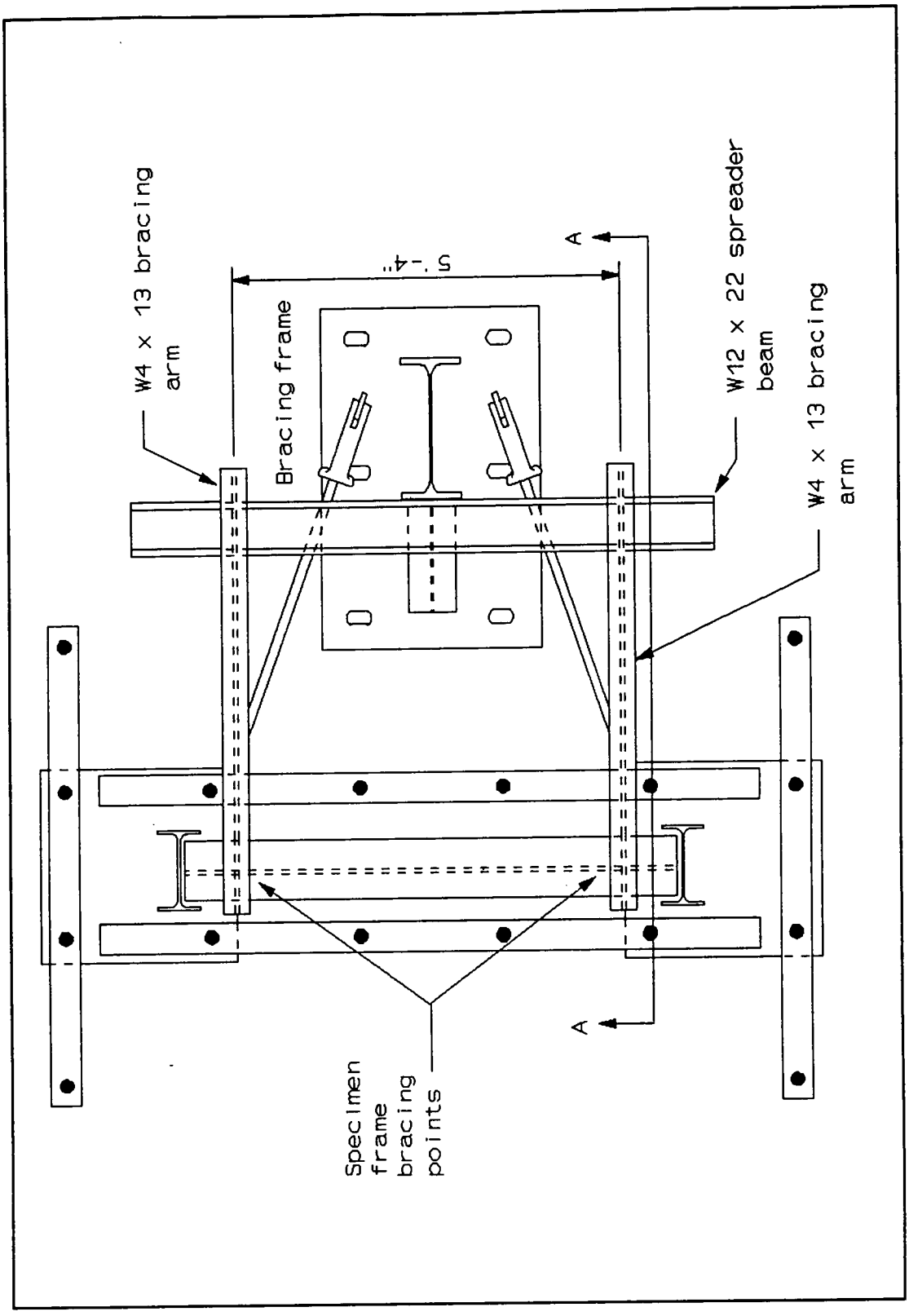


Figure 3.7: Specimen bracing; plan

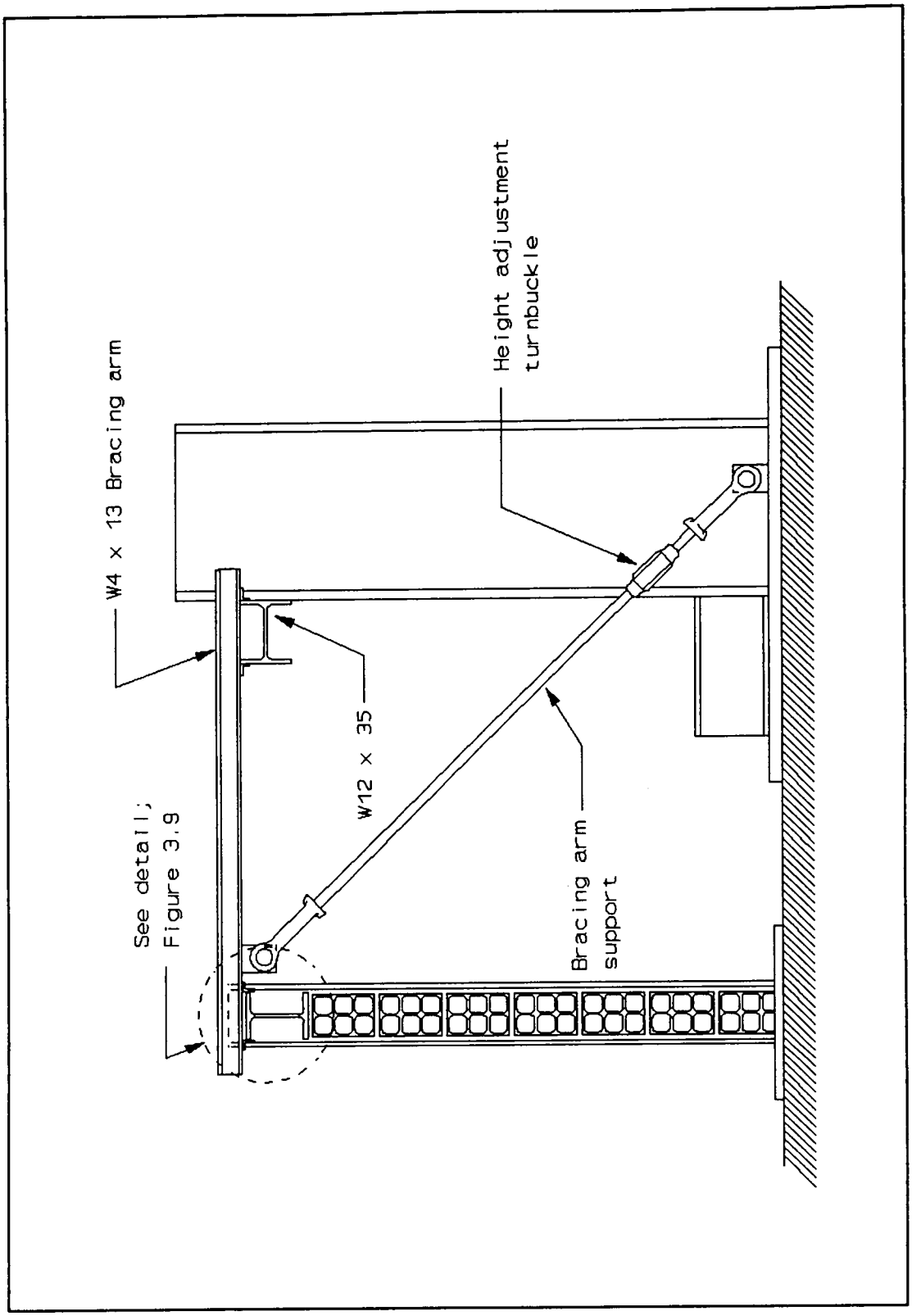


Figure 3.8: Specimen bracing; section

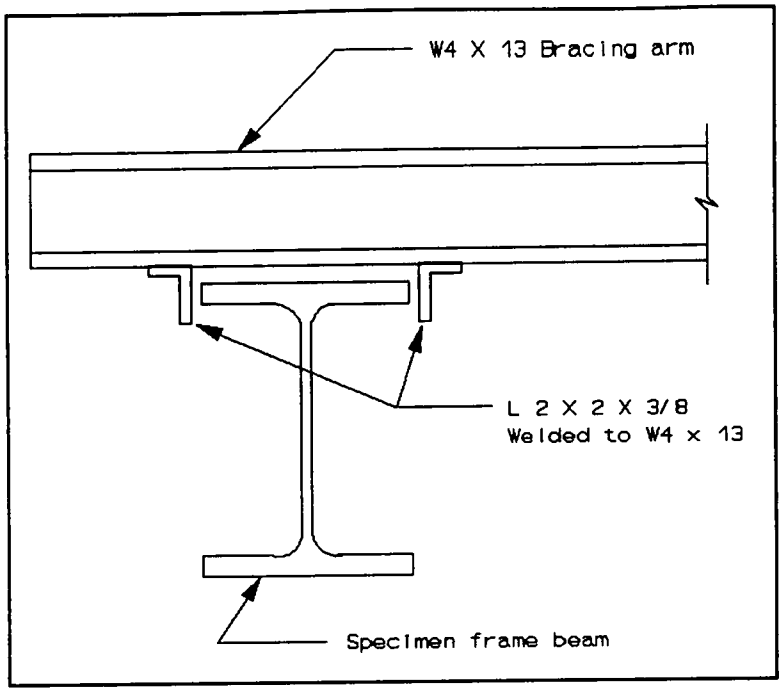


Figure 3.9: Bracing detail

3.5 Laboratory Setup

A structural laboratory, with a strong floor and a 3 ton rail crane, was used for the testing program. The concrete strong floor had 1¼" tie rod holes spaced at 24" on center in both directions. This was suitable for attaching the reaction frame and the specimen frames to the slab.

The reaction frame was brought in and assembled before any specimen frames were present. Test setup construction included assembling the reaction frame, specimen frame and the out-of-plane bracing structure. There was room in the lab for a full test setup and another specimen frame.

There was a required curing period of 30 days for each panel. The extra room in the lab allowed for a "staggering" of tests in that, while one frame was being instrumented to be tested, another frame could be constructed. This shortened the waiting period between test from the 30 day curing period to approximately 15 days. Figure 3.10 illustrates the floor plan of the laboratory with a test setup and another specimen frame. The out-of-plane bracing frame is not shown.

3.6 Instrumentation

Prior to testing, the specimen frames and panels were instrumented with various data collection devices. For displacement measurements, linear variable displacement transducers, (LVDTs), were mounted in various positions. Figures 3.11 and 3.12 depict the locations of the LVDTs. Figure 3.11 illustrates the positioning of the stationary and relative LVDTs.

The stationary LVDTs measured overall movement of the frame and panel together. The relative LVDTs gauged the movement of the panel with relation to the confining frame. Figure 3.12 shows the location of the panel LVDTs: these indicated relative movement between the individual clay tile. Frames were fabricated to hold the stationary LVDTs in place. The relative and panel LVDTs were fastened to the specimen frame with an epoxy via a bracket that held the LVDT. The travel range of the LVDTs varied from ±1˝ to ±3˝.

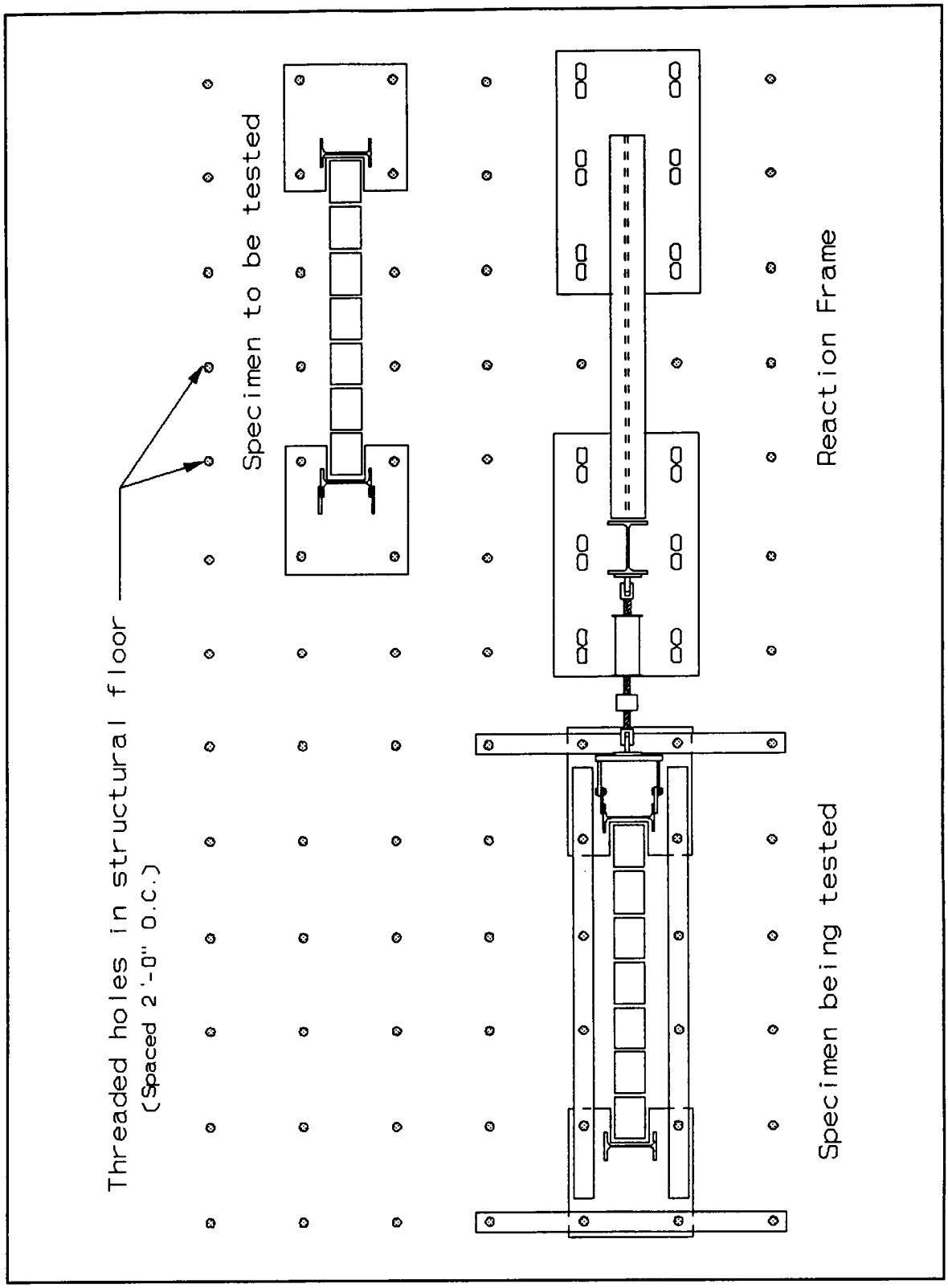


Figure 3.10: Partial lab floor plan

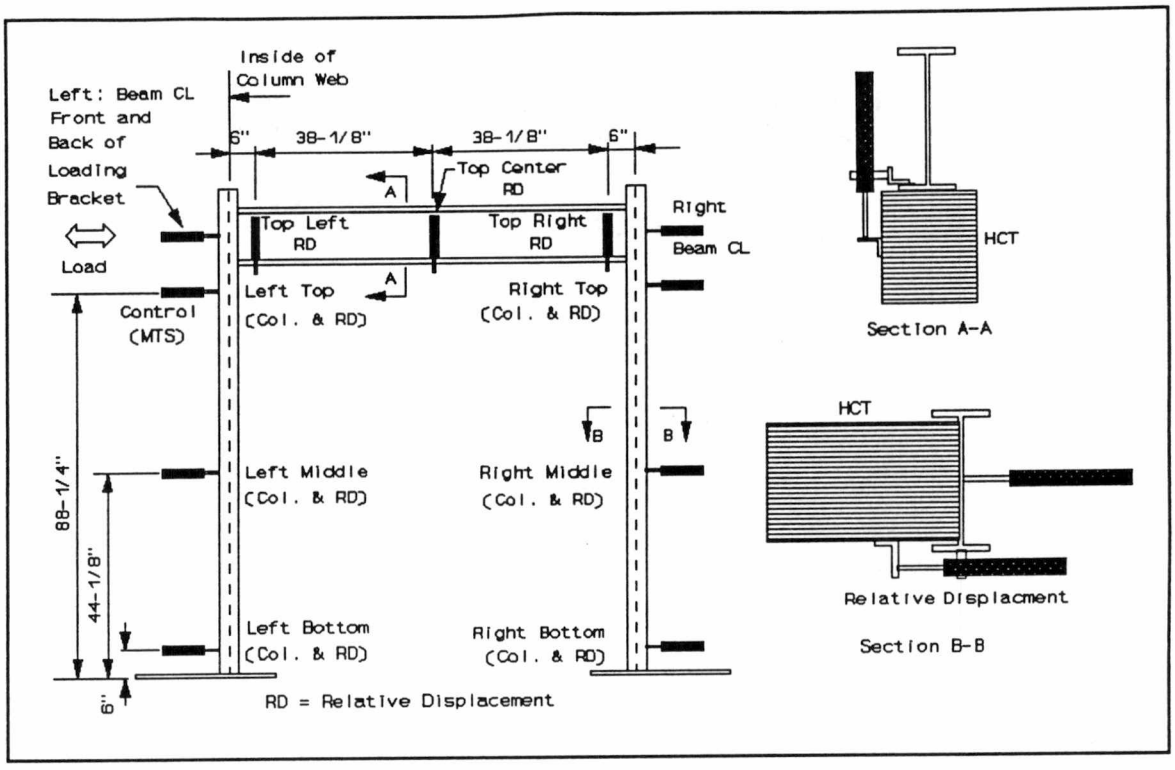


Figure 3.11: LVDT placement

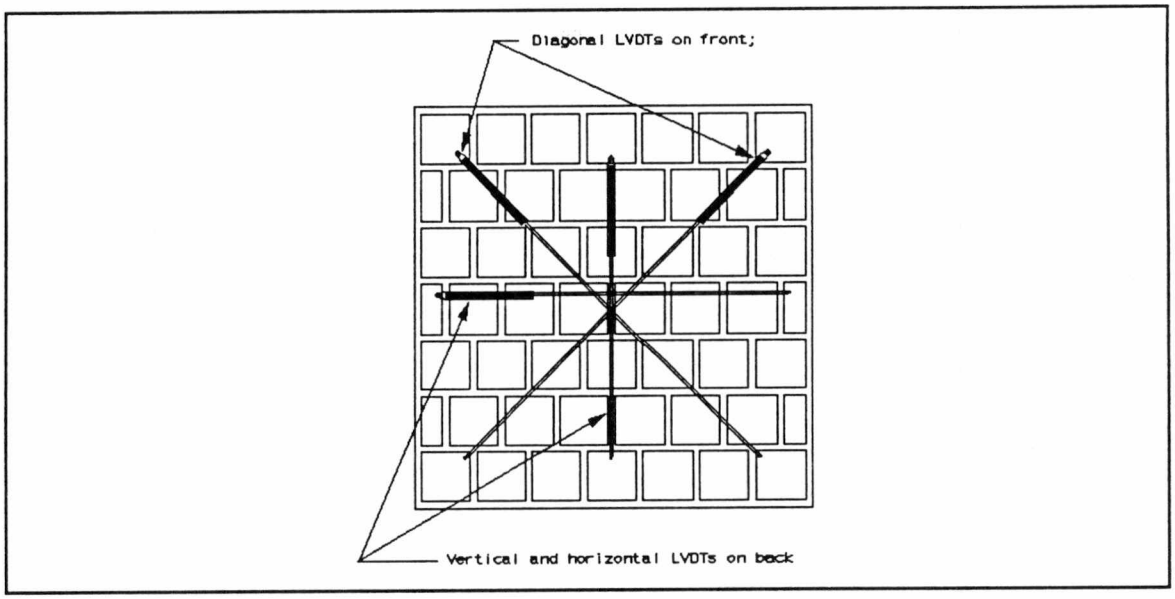


Figure 3.12: Panel LVDT placement

The confining frame was also instrumented with strain gages at various points on the beam and columns. Figure 3.13 shows the locations of the strain gages. As shown in figure 3.13, the strain gages located opposite each other on the two flanges of the column were wired in pairs in a half bridge configuration. This yielded a true average reading of strain values at that particular position in the column. The strain gages located on the beam of the confining frame were wired in a similar manner. The strain gages opposite each other on the same flange of the beam were wired together in the half bridge configuration. All of the strain gages were wired through a Vishay 2100 conditioner for excitation and amplification.

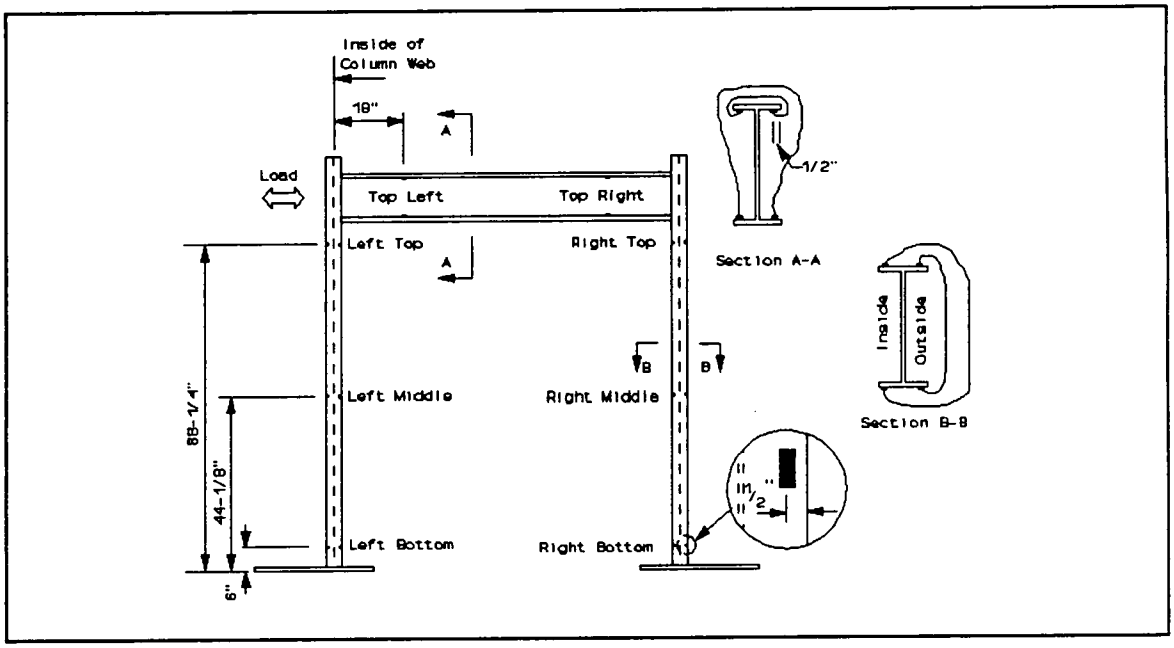


Figure 3.13: Strain gage locations

Load, displacement, and strain measurements were all collected through a central data collection system. Figure 3.14 is a schematic of the instrumentation and control systems for a typical test. The LVDTs were connected to a STB 884/SCV terminal block. The LVDTs were electrically excited by an external source at this point. From here they were run into the Megadac 3008 data collection system. The strain gage connections ran from the aforementioned conditioner into the data collection computer. The Megadac data collection system was connected to an IBM PS/2 via an IEEE 488 interface. Digital monitors or various real time plots were viewed through this computer during testing.

3.7 Testing Procedure

The testing procedure was divided into three distinct areas. There were pre-test activities, loading the specimen and collecting data, and post-test activities.

3.7.1 Pre-Testing Requirements

The first requirement of the testing was to erect the steel confining frame. The connections of the specimen frame were tightened with an impact wrench using the "turn of the nut" method to obtain a slip-critical connection. The specimen was then plumbed and connected to the strong floor.

The infill was then placed into the frame. The mortar mix used was ½ bag of type N mortar mixed thoroughly with seven

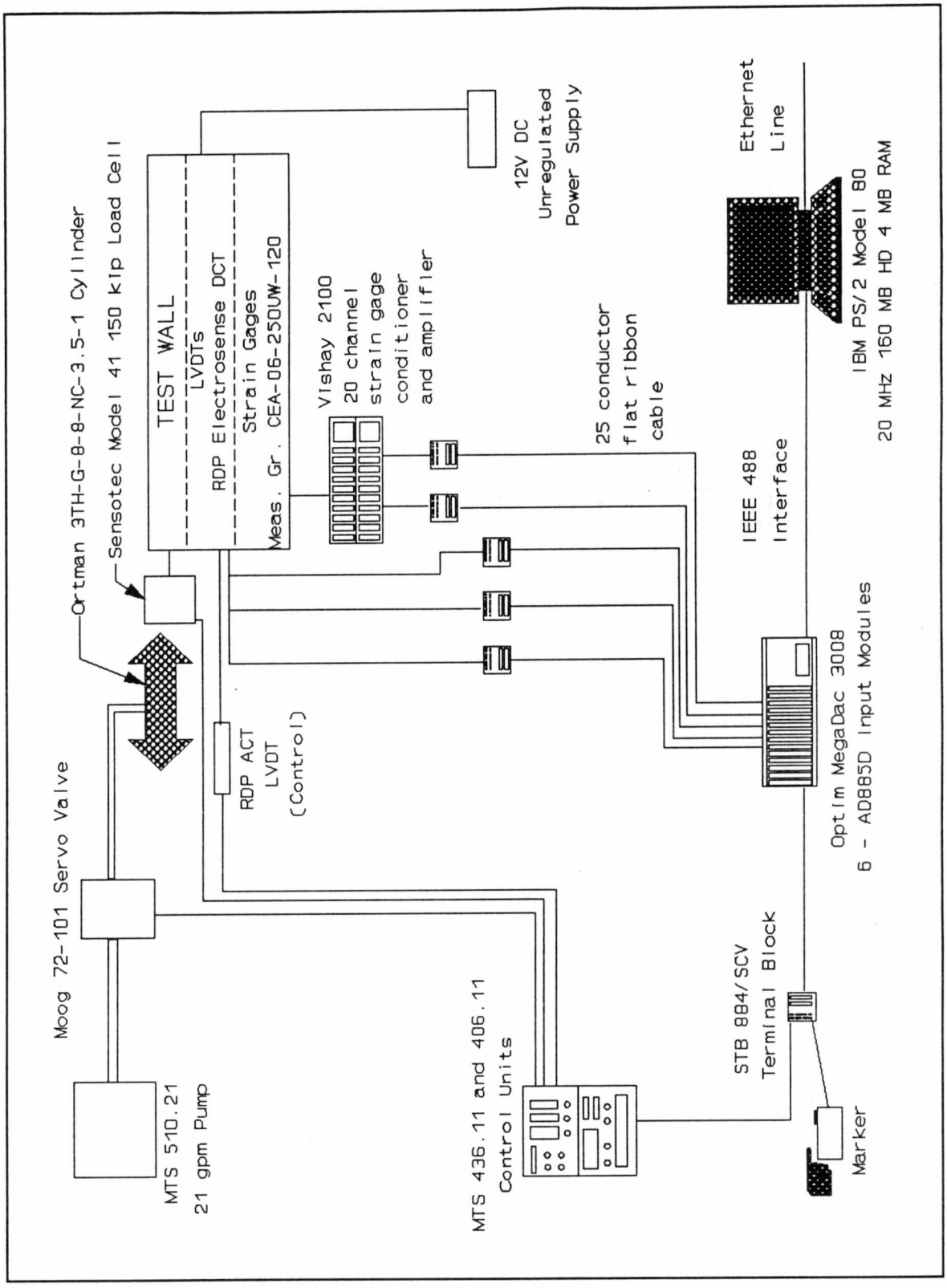


Figure 3.14: Instrumentation Schematic

shovelfuls of natural river sand. Water was added to obtain suitable workability. The wall was laid seven courses high of seven tile each. The head joints and bed joints were approximately ¾" thick. The bottom course had a mortar joint between it and the floor. There was a mortar joint between the tile and the webs of the columns; however, there was no mortar placed between the tile and the column flanges. During the construction of the clay tile panel, nine 2" by 2" by 2" mortar cubes were made according to ASTM C109 (American Society for the Testing of Materials). These nine cubes were made in groups of three from three different batches of mortar. One cube from each batch was tested at 30 days. The remaining six cubes were tested on the day of the full test.

Instrumentation of the specimen frame then proceeded. The LVDTs and strain gages were attached as discussed in section 3.5. The LVDTs were physically moved to within 0.050" of their null position. A final balance of the LVDTs was performed with the Megadac to "zero" the LVDTs before testing. A shunt calibration was performed on the strain gages with the conditioner to ensure that the gages were working. At this point, before the ram was attached to the specimen frame, it was cycled back and forth several times at some small increment to confirm that there were no anomalies present in the hydraulic system. The ram was then attached to the specimen frame. A pre-test crack map of the specimen panel

was drawn in order to compare with crack maps that would be drawn during and after testing.

3.7.2 Testing

The ram and load cell configuration is illustrated in figure 3.15. The specimen frame was loaded with an Ortman ±8" travel hydraulic ram. The load was measured with a Sensotec Model 41 150 kip load cell. The hydraulic ram was controlled by a MTS control unit and fed by a MTS 21 gpm pump. The tests were run on deflection control and this deflection was monitored by an AC excited LVDT that was run through the MTS control system. A deflection was preset and the MTS applied a load with the ram until the control LVDT measured the preset deflection.

The loading of the specimen frame was cyclic in nature. The initial deflection was preset at approximately 40% of the predicted ultimate load divided by the calculated initial stiffness. The specimen was loaded to this deflection in compression and tension. This cycle was repeated at least twice for each deflection value up to about 1" or greater. From this value of deflection, the specimen was loaded only once in tension and once in compression. Table 3.1 is a break-down of the deflection increments and number of cycles for each increment for frame 2. Frames 17 had a similar loading history.

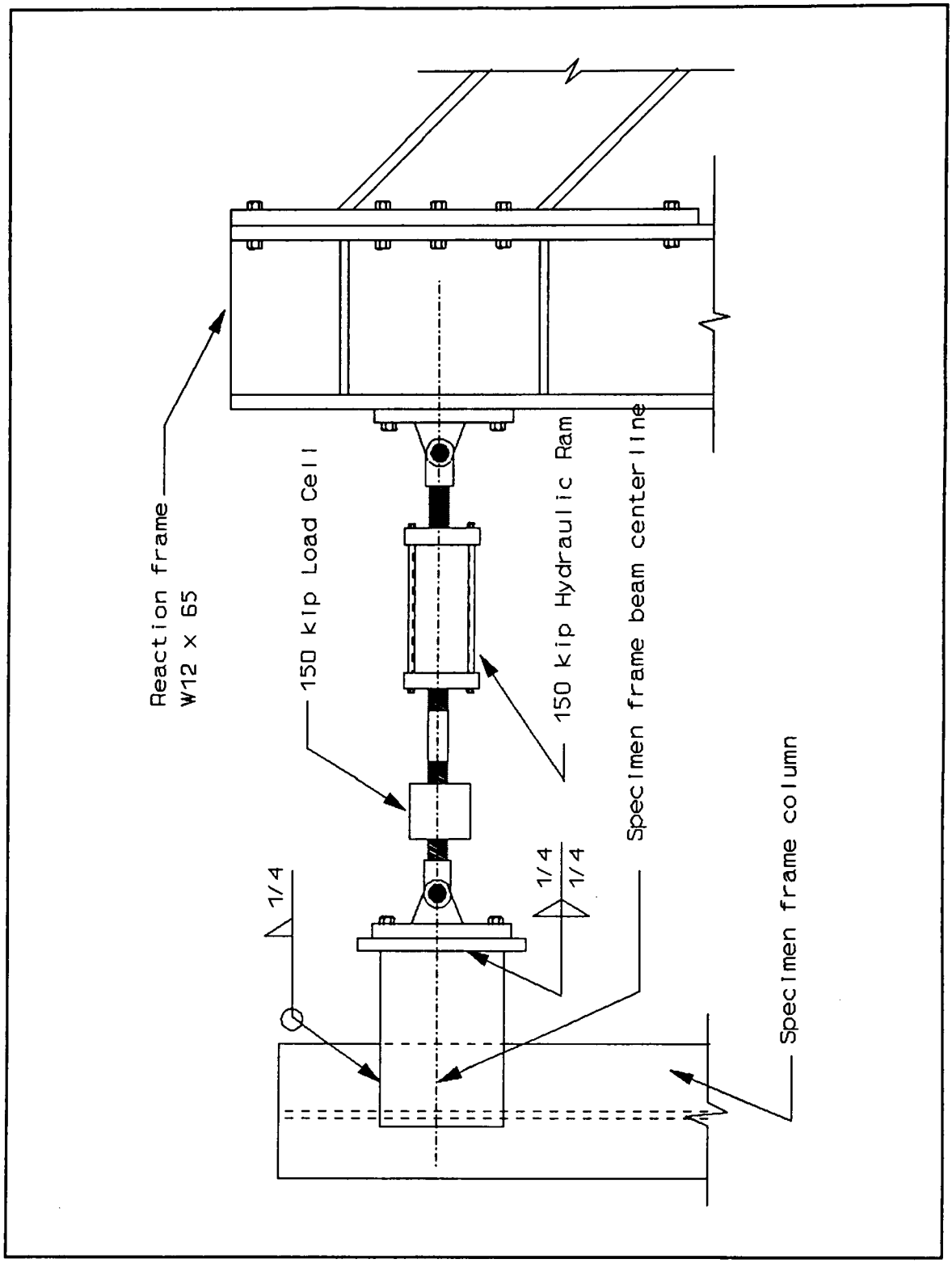


Figure 3.15: Ram and Load cell configuration

Loading No.	Deflection (inches)	Number of Cycles Frame 2, Frame 17
1	0.05	3, 2
2	0.10	3, 2
3	0.15	3, 2
4	0.20	3, 2
5	0.25	3, 2
6	0.30	3, 2
7	0.40	3, 2
8	0.50	3, 2
9	0.60	3, 2
10	0.70	3, 2
11	0.80	3, 2
12	0.90	3, 2
13	1.00	1, 1
14	1.20	1, 1
15	2.00	1, 1

Table 3.1: Deflection increment summary

The deflection cycles continued until well past peak load. During the test, when the clay tile began to break and fall from the frame, the test would be stopped momentarily and the panel and relative displacement LVDTs would be removed to prevent damage. Photographs and videos of "major events" were taken during testing.

3.7.3 Post-Testing Activities

Loading of the specimen frames usually ceased when the full interface between the tile and the frame had been lost and clay tile began to fall out of the frame. At this point, a post-loading crack map was drawn and the remaining tile were knocked out of the frame. For several tests, the bare frame was loaded for several cycles to determine the bare frame stiffness. The mortar cubes were tested in compression to determine the mortar strength of the wall at the time of testing.

Chapter 4: GENERAL SYSTEM BEHAVIOR

4.1 Introduction

The composite behavior of the frame-infill system and bare frame behavior are considered in this chapter. As outlined in chapter three, the frames studied are numbers 2 and 17. Both frames are constructed with W10 x 30 columns and a W12 x 35 beam with simple connections. The difference between the two frames is the aspect ratio. Frame 2 was constructed with a panel ratio of 1:1 with the dimensions being 7'-4" by 7'-4". The clay tile panel for frame 17 was 11'-4" long by 7'-4" which is an aspect ratio of approximately 1.5:1.

The emphasis of this study is primarily the determination of the load-deflection relationships of the system. Figure 3.11 illustrates the placement of the LVDT's for a typical test specimen. The numbering system for the LVDT's is shown in figure 4.1. This numbering system is referred to in reference to specific LVDT's throughout this study. Several of the LVDT symbols in figure 4.1 are assigned two numbers. The first number represents the frame LVDT and the second represents the relative panel-frame displacement LVDT. Panel deformations and frame-panel relative displacements are discussed in chapter 5 and 6 respectively.

For both frames, six loops were extracted and used to study the behavior of the frame. The entire load-deflection

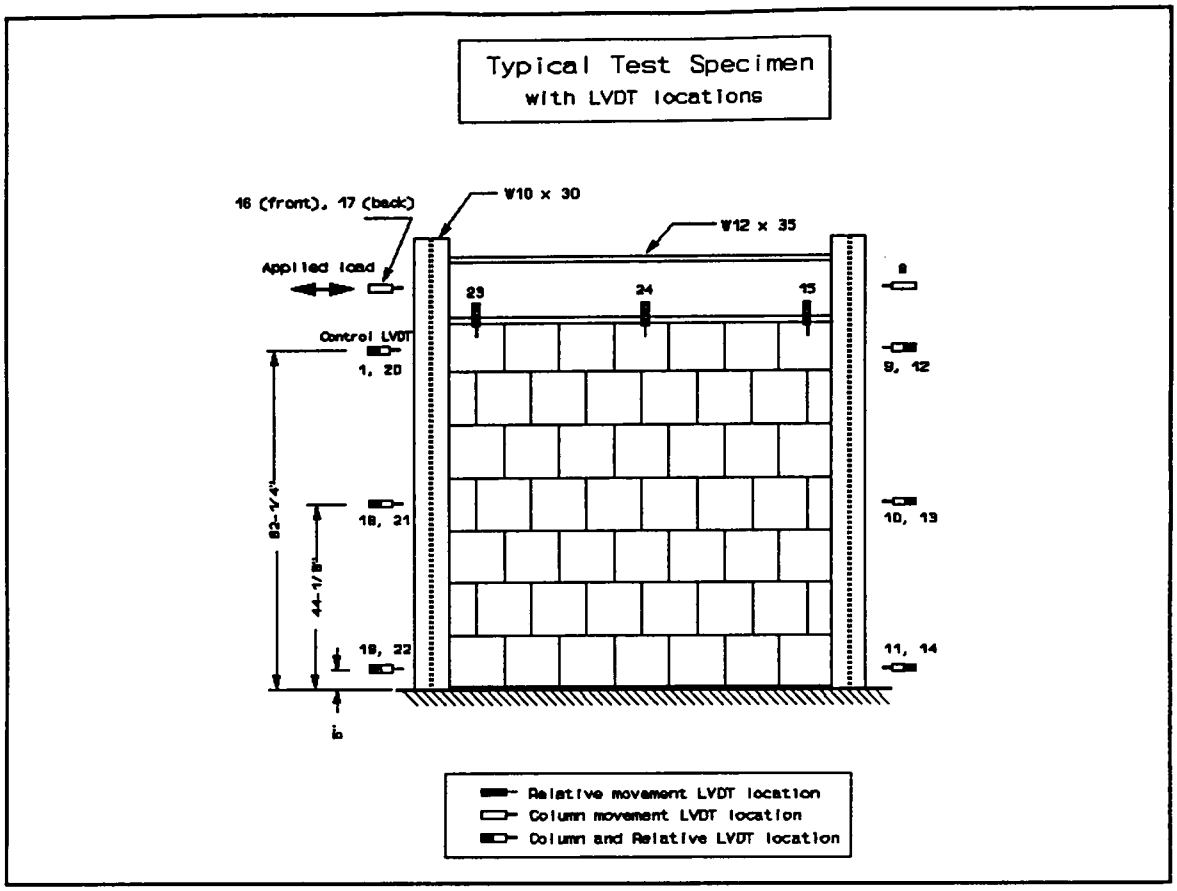


Figure 4.1: Lvdt numbering scheme

hysteresis for frames 2 and 17 are shown in figures 4.2 and 4.3 respectively. Each of the six loop or deflection cycle represented significant events that occurred during testing. Figure 4.4 illustrates the six loops for frames 2 and 17. Each of these loops represents the first cycle for a particular deflection increment. Recall that each deflection increment consisted of two or three cycles.

Several envelope plots have been developed. All envelope plots, a load-deflection plot for example, were developed by taking the point of maximum compression of the first loop for

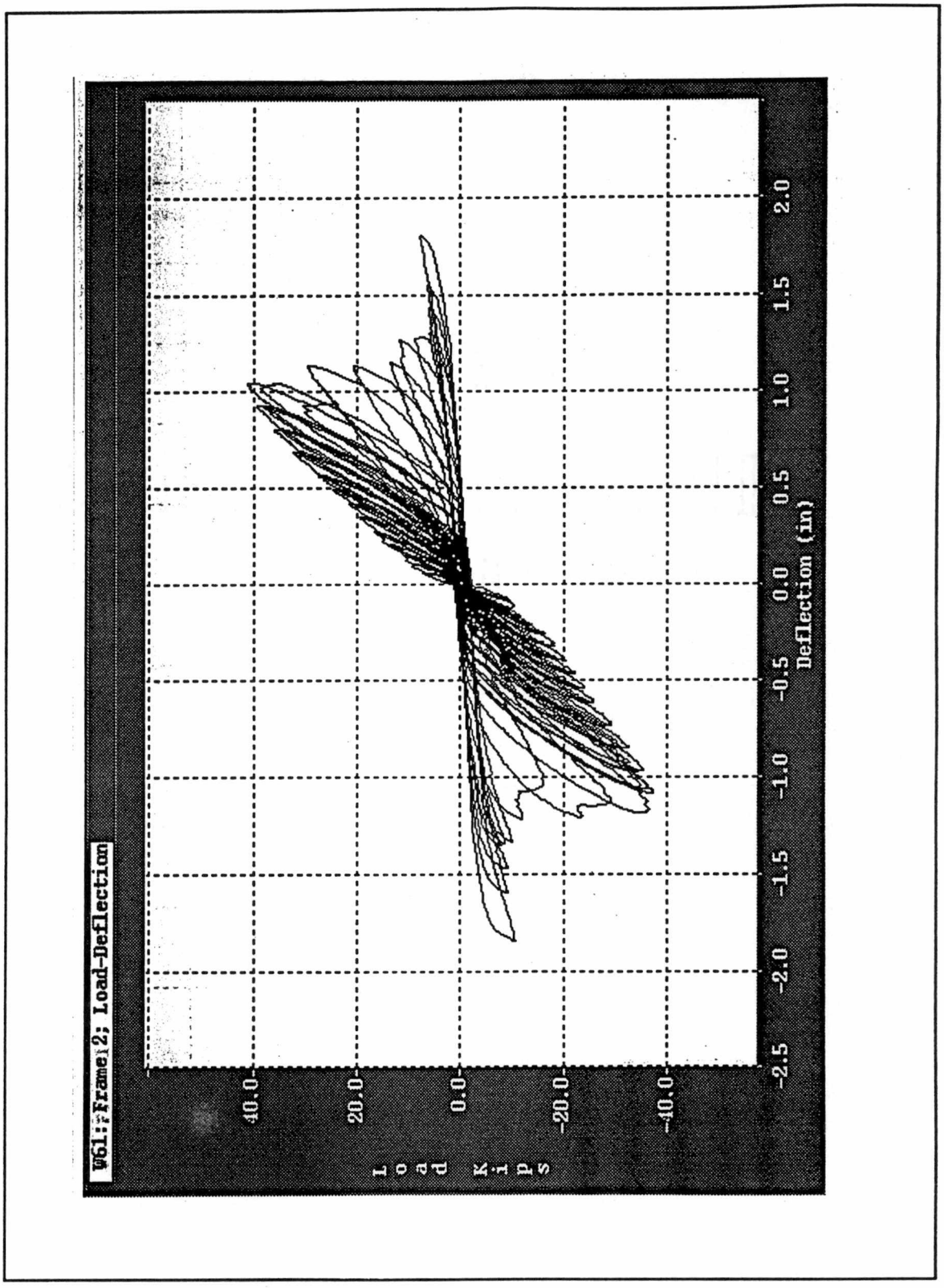


Figure 4.2: Frame 2 hysteresis

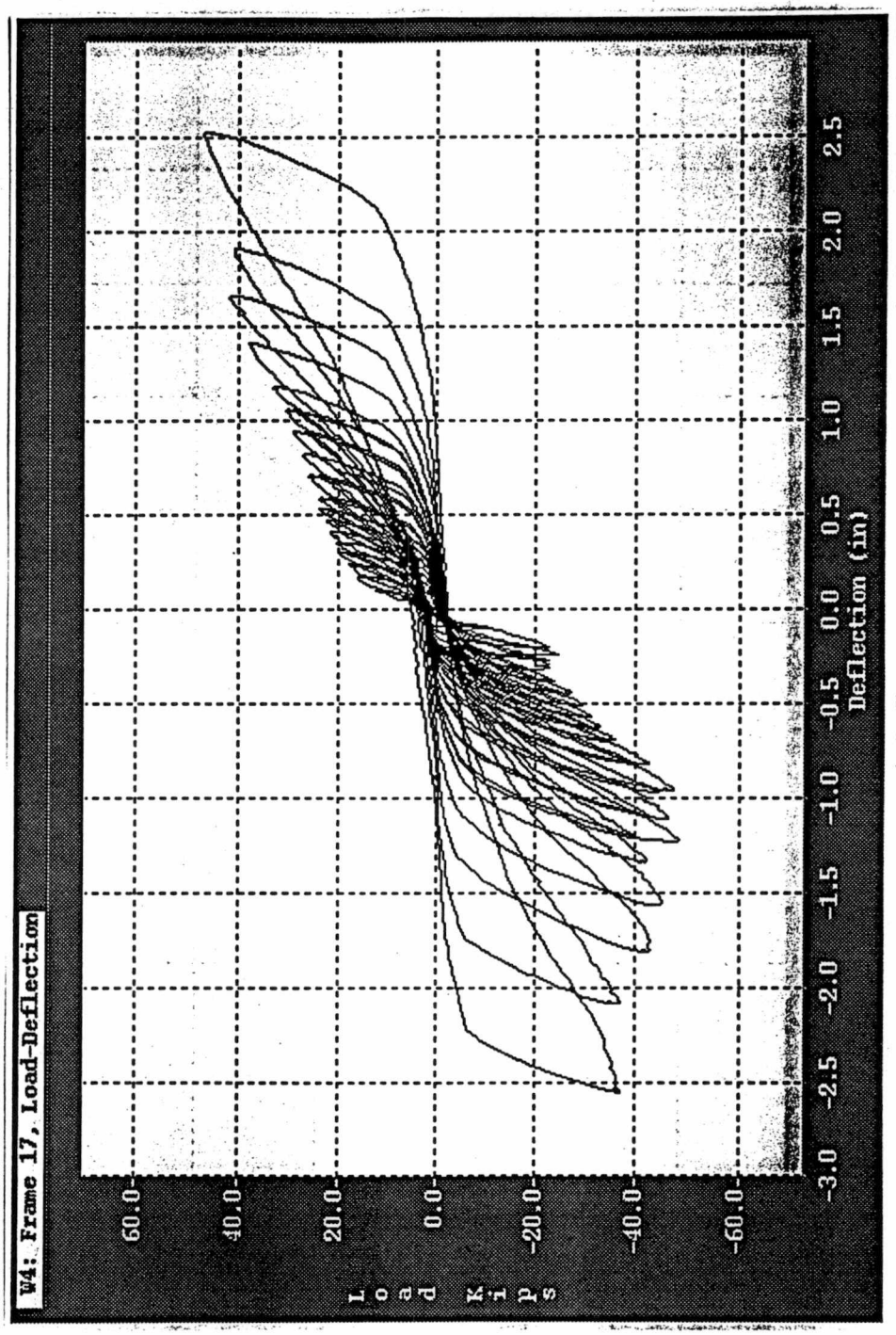


Figure 4.3: Frame 17 hysteresis

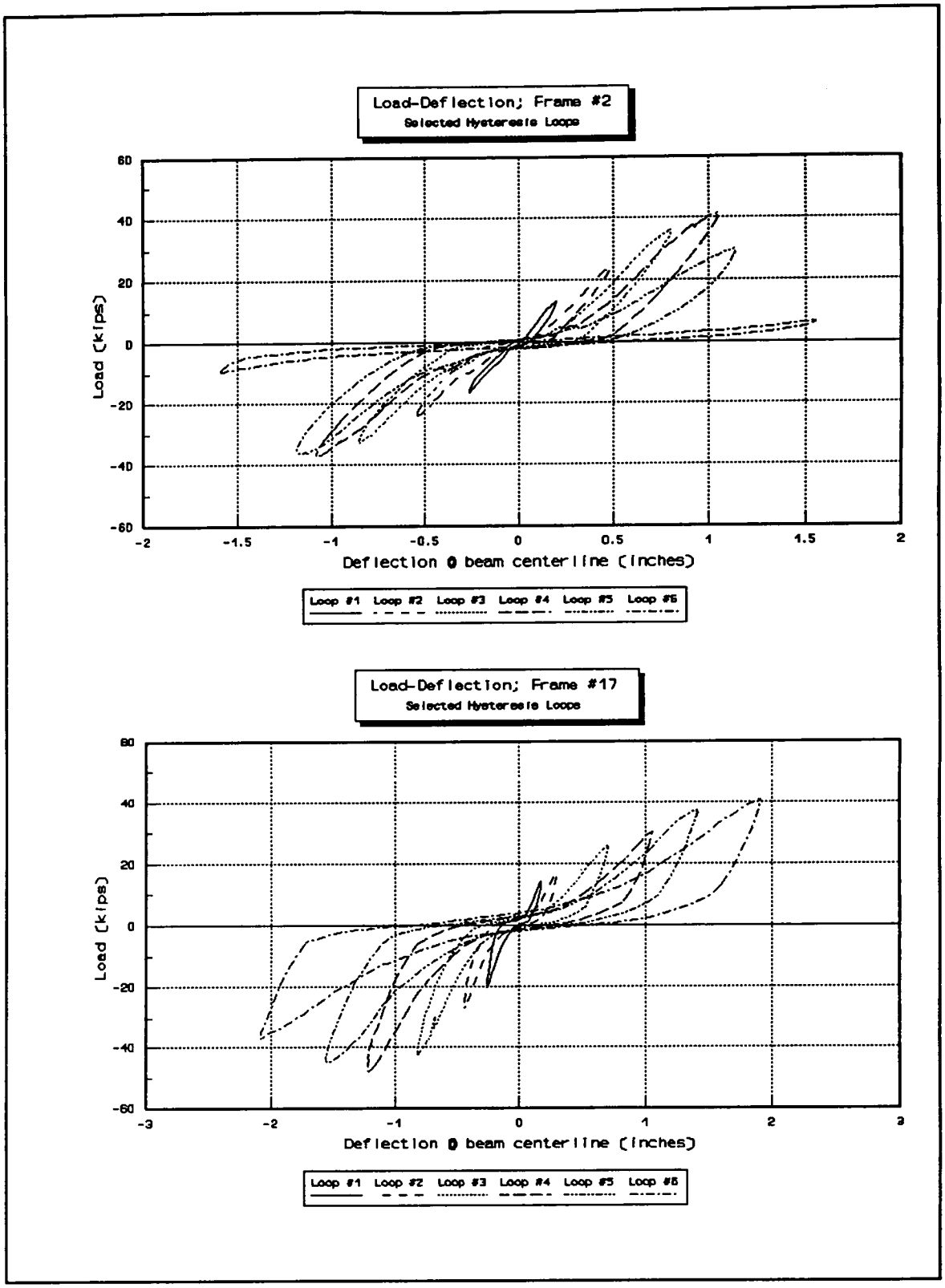


Figure 4.4: Selected deflection cycles

a particular deflection increment and using these as points for the singular curve plot or envelope. The points for these curves are not limited to the maximum compression points of the six selected cycles, but rather include points of maximum compression from the entire hysteresis. The sign convention of all straight line plots has been negated in order to give a positive load and deflection when the system is under compression.

4.2 Envelope behavior

The load-deflection envelopes generate valuable information about the behavior of the infilled frames. However, they cannot be viewed as monotonic load to failure plots. Due to the cyclic nature of the loading, quantifying characteristics from these plots could be erroneous; therefore, only general behavioral properties are related to these plots.

4.2.1 Stiffness and softening of the system

Figure 4.5 depicts the singular load-deflection curves of both frames 2 and 17. Both systems exhibit a definite softening after the first deflection increment. The initial stiffness of the systems up to this point is somewhat in question when taken from the load-deflection envelope. Figure 4.6 illustrates the first loop or deflection cycle for frame 2. The slopes represented by lines one and two are the initial tangent stiffness and secant stiffness at

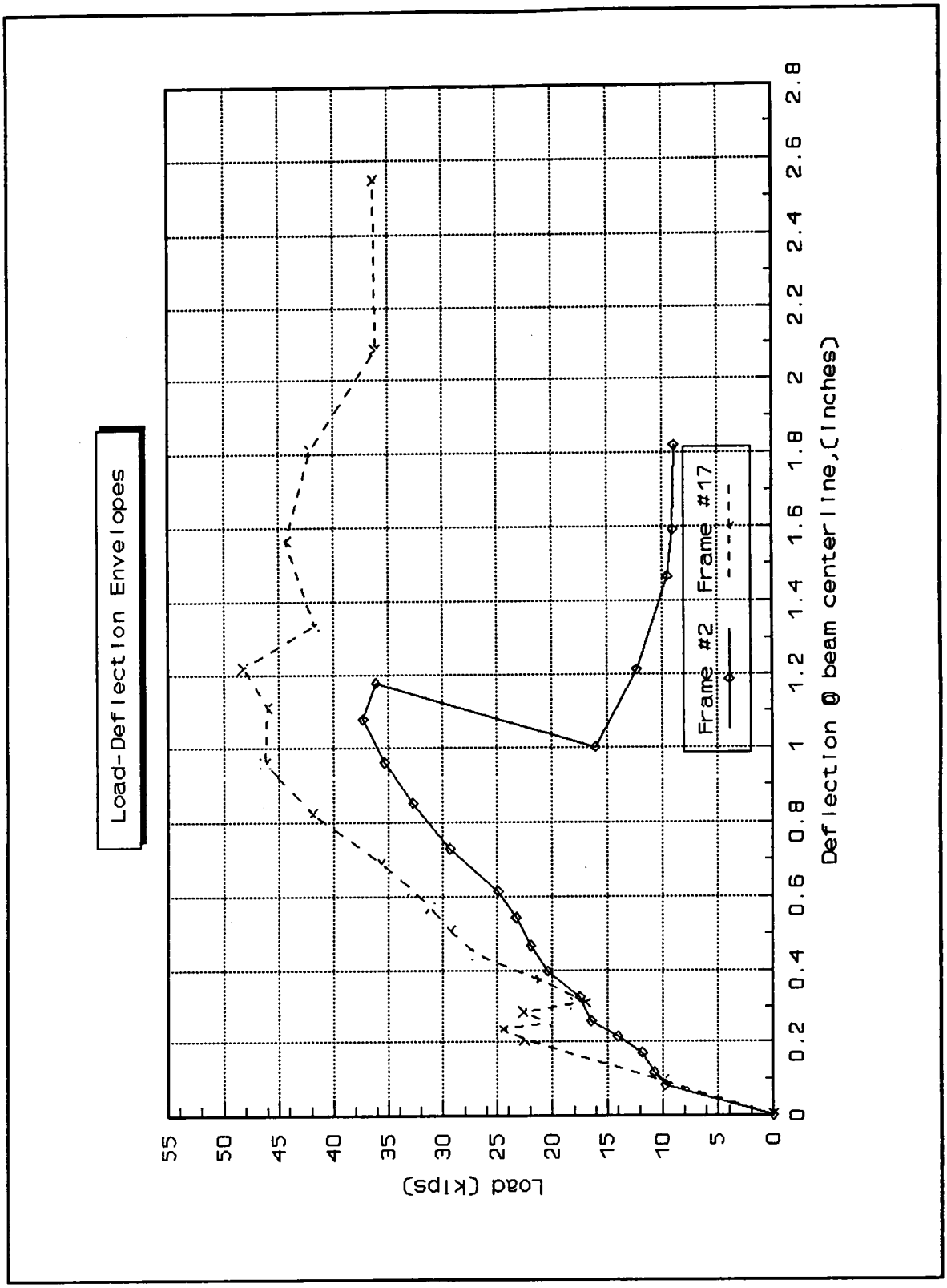


Figure 4.5: Load-deflection envelope

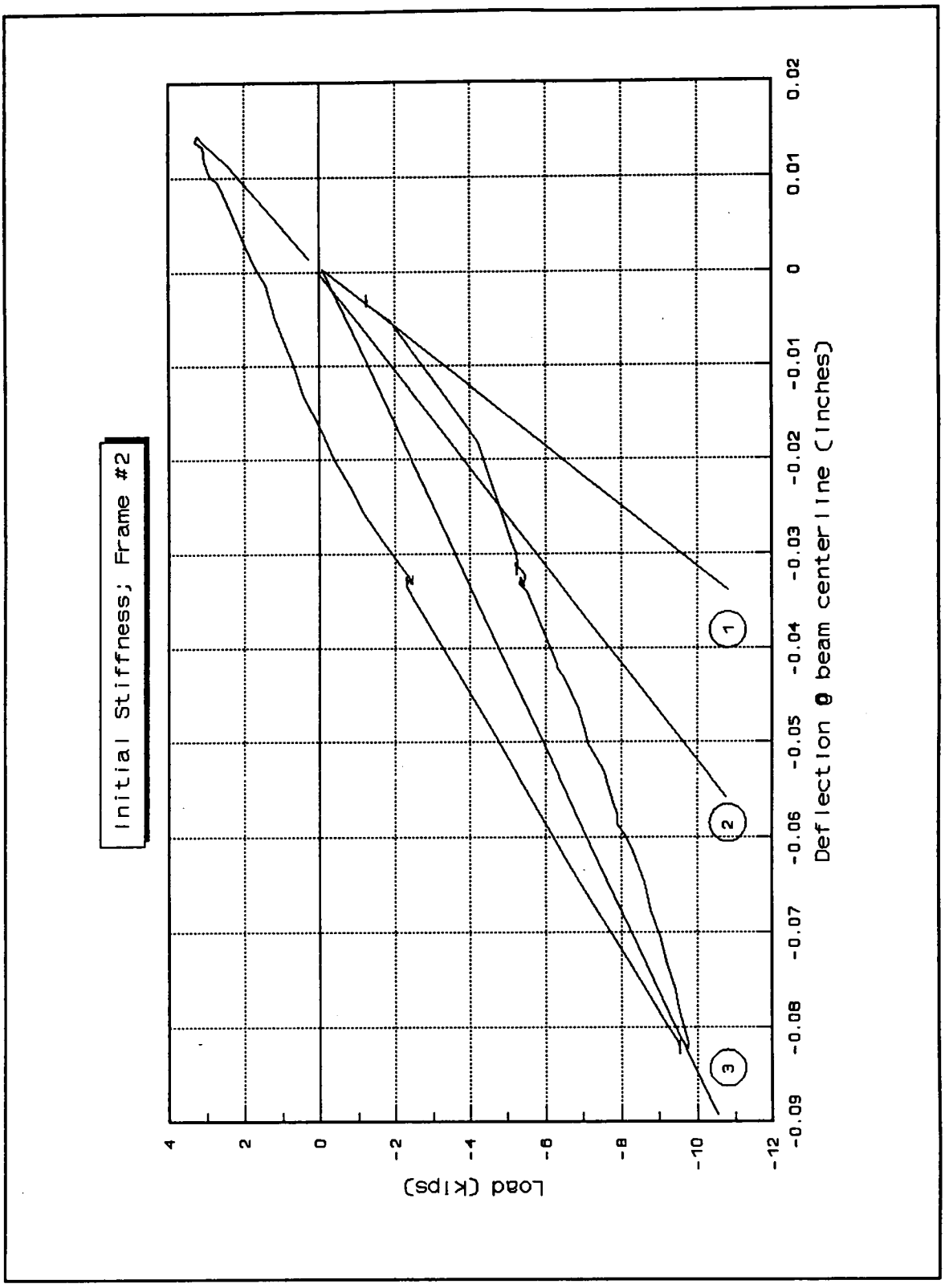


Figure 4.6: Initial stiffness

approximately 50% of the maximum load for the first deflection cycle. Frame 2 had an initial tangent stiffness of 320 kips/inch and a secant stiffness of 193 kips/inch. This indicates that there is considerable softening of the system throughout the first 0.025 inches of deflection, which is the deflection that corresponds to one-half of the maximum compressive load. Jamal's suggested initial stiffness, (Jamal, 1993), yields an initial stiffness of 351 kips/inch. This predicted stiffness is within 10% of the actual initial tangent stiffness. The stiffness represented by the slope of line three is 116 kips/inch. This is the initial stiffness that would be obtained from the envelope load deflection plot.

Due to technical difficulties, the first two deflection cycles of frame 17 were not recorded with the data collection system. The first deflection increment was repeated; however, an accurate initial stiffness cannot be obtained for frame 17. The repeat cycle of the first deflection increment, which is the third cycle, is analyzed for stiffness. For comparison purposes, the stiffness for the third cycle of frame 2 is also given. Figure 4.7 illustrates the third deflection cycles for both frames.

The third cycle of frame 2 produced a stiffness of 125 kips/inch. As indicated by the slope line in figure 4.7, the stiffness is taken as the slope of the compressive loading portion of the loop. This stiffness may be compared to the secant stiffness of the initial deflection increment. The

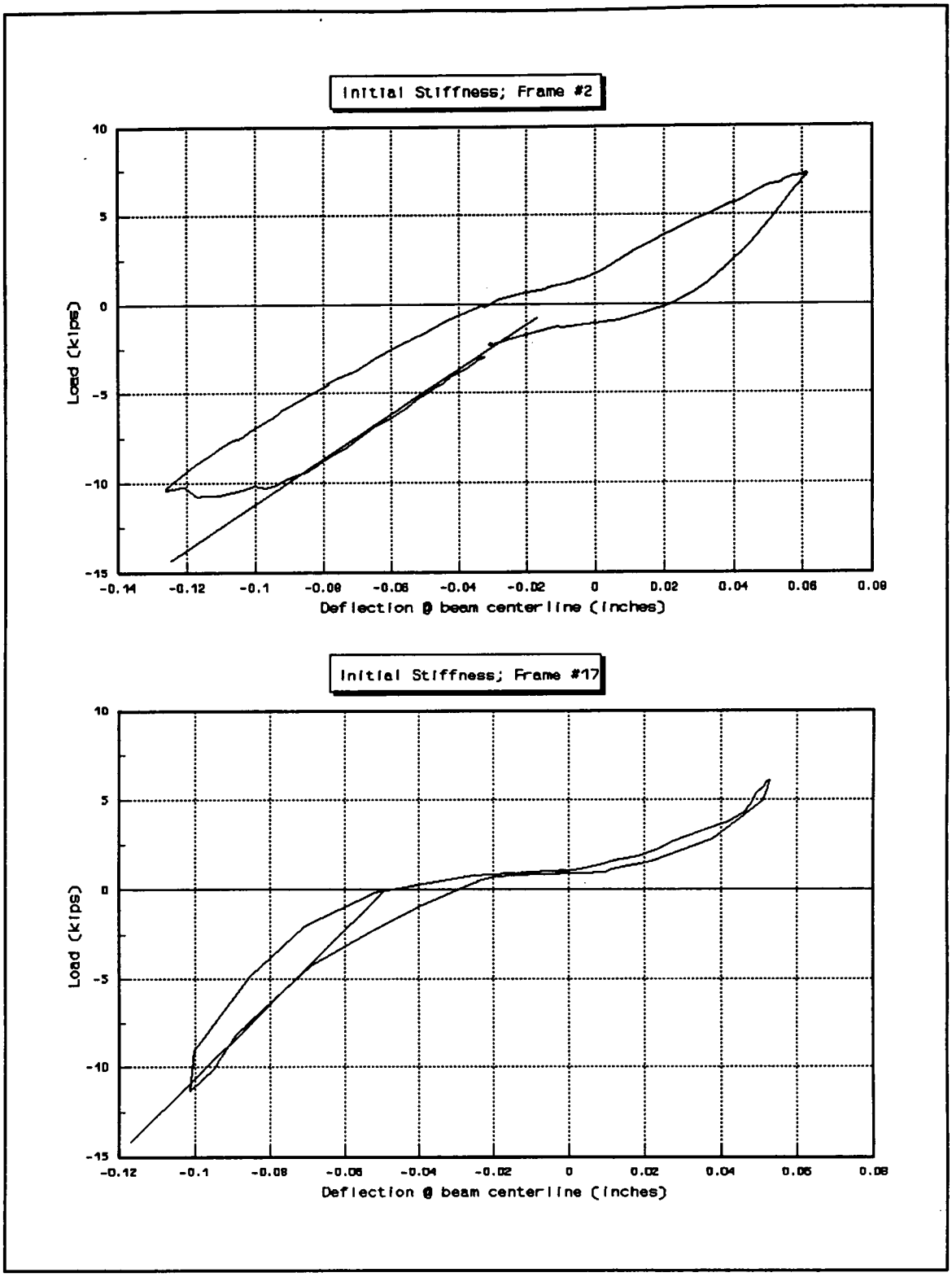


Figure 4.7: Third cycle stiffness

initial secant stiffness, as previously mentioned, is 193 kips/inch. This indicates further stiffness degradation. The third cycle of frame 17 produces a stiffness of 214 kips/inch. This is significantly stiffer than frame 2 during the same cycle and deflection increment. This is attributed to the larger aspect ratio of frame 17.

The load-deflection envelope for both frames, illustrated in figure 4.5, indicates a softening point for both frames. Frame 17 exhibits significant softening at 24.5 kips and a deflection of 0.23 inches, corresponding to approximately 50% of the ultimate compressive load for the system and about 18% of the ultimate deflection. Diagonal cracking became visible two deflection cycles after the softening point. As noted by Stafford-Smith and Carter (1969), this is the result of a tension failure of the infill along the compressive diagonal. The load was less for the next few cycles before increasing again.

Frame 2 exhibits a continuous increase in load until ultimate. Frame 2 softens significantly at a load of 10 kips and a deflection of 0.08 inches. This corresponds to approximately 26% of the ultimate load and 7% of the ultimate deflection. Both of these are considerably smaller percentages than for frame 17. This point in frame 2 coincided with visible cracks forming at the beam-infill interface. Panel cracking did not occur until the compressive load had reached 40% of the ultimate load.

Frame 17 had not formed cracks at the interface by the same time in it's loading history that frame 2 began to lose the interface bond. This may be attributed to the larger aspect ratio, which gives the system a larger bonding surface area. This indicates that the loss of the beam-infill interface is the onset of softening of the system.

4.2.2 Ultimate load and post-ultimate behavior

The ultimate compressive loads for frames 2 and 17 were 37.4 kips and 48.2 kips respectively. Frame 2 reached it's ultimate load at a deflection of 1.08 inches, while frame 17 attained an ultimate load at a deflection of 1.22 inches. The ultimate deflection of frame 17 was 12% higher than that of frame 2, while the ultimate load was 23% higher. A detailed study of the behavior of the system leading up to the ultimate loads is presented in section 4.3.

A comparison of actual to predicted ultimate loads is made using equation 2.1 for predicted ultimate load (Holmes, 1961). For convenience, this equation is shown again below.

$$H = \frac{24EI\varepsilon d}{H^3\left(1+\frac{I}{I_o}\cot\theta\right)\cos\theta} + Af_c\cos\theta \qquad \text{EQ. 2.1}$$

The second term of the equation uses the area of the equivalent compressive strut. Holmes (1961) suggested that

this be equal to td/3. This formula over-estimates the area of the diagonal compressive strut. A closer approximation for the area of the compressive strut is the length of contact, α, multiplied by the thickness of the infill. Stafford-Smith and Carter (1969) suggested that the length of contact is given by $\pi/2\lambda$, where λ is the relative stiffness parameter developed by Stafford-Smith and Carter (1969). The value for the panel compressive strength, f_c, in EQ. 2.1 was obtained from prism testing conducted by Boyd (1993). This formula, along with Jamal's area reduction coefficients (Jamal, 1993), was used in the computation of the equivalent strut area. These reduction coefficients were 0.71 for a pinned frame and 0.66 for 50% secant stiffness.

Employing the use of these formulae, frame 2 yielded a predicted ultimate compressive load of 41.43 kips. This is 11% higher than the actual ultimate load of 37.3 kips. Frame 17 produced a predicted ultimate load of 50.97 kips, which is 6% higher than the actual load of 48.2 kips.

Frame 2 experienced an extreme drop in load following the ultimate load. From this point, additional deflection was accompanied by decreasing load. The occurrence of this characteristic was used to terminate the test. Frame 17, however, continued to hold a load comparable to it's ultimate with increased deflection. The deflection reached 2.56 inches while maintaining a load of 36 kips. This is more than twice the ultimate deflection with a drop in load of 25% from the

ultimate load. This seems to imply that the use of a larger aspect ratio increases post-ultimate ductility of the system.

4.2.3 Bare Frame Envelope Behavior

Frames 2 and 17 were both loaded cyclicly after the test was completed and the infill was removed. Figure 4.8 illustrates the load-deflection envelopes for both frames. These envelopes were obtained in same manner as described in section 4.1. The bare frames were not loaded to failure, but were simply loaded with three or four deflection cycles. Upon examination of the strain gage data, the steel members of frame 2 had not yielded anywhere. However, frame 17 experienced some slight yielding in the windward column at the mid-height during the infill testing.

Both bare frames behave identically. In fact, an overplot of the two envelopes reveals that they are almost the same curve. This was probably due to the pinned connections of the frame. With essentially no moment being transferred to the beam, the bare frame was essentially behaving as two cantilevered beams. The stiffness, using $3EI/L^3$, was 3.56 kips/inch. This is compared to the initial envelope stiffness of both frames of 4.04 kips/inch. This indicates that the presence of the infill dramatically increases the stiffness of the system.

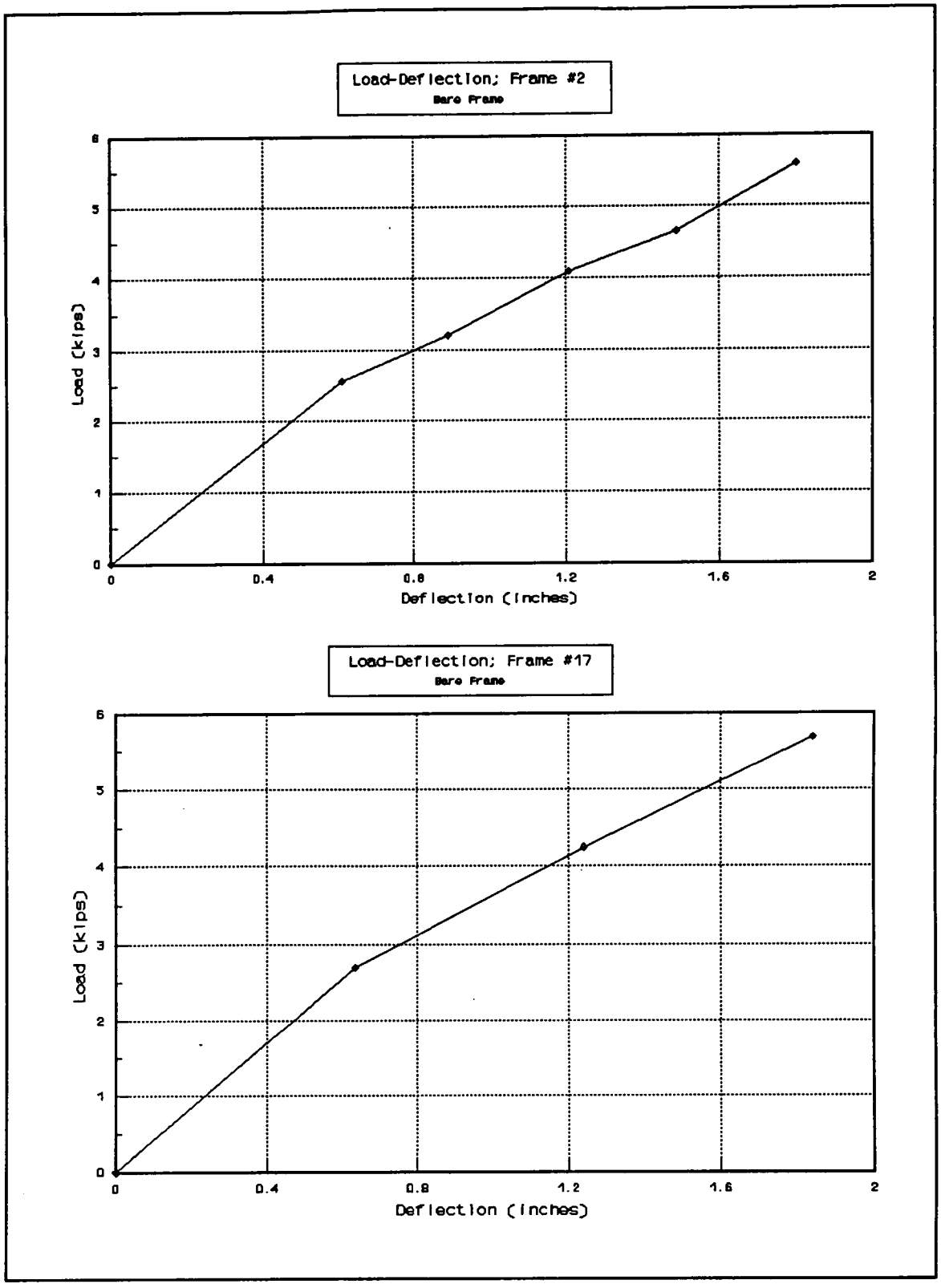


Figure 4.8: Bare frame load-deflection envelopes

4.3 Hysteretic Behavior

Figures 4.2 and 4.3 illustrates the entire hysteresis of frames 2 and 17. As described in section 3.6.2, loading of the frame was cyclic in nature. A schedule of deflection increments was pre-determined. Each frame was cycled in tension and compression to each of these deflections. Each deflection cycle was run three times for frame 2 and twice for frame 17. In each case, the repeated deflection cycles produced a slightly decreased load from that of the first cycle for any particular deflection increment. As previously mentioned, six hysteresis loops for each frame were extracted for study. Each of these loops was chosen due to similar behavior between the two frames for that particular deflection increment cycle.

4.3.1 Frame 2 Hysteresis

Figures 4.9 through 4.14 illustrate each of the six hysteresis loops studied along with the corresponding deflected shape of the frame. The deflected shape of the frame is illustrated at the maximum compressive load for the cycle. Figure 4.9 depicts a deflection cycle of 0.261 inches at the beam centerline. This was where stair step cracking had become noticeable on the front and back of the infill panel; therefore, a tension failure in the infill along the compression diagonal had occurred. Mortar spalling had begun to occur at the beam-infill interface by this point in the

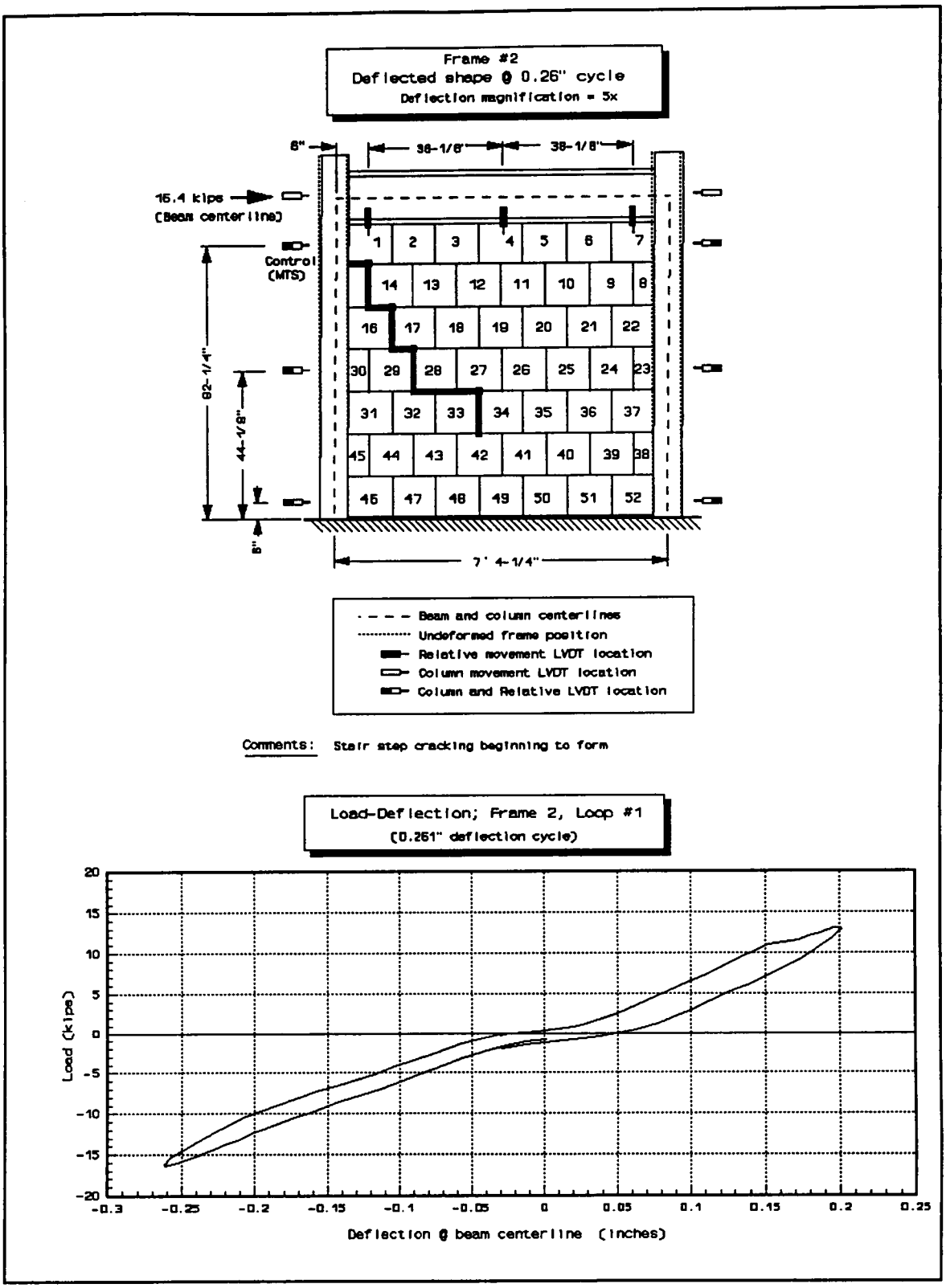


Figure 4.9: Frame #2; Loop #1

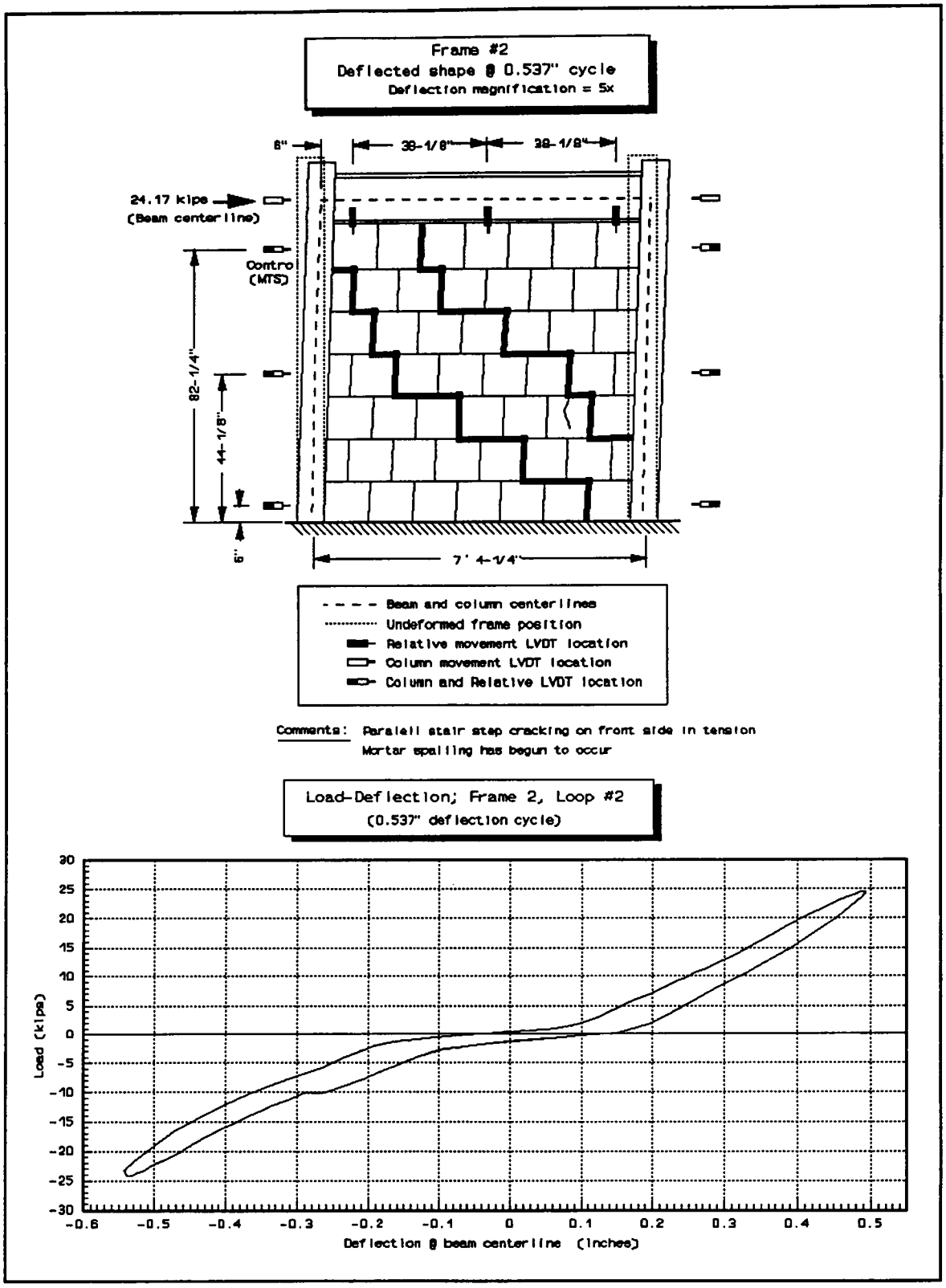


Figure 4.10: Frame #2; Loop #2

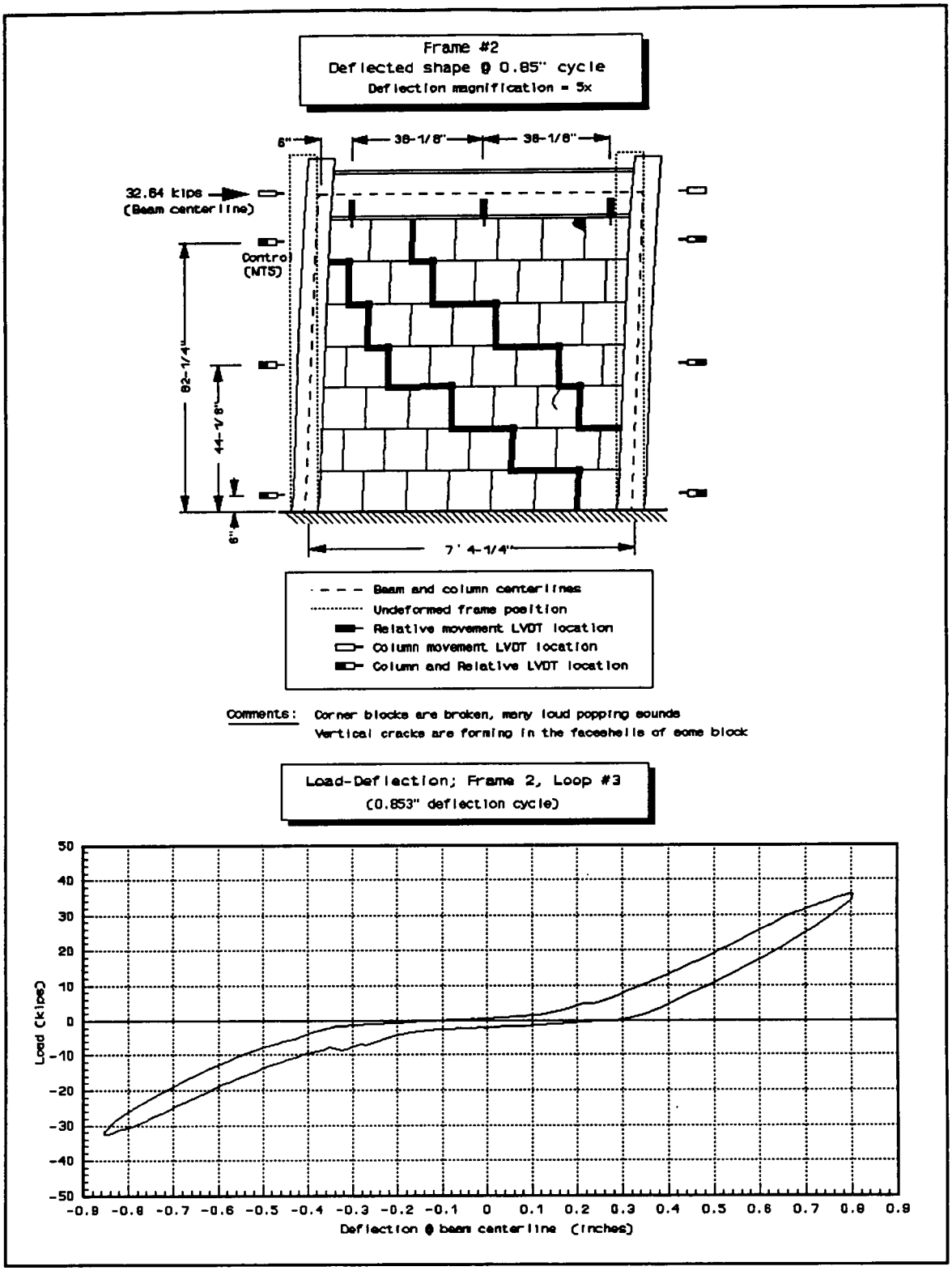


Figure 4.11: Frame #2; Loop #3

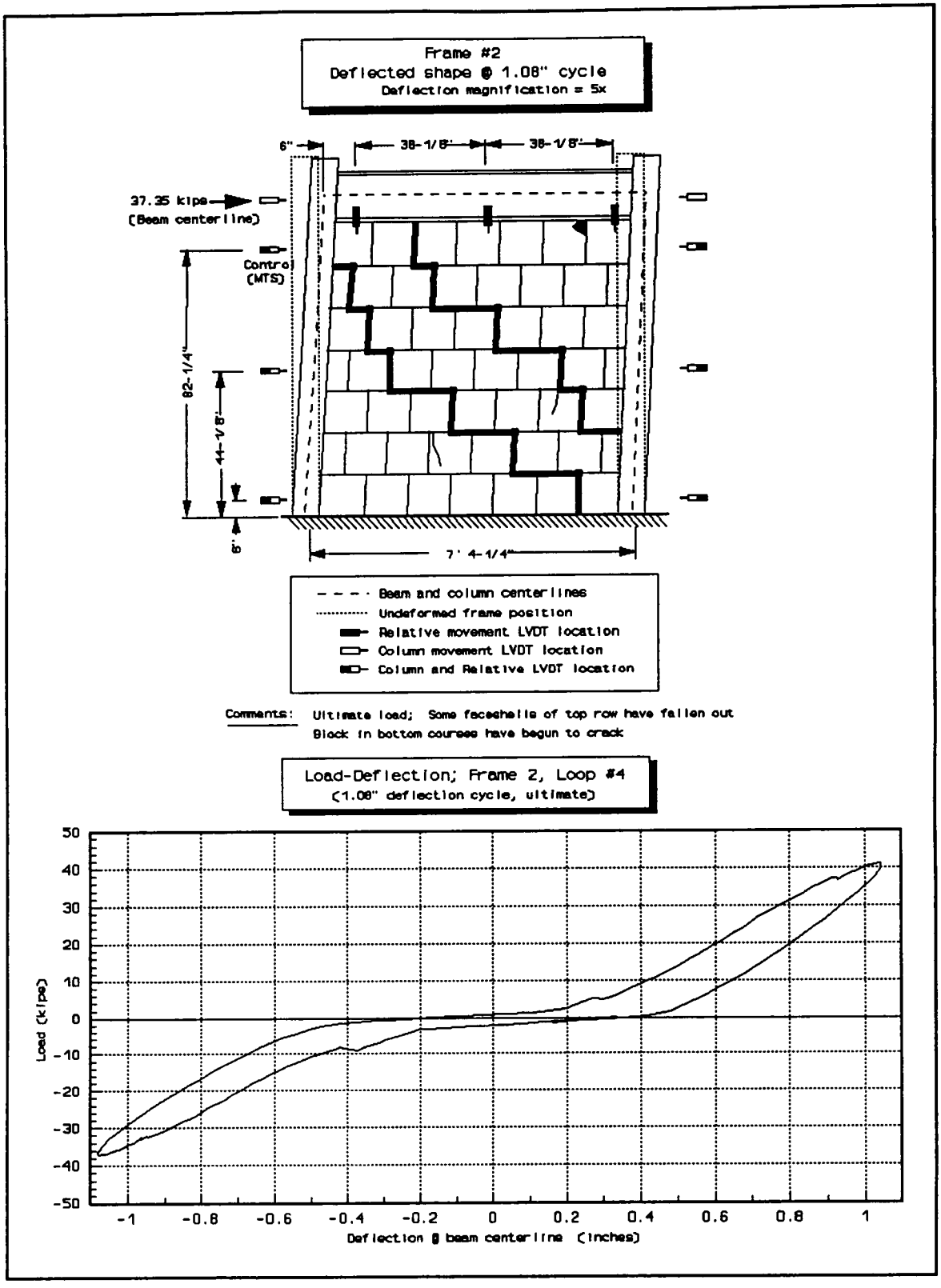


Figure 4.12: Frame #2; Loop #4

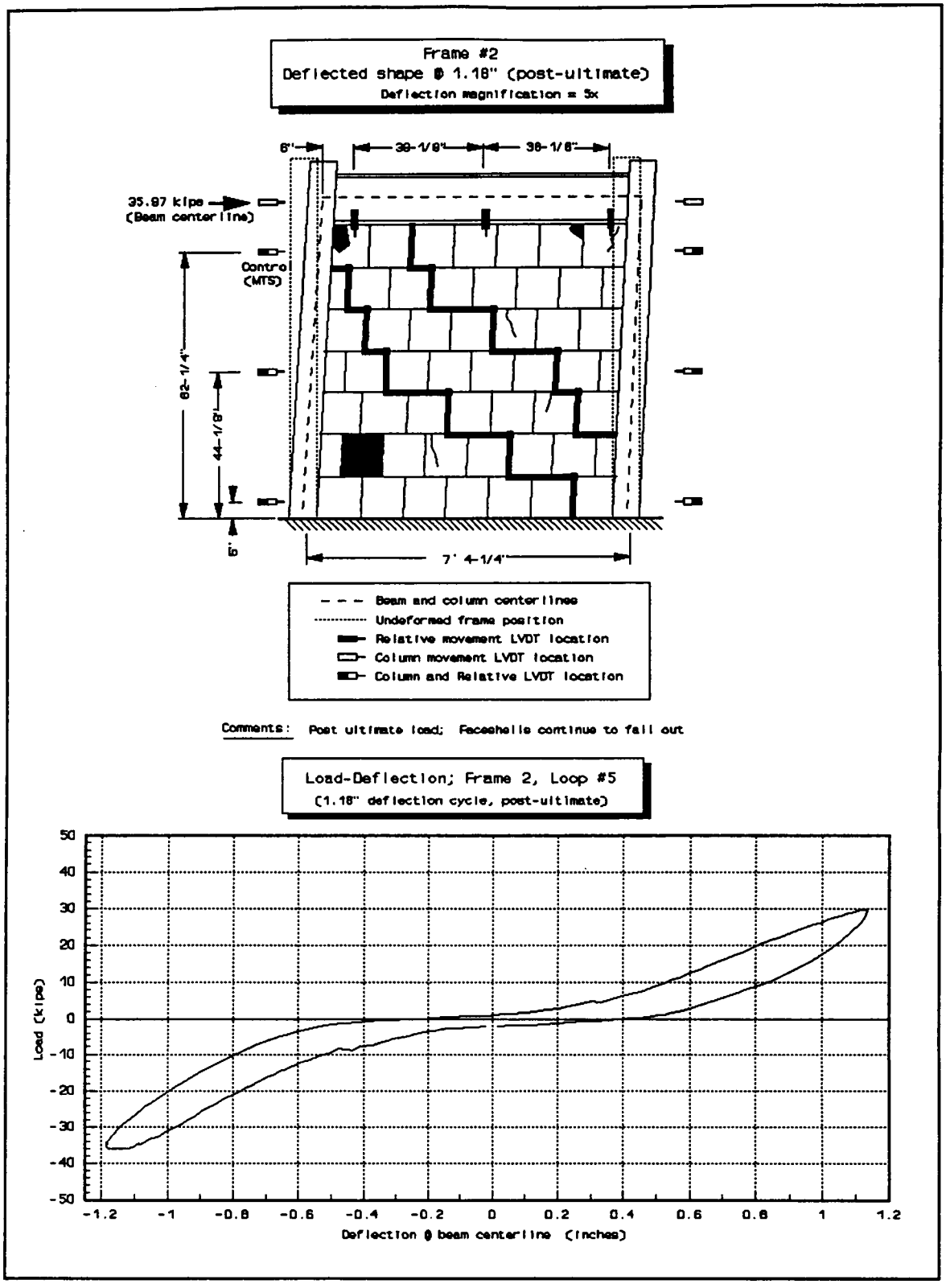


Figure 4.13: Frame #2; Loop #5

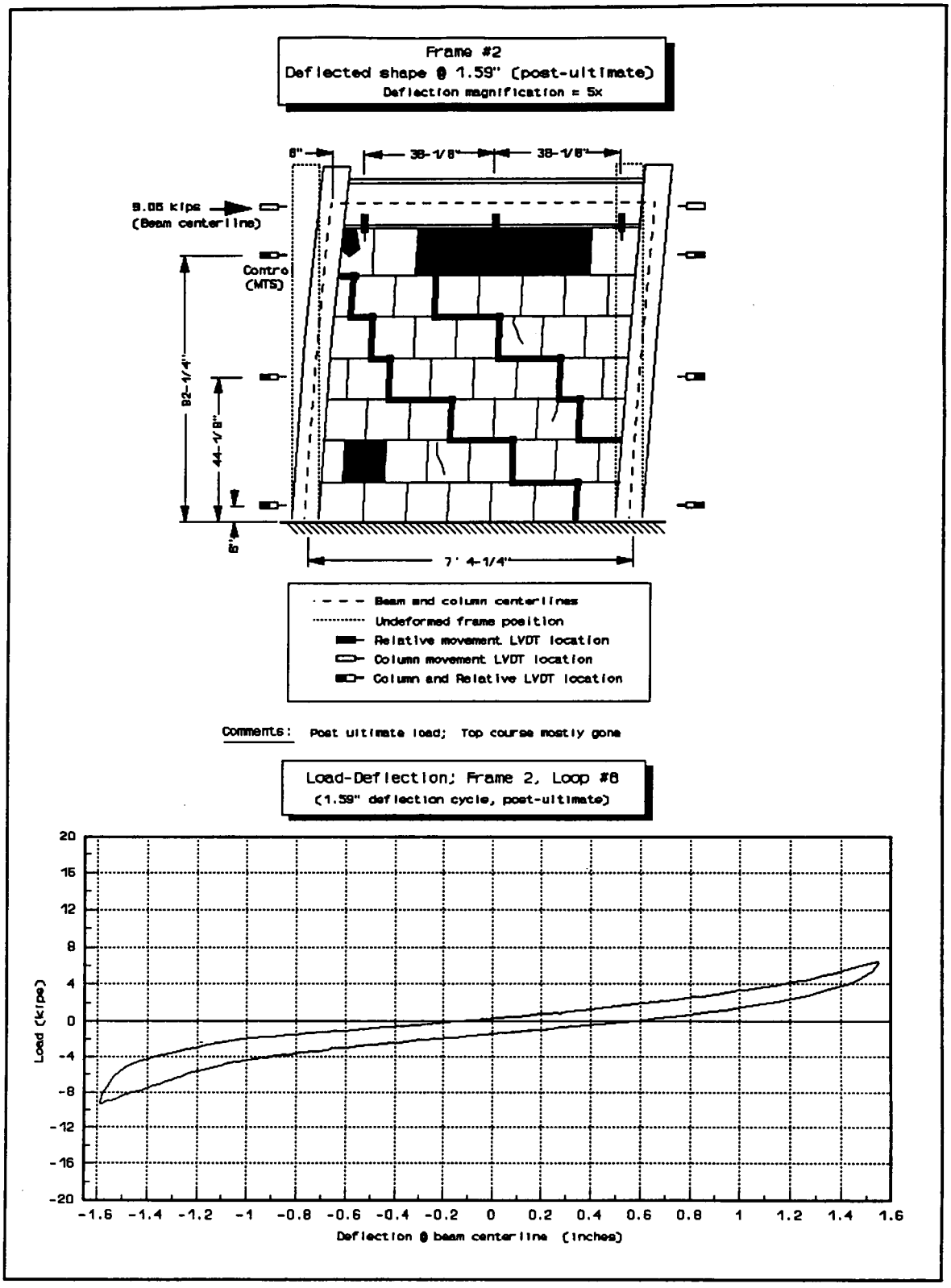


Figure 4.14: Frame #2; Loop #6

loading history. The maximum compressive load for the cycle was 16.4 kips. The stiffness of the system, for this loop and successive loops, is taken as a line parallel to the compressive loading portion of the curve. The stiffness of the frame during this cycle is 63 kips/inch. This was a degradation of 67% from the initial secant stiffness of 193 kips/inch in the first cycle.

Figure 4.10 illustrates a deflection cycle of 0.537 inches. At this point, parallel stair step cracking has formed in the panel from floor to beam. This visually defines the compressive strut in the panel. During several cycles previous to this one, loud popping in the panel had been observed. This is thought to indicate web splitting in the hollow clay tile. The maximum compressive load for this cycle was 24.17 kips. The stiffness of the system for this cycle had further degraded to 48 kips/inch.

Figure 4.11 represents a deflection cycle of 0.853 inches, in which the frame experienced a maximum compressive load of 32.64 kips. At this point, several tile have cracked in the face shells and the face shell of tile six, on the top row, had broken off in the corner. This can be seen in the deflected shape of figure 4.11. The stiffness of the system at this point was 48 kips/inch, indicating no stiffness degradation taking place since the 0.537 inch deflection cycle.

Figure 4.12 depicts the 1.08 inch deflection cycle, the deflection cycle in which the frame experienced the ultimate load of 37.35 kips. There was continued crack formation in the face shells of the panel. The stiffness for the ultimate cycle is also 48 kips/inch. There had been little to no stiffness degradation near and including the ultimate load.

The last two loops studied are post-ultimate deflection cycles. Figure 4.13 illustrates a deflection cycle of 1.18 inches. The frame experienced a maximum compressive load of 35.97 kips. This was a drop in load of approximately 4% from the ultimate load for the frame. There was continued crack formation in the panel tile. The face shell of block 44 had fallen out, as depicted in figure 4.13. There was also increased mortar spalling from the beam-infill interface. The stiffness of the system had fallen to 40 kips/inch.

Figure 4.14 illustrates a deflection cycle of 1.589 inches. This deflection cycle was the next to last cycle for frame 2 with the infill intact. The frame experienced a maximum compressive load of 9.06 kips. As shown in figure 4.14, most of the top course was gone. This was perhaps one of the contributing factors of the stiffness degradation. The stiffness of the system has fallen to 4.4 kips/inch. This was a drop of 91% from the stiffness of the system at ultimate.

4.3.2 Frame 17 Hysteresis

Figures 4.15 through 4.20 illustrate the six loops studied for frame 17. Figure 4.15 depicts a cycle and deflected shape for a deflection of 0.257 inches. The frame experienced a maximum compressive load of 20.40 kips for this cycle. Significant cracking noises had taken place prior to this cycle and diagonal cracking had become visible. There had also been some slight mortar spalling. The stiffness of the frame for this cycle was 114 kips/inch. As mentioned previously, the first two deflection cycles of frame 17 were not recorded and an initial stiffness could not be obtained. This was a drop in stiffness of approximately 47% from the third cycle of frame 17.

Figure 4.16 represents a deflection cycle of 0.44 inches. During this cycle, the frame experienced a maximum compressive load of 26.80 kips. Banded diagonal cracking became visible during this deflection cycle. The stiffness of the system for this cycle was 93 kips/inch.

Figure 4.17 illustrates a deflection cycle of 0.852 inches during which the frame experienced a maximum compressive load of 41.88 kips. Several cycles previous to this, the panel had begun to experience some slight corner crushing. As depicted in figure 4.17, the corner of the face shell of block ten in the top row fell off in the compression half of the cycle. Vertical cracking in tile along the compression diagonal had

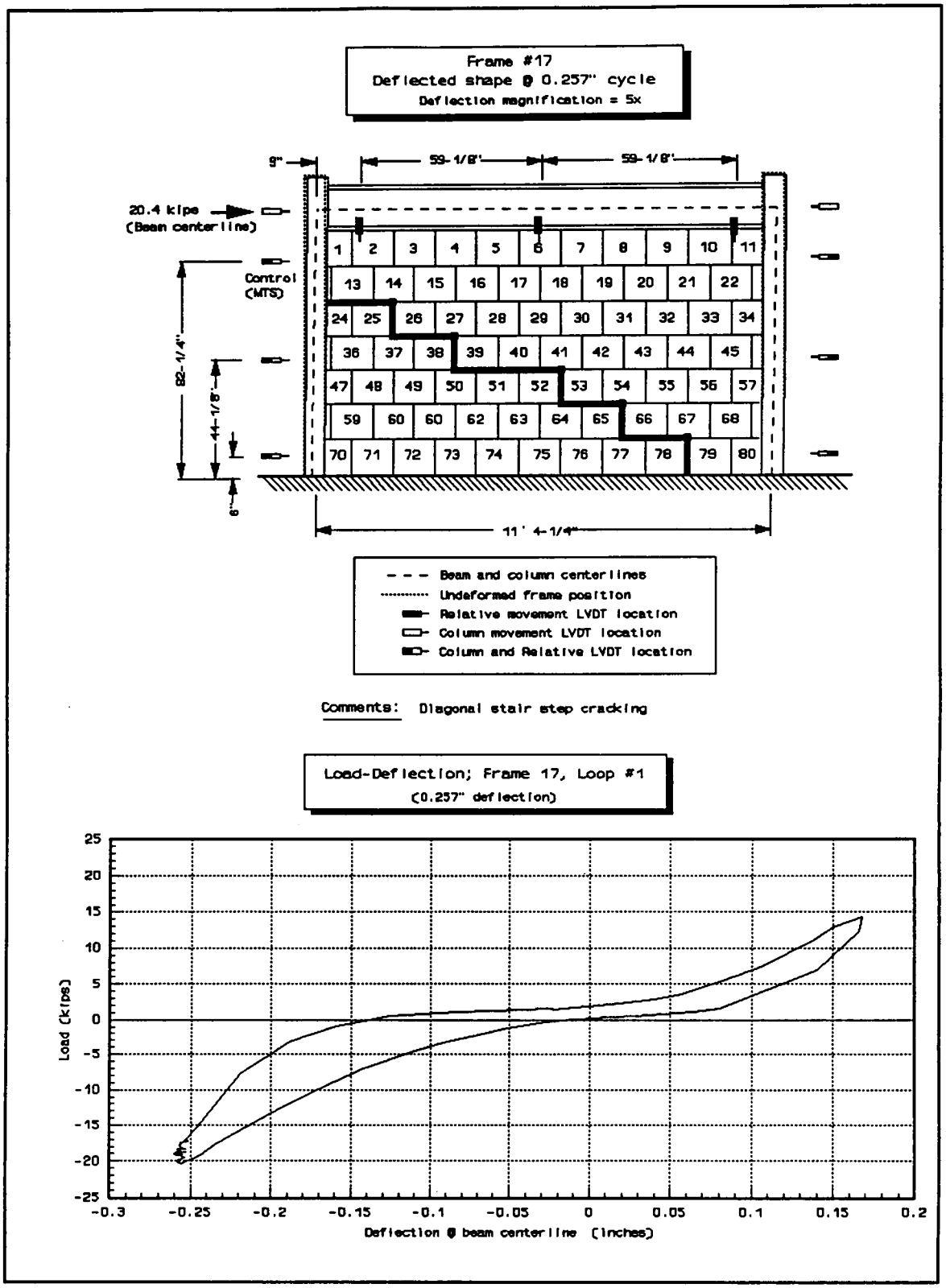


Figure 4.15: Frame #17; Loop #1

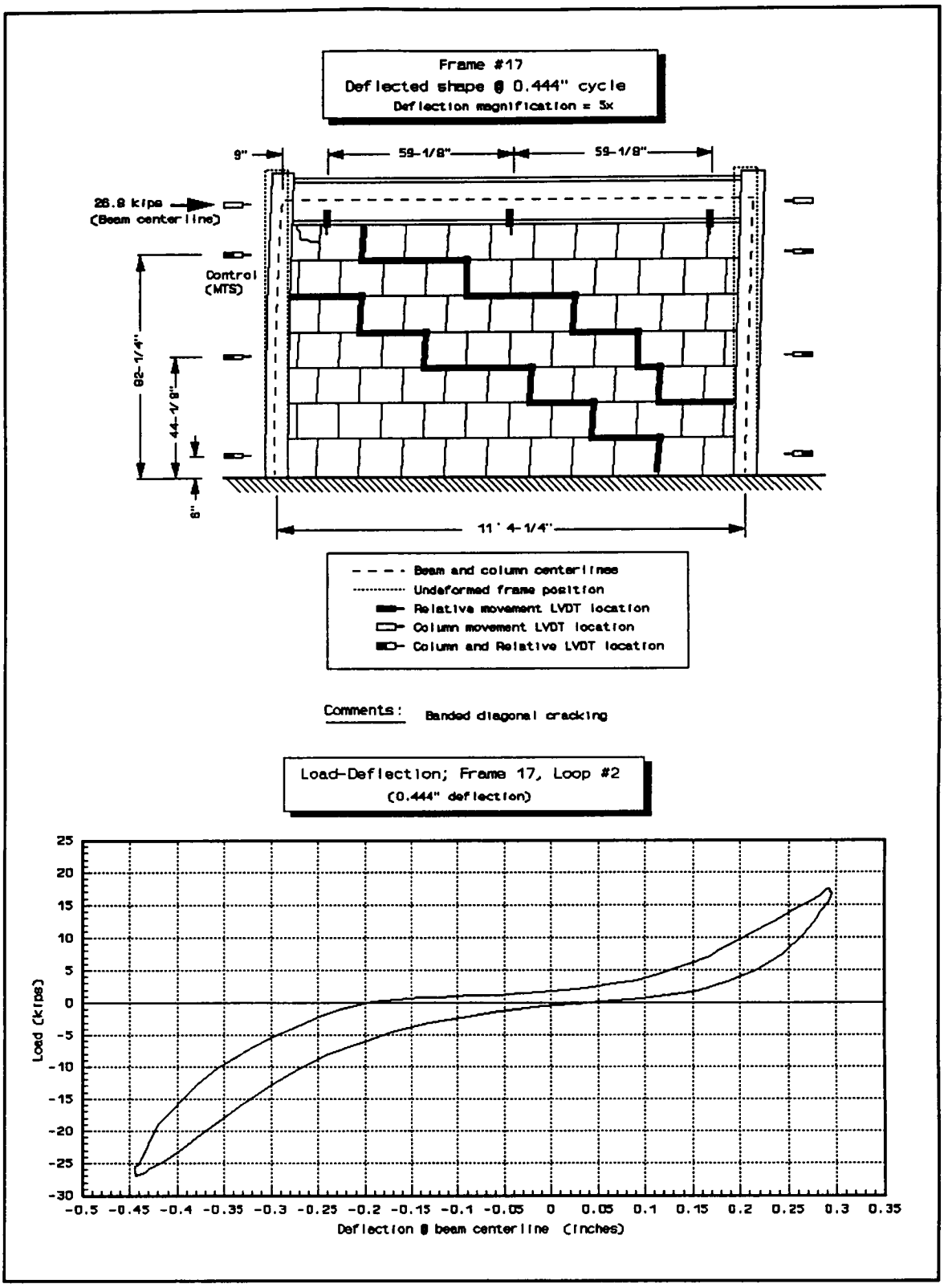


Figure 4.16: Frame #17; Loop #2

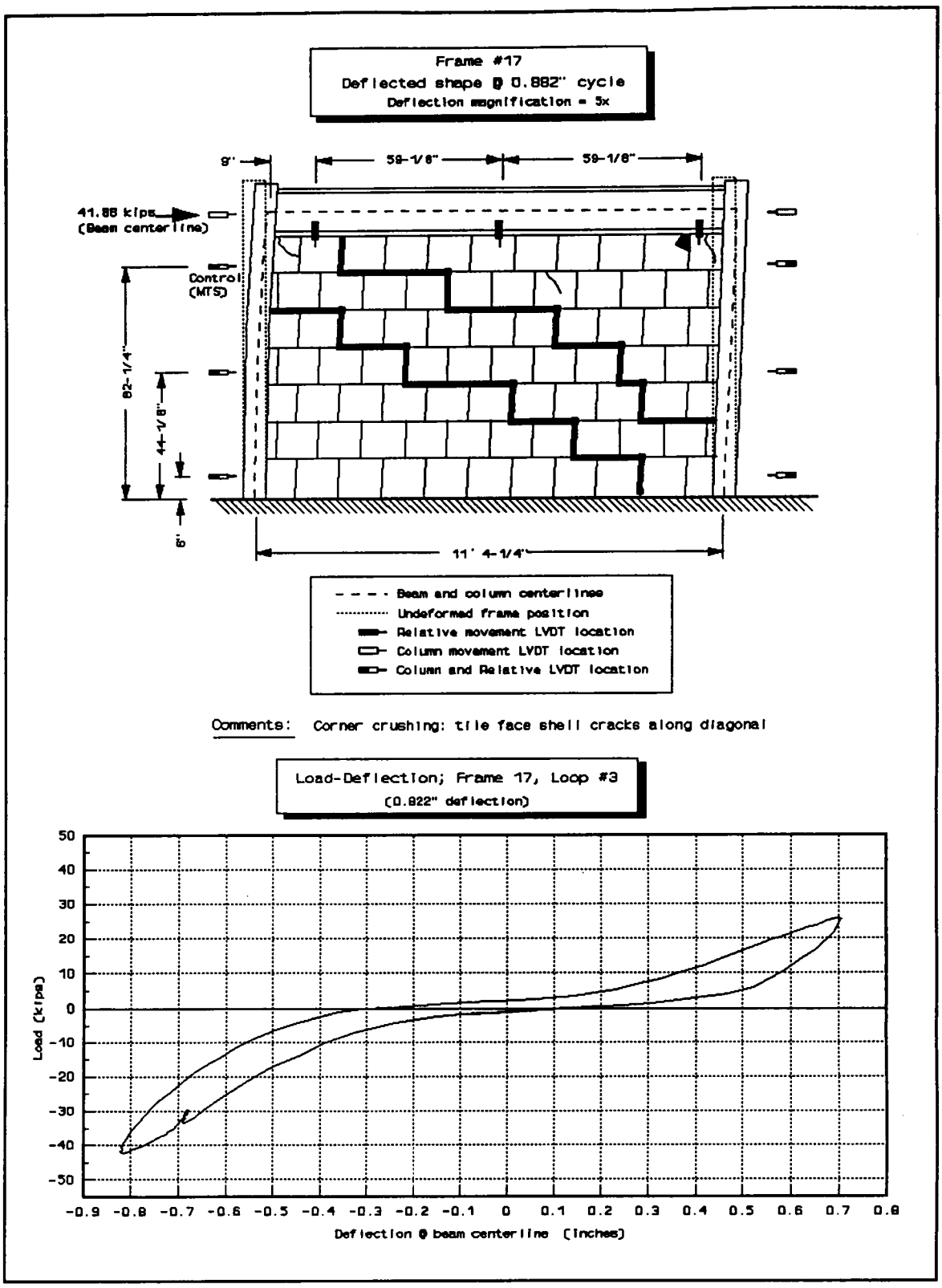


Figure 4.17: Frame #17; Loop #3

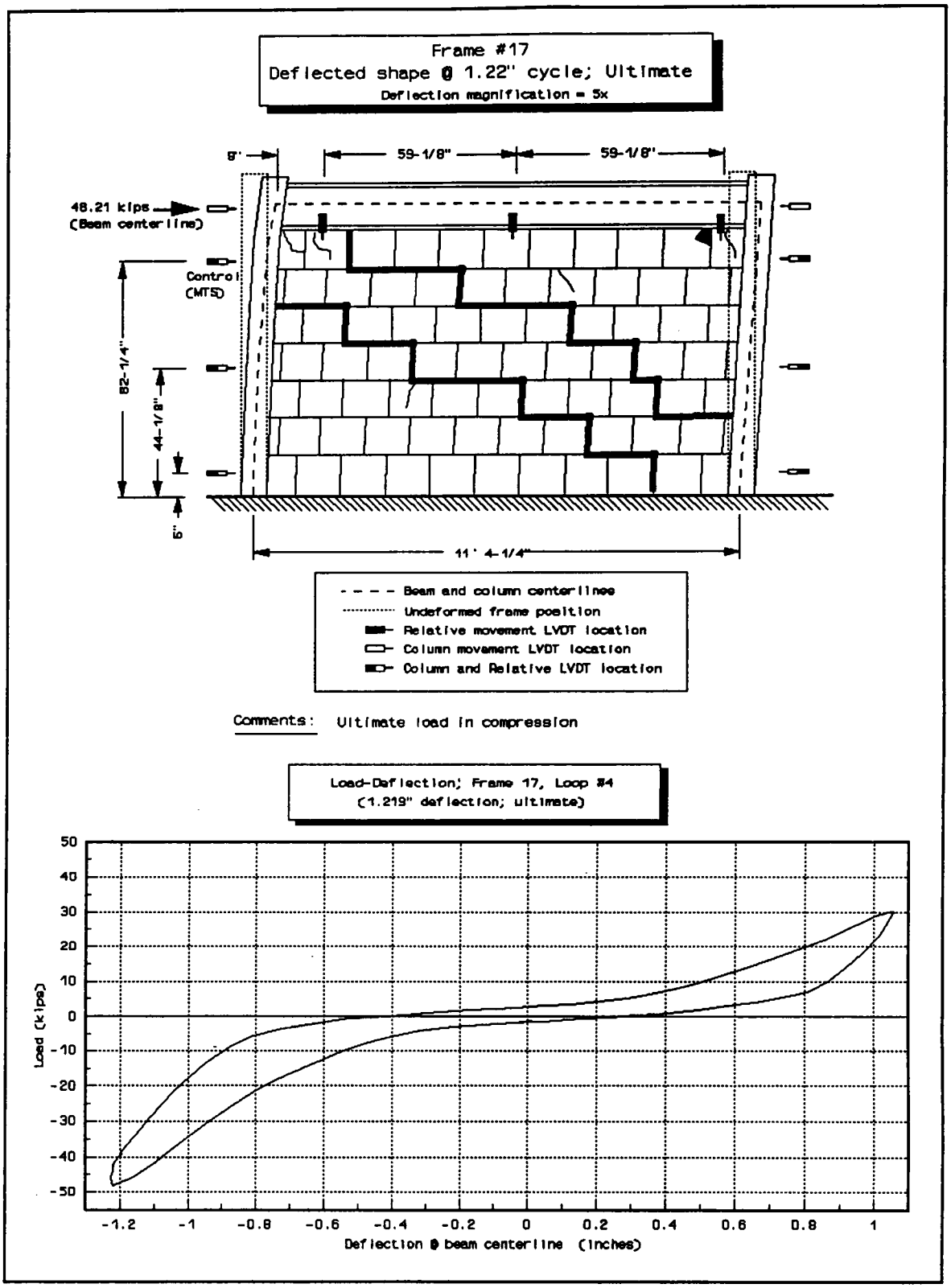


Figure 4.18: Frame #17; Loop #4

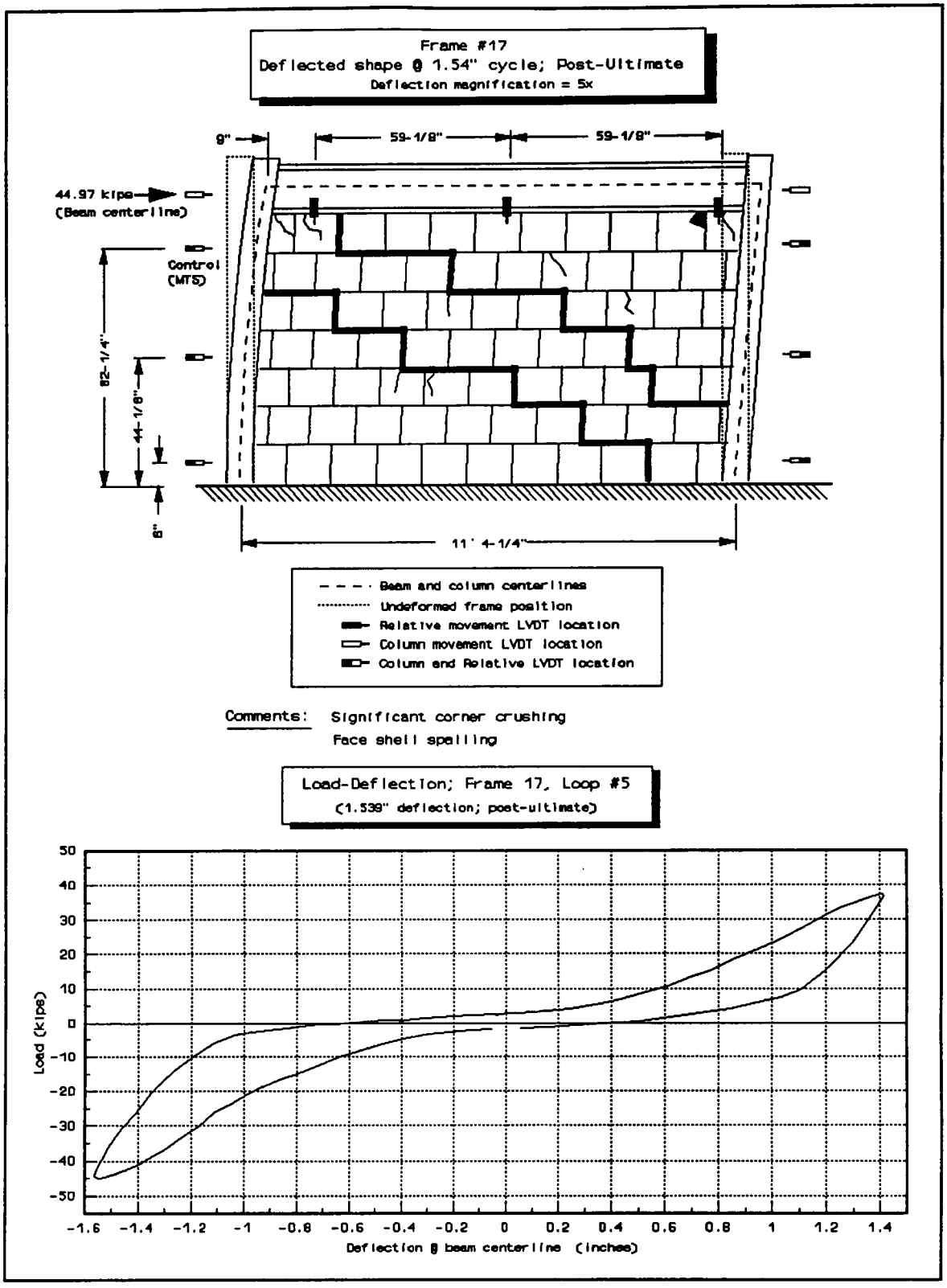


Figure 4.19: Frame #17; Loop #5

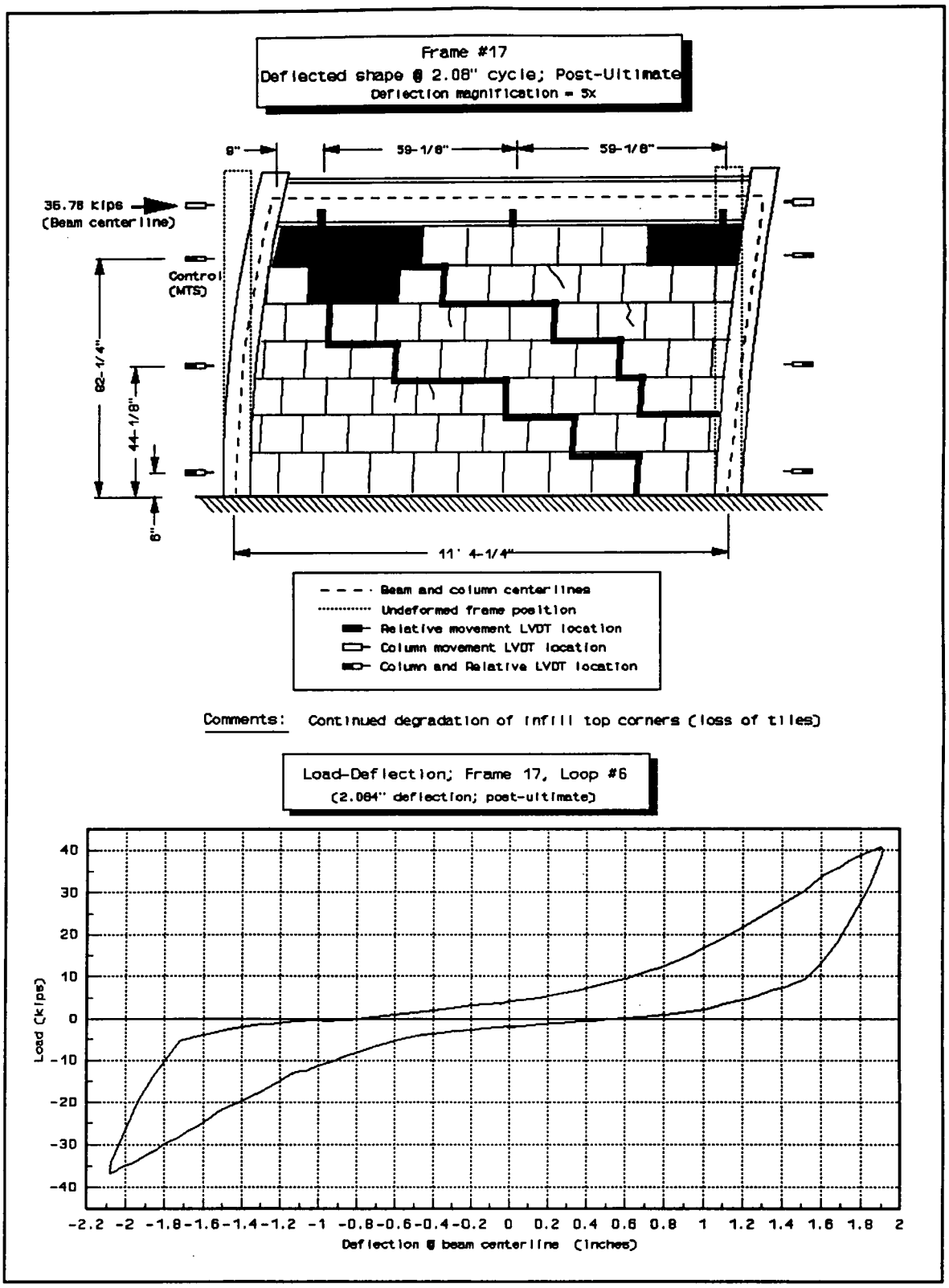


Figure 4.20: Frame #17; Loop #6

also been observed by this point. The stiffness of the system had degraded to 78 kips/inch.

A deflection cycle of 1.22 inches is illustrated in figure 4.18. This was the cycle in which the frame attained its ultimate load of 48.2 kips. Significant cracking had occurred in the tile. The stiffness of the system was 72 kips/inch during the ultimate load cycle. Deflection increments from this point were cycled only one time for the frame.

Figure 4.19 represents a post-ultimate deflection cycle of 1.54 inches. The maximum compressive load for this cycle was 44.97 kips. This was a drop in load of 7% from ultimate with an increase in deflection of 26% beyond the ultimate load deflection. Significant corner crushing and face shell spalling had occurred prior to and during this cycle. The stiffness of the system for this cycle was 45 kips/inch. This was a decrease of roughly 37% from the stiffness of the system at ultimate.

Figure 4.20 depicts a deflection cycle of 2.08 inches. The maximum compressive load for this cycle was 36.78 kips. There was continued degradation of the infill, especially at the top corners. Several whole tile had fallen out, as can be seen in figure 4.20. The stiffness of the system was 25 kips/inch.

4.4 System Energy Absorption

The energy absorbed by the system during any particular deflection increment is taken as the area inside the

hysteretic loop for that cycle. Figure 4.21 illustrates a plot of energy absorption by the system for each hysteresis loop versus the deflection of the frame. Frame 2 continues to absorb increasing energy up to a point slightly past ultimate. This roughly corresponded to the time when the top course of the panel began to disintegrate. The maximum energy absorbed by frame 2 for a particular loop was approximately 17.3 kip-inches. From this point, the energy absorption begins a steady decline with increasing deflection.

Frame 17 however, continues a steady increase in energy absorption far past the ultimate deflection. This was probably due to the fact that more of the infill was left intact past the ultimate load for frame 17 compared to frame 2. The maximum energy absorption that was recorded for frame 17 was 48 kip-inches. This is almost three times the maximum energy absorbed by frame 2. From the shape of the energy-deflection curve, frame 17 probably would have continued to absorb an increasing amount of energy with increasing deflection.

4.5 Bare Frame Hysteresis

Figure 4.22 illustrates the bare frame load-deflection hysteresis for frames 2 and 17. Both bare frames behaved in a similar manner. Both frames were subjected to a maximum deflection of approximately 1.77 inches and experienced a maximum load 5.5 kips for frame 2 and 5.75 kips for frame 17.

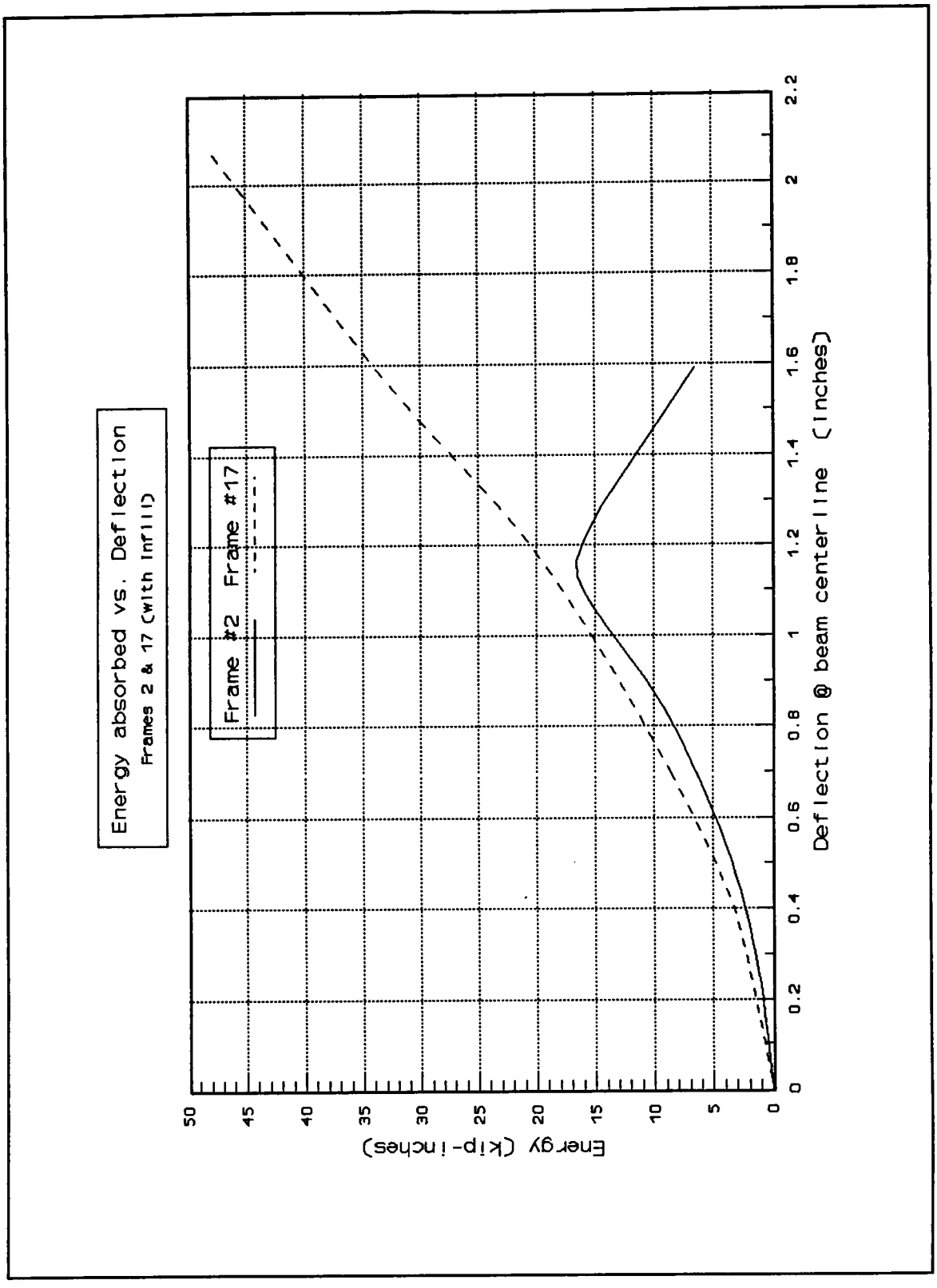


Figure 4.21: Energy absorption

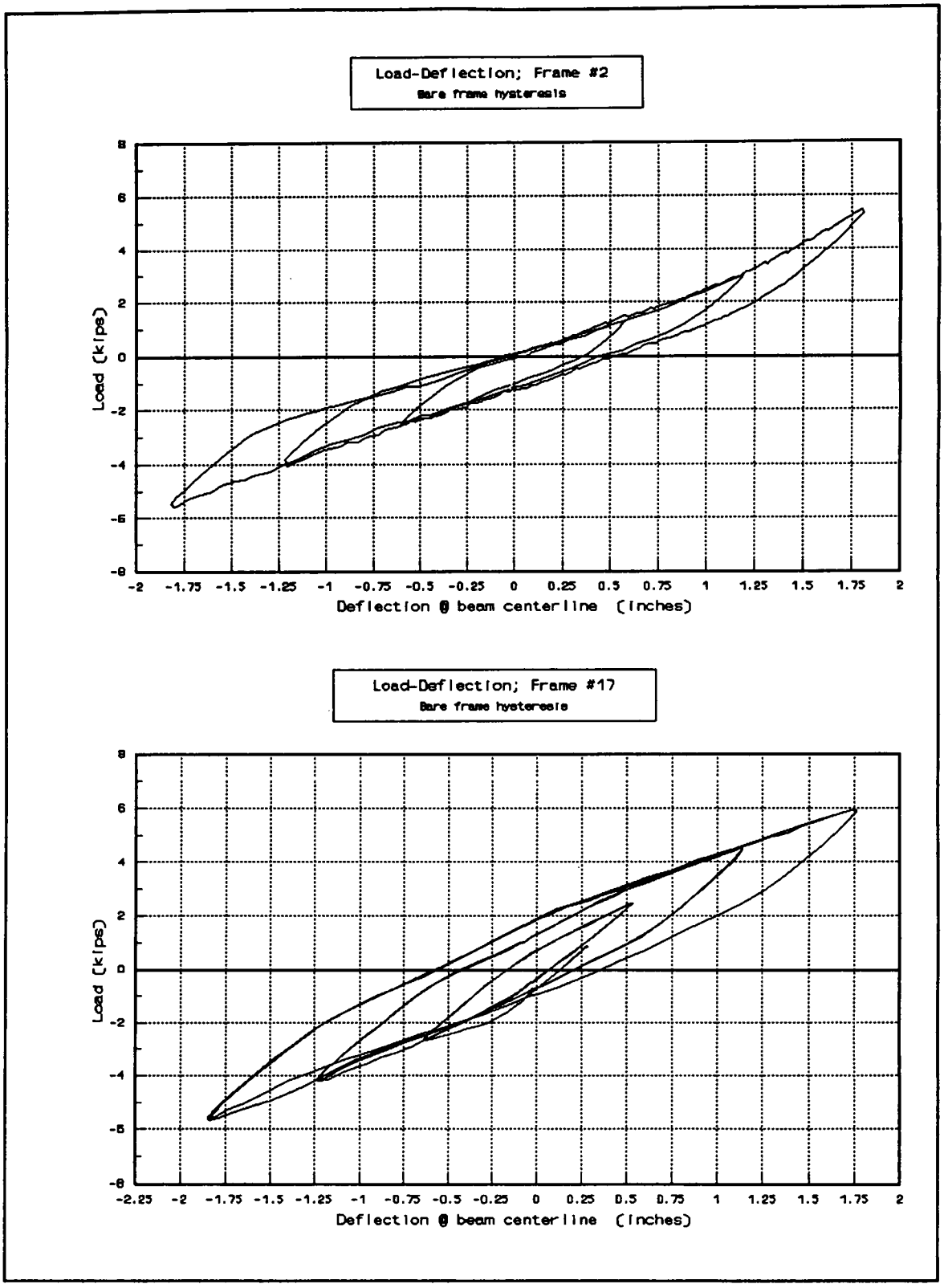


Figure 4.22: Bare frame hysteresis

Frame 2 did not experience any stiffness degradation during the bare frame testing. The initial and final stiffness for the frame was 2.4 kips/inch. Frame 17 had an initial stiffness of roughly 3.2 kips/inch. After the first deflection cycle of 0.6 inches, the stiffness of the system was reduced to approximately 2.5 kips/inch.

Energy absorbed versus deflection for the bare frames is shown in figure 4.23. The maximum energy absorbed by frame 2 with the infill still intact was 17.3 kip-inches at a deflection of 1.18 inches. The bare frame, at this same deflection, only absorbed 2.1 kips-inches. Frame 17 absorbed 32.53 kip-inches at a deflection of 1.54 inches. The bare frame, at the same deflection absorbs 3.75 kip-inches. For both frames, the energy absorbed by the system with the infill intact was approximately eight times that of the bare frame at the same deflection.

4.6 Frame Comparison and Summary

Both frame 2 and 17 behaved similarly up to their ultimate loads. Pre-ultimate behavior of the systems was distinguished by mortar spalling beginning at the beam-infill interface and then throughout the mortar joints of the entire panel. Next, diagonal cracking was observed at approximately the same load and close to the same deflection for both frames. The panel cracking load for frame 2 was 24.17 kips, which was approximately 65% of the ultimate load. Panel cracking

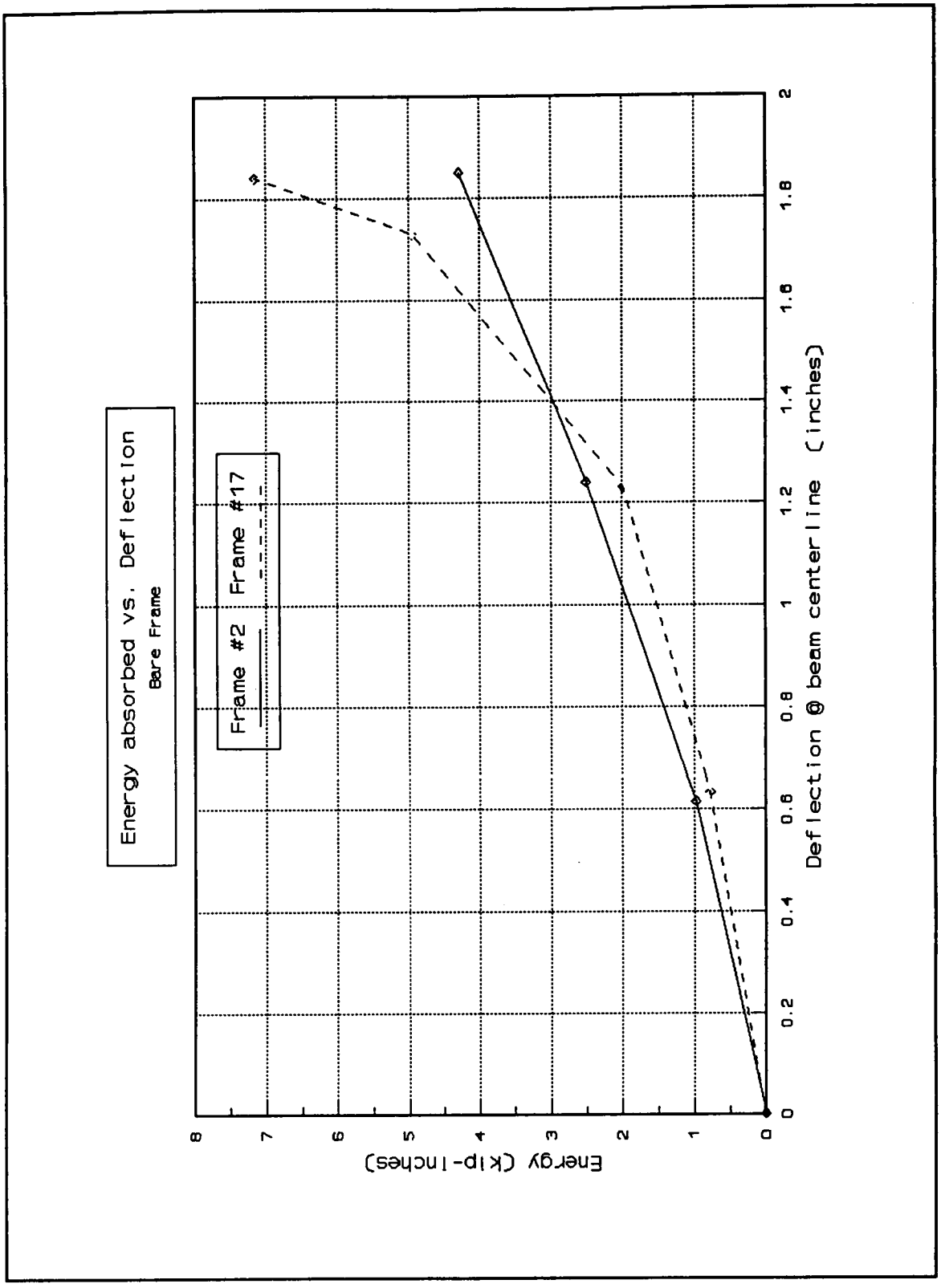


Figure 4.23: Bare frame energy absorption

occurred at a load of 25.45 kips of frame 17. This was roughly 53% of the ultimate load for the frame. After the diagonal cracking was observed, banded diagonal cracking appeared. This visually defined the compressive diagonal of the panel. This was followed by face shell cracking of the clay tile and eventually led to face shell spalling. This was the result of the face shells splitting away from their webs and it occurred mostly in the top two courses.

Both systems exhibited significant post-ultimate strength. Frame 2 experienced a sharp drop in load several cycles after ultimate; however, the system still carried a load of roughly 30% of the ultimate load for several cycles after ultimate and after the top course had begun to disintegrate. Frame 17 experienced a drop in load of about 6 kips following it's ultimate load of 48.2 kips. From here, the frame gained load slightly and then dropped off to roughly 36 kips and maintained this compressive load for the remainder of the test. This maintained post-ultimate load was 75% of the maximum compressive strength of the system. This indicates that the greater aspect ratio, although it may not increase cracking load, does significantly increase ultimate and post-ultimate loads. This is achieved in part by decreasing the angle that the compressive strut makes with the horizontal, thus causing the panel compressive diagonal to be able to resist more horizontal force.

The stiffness degradation of both is was similar. Figure 4.24 illustrates the stiffness of the systems at the maximum compressive loads for each of the six studied cycles. The stiffness values in figure 4.24 were taken as the slope of the major portion of the compressive loading curve. This is illustrated in figure 4.7. As mentioned previously, an initial stiffness for frame 17 was not obtained; therefore, the third cycle stiffness was used as the initial stiffness in figure 4.24. The initial stiffness would be somewhat higher. Both of the stiffness degradation curves behave alike. The frames experience a sharp drop in stiffness up to about 25% of their ultimate deflection. Both curves begin to level off and the stiffness remains somewhat constant up to the ultimate deflection. From here both stiffnesses begin to drop, with frame 2 decreasing at a faster rate than frame 17. At ultimate and after ultimate, frame 17 maintains a stiffness roughly 38% greater than that of frame 2.

As can be seen in figures 4.9 to 4.20, all the load-deflection hysteresis loops behave in a similar manner. As each frame was loaded, there was a portion of the load-deflection curve where there was increased deflection without a significant increase in load. This was due in part by some sliding that occurs between the beam and the infill panel. This phenomenon will be examined further in chapter 6. The effect became more pronounced in later deflection cycles where the beam-infill interface had been lost. After the slippage,

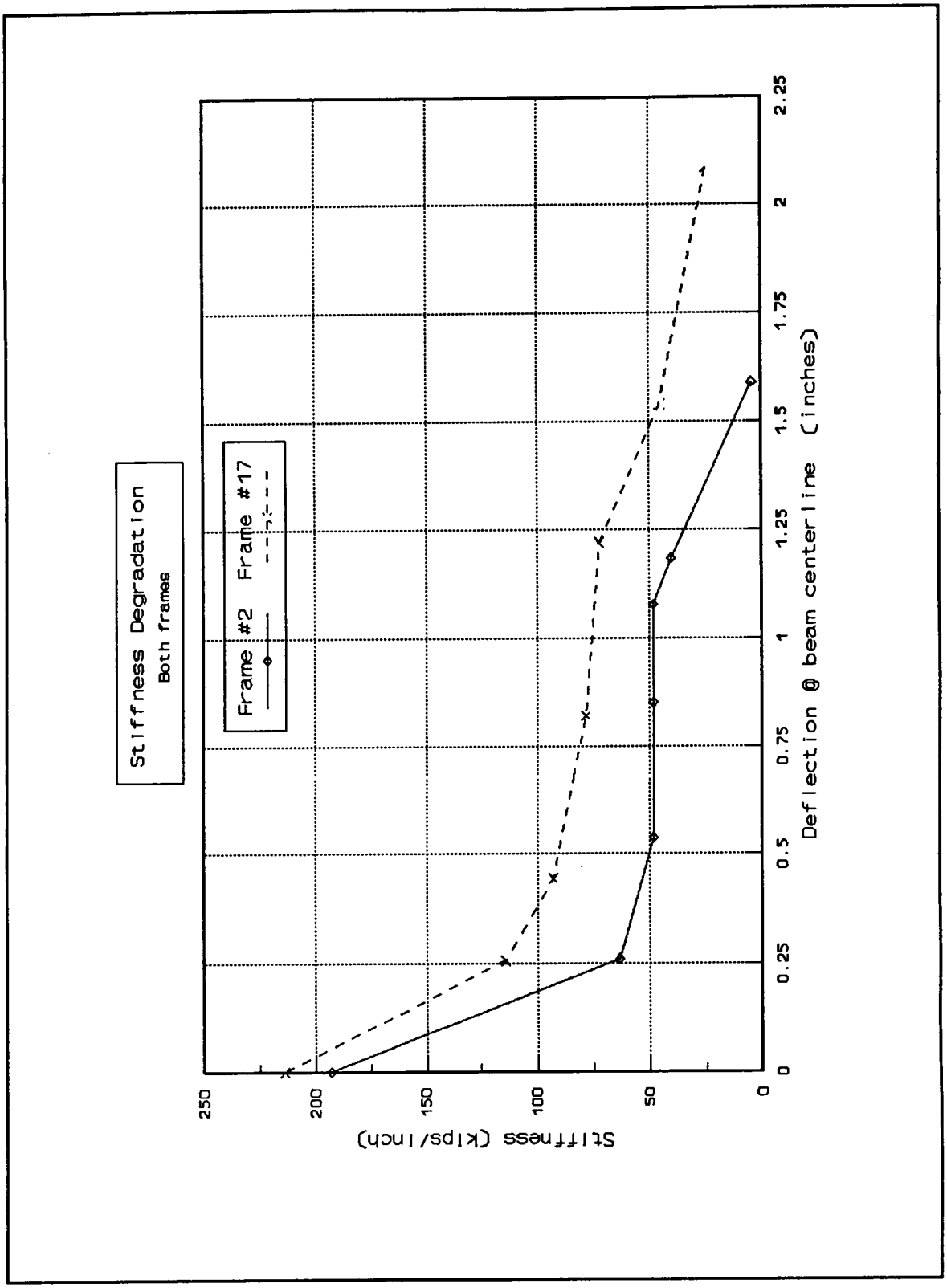


Figure 4.24: Stiffness degradation

the frame engaged the infill and the system stiffness increased dramatically. Eventually, as the panel disintegrated, the response and stiffness of the system approached the bare frame response. This can be seen for frame 2 in figure 4.25. This is a comparison of the sixth load-deflection loop studied to the last load-deflection loop of the bare frame. Figure 4.26 illustrates the same comparison for frame 17. As can be seen from the plot, frame 17 did not degrade to the bare frame response. This plot reinforces the positive attributes of a larger aspect ratio.

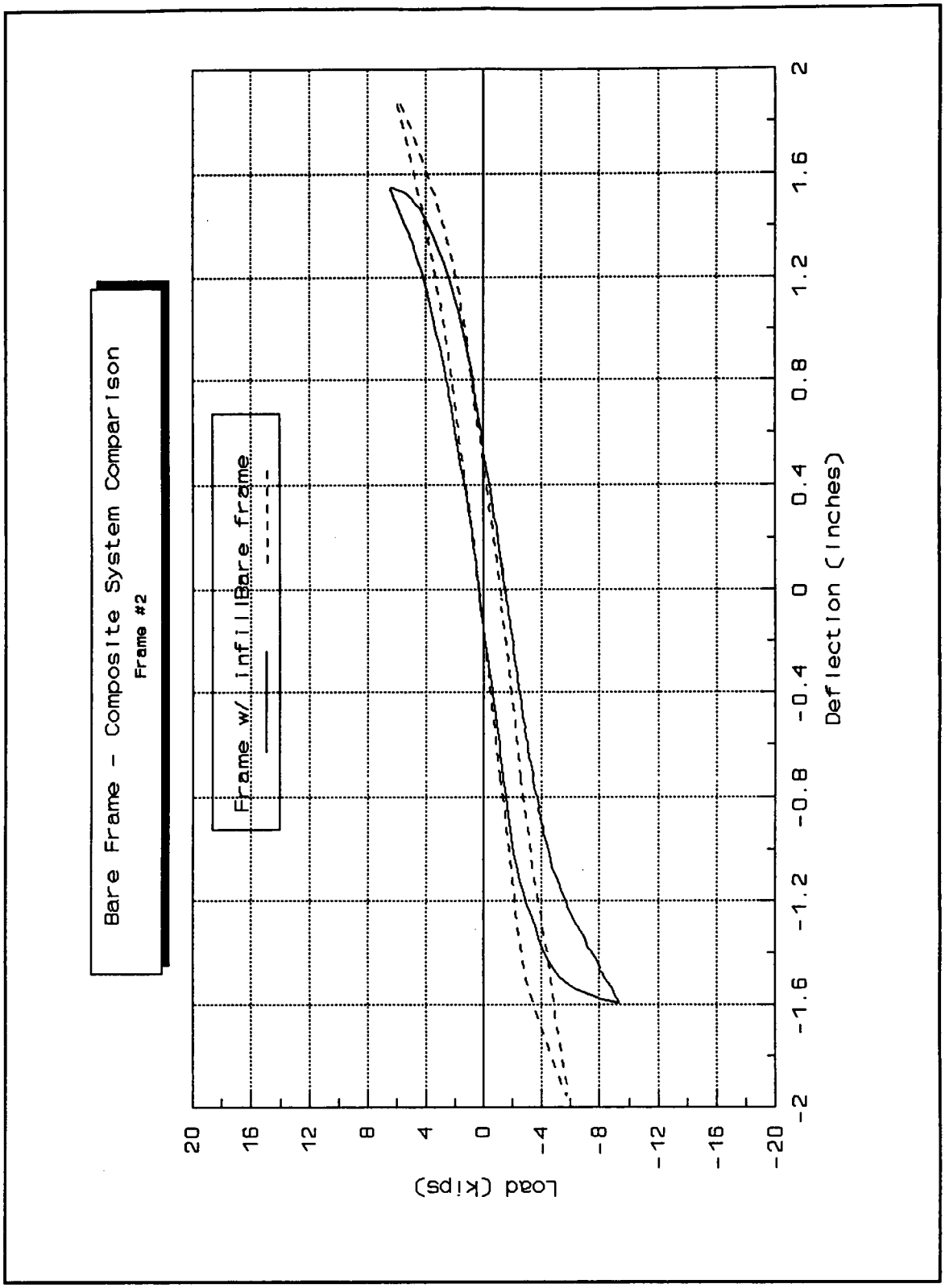


Figure 4.25: Composite - bare frame comparison; Frame 2

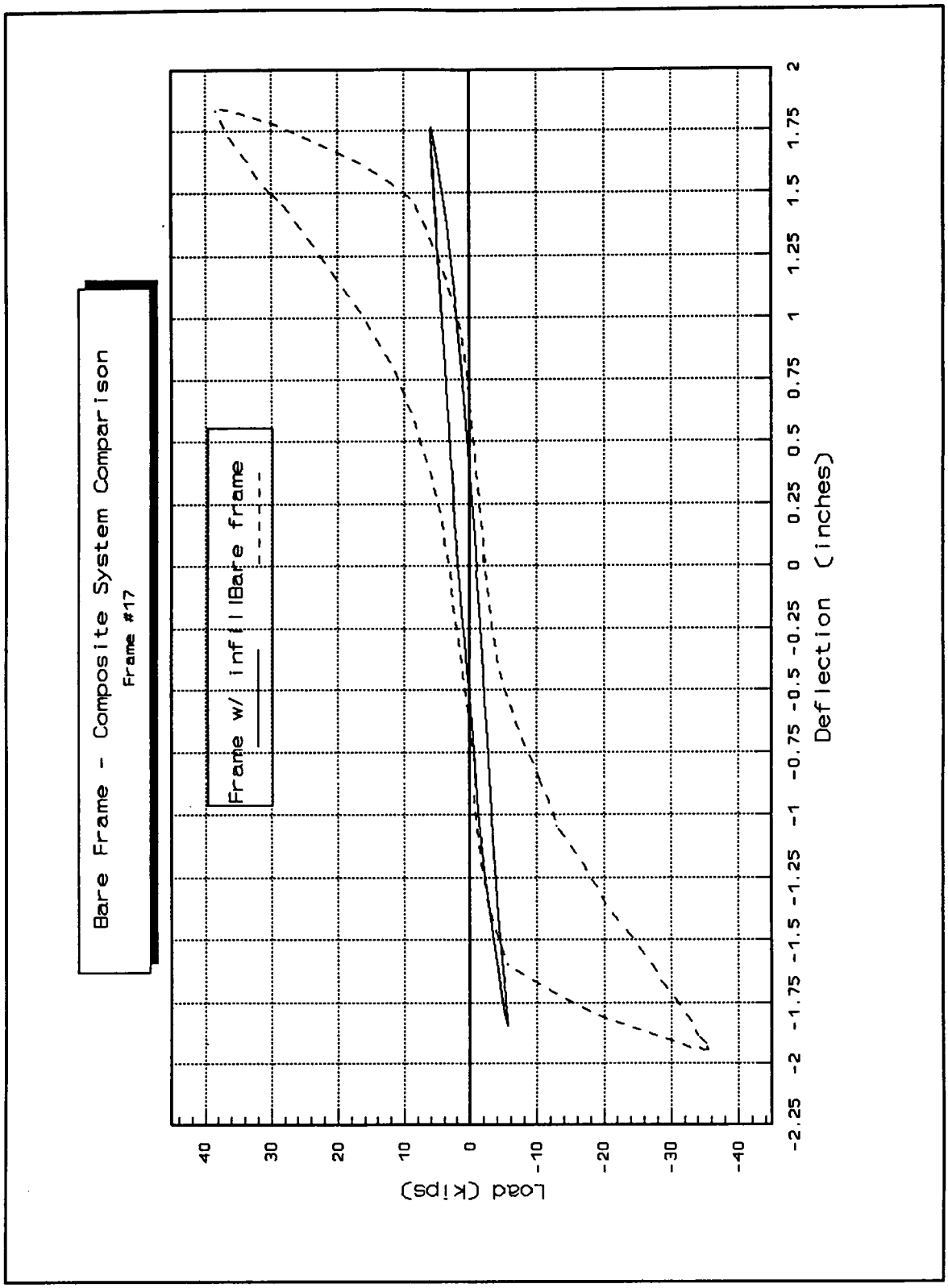


Figure 4.26: Composite - bare frame comparison; Frame 17

Chapter 5: **PANEL BEHAVIOR**

5.1 Introduction

The load-strain relationships of the infill panel are examined in this chapter. The hysteretic load-deflection behavior of the panel is also scrutinized. All of the load-strain and stress-strain envelopes presented in this chapter have been developed in the same manner as the previously studied envelopes. That is, the envelopes were constructed from the points of maximum compression from the load-deflection hysteresis. The difference here was that the panel LVDT's had to be removed just after the ultimate load was achieved to avoid damaging the LVDT's. The panel deformations were taken from the panel LVDT's, as pictured in figure 3.12.

5.2 Load-Strain Relationships

Figure 5.1 illustrates the load-strain curve of the compression diagonal for both frames 2 and 17. The load represented in this plot was the horizontal load at the beam centerline. Figures 5.2 and 5.3 are the load-deflection envelopes for each frame annotated with test event descriptions. The compressive strut of frame 2 softened considerably at a load of 10 kips and a strain of roughly 0.015×10^{-3}. As indicated in figure 5.2, this was where diagonal cracking became visible. Once the diagonal cracking

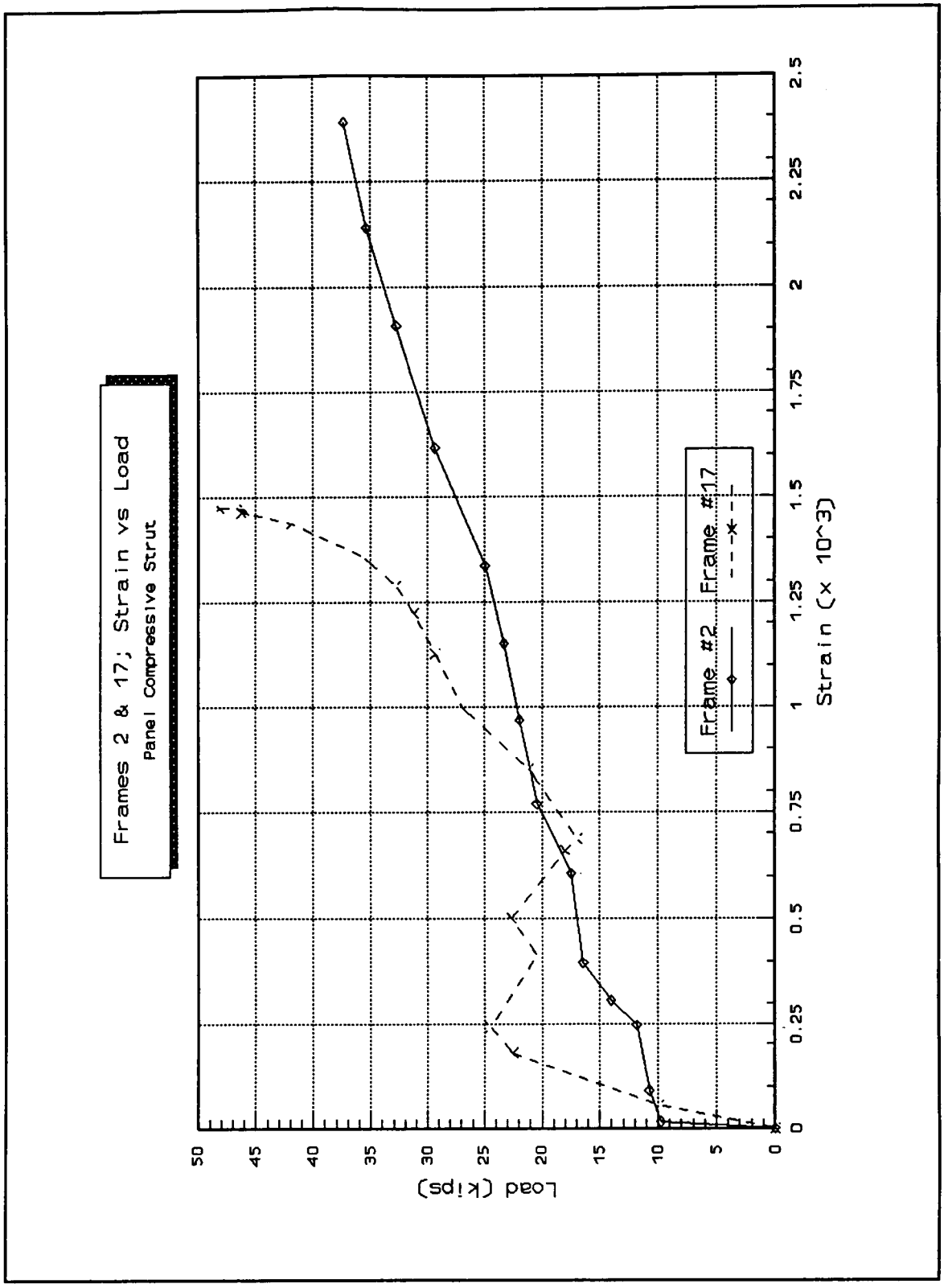


Figure 5.1: Load-strain, Compressive diagonal

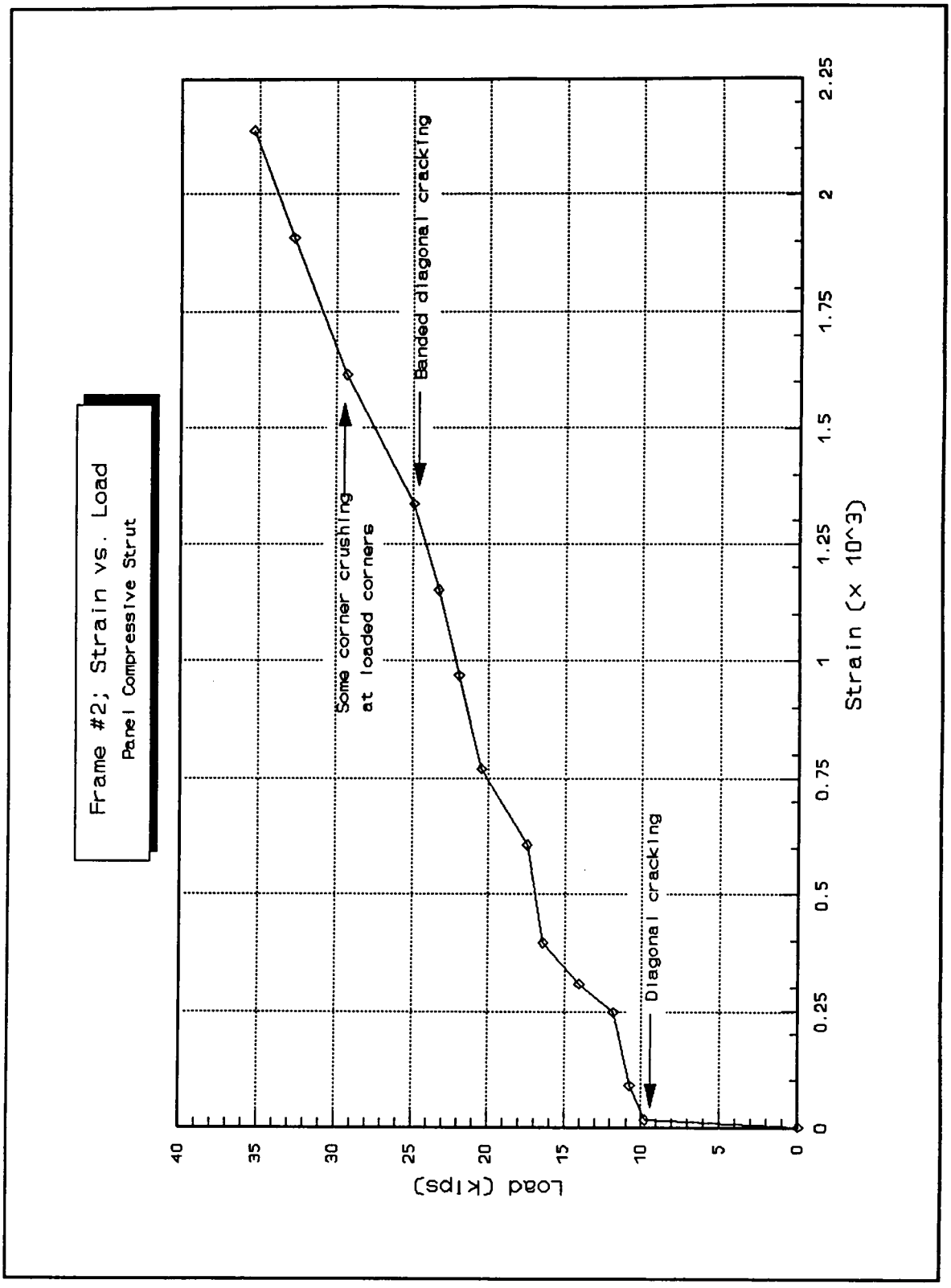


Figure 5.2: Frame #2; Compressive diagonal strain

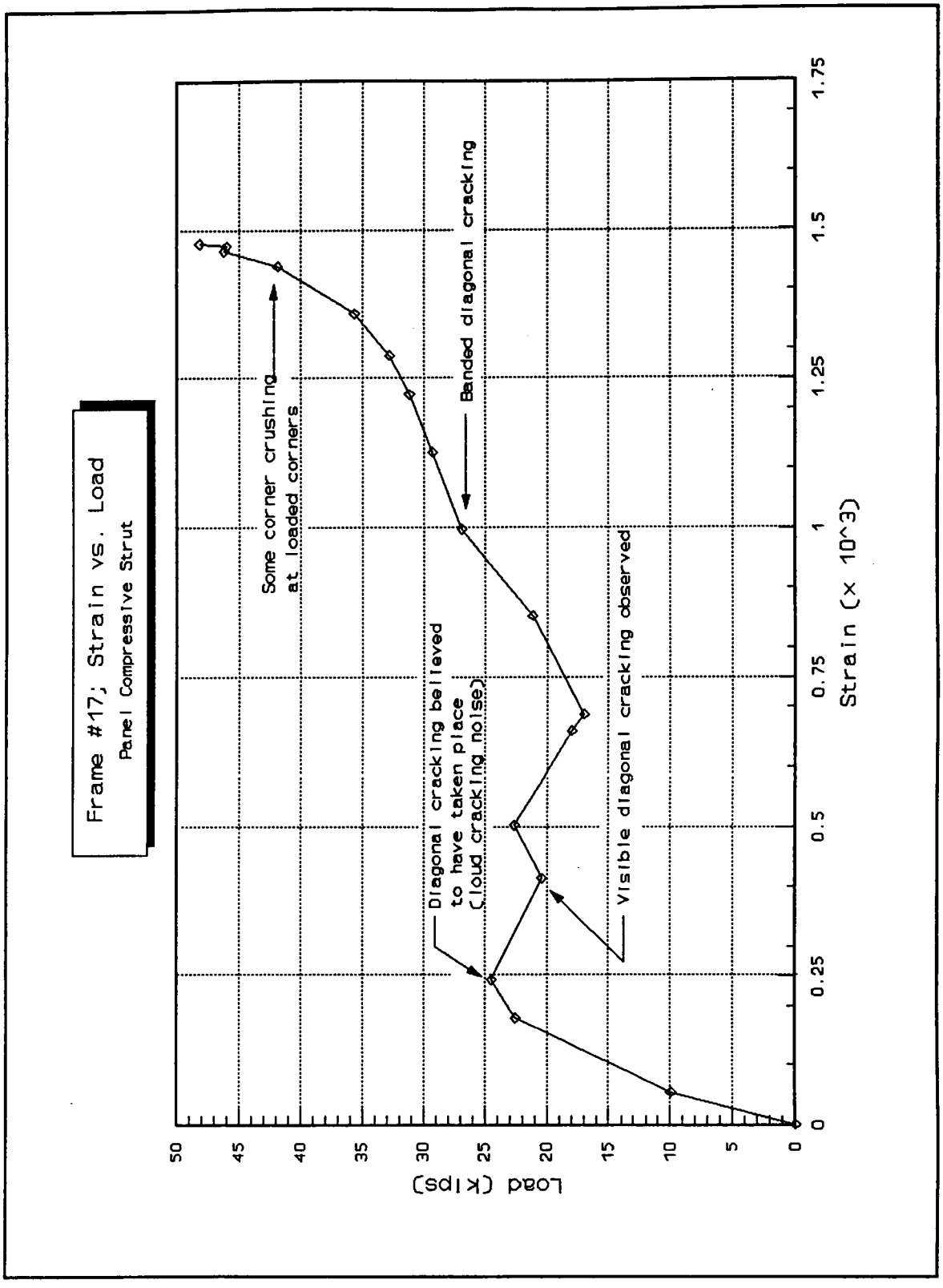


Figure 5.3: Frame #17; Compressive diagonal strain

had occurred, there was less confinement of the compressive strut and this allowed larger strains to occur in the strut. Banded diagonal cracking became visible at a load and strain of 25 kips and 1.33 x 10^{-3} inches/inch. As noted in figure 5.2, corner crushing in the loaded corners of the strut was observed shortly before reaching ultimate. There was a slight decrease in the stiffness of the strut after corner crushing commenced.

Although frame 17 experiences some softening at 10 kips, the load-strain envelope remained fairly linear to a load of about 22.5 kips before there was significant softening of the strut. As noted in figure 5.3, although diagonal cracking was not visible until later, diagonal cracking probably occurred between 22 and 24 kips where the envelope began to soften. At a strain of 0.70 x 10^{-3}, the load began to increase and as it neared the ultimate load, there appeared to be a "strain hardening" effect in the envelope. There was very little increase in strain prior to the ultimate load. This was presumably due to a lesser degree of degradation of the compressive strut, which in turn was due to the larger equivalent compressive strut area for frame 17.

Figure 5.4 illustrates the tension diagonal load-strain envelope for both frames. The load-strain envelope of the tension diagonal for frame 2 remains linear up to a load of 10 kips where a tension failure occurs in the panel. The strain in the tension diagonal was negligible when the failure

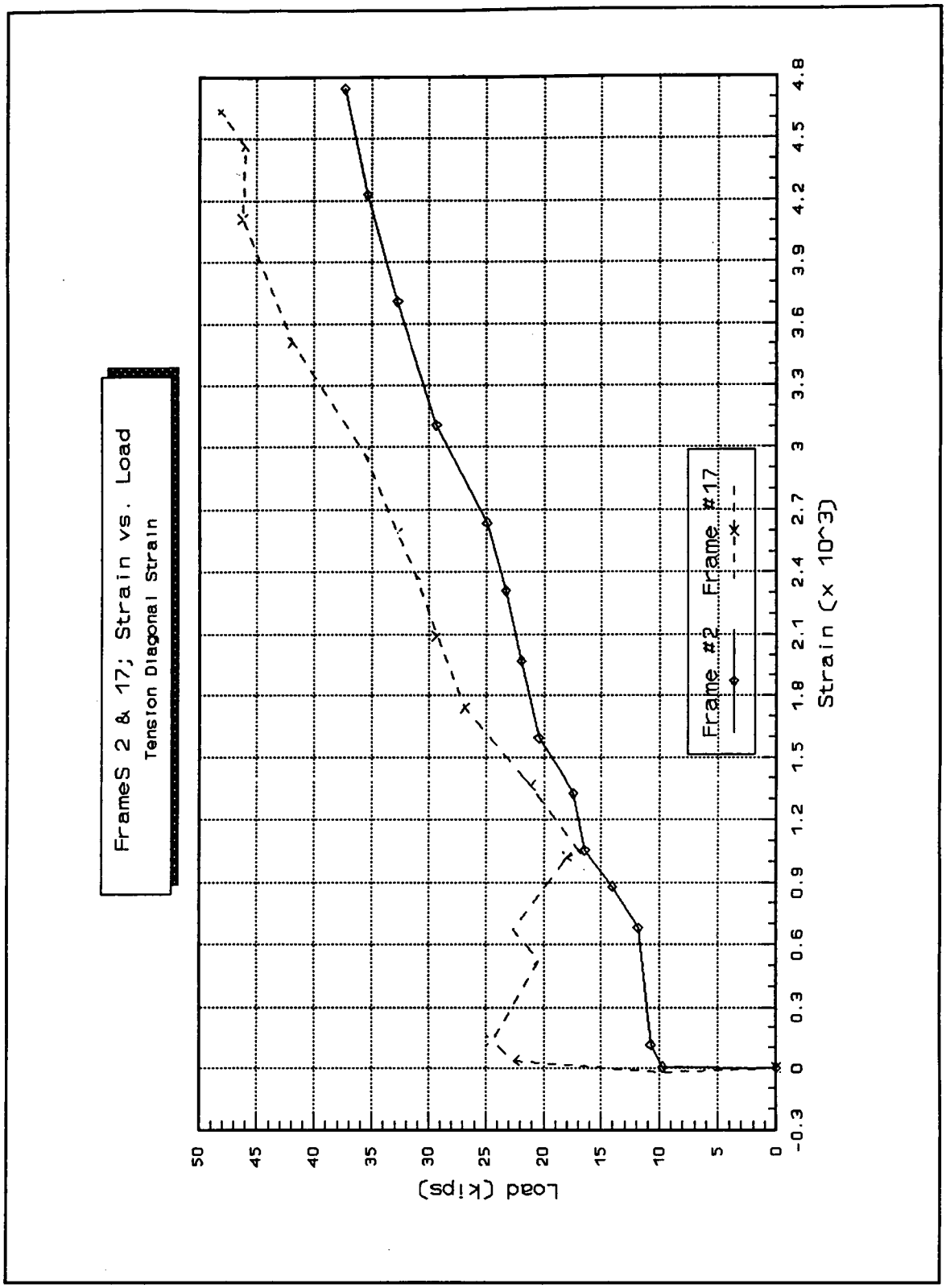


Figure 5.4: Load-strain envelope; tension diagonal

occurred. This tension failure occurred at approximately the same time the compression strut began to soften. The increase in strain from this point was due to an opening of the tension crack along the compression diagonal, not plastic deformation.

The tension failure in panel 17 also occurred about the same time that its compression strut began to soften. As can be seen in figure 5.4, the tension diagonal of frame 17 was in slight compression, although negligible strain, during the first cycle. This may have been an anomalous reading due to a slight offset of the LVDT from the start of the test. The tension failure occurred at about 22.5 kips and the same drop in load was seen as in all the load-deflection and load-strain envelopes for frame 17. From here, the load increased at considerably lower strains for the same given load as compared to frame 2. This indicates that for the same load, the tension cracking of a panel with a larger aspect ratio will not be as severe as for a smaller aspect ratio.

Figure 5.5 illustrates the vertical strain versus load envelope for frames 2 and 17. The load-strain envelope for frame 2 behaved almost identically to the load-strain envelope for the tension diagonal of that frame. The sole difference was that the strains were slightly less for the corresponding loads. The vertical strain versus load envelope for frame 17 behaved the same as for the tension diagonal up to the point of the tension failure of the panel. After the drop in load that was seen after the panel softening, the curve behaved

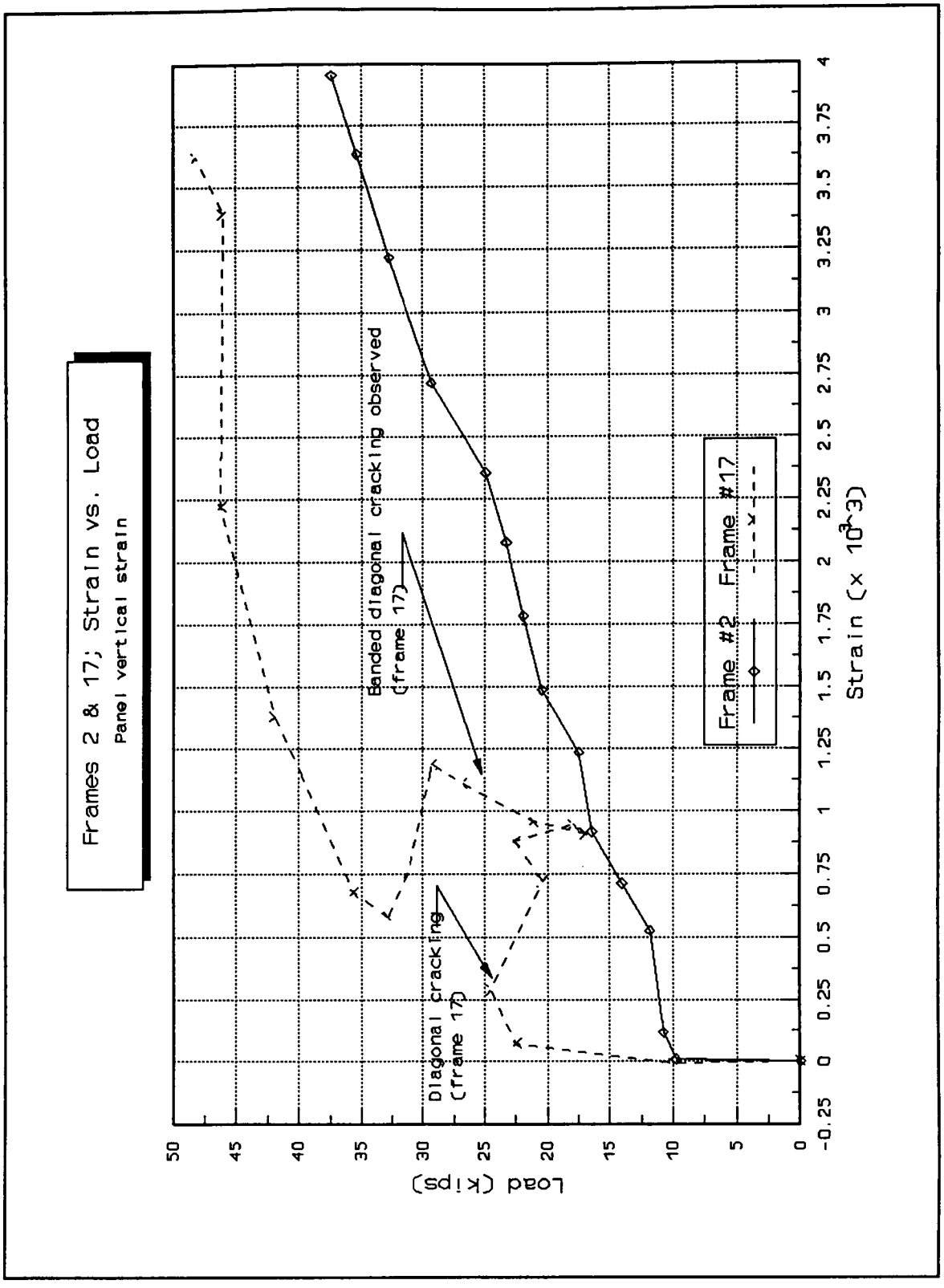


Figure 5.5: Load-strain envelope, panel vertical

rather erratically. As shown in figure 5.5, this was the region in between singular and parallel stair step cracking. Tension cracking of the mortar joint is the most likely cause of the erratic behavior. During this time, the panel was loaded up to approximately 30 kips with a slight increase in strain. At this point, there was a decrease in vertical strain with increasing load for several cycles. This could be attributed to a poisson effect because, as will be seen, the horizontal strain during this period was increasing in tensile strain.

Figure 5.6 depicts the panel horizontal strain versus load envelopes for both frames. Both curves behave similarly to their vertical strain counterparts with the exception that the horizontal strains were somewhat less than the vertical strains. Frame 17 exhibited some slight compression up to 10 kips, which was where the tension failure of the panel took place. Figures 5.7 and 5.8 illustrate a comparison of the panel vertical and horizontal strains versus load for both frames 2 and 17. As seen in these figures, after the tension failure along the compression diagonal, the vertical displacement of the panels was greater than the horizontal displacement. This effect was somewhat more pronounced in frame 2 than frame 17. This is in agreement with the findings of Moghaddam (1988), who suggested that in order to suppress the diagonal cracking, containment of the horizontal, but primarily the vertical, displacements must be obtained.

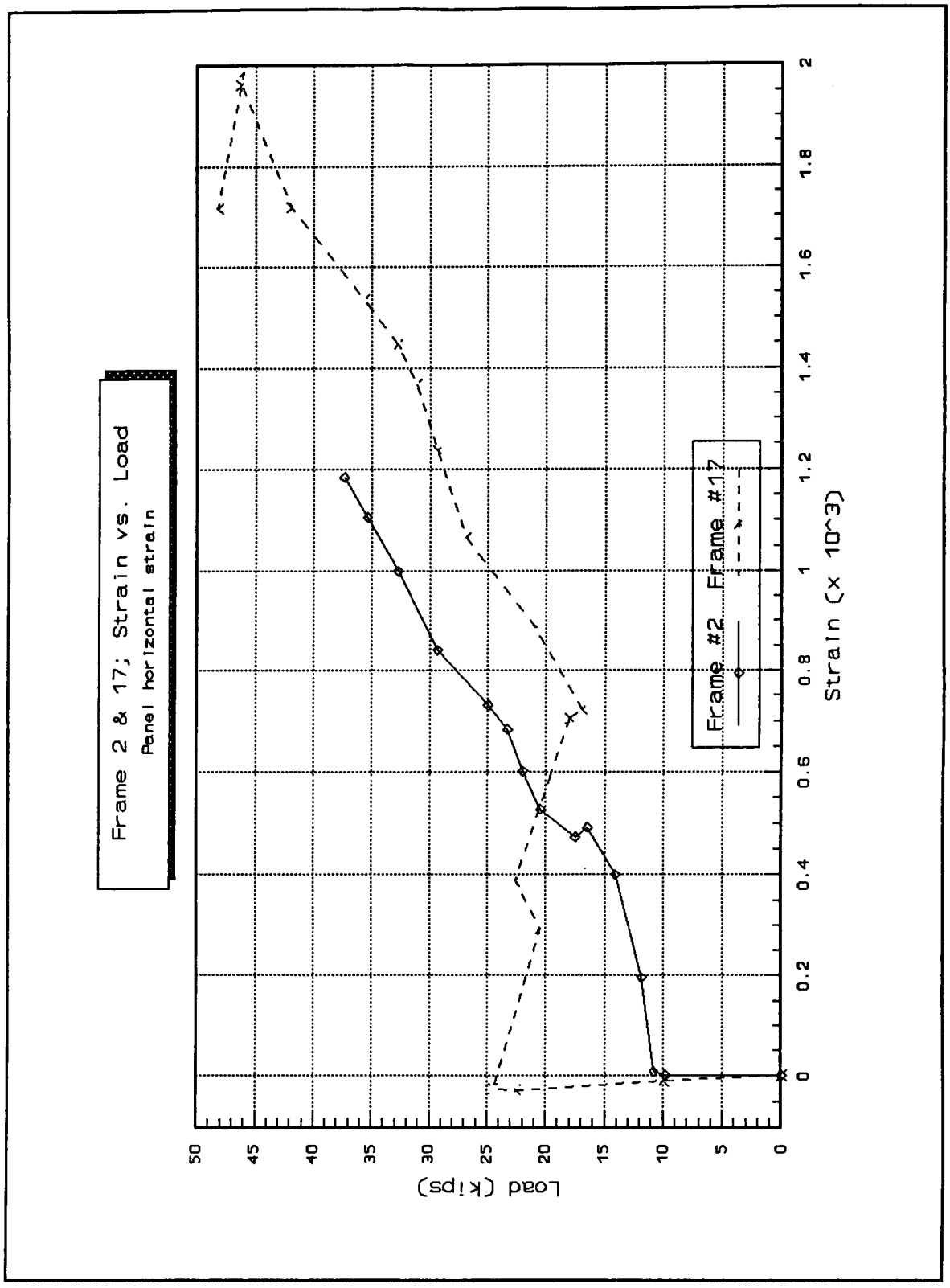


Figure 5.6: Horizontal load-strain; both frames

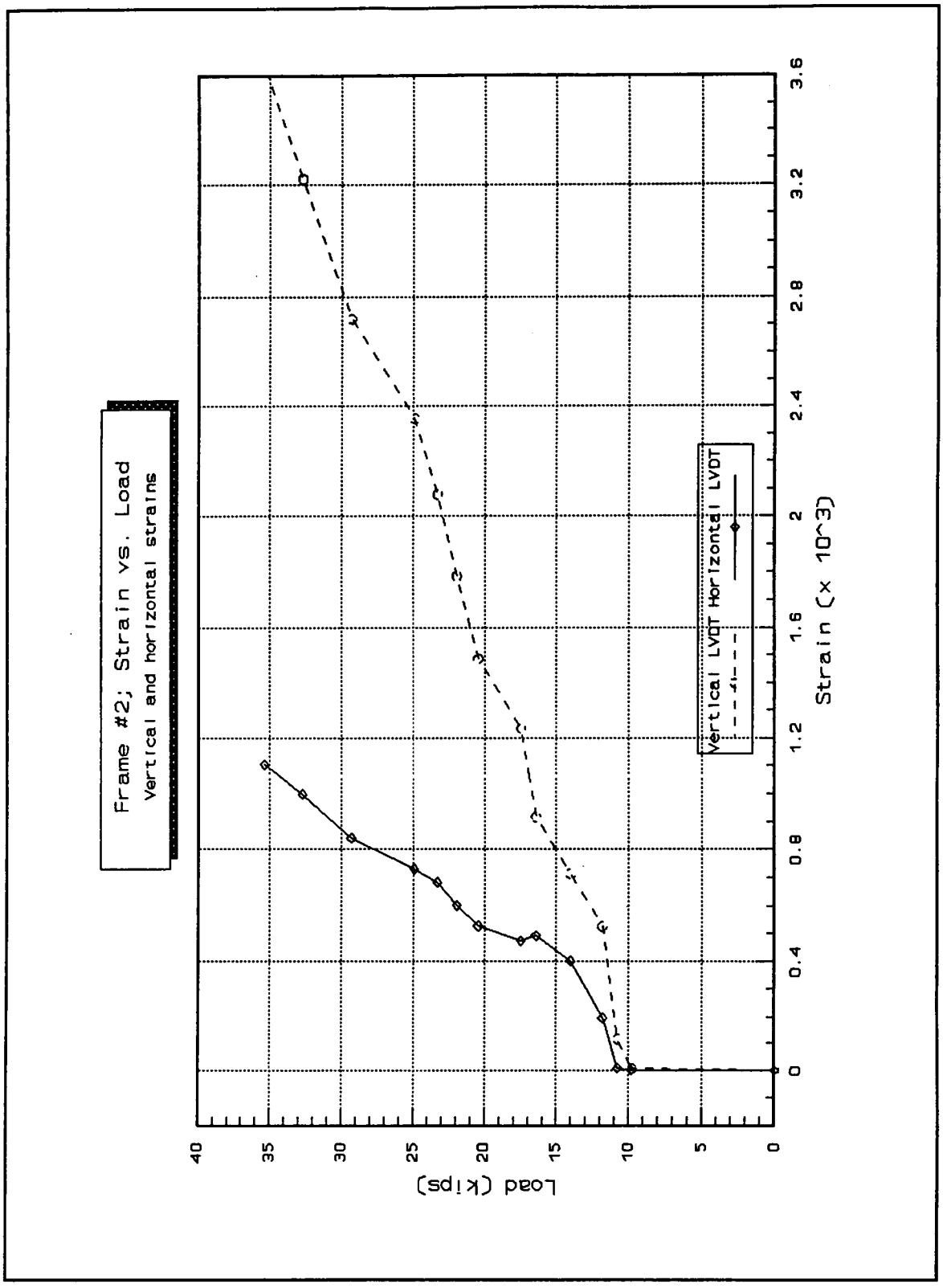


Figure 5.7: Frame #2; Vertical and horizontal load-strain

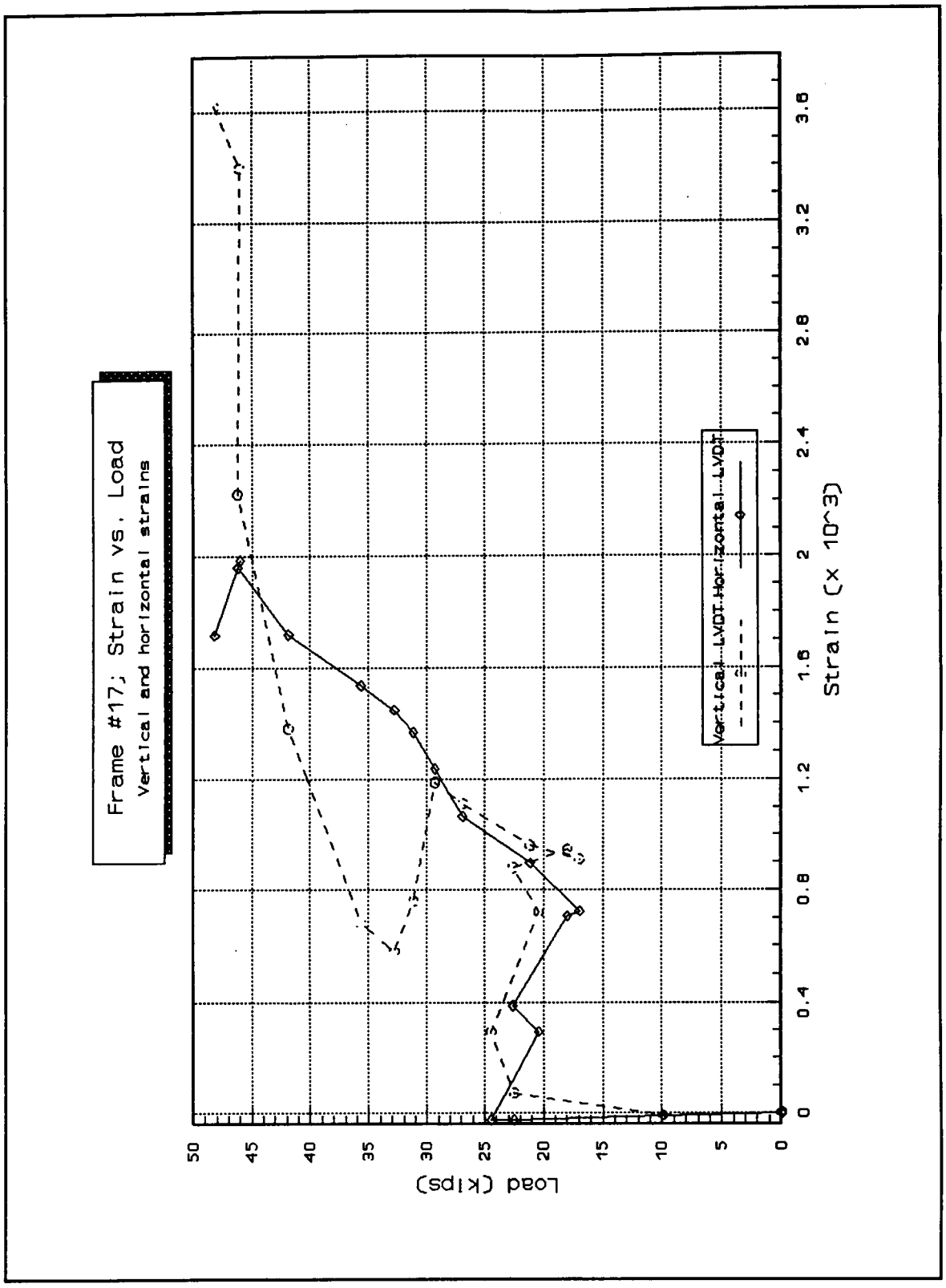


Figure 5.8: Frame #17; Vertical and horizontal load-strain

5.3 Stress-Strain Relationships

Figure 5.9 illustrates the stress-strain envelope of the compressive strut for both frames 2 and 17. The load used in calculating the stress was the diagonal load in the strut, rather than the horizontal racking load. The diagonal load in the strut was statically determined by dividing the horizontal racking load by the cosine of the angle that the strut makes with the horizontal. The area used in the calculation of stress in the compressive strut was the area obtained in section 4.2.2. The stress-strain envelopes obviously behave in the same manner as the load-strain envelopes. The stress-strain envelope of frame 2 was linear up to a stress of approximately 170 psi, which corresponded to a strain of 0.015 x 10^{-3} inches/inch. From this point, the strut softened considerably and increased to an ultimate stress of 650 psi and an ultimate strain of 2.39 x 10^{-3} inches/inch. The compressive strut of frame 17 softened slightly at a stress of 120 psi, but remained fairly linear up to a stress of 270 psi and a strain of 0.18 x 10^{-3} inches/inch. This indicates that for the frame with the larger aspect ratio, the compressive strut was more ductile up to the point of "yielding" of the material.

The post-softening behavior of frame 17 is much different than frame 2. The strain hardening effect is also seen in the stress-strain envelope of the compressive strut for frame 17. Frame 17 increased rapidly, relative to the rate of strain

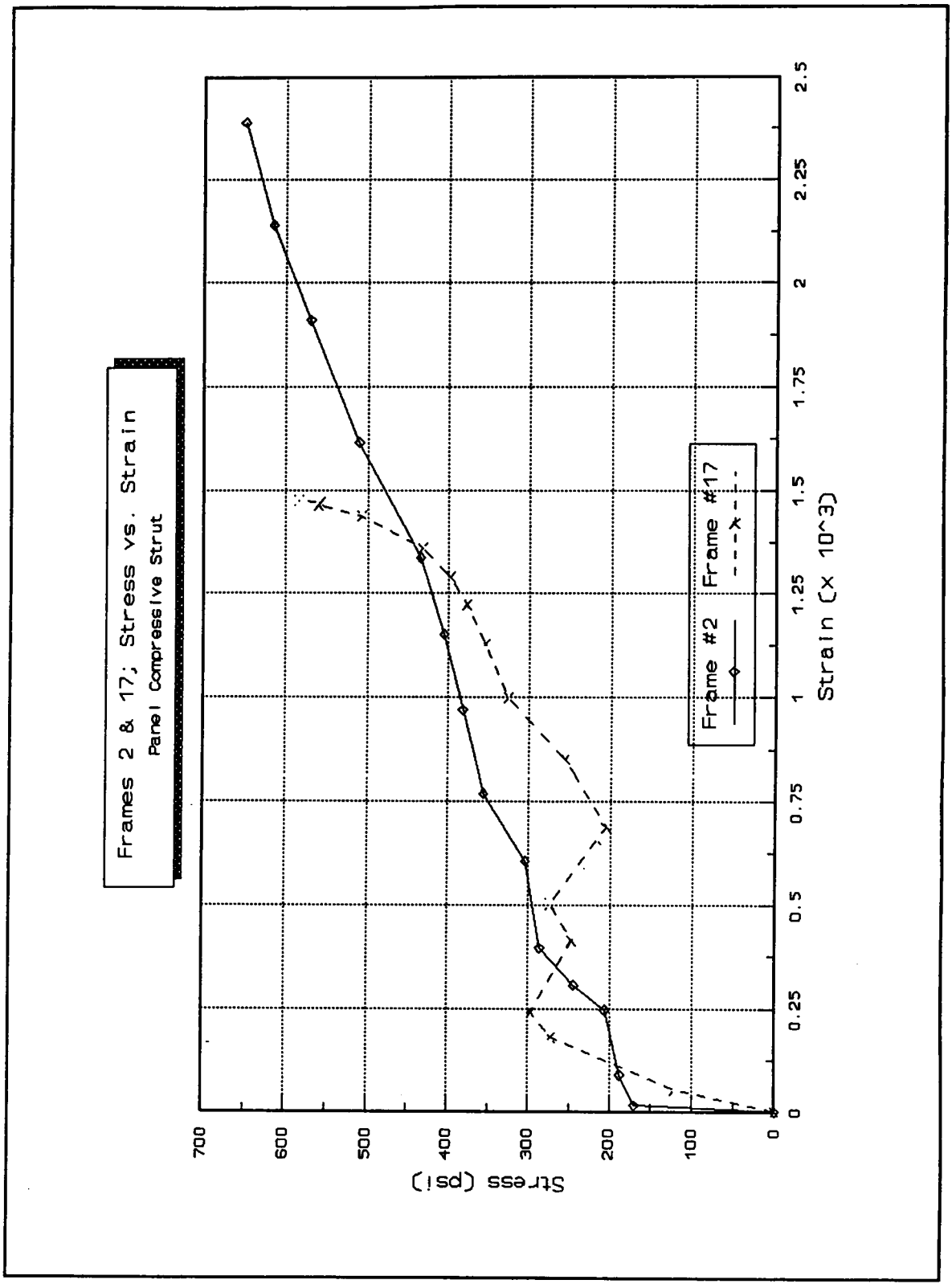


Figure 5.9: Compressive strut; Stress-strain envelopes

increase, to it's ultimate stress of 583 psi, which coincided with an ultimate strain of 1.48 x 10^{-3} inches/inch. This was approximately 90% of the stress in the compressive strut at ultimate and 60% of the ultimate strain for frame 2. The lower stress of the compressive strut for frame 17 was due to the smaller angle that the strut makes with the horizontal and the larger strut area of the panel.

Figure 5.10 illustrates a stress-strain curve obtained from a four high prism (cores vertical) compression test conducted by Boyd (1993). The ultimate stress of the prism test was somewhat lower than the ultimate stresses of the compressive struts of the panels. This is to be expected since there was no lateral confinement in the prism tests. The ultimate strains of the panels are comparable to the prism test. The ultimate strain of the prism test was roughly 0.0015 inches/inch. The ultimate strain of the compressive strut for frame 2 was 0.00239 inches/inch. The ultimate strain of the strut for frame 17, which, due to the strut angle, was closer to cores vertical condition of the prisms, was 0.00148. This was only a 1.3% difference from the prism ultimate strain.

5.4 Panel Hysteretic Behavior

The hysteretic behavior of the panel is considered in this section. As previously mentioned, the panel LVDT's were removed immediately after the ultimate load had been achieved. Therefore, the first four of the six load-deflection

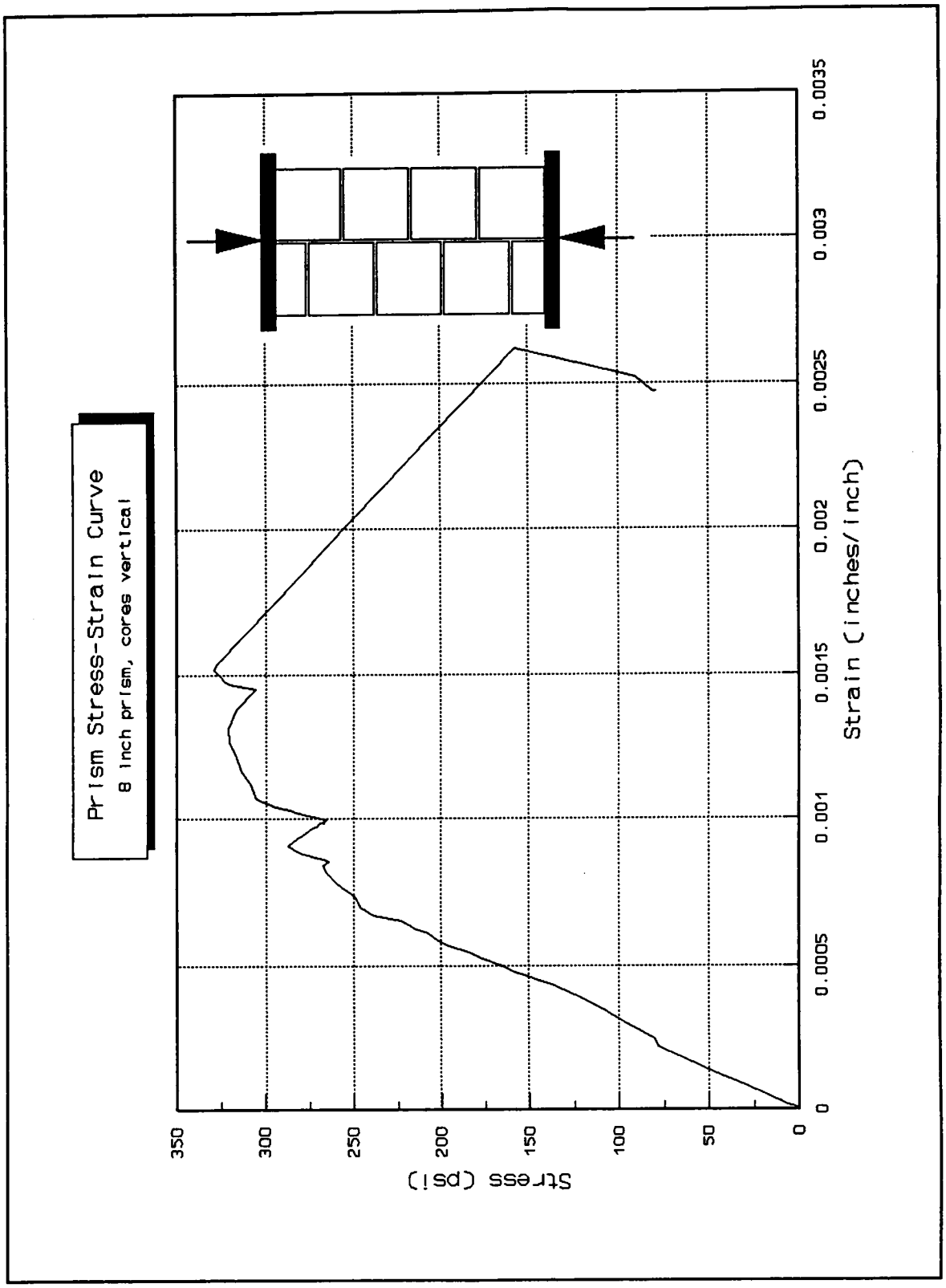


Figure 5.10: Prism stress-strain curve (after Boyd, 1993)

hysteresis loops studied in chapter four are investigated for the panel. The terms 'tension diagonal' and 'compressive diagonal' refer to the time frame when the frame was loaded in compression. The load for all panel hysteresis loops was the horizontal racking load.

5.4.1 Frame #2; Panel Hysteresis

Figure 5.11 depicts the load-deflection hysteresis for LVDT #27 of frame 2. Loop one represents the point where diagonal cracking was first observed. Loop two illustrates the hysteresis loop where banded diagonal cracking was noticed. In this loop, a flat portion of the load deflection curve was noticed on either side of zero during the loading and unloading segments of the cycle. This phenomenon was seen in the load-deflection curves for the beam centerline deflection. During testing, it was thought that this was due to an interface slippage between the beam and the panel at low loads. However, the fact that the flat portion exists in the panel LVDT load-deflection hysteresis indicates that this phenomenon was, at least in part, due to the non-linear properties of the material. This topic is investigated further in chapter 6 where comparisons are made between the relative and frame LVDT's.

Figure 5.12 illustrates the load-deflection hysteresis for LVDT #28 of frame 2. Loop one represents the approximate time that diagonal cracking in compression occurred. This

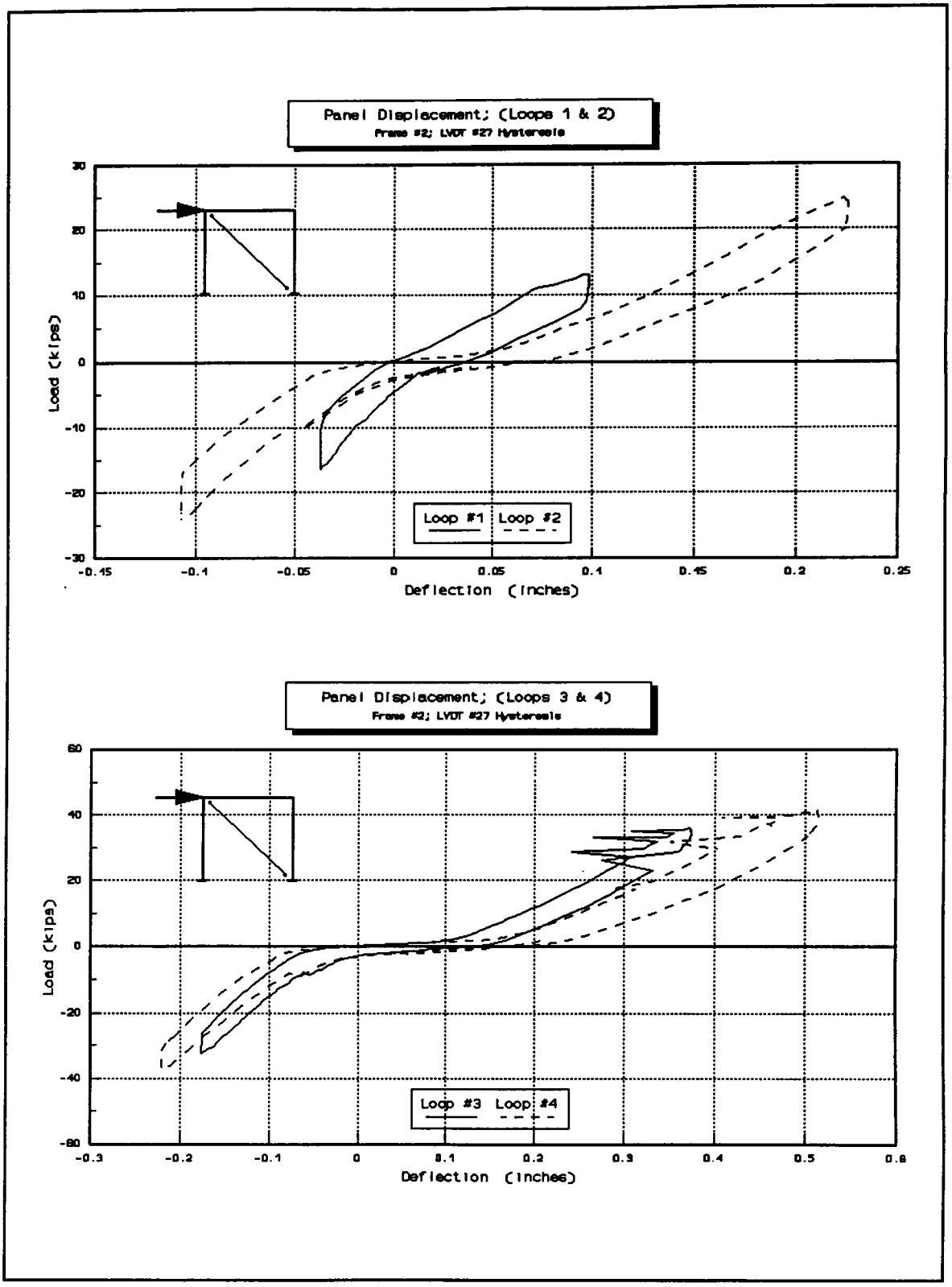


Figure 5.11: Frame #2; LVDT #27 hysteresis

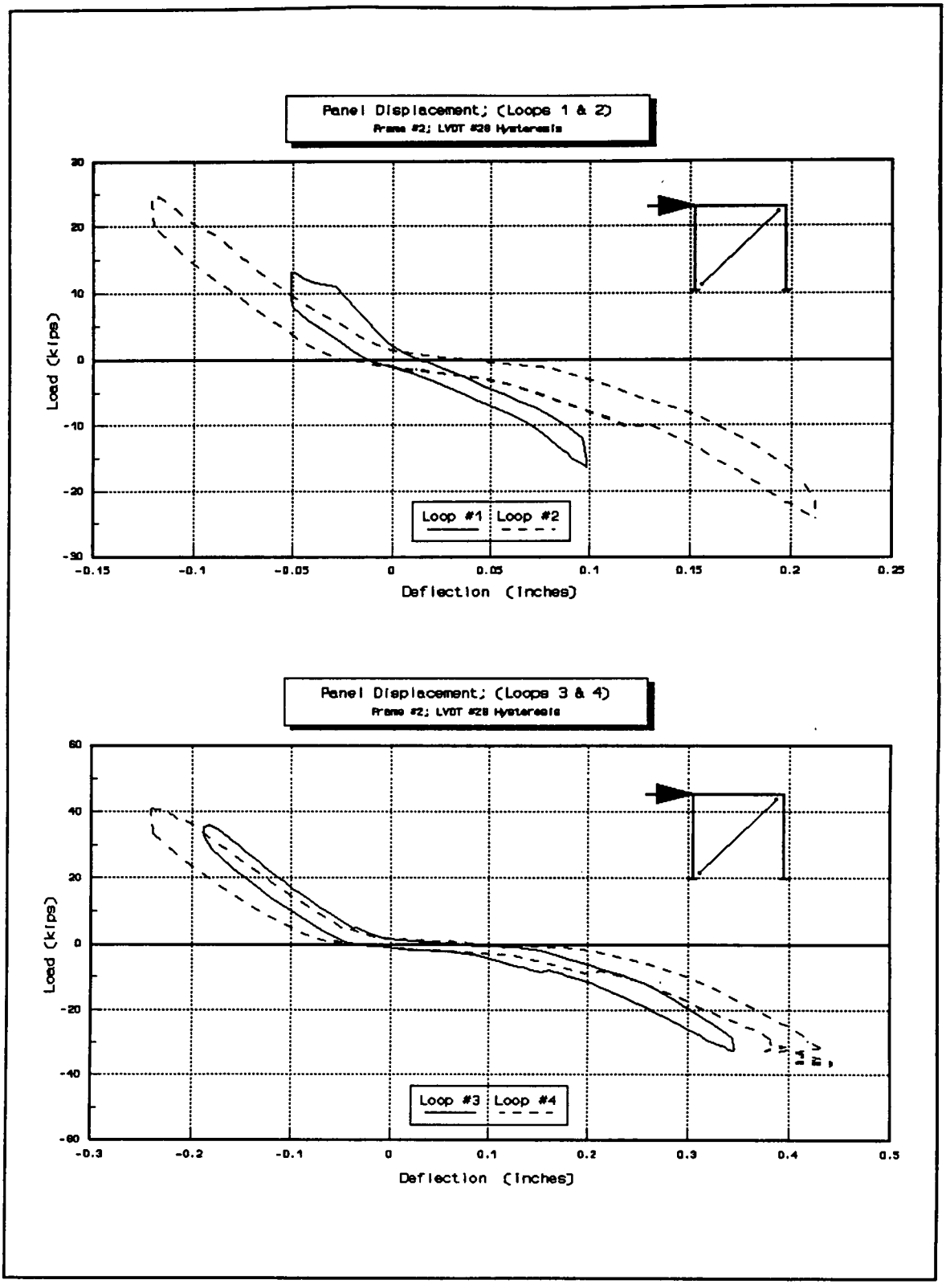


Figure 5.12: Frame 2; LVDT #28 hysteresis

corresponds to a tension failure in the panel. It can be seen, in the tensile or positive deflection portion of the plot, that there was a significant loss of stiffness from the compressive portion of loop one to loop two. The tensile deformations were consistently almost twice that of the compressive deformations for LVDT #28. The "sliding" effect was seen in the compressive loading portion of loops three and four. This corresponded to the time frame in which LVDT #28 was the tension diagonal. The effect may have been due partially to material properties, but in the tension diagonal LVDT, this effect was probably the stair step crack opening up after the tension failure in the mortar has occurred.

Figures 5.13 and 5.14 depict the four load-deflection hysteresis loops of the panel horizontal and vertical LVDT's, respectively. These loops behave quite differently from the diagonal hysteresis loops. Both the horizontal and the vertical remain in tension from the time frame of loop one to the end of the test. During all four hysteretic loops of frame 2, the maximum tensile load and the maximum compressive load for each particular loop was roughly the same, while the deflection of the horizontal LVDT during the compressive load was somewhat less than that of the tensile loading. All of these loops, possibly with the exception of loop one, were for the most part, simply measurements of the horizontal distance of the opening and closing of the diagonal tension crack that had formed in the panel previously.

The panel vertical deflections of frame 2 also remained in a tensile deflection throughout the testing. The vertical hysteresis of the panel behaves much the same as for the horizontal of the panel. One difference was that the vertical LVDT achieved significantly greater deflections as compared to the coincident horizontal deflection. The deflections of the vertical LVDT were roughly the same during the tension and compressive loading of the same cycle. This was in contrast to the horizontal panel deflections.

5.4.2 Frame #17; Panel Hysteresis

Figure 5.15 illustrates the load-deflection hysteresis for LVDT #27 of frame 17. The compressive loading portion of loops one and two represent the point where diagonal and banded diagonal cracking occurred in the panel. The compressive diagonal of frame 17 was much stiffer than that of frame 2 in the same deflection increment. The flat portion of the load deflection curve that was also seen in frame 2 was not observed in the compressive diagonal until loop three. This probably indicates that plastic deformation of the panel strut did not occur as soon in frame 17 as it did in frame 2.

Figure 5.16 depicts the load deflection hysteresis of LVDT #28 of frame 17. Loop one represents the approximate time that the tension failure took place. This was during the compressive loading portion of the curve. As can be seen in figure 5.16, after the diagonal cracking had occurred, there

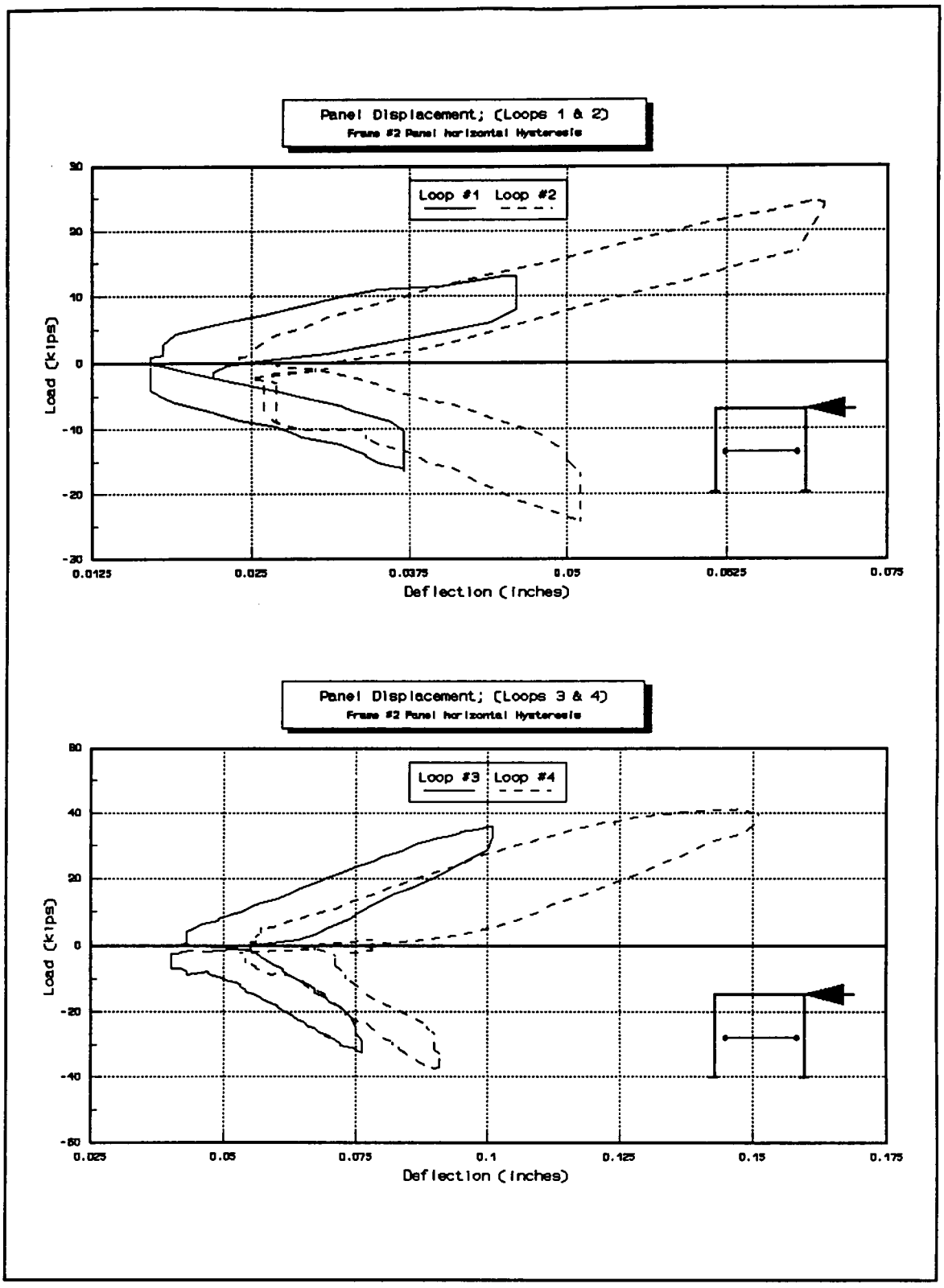


Figure 5.13: Frame #2; Panel horizontal hysteresis

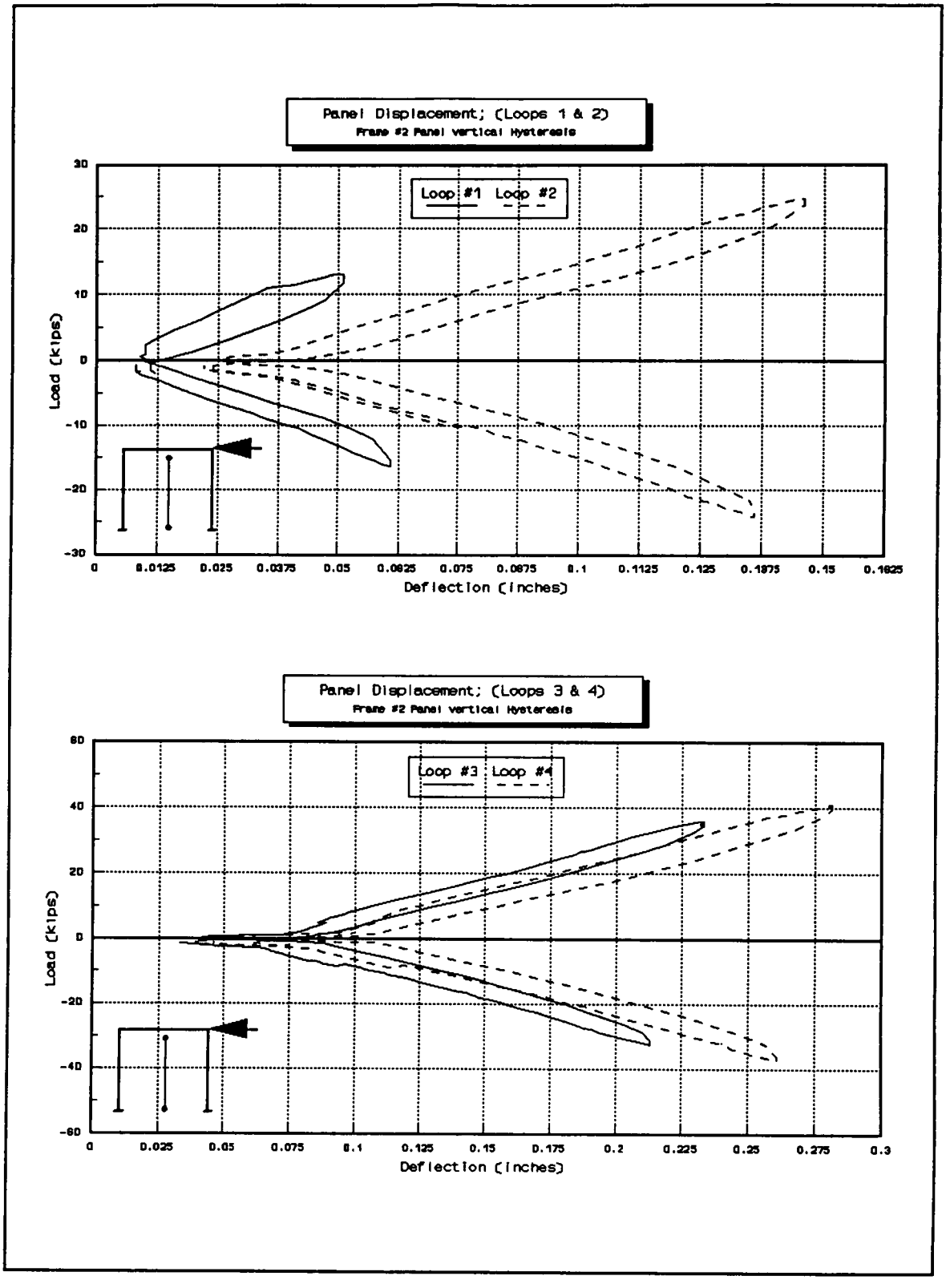


Figure 5.14: Frame #2; Panel vertical hysteresis

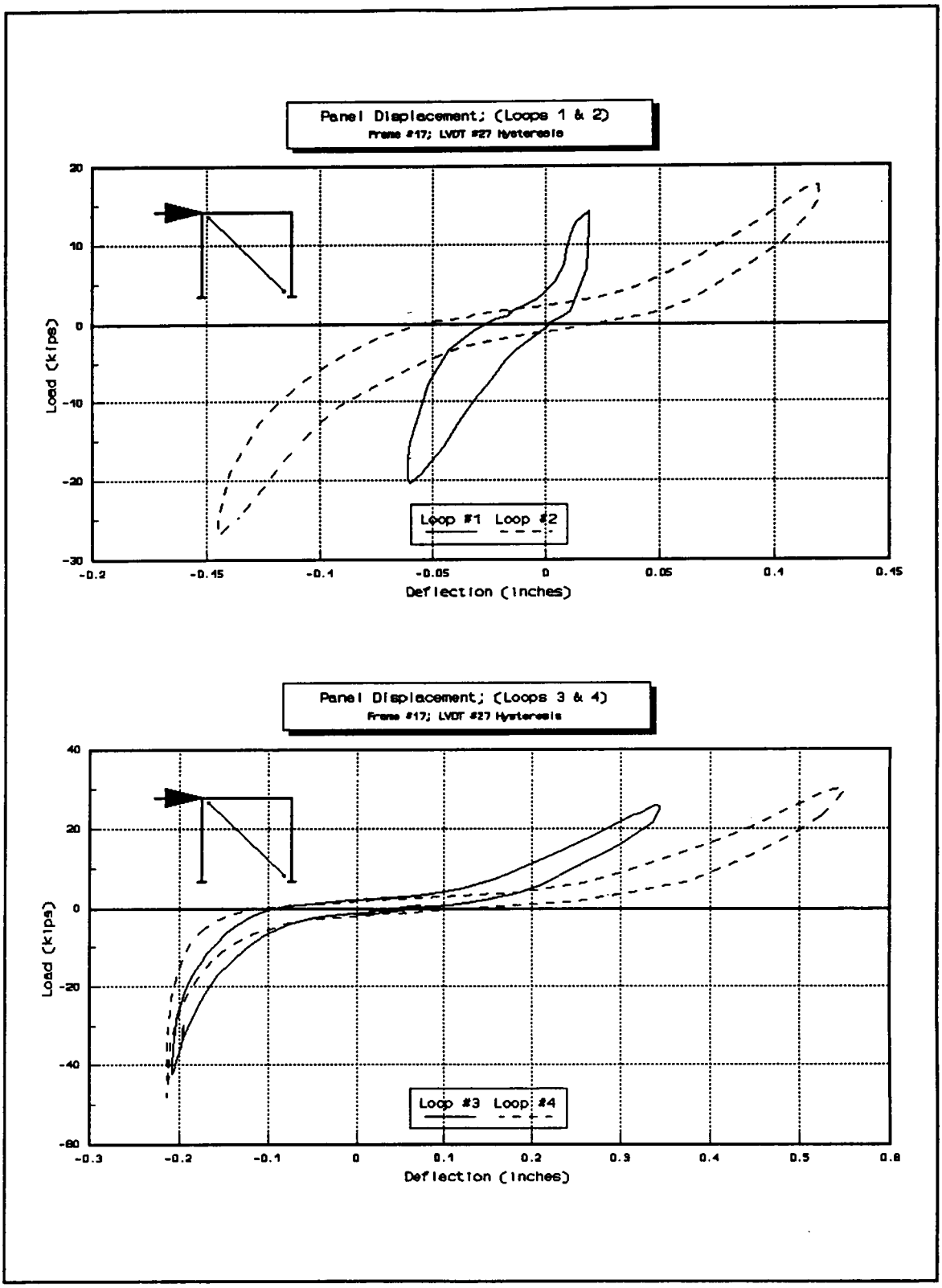


Figure 5.15: Frame #17; LVDT #27 hysteresis

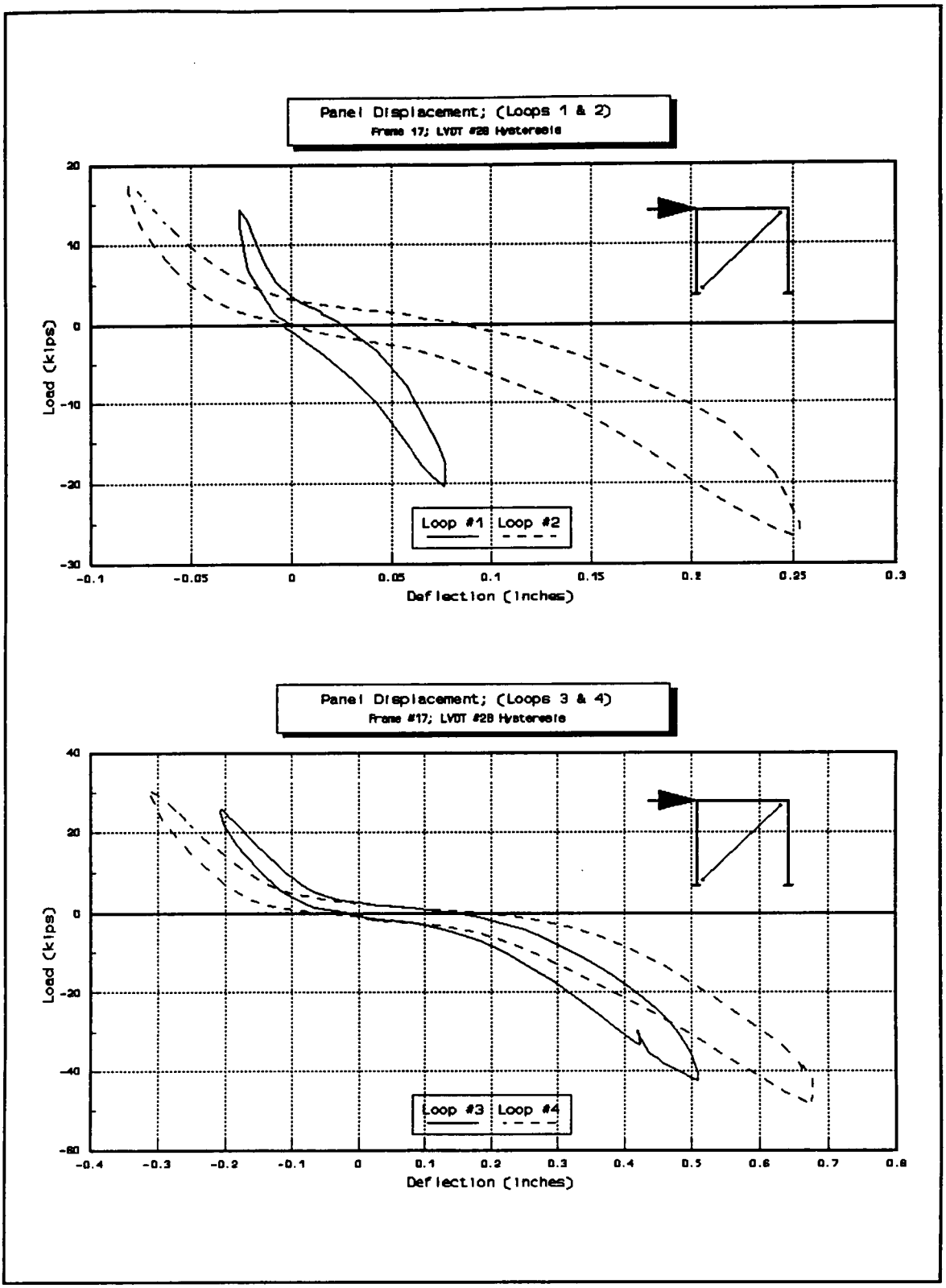


Figure 5.16: Frame 17; LVDT #28 hysteresis

was a large increase in deflection at the maximum compressive load. Once banded diagonal cracking had occurred, after loop three, the deflection more than doubled at the maximum compressive load. This indicated, as in frame 2, that the stair step crack was opening further after the tension failure in the mortar had occurred.

Figures 5.17 and 5.18 illustrate the four load-deflection hysteresis loops of the panel horizontal and vertical LVDT's, respectively. The horizontal and vertical LVDT's remain in tensile strain from the time of diagonal cracking to the end of the test. For frame 2, the panel vertical strains were significantly greater than that of the horizontal strains at the maximum compressive loads. This effect was present in frame 17 for loops three and four, though not as pronounced. In fact, the vertical strains at the compressive loads from loops one and two were slightly less than the horizontal strains.

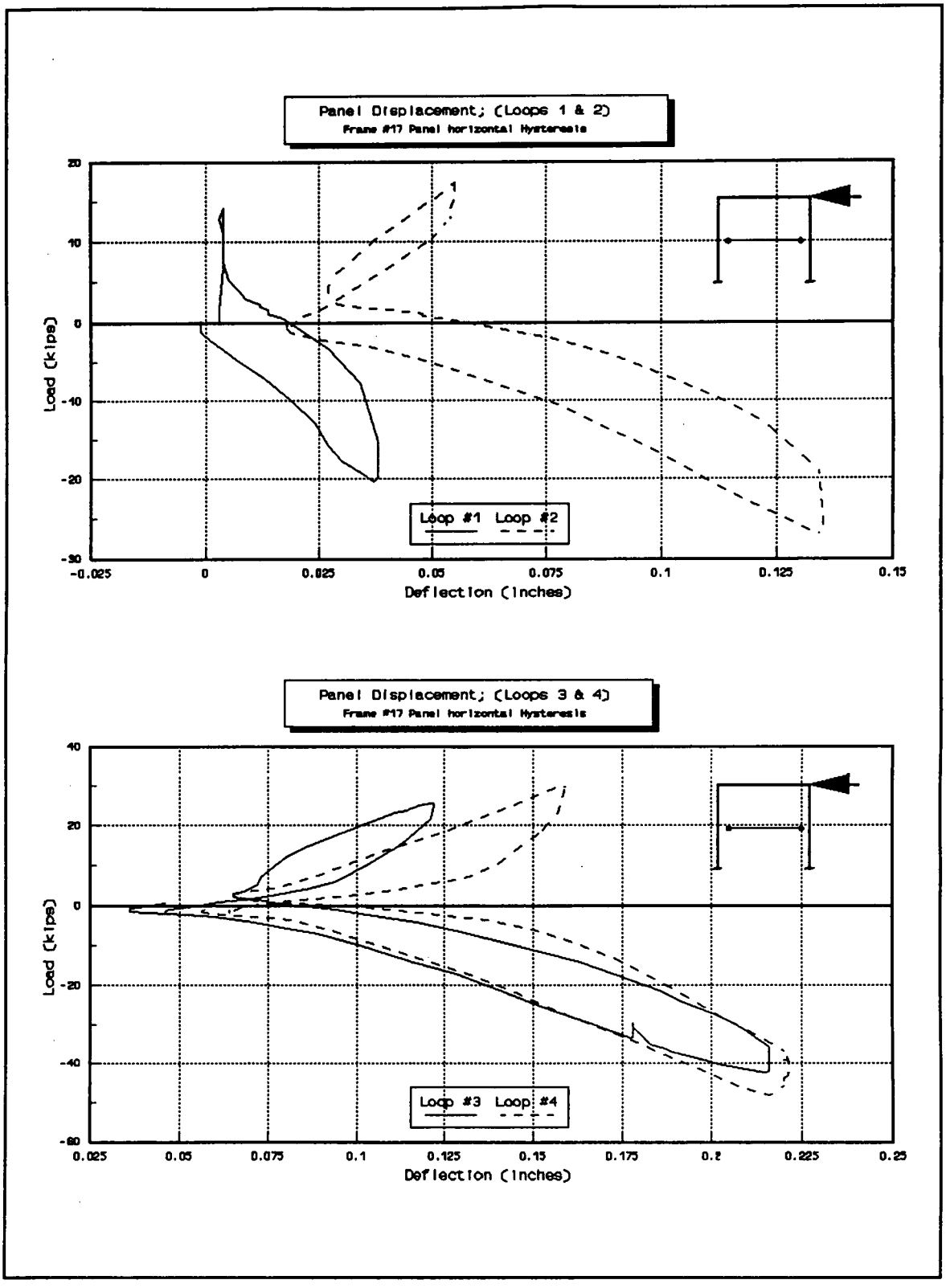


Figure 5.17: Frame 17; Panel horizontal hysteresis

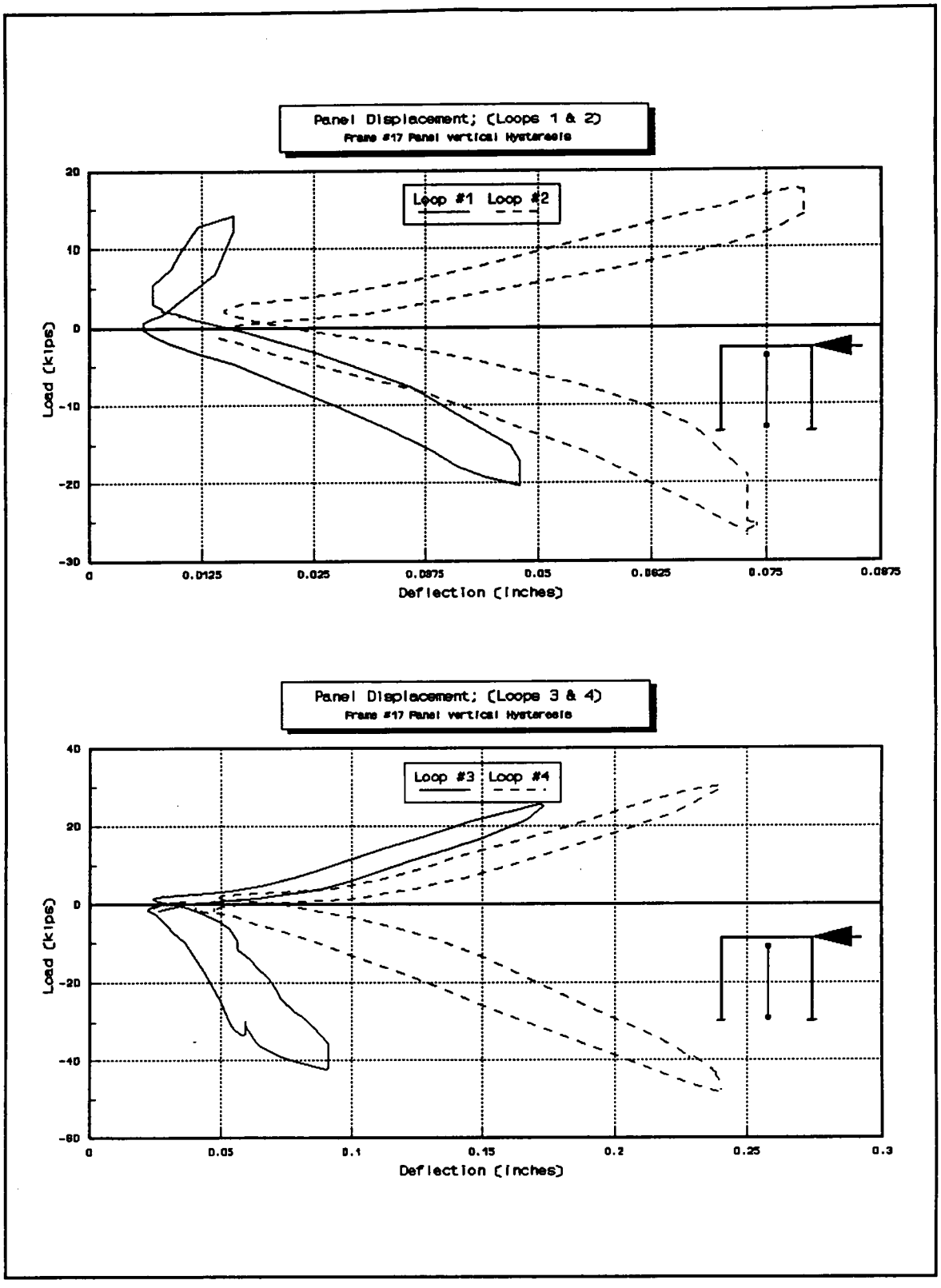


Figure 5.18: Frame 17; Panel vertical hysteresis

Chapter 6: **FRAME-PANEL RELATIVE MOVEMENT**

6.1 Introduction

The displacements of the panel relative to the frame are considered in this chapter. Each individual relative LVDT load-displacement hysteresis is examined first. Referring to figure 4.1, plots were constructed of the displacement of LVDT's 12, 13, 20, and 21 versus the beam centerline displacement. These LVDT positions correspond to the top and mid-height positions of the columns on either side of the frame. Lastly, a comparison of behavior is made between the load-deflection hysteresis of the four aforementioned LVDT's and the hysteresis of frame LVDT's at the same elevations.

6.2 Relative hysteresis

LVDT's were attached to the columns and the beam around the perimeter of the panel in order to gage relative displacement between the panel and the frame. The load-deflection hysteresis curves and centerline versus relative deflection curves of frames 2 and 17 for four of the six loops studied in chapter's 4 and 5 are examined first. A positive displacement indicates an extension of the LVDT or an opening of the gap. The panel and relative LVDT's were removed just after the ultimate load was achieved to avoid damage. In the interest of clarity, each of the load-deflection hysteresis curves

illustrates the test specimen showing the location of the respective LVDT.

6.2.1 Frame 2 Relative Hysteresis

Figures 6.1 through 6.9 illustrate the load-deflection curves for frame 2. Figure 6.1 depicts all four loops for LVDT 12, the top relative LVDT on the leeward side of the frame. All four loops exhibit similar behavior. The flat portion of the curves indicates that there has been significant deterioration of the panel-beam interface, and that gapping is occurring. As the specimen was loaded in compression, the frame pushed away from the panel, indicating that there was no tensile bond between the panel and the columns by this point. This is shown by the positive flat-line increase in deflection in the compressive loading portion of the curve. The lateral deflection of the windward column was slightly greater than the leeward column; therefore, the system reached a point in compression where the infill engaged the leeward column again. From this point, the relative deflection decreased, which may indicate some mortar crushing and probably some plastic deformation of the tile in the latter stages. The decrease in deformation with increasing compressive load was significantly greater in loop four as compared to loop one.

As the specimen was loaded in tension, the leeward column was pulled towards the panel, thus closing the gap between the

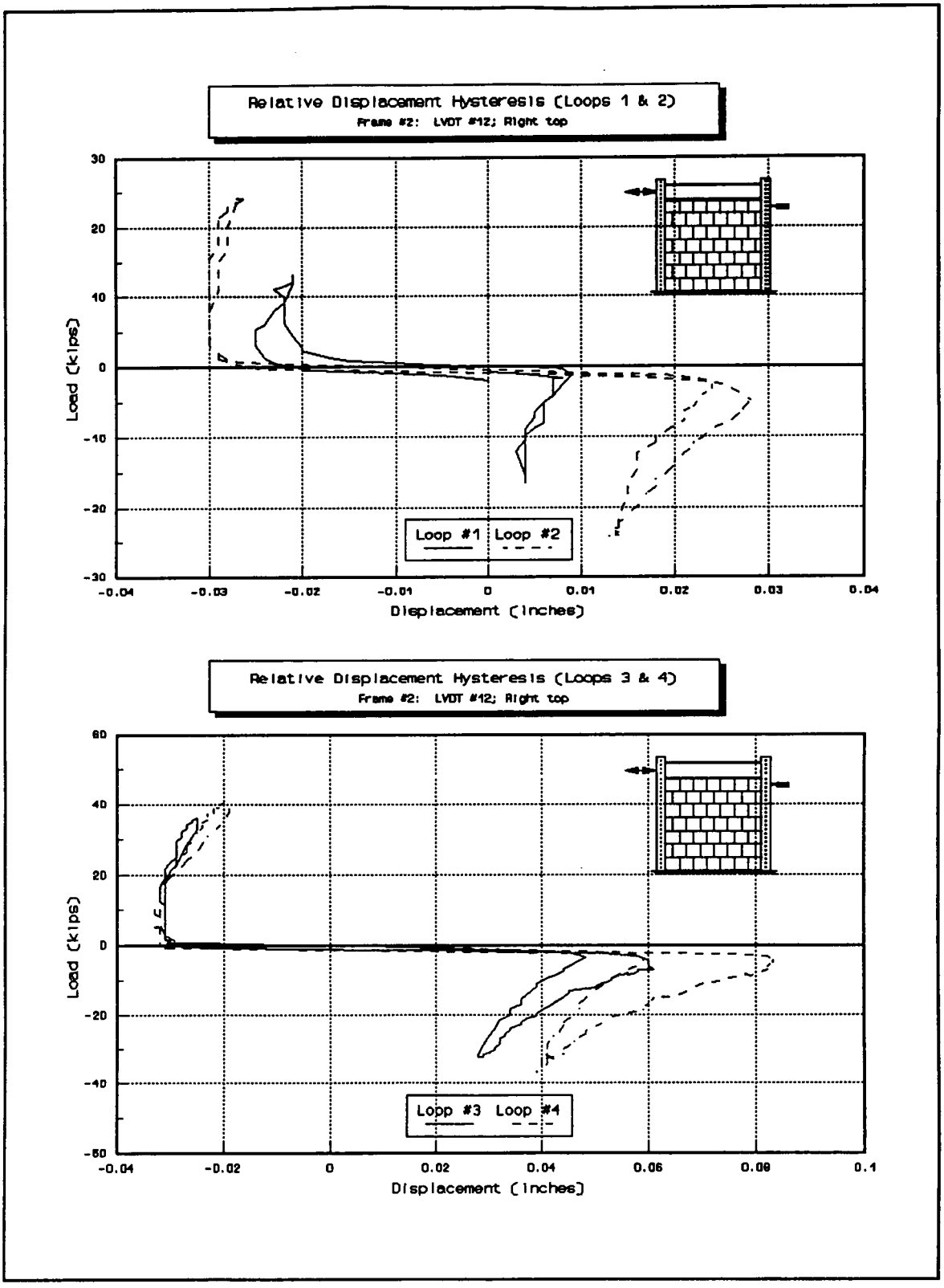


Figure 6.1: Frame 2; LVDT 12 hysteresis

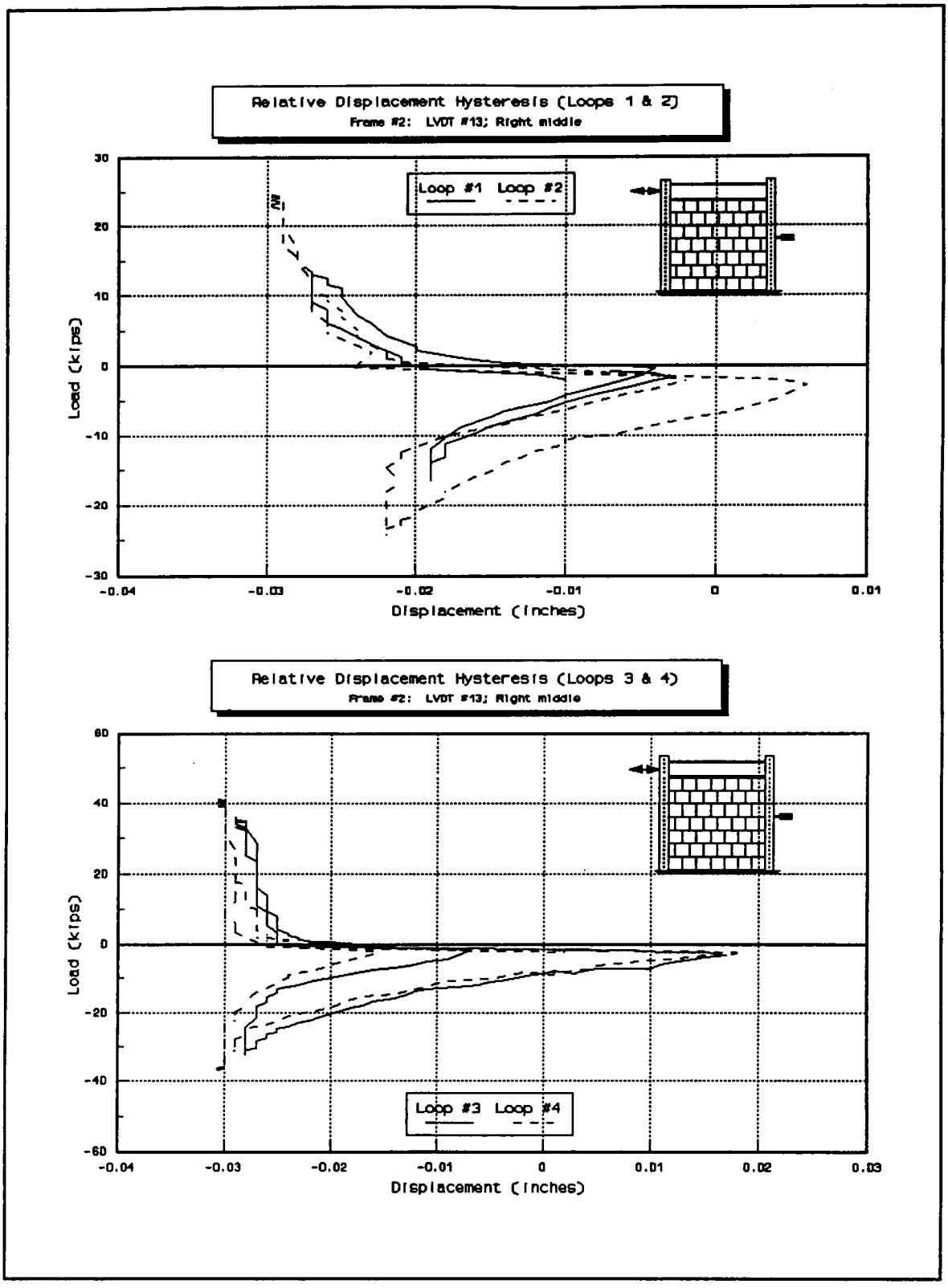


Figure 6.2: Frame 2; LVDT 13 hysteresis

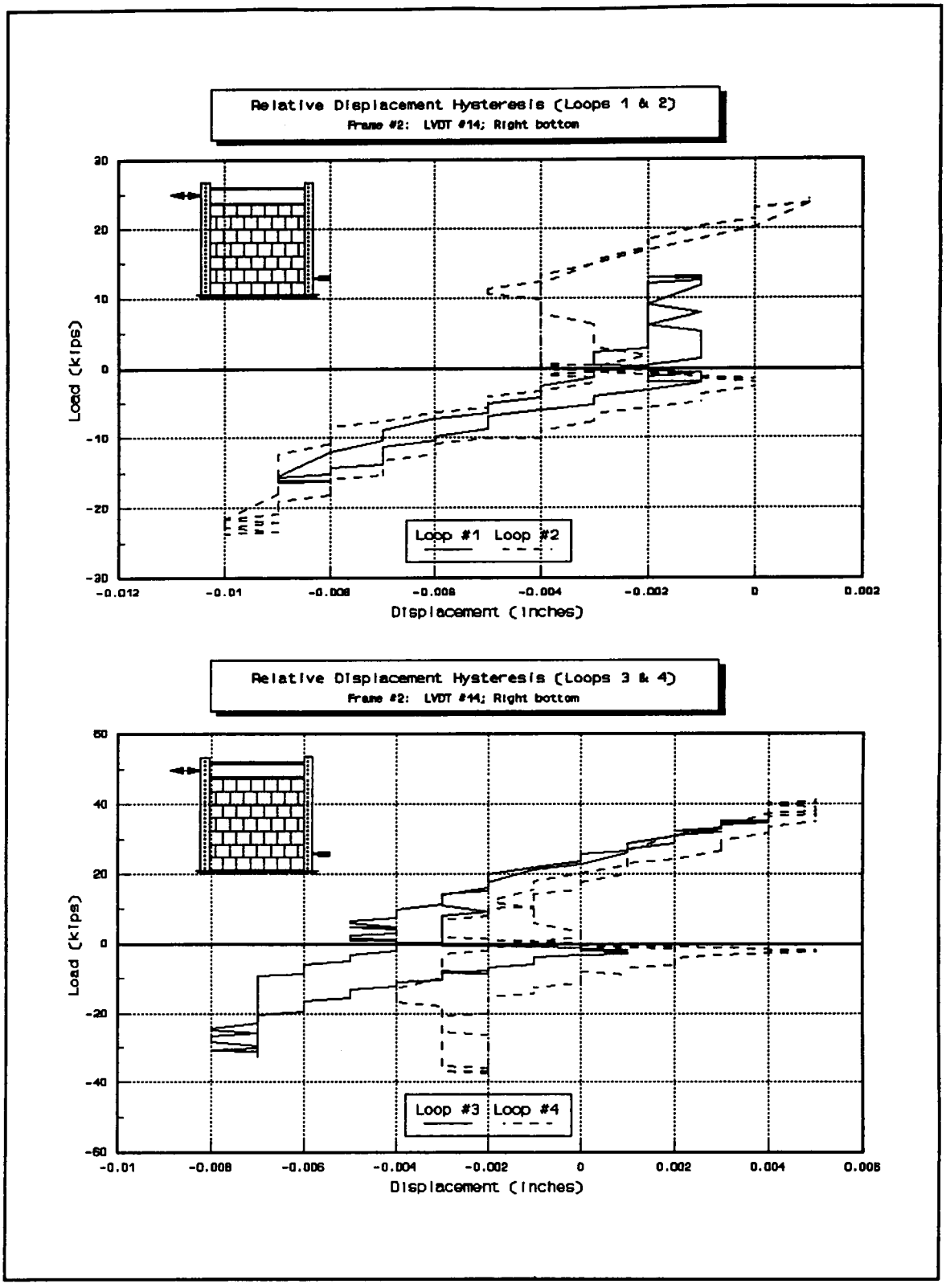


Figure 6.3: Frame 2; LVDT 14 hysteresis

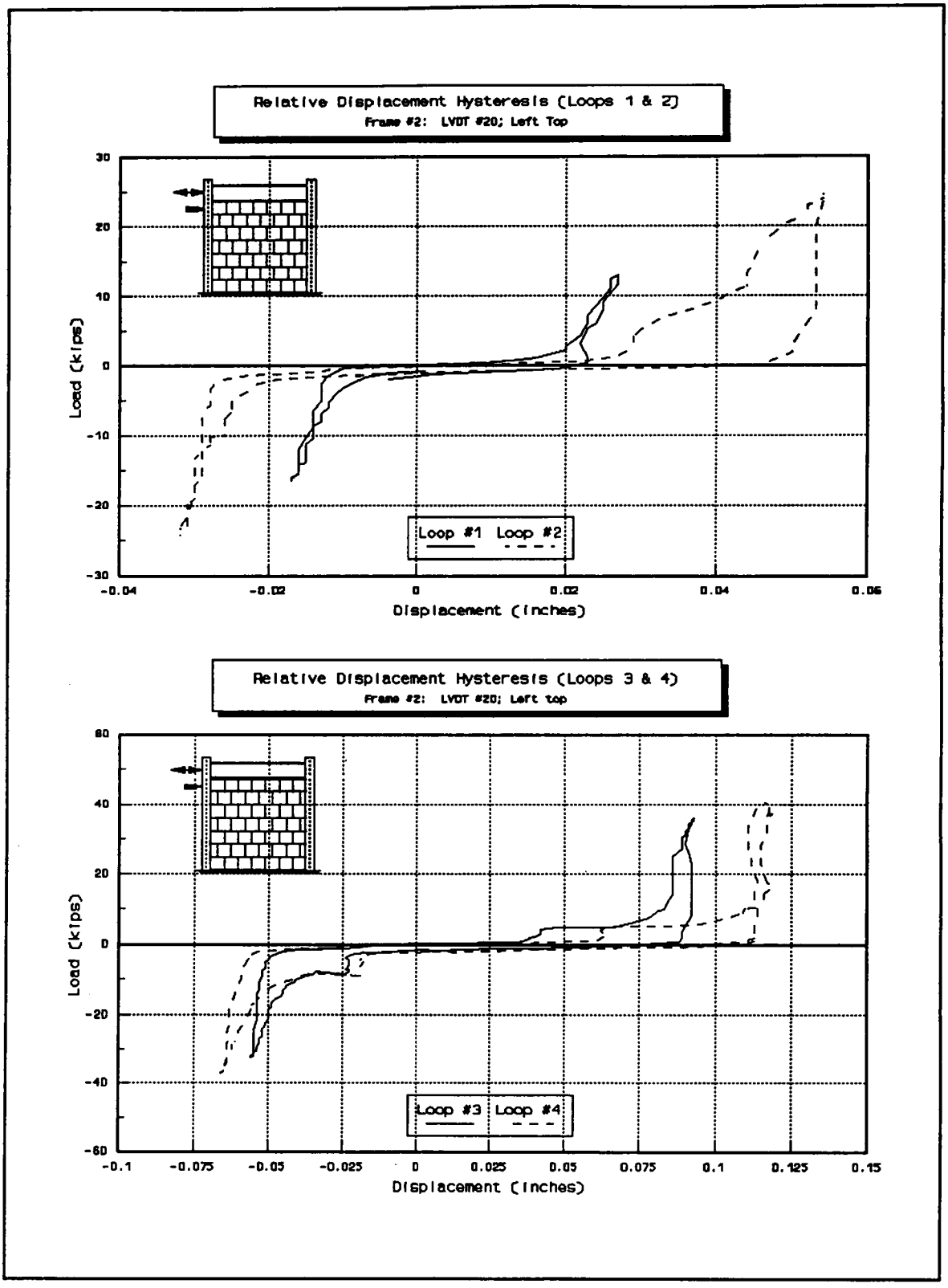


Figure 6.4: Frame 2; LVDT 20 hysteresis

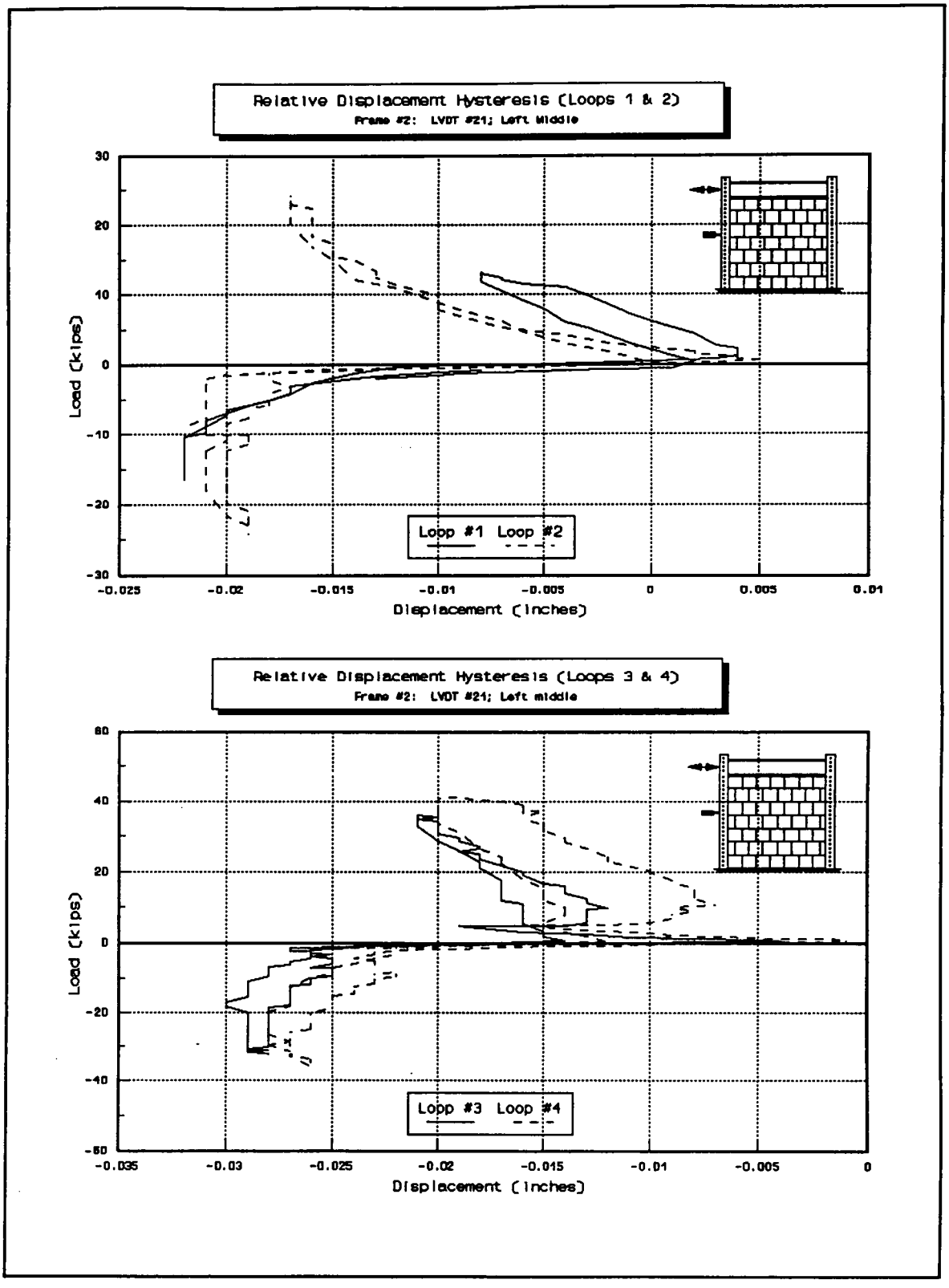


Figure 6.5: Frame 2; LVDT 21 hysteresis

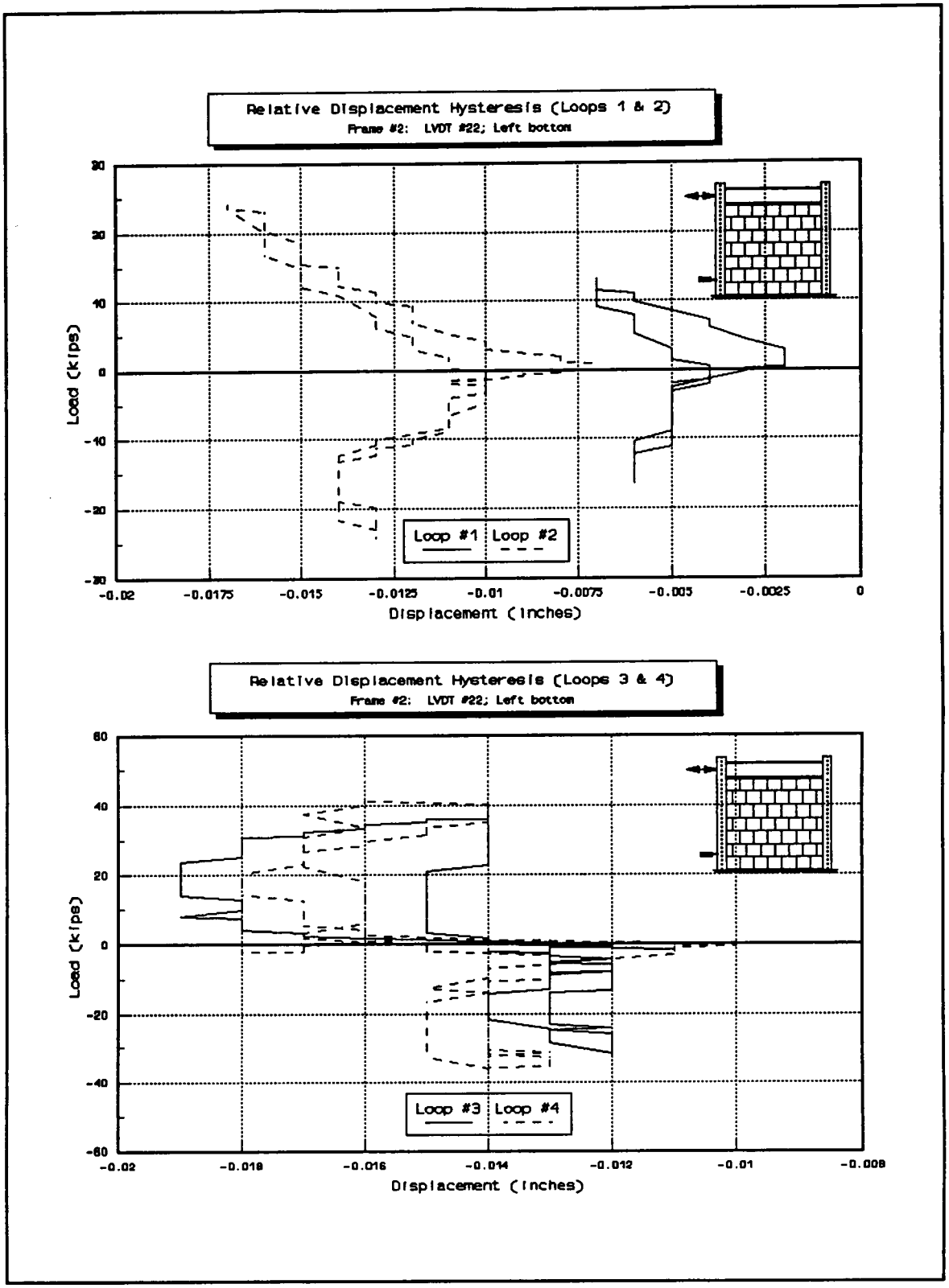


Figure 6.6: Frame 2; LVDT 22 hysteresis

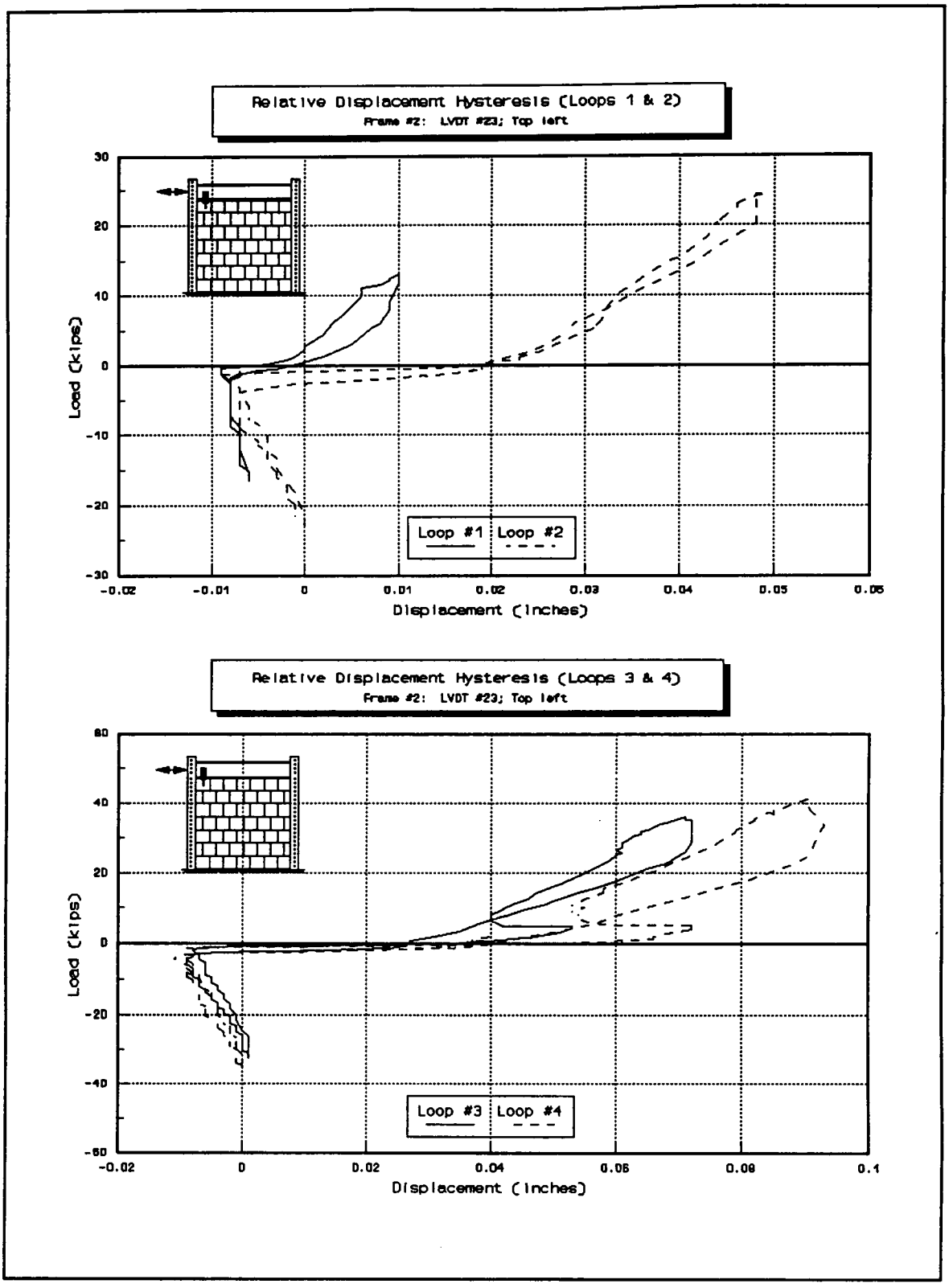


Figure 6.7: Frame 2; LVDT 23 hysteresis

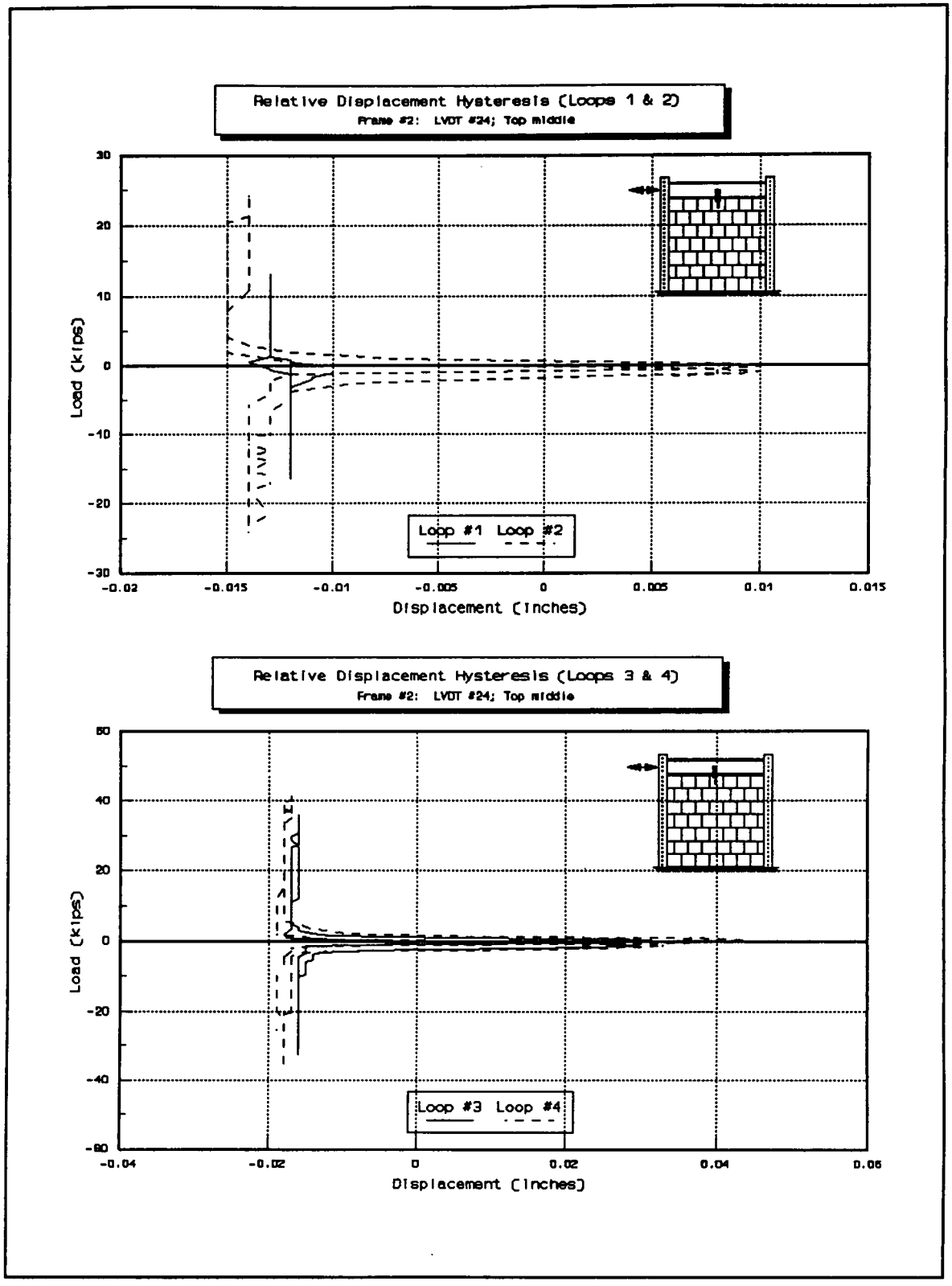


Figure 6.8: Frame 2; LVDT 24 hysteresis

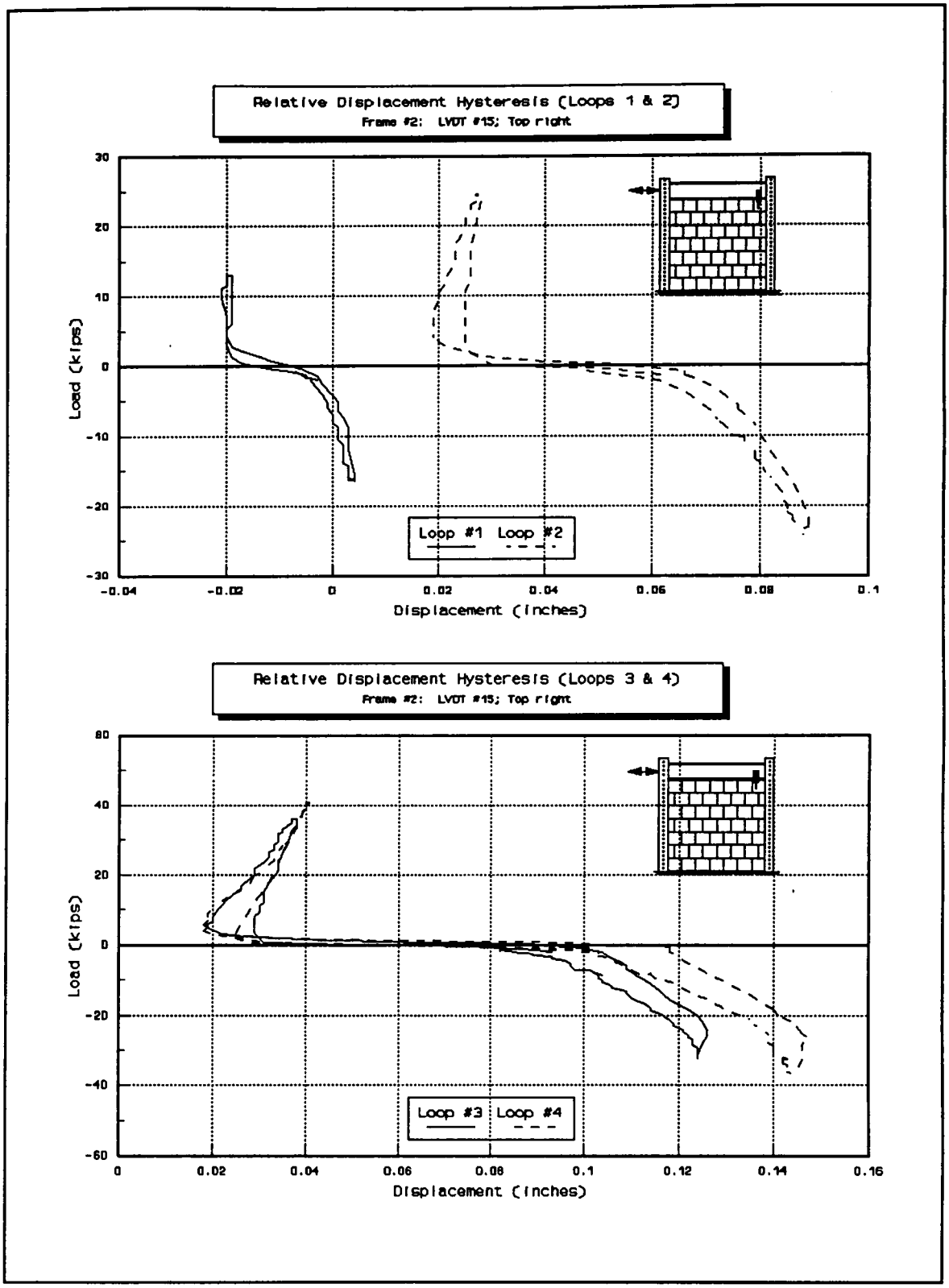


Figure 6.9: Frame 2; LVDT 15 hysteresis

panel and the frame. This is accounted for with the flat-line portion of the tensile segment of the curve. As the frame engages the panel, the relative deflection remains fairly constant with increasing load for loops one and two. The tensile portion of loops three and four, exhibited a slight increase in deflection after the panel had engaged the wall.

Figure 6.10 depicts the relative displacement of LVDT 12 versus the beam centerline displacement for all four loops. All four loops behave similarly with the hysteresis curve opening up as the system approaches ultimate. Figure 6.10 can be used to validate the above described behavior due to the fact that these curves behave similarly to the load-deflection hysteresis curves for LVDT 12.

Figure 6.2 illustrates the four hysteretic loops for LVDT 13, which was the LVDT located at panel mid-height on the leeward column. The behavior of this relative displacement hysteresis was quite different from that of LVDT 12. As the system was loaded compressively, there was a steady increase in deflection accompanied by an increase in load with no flat-line portion. This demonstrates a lesser degree of panel-frame separation at the mid-height. The decrease in relative deflection cannot be explained by mortar crushing because during the dismantling of the system after testing, there was little mortar joint degradation between the column and panel observed at this elevation. Figure 6.11, the beam centerline

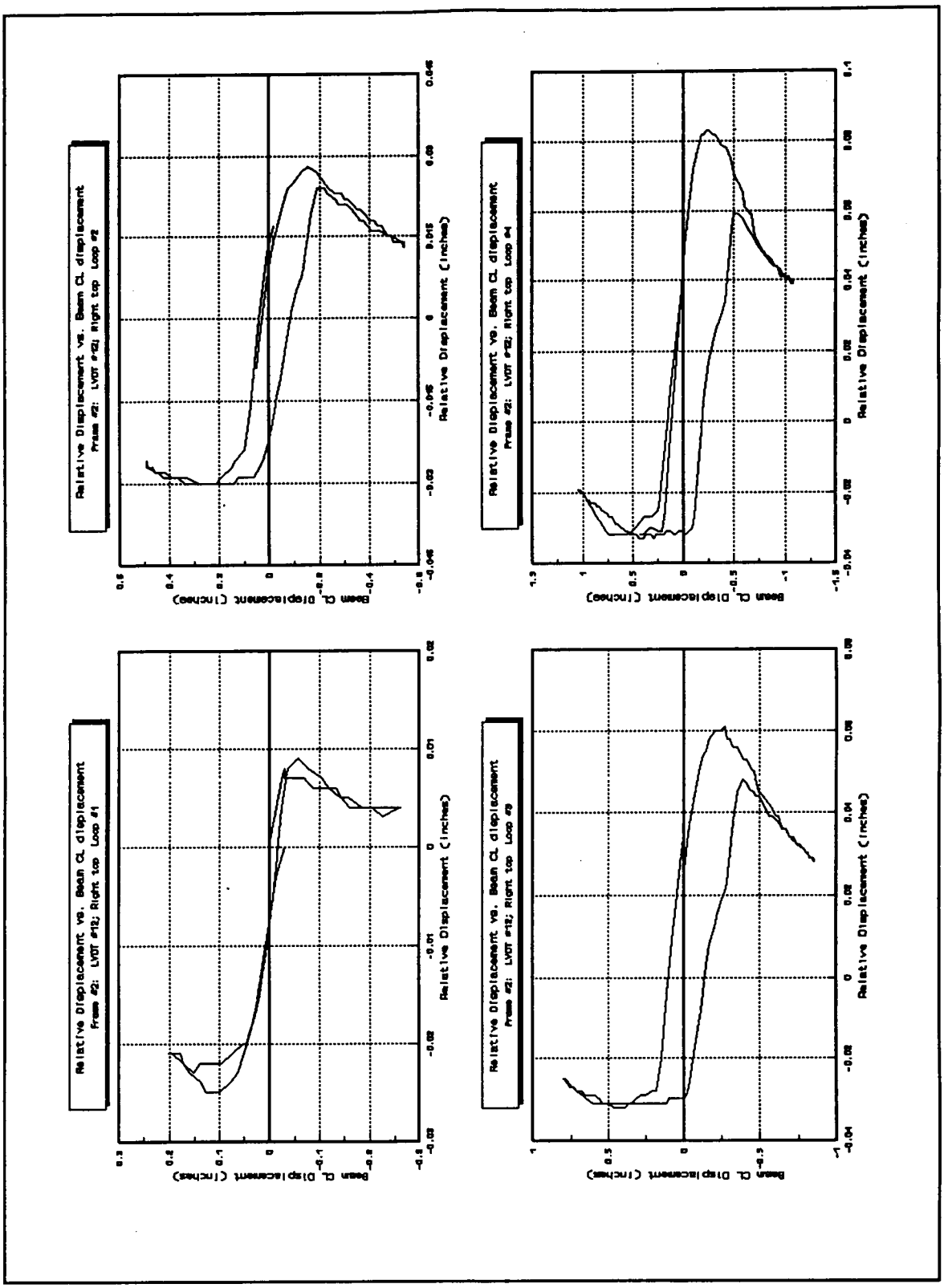


Figure 6.10: Frame 2; LVDT 12 vs. Beam CL deflection

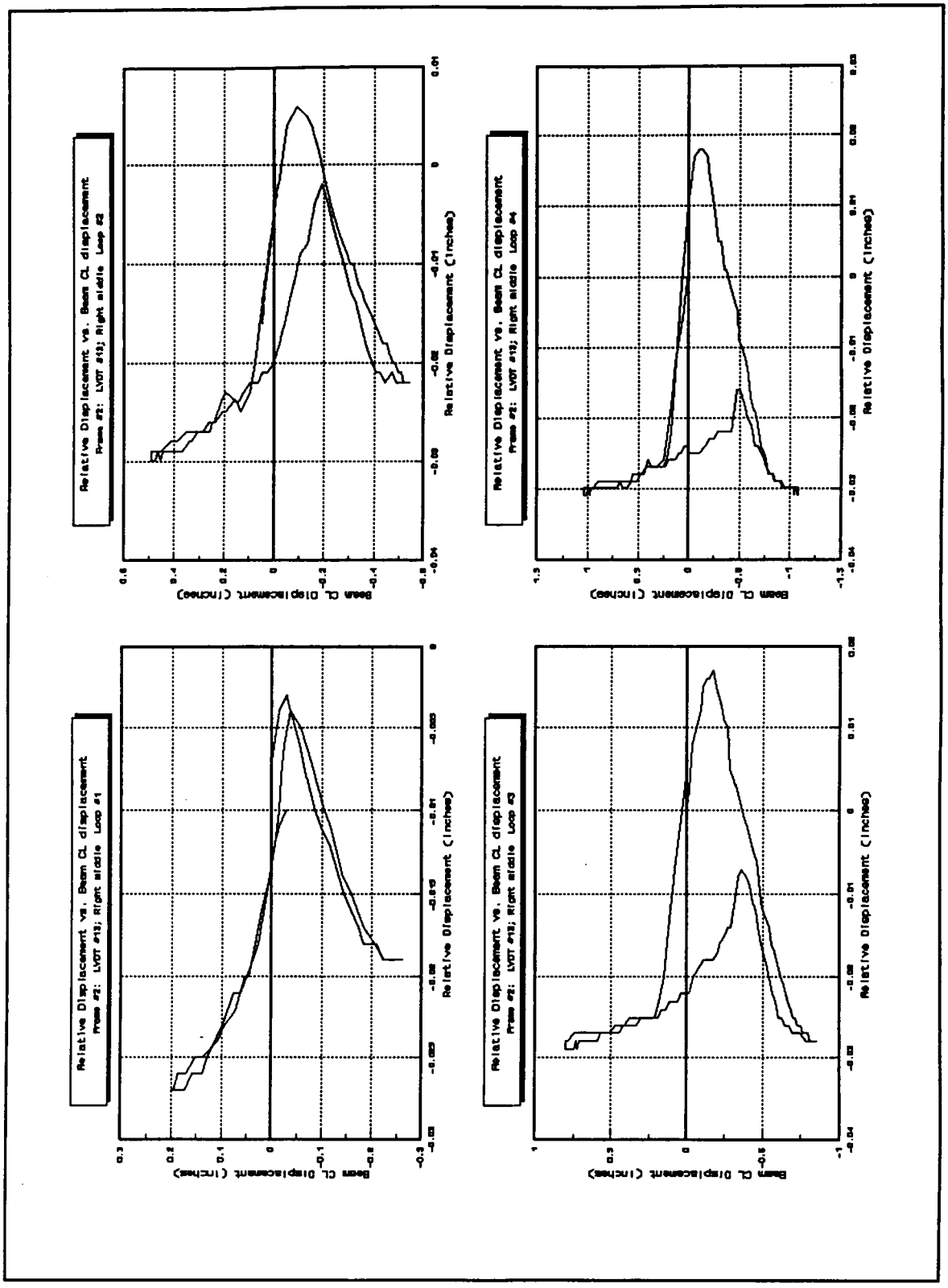


Figure 6.11: Frame 2; LVDT 13 vs. Beam CL deflection

displacement versus LVDT 13 displacement, demonstrates similar behavior as that of the load-deflection hysteresis.

Figure 6.3 illustrates the load-deflection hysteresis for LVDT 14. This corresponds to a relative displacement at six inches from the floor level. The behavior of this hysteresis for the entire test was rather erratic. Closing of the gap during compressive loading and opening of the gap during tensile loading was observed. Upon removal of the panel after testing, there was little mortar crushing observed in this area.

Figure 6.4 represents the load-deflection hysteresis for LVDT 20. The deflection decreases slightly after the initial gap closes indicating some mortar deformation and crushing. It is likely that the deflection decrease was due to some small non-linear deformation of the tile since this LVDT was connected to a tile that was part of the compression diagonal. Overall, the behavior indicates a stiff joint. The total compressive deflection was 0.01 inches in loop one and increased only to 0.055 inches in loop four. The tensile displacements were about twice the compressive displacements. The compressive behavior of LVDT 20 was identical to the tensile behavior of LVDT 12, the leeward column counterpart. This was a common characteristic for all the relative LVDT's. Figure 6.12 illustrates the beam centerline deflection versus the relative displacement for LVDT 20, indicating similar behavior as that of the load-deflection hysteresis.

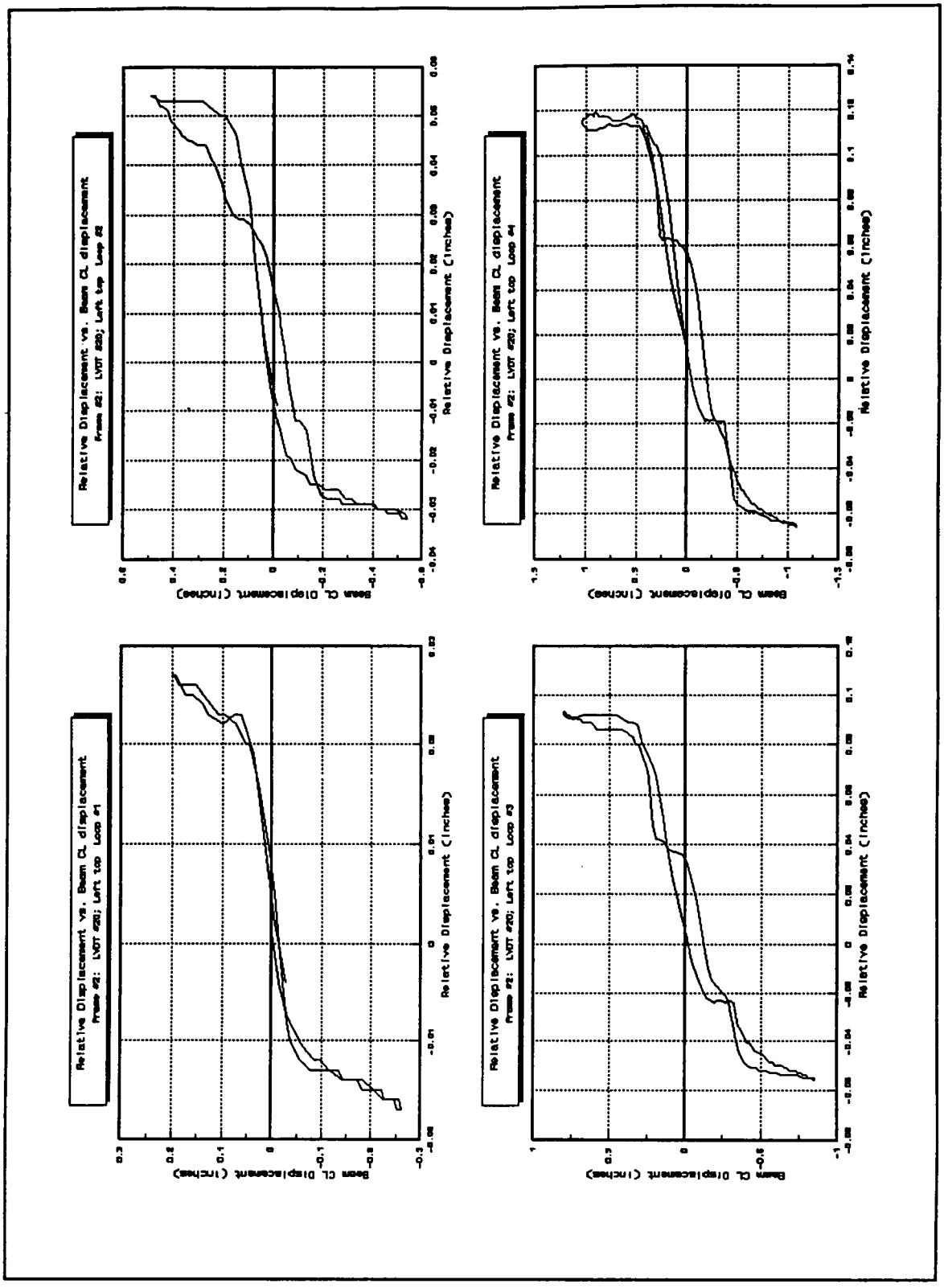


Figure 6.12: Frame 2; LVDT 20 vs. Beam CL deflection

Figure 6.5 depicts the load-deflection hysteresis for LVDT 21, which was located at panel mid-height on the windward column. The hysteresis demonstrated comparable behavior to that of it's counterpart on the leeward column. However, as the system reached it's maximum compressive load for each cycle, there was a slight decrease in the relative displacement. This may be accounted for by some head joint crushing along the panel. Figure 6.13 illustrates the beam centerline deflection versus the relative displacement of LVDT 21, which also exhibits similar behavior.

Figure 6.6 illustrates the load-deflection behavior of LVDT 22, which was located on the bottom windward column. There was an offset of the hysteresis loops between loop one and loop two. This indicates that there may have been some cracking of the tile at some time between these two loops or a slippage of the LVDT. This would shift the zero point of the LVDT.

Figure 6.7 represents the load-deflection hysteresis of LVDT 23, which was located at the top left corner of the beam-panel interface. With all four loops, the deflection was positive, indicating an opening of the gap both in compressive and tensile loadings. Although the frame connections were designed as simple connections, some moment was probably transferred to the beam and in compressive loading, the loaded end of the beam may have been slightly lifted away from the panel. The opening of the interface in tensile loadings was

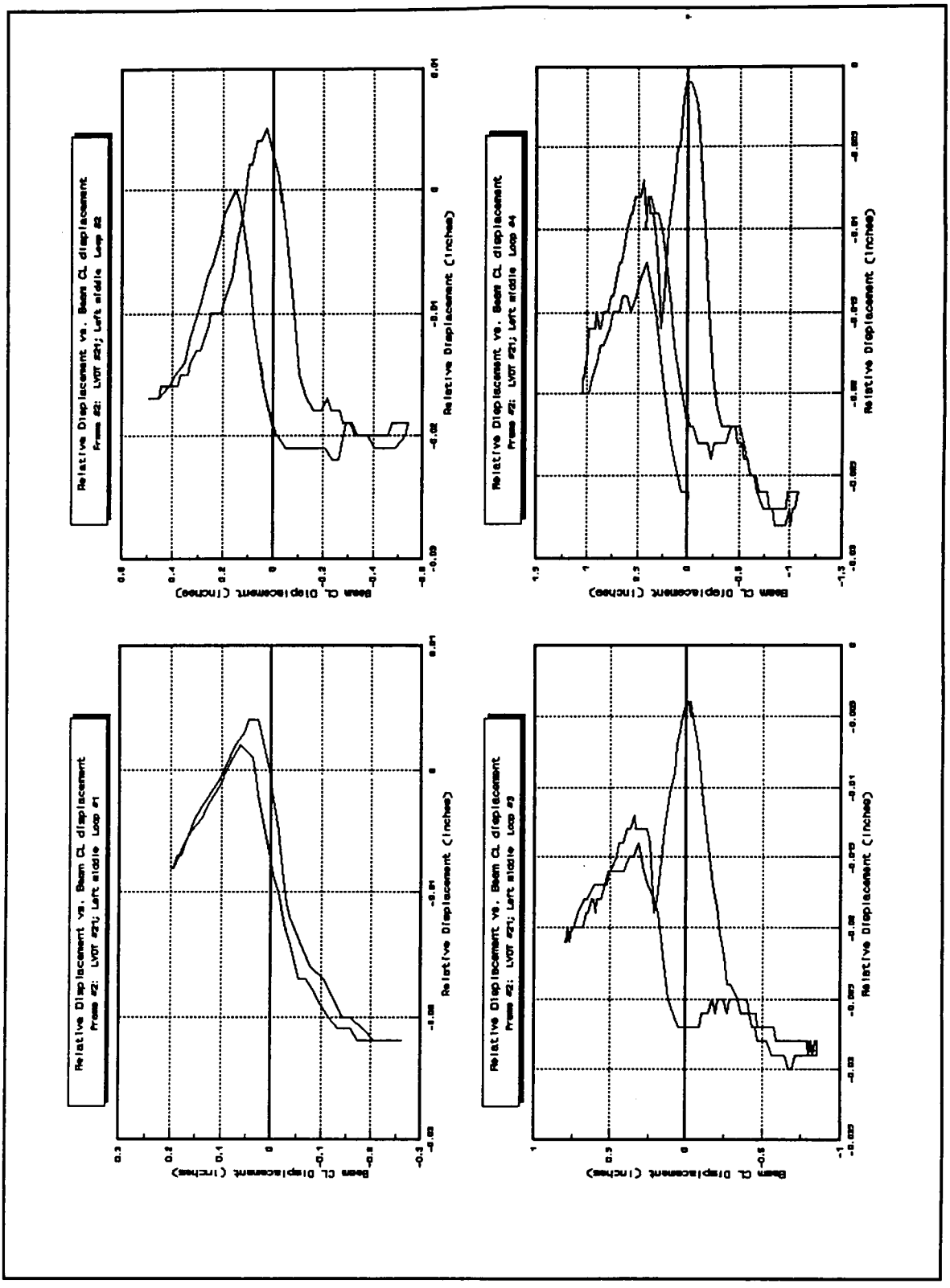


Figure 6.13: Frame 2; LVDT 21 vs. Beam CL deflection

as much as five to eight times that of the opening during compression.

Figure 6.8 illustrates the load-deflection behavior of LVDT 24. This LVDT was located on the beam-panel interface at the mid-point of the panel. In both compressive and tensile loadings, there was a flat-line decrease in relative displacement. This indicates that the interface was closing as the system was loaded in compression and tension. As noted in chapter 5, through observation of the vertical panel strains, at maximum compressive and tensile loadings, the vertical strains were always increasing. This is reflected in the always decreasing relative deflection of LVDT 24.

Figure 6.9 illustrates the load-deflection hysteresis of LVDT 15, which was located at the beam-panel interface in the leeward corner of the panel. Between loops one and two, there was a shift of the LVDT's zero point. As with LVDT 22, in the bottom windward corner, there was probably some corner crushing of the tile that would account for this slip. In compression, the curve behaves as expected, there was an increase in relative deflection meaning that the gap was opening with increasing load. As the frame was loaded in tension, the beam-panel interface closes with a slight opening as the frame reached it's maximum tensile load for the loop. This can be explained in the same manner as the opening of the beam-panel gap at the windward corner during compressive loading. In other words, the behavior of LVDT 15 and 23 were

identical by comparing the tensile and compressive behavior of each respective LVDT.

6.2.2 Frame 17 Relative Hysteresis

Figures 6.14 through 6.22 illustrate the load-deflection hysteresis for the relative LVDT's of frame 17. Figure 6.14 represents the four loops studied for LVDT 12. The four loops exhibit the same behavior as that of LVDT 12 for frame 2. As compared with frame 2, the relative displacements for this LVDT were significantly greater. Figure 6.23 depicts the beam centerline deflection versus LVDT 12 displacement.

Figure 6.15 illustrates the load deflection hysteresis of LVDT 13, which was located at the panel mid-height on the leeward side of the wall. There was a shift in the zero point of the LVDT before loop one. This may have been the result in cracking of the mortar joint around the tile to which the LVDT was connected; thus, allowing the tile itself to shift. The load-relative displacement behavior for this LVDT was somewhat different from that of the same LVDT for frame 2. The compressive loading portion of the curves behaved similarly. As the frame was loaded in compression, the panel-column interface began to open until the panel was engaged by the windward column. From here, the panel-column interface gap decreased. Again, there was insignificant mortar crushing observed upon dismantling the frame at this location;

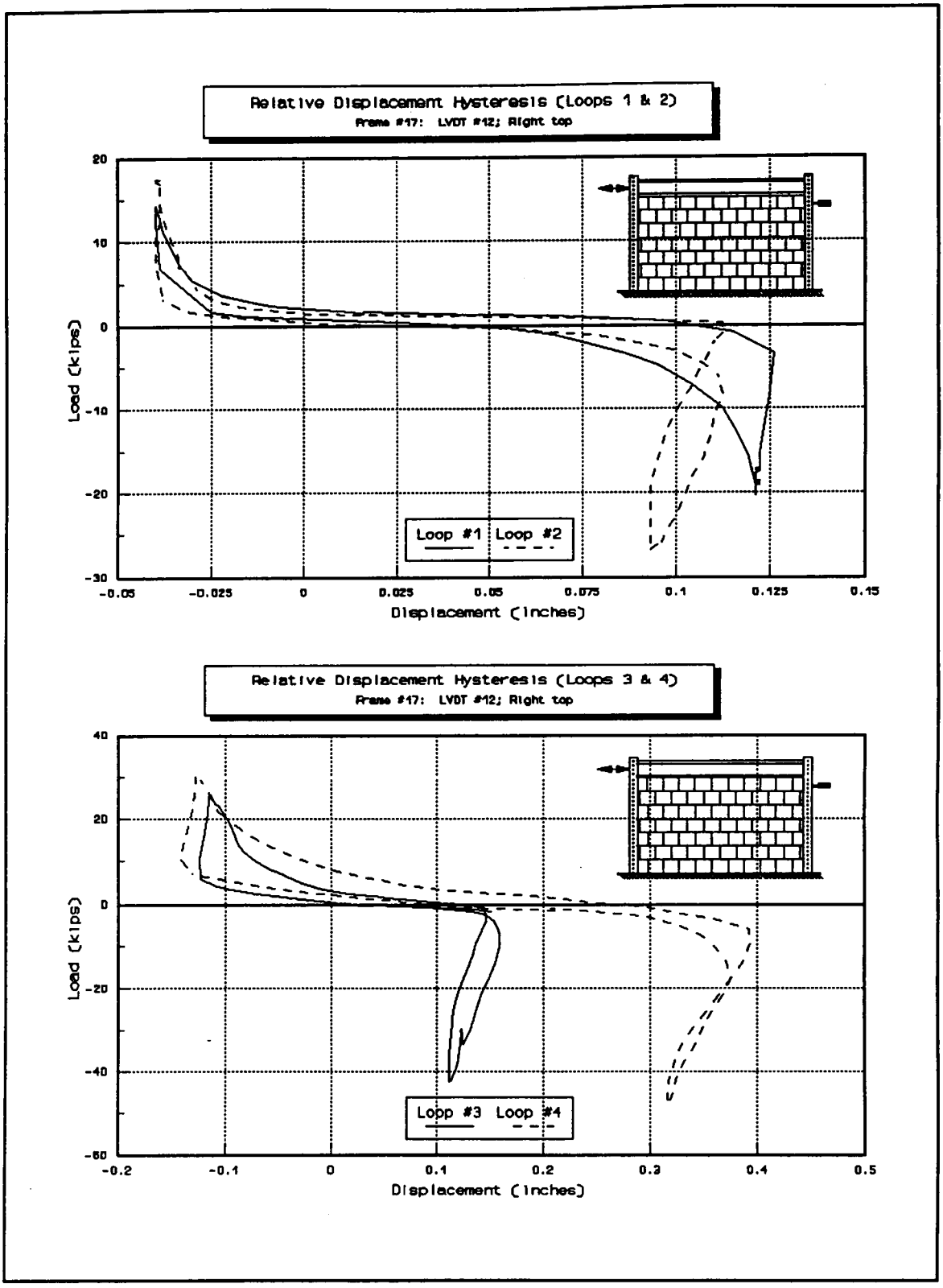


Figure 6.14: Frame 17; LVDT 12 hysteresis

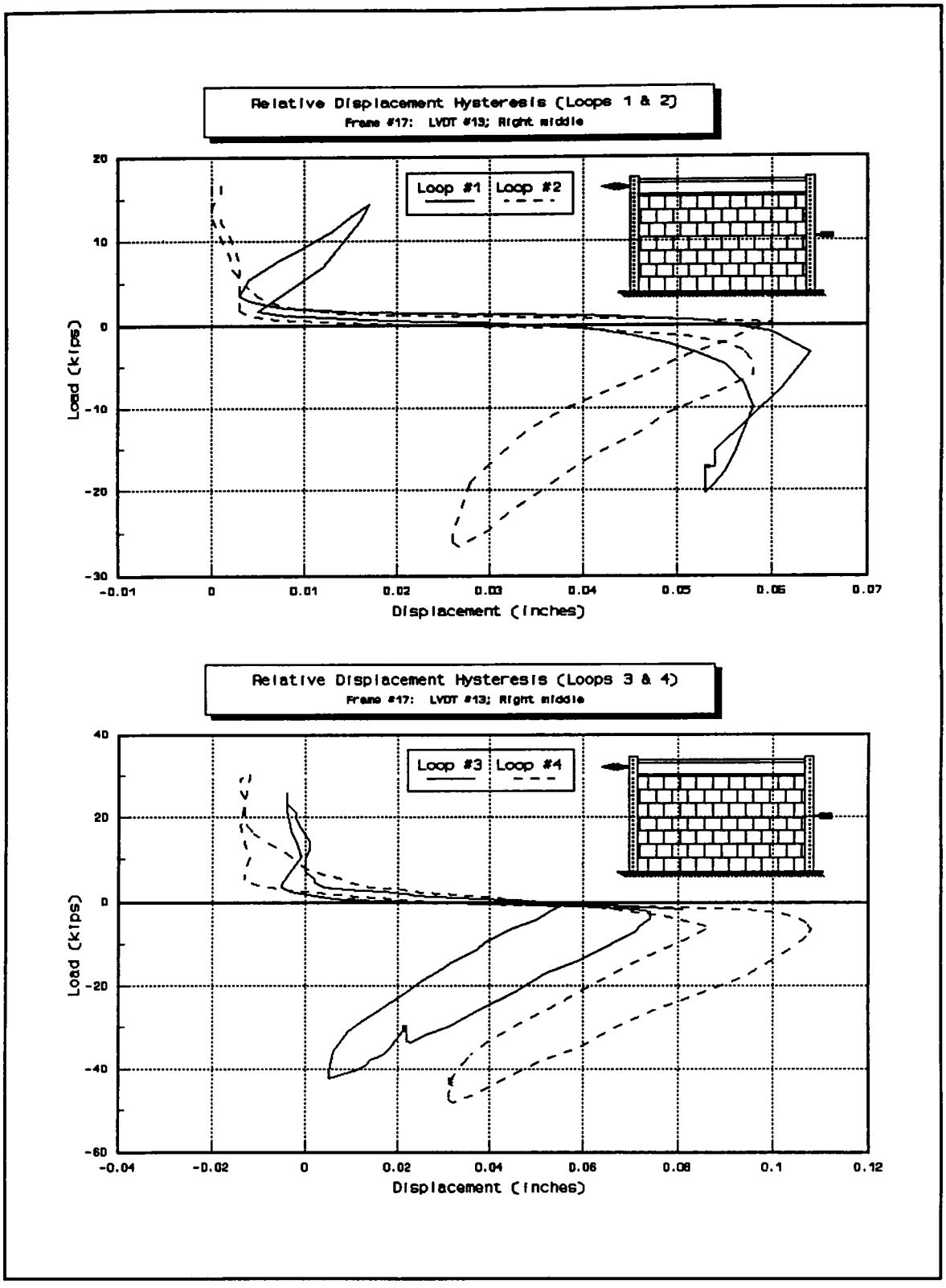


Figure 6.15: Frame 17; LVDT 13 hysteresis

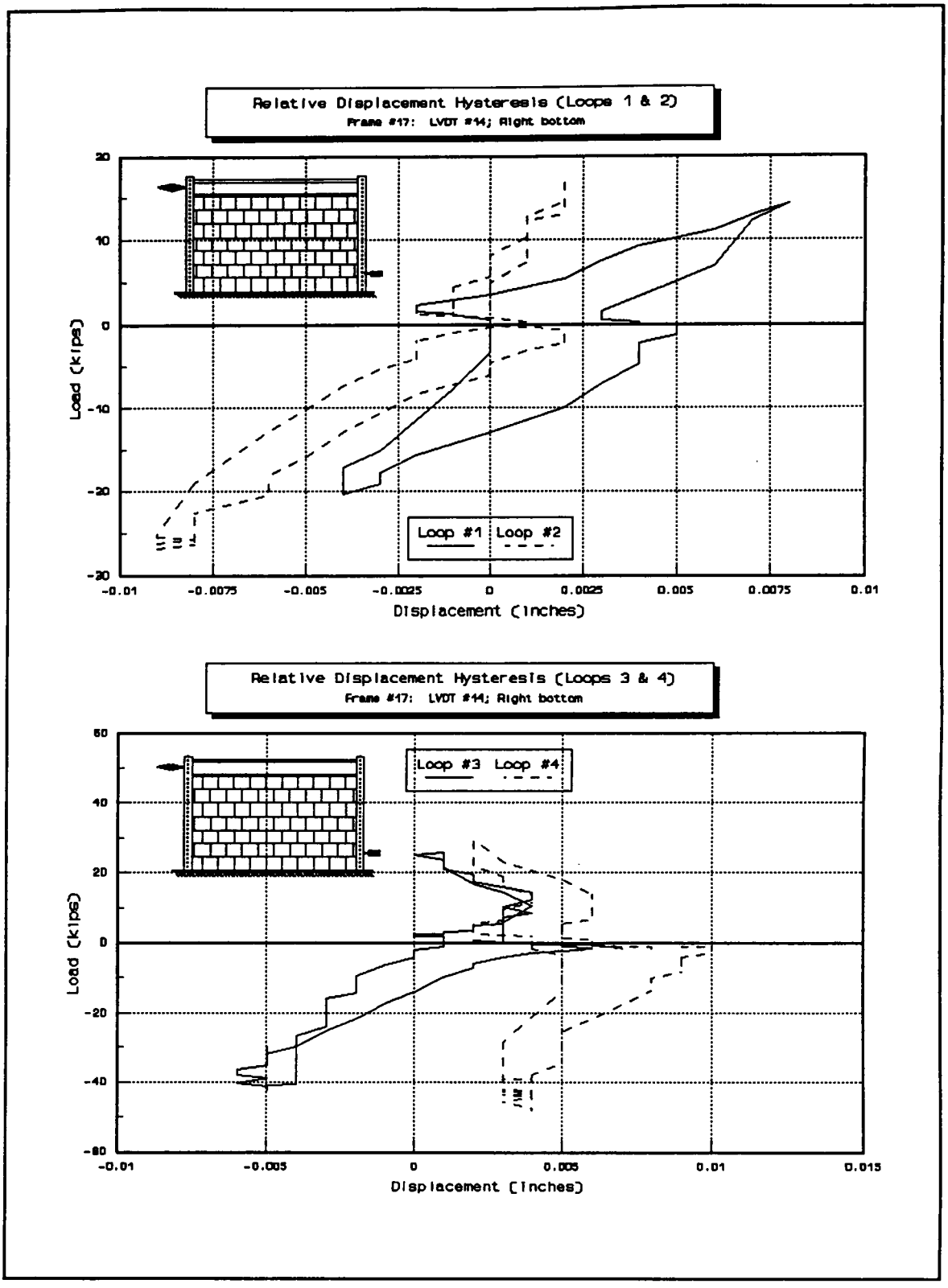


Figure 6.16: Frame 17; LVDT 14 hysteresis

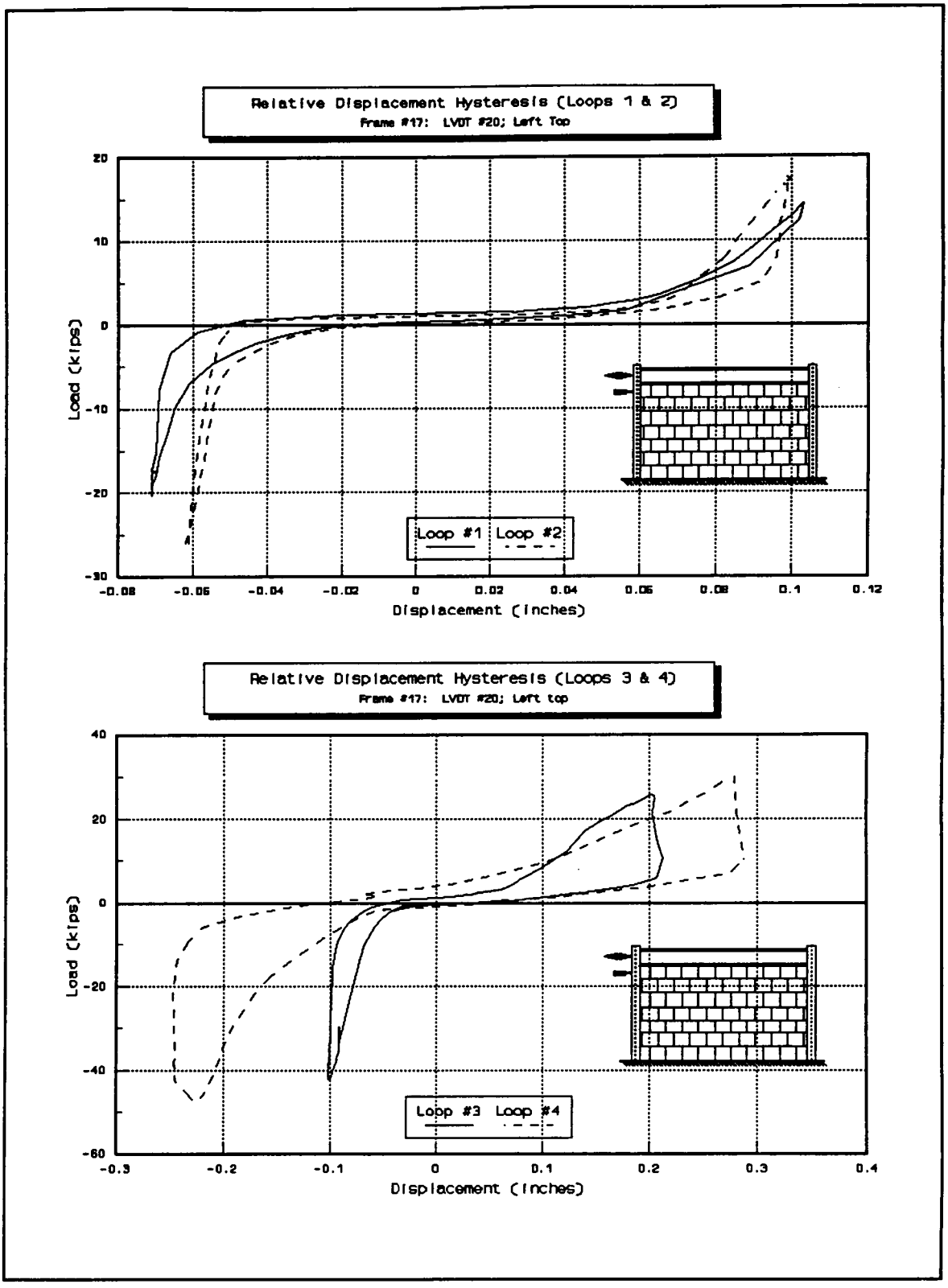


Figure 6.17: Frame 17; LVDT 20 hysteresis

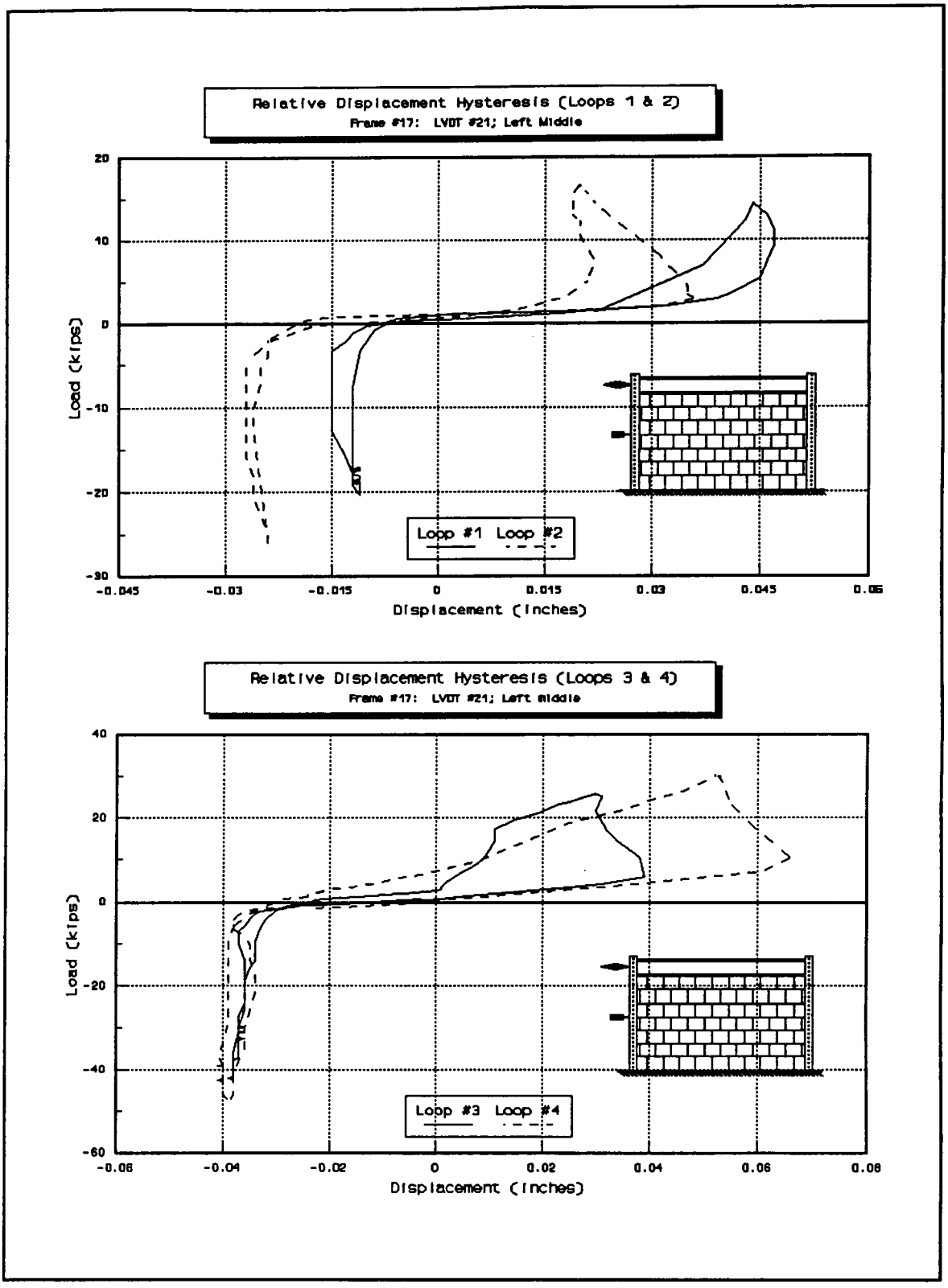


Figure 6.18: Frame 17; LVDT 21 hysteresis

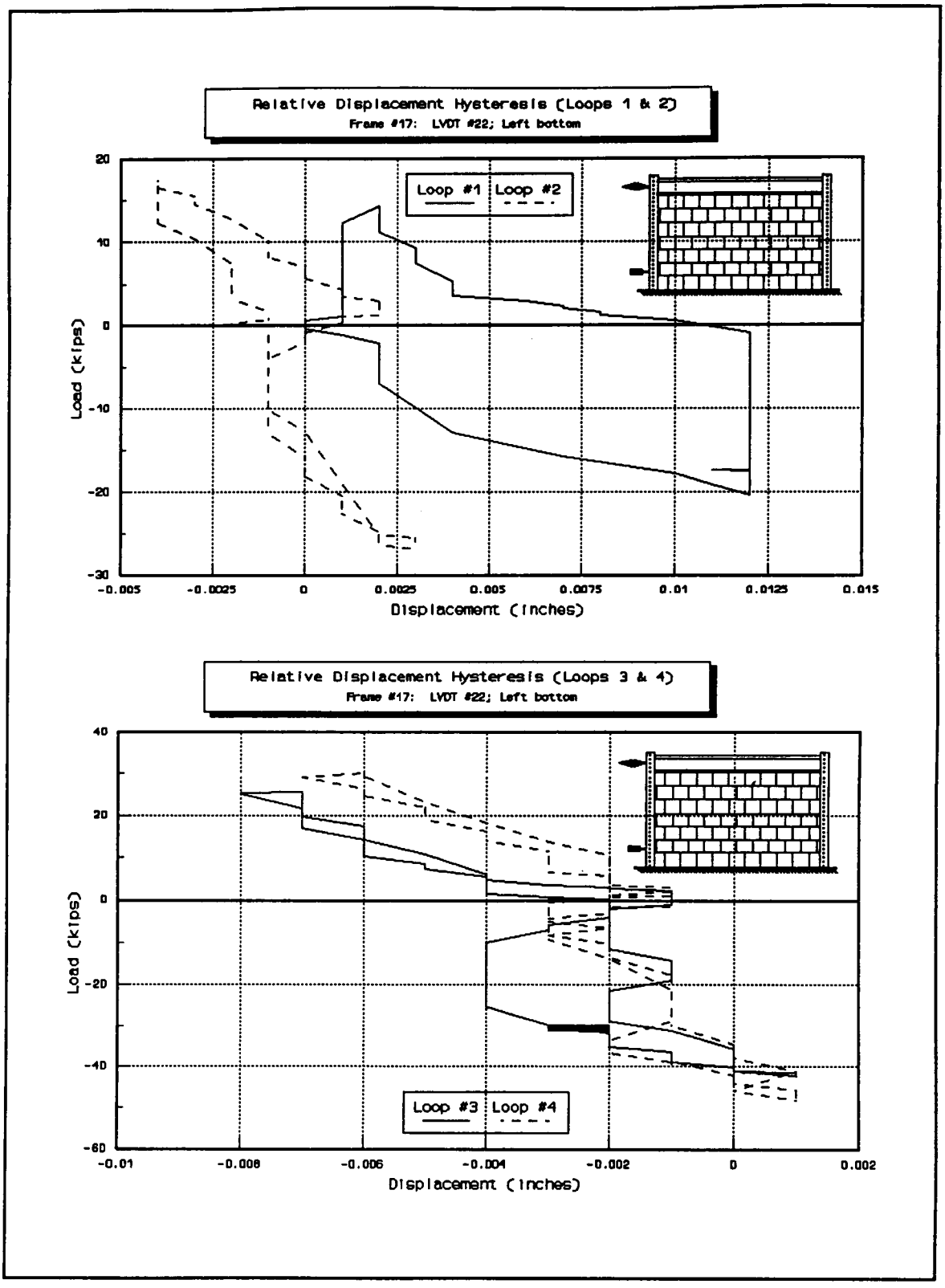


Figure 6.19: Frame 17; LVDT 22 hysteresis

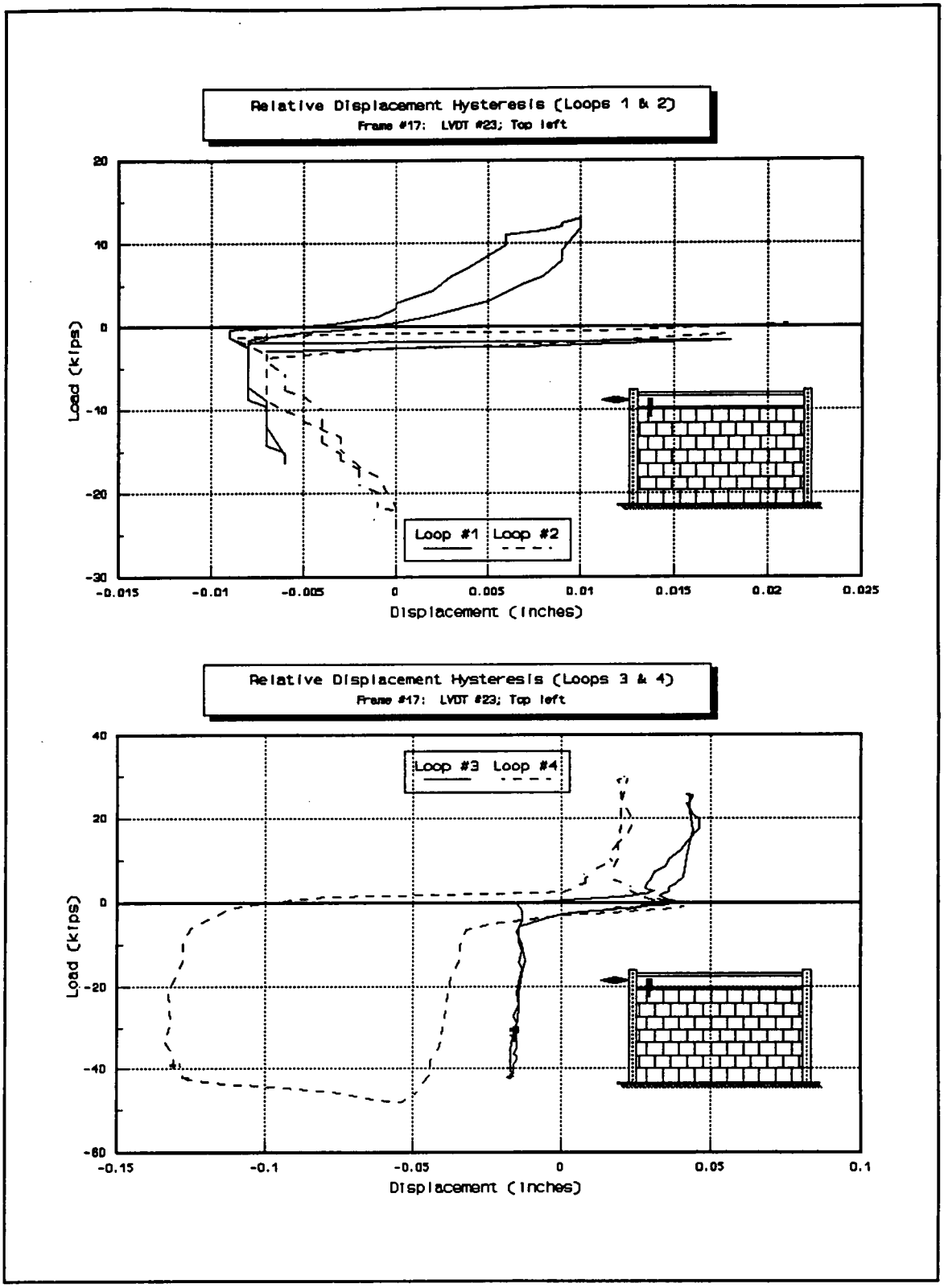


Figure 6.20: Frame 17; LVDT 23 hysteresis

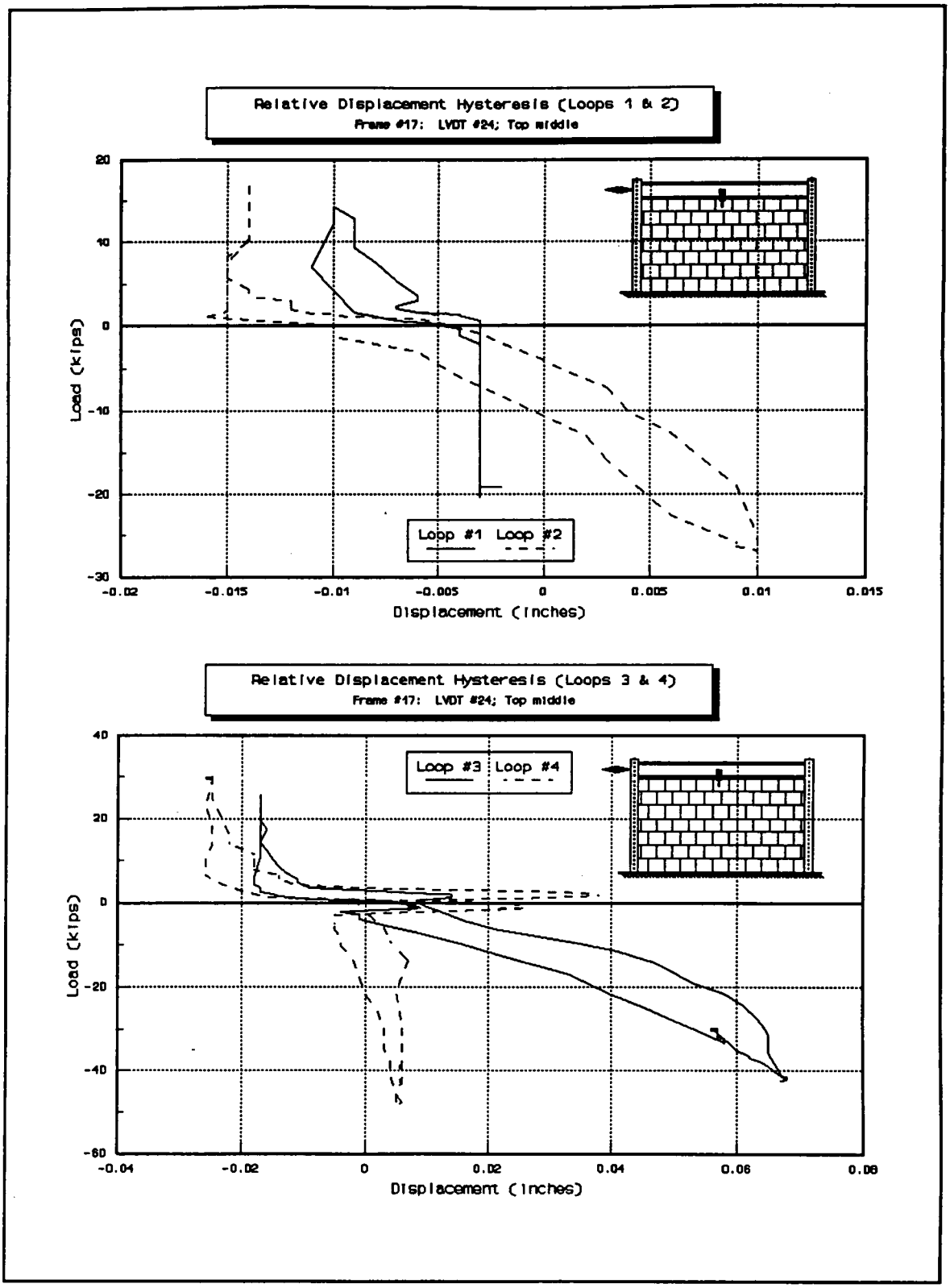


Figure 6.21: Frame 17; LVDT 24 hysteresis

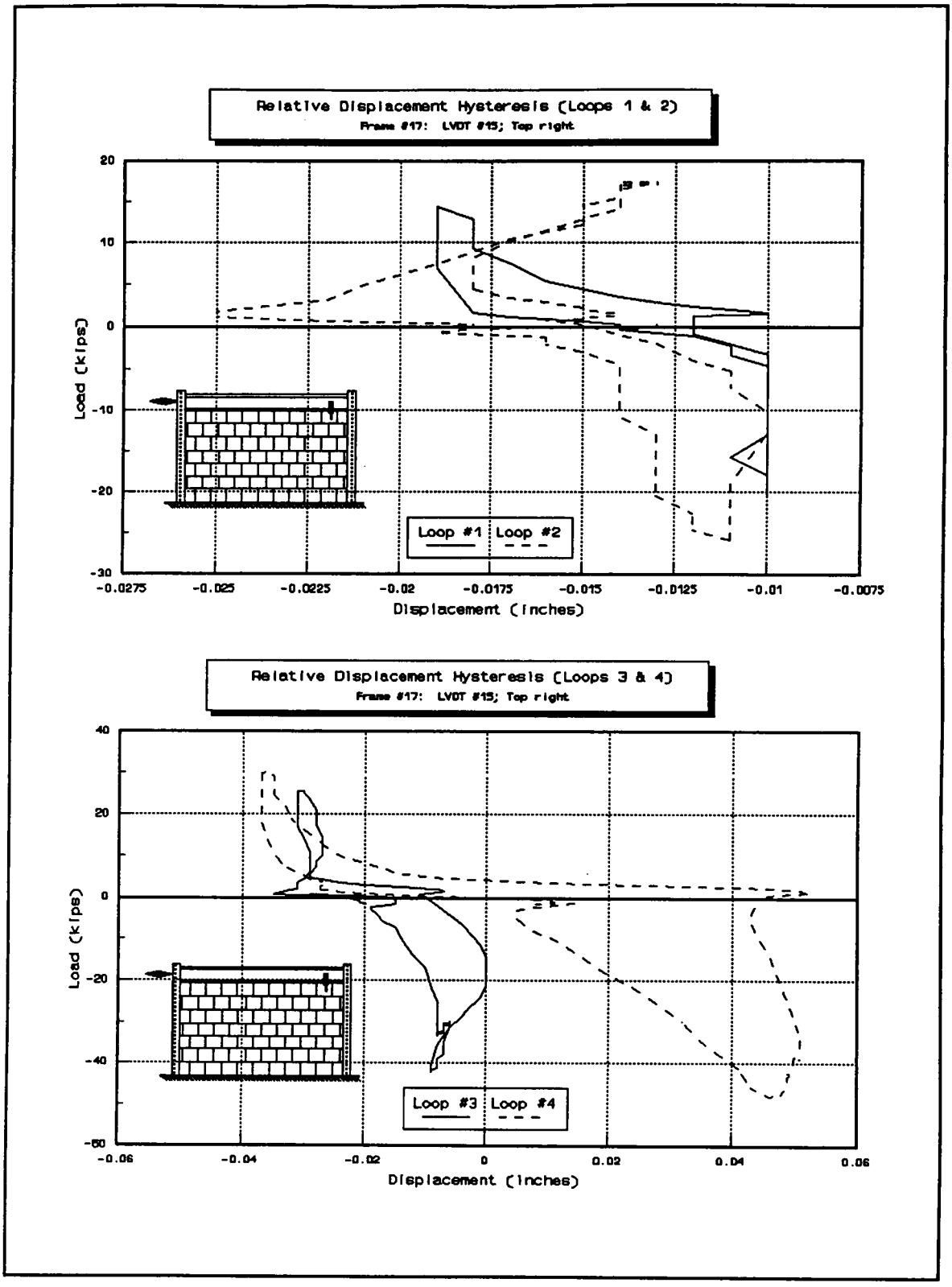


Figure 6.22: Frame 17; LVDT 15 hysteresis

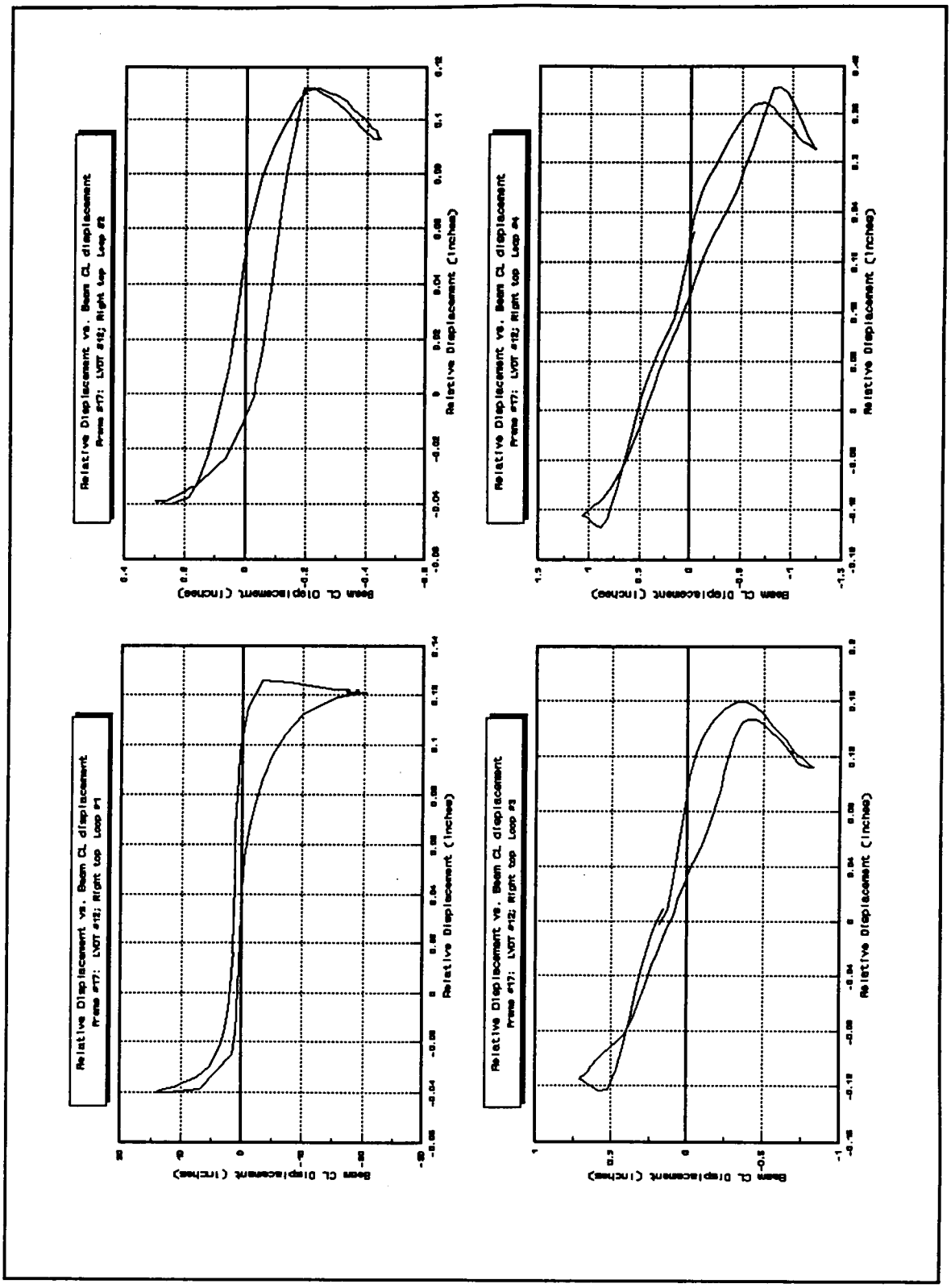


Figure 6.23: Frame 17; LVDT 12 vs. Beam CL deflection

therefore, some of the compressive displacement may have been non-linear deformation of the tile adjacent to the column. With the exception of loop one, the tensile loading portion of the load-deflection curve behaved the same as that of frame 2. As the leeward column engaged the panel in loop one, there was an increase in the relative displacement. Figure 6.24, the beam centerline displacement versus the relative displacement for LVDT 13, verifies this behavior.

The behavior of the load-relative displacement hysteresis for the bottom leeward corner of the panel for frame 17 was not as erratic as that of frame 2. Figure 6.16 illustrates the behavior for this LVDT. As can be seen in figure 6.16, there was a shift in the hysteresis curve between loops two and three. This was during the time that corner crushing was observed and the tile to which the LVDT was connected may have become cracked enough to cause this shift.

Figure 6.17 illustrates the load-deflection hysteresis for the top windward corner of the panel. As with the top leeward corner of the panel, all four loops exhibit the same behavior as the same LVDT for frame 2. LVDT 20 for frame 17 did exhibit a greater amount of gapping. Figure 6.25 confirms this behavior with the beam centerline-relative displacement hysteresis.

Figures 6.18 and 6.19 show the load-deflection hysteresis for LVDT's 21 and 22. These correspond to the panel mid-height and panel bottom corner of the windward column. The

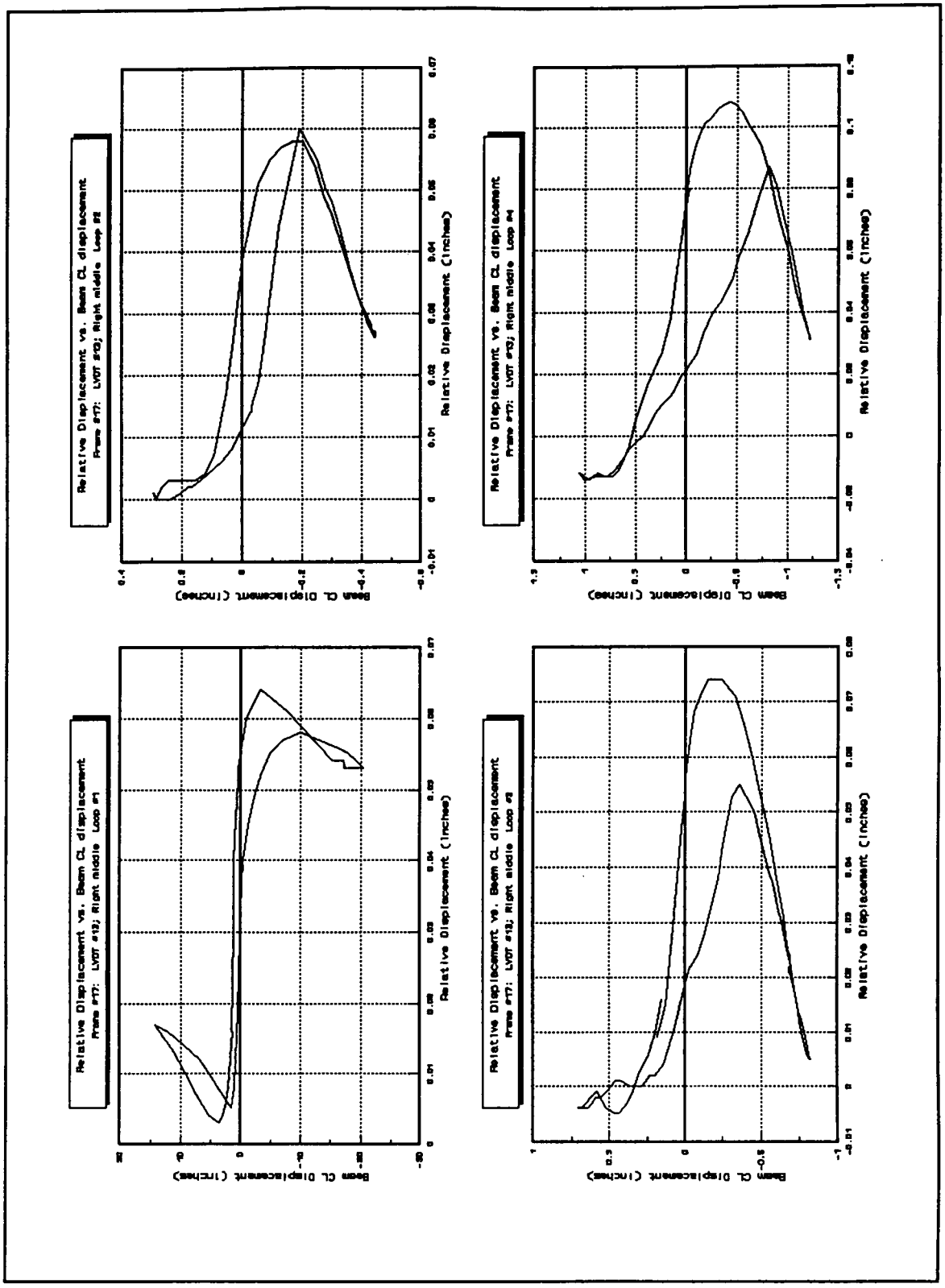


Figure 6.24: Frame 17; LVDT 13 vs. Beam CL deflection

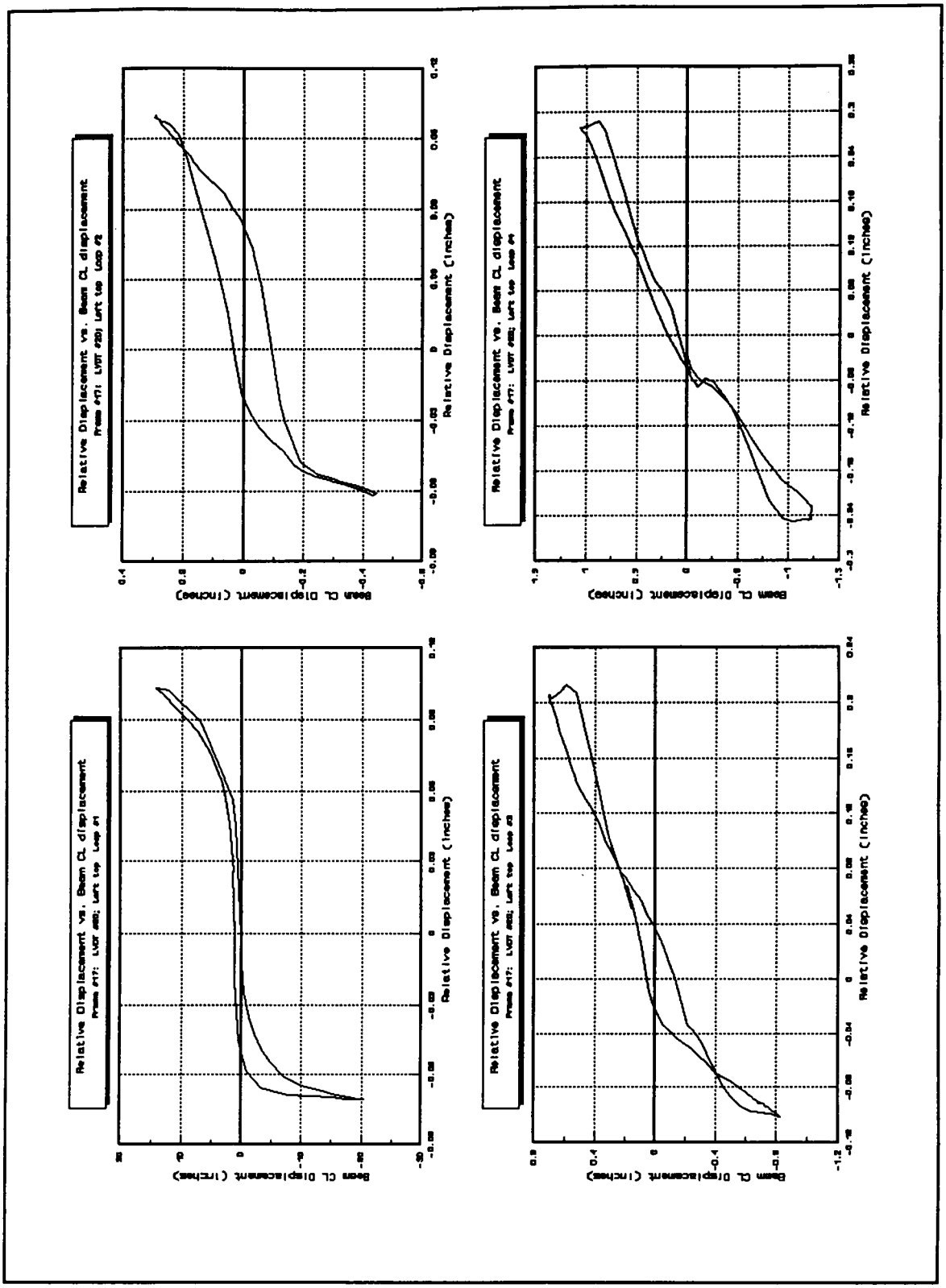


Figure 6.25: Frame 17; LVDT 20 vs. Beam CL deflection

tensile behavior of the panel-frame mid-height relative displacement behaves in the same manner as the leeward column counterpart. The behavior during the compressive loading was different in that there was no relative displacement once the column engaged the panel. The beam centerline displacement versus the relative displacement at the panel mid-height is shown in figure 6.26.

Figure 6.20 through 6.22 illustrate the relative displacement hysteresis curves for the beam-panel interface. Figure 6.20, load-relative deflection hysteresis for the top windward corner of the panel, behaves the same as it did for frame 2 except at the ultimate compressive load. During this increment, the deflection remained constant up to the maximum compressive load, at which time there was a sudden opening of the beam-panel interface gap. This can be accounted for by corner crushing of the tile in the loaded corner.

Figure 6.22 represents the load-relative displacement hysteresis at the beam-panel interface of the top leeward corner of the panel. Loops one and two demonstrate some erratic behavior, but remain within a range of displacements somewhat smaller than the frame 2 counterpart. The compressive loading portion of loop four, which was the ultimate load increment, caused a significant increase in the size of the beam-panel gap. This is accounted for in the fact that the beam-panel interface was completely destroyed by this point in the loading history.

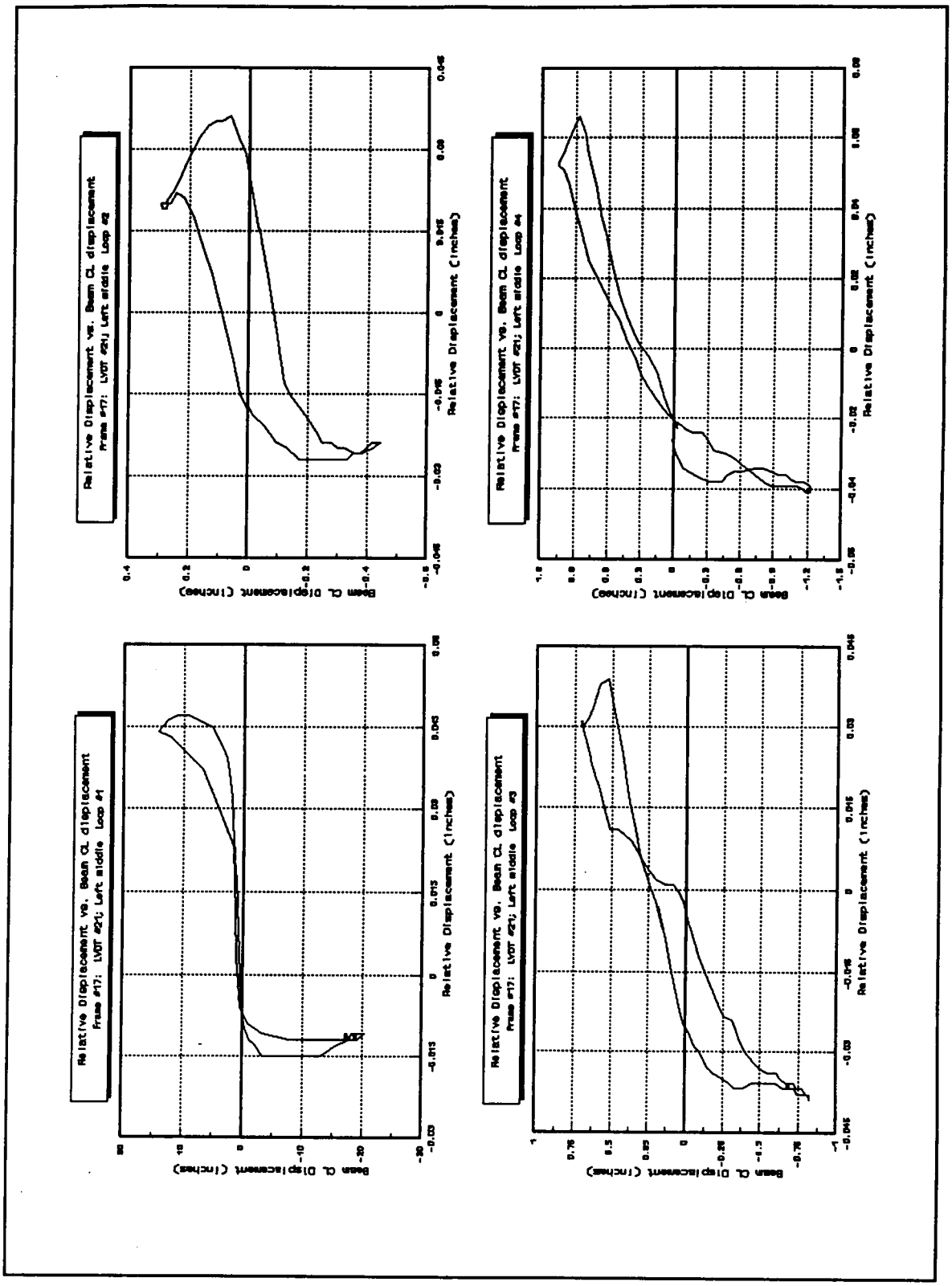


Figure 6.26: Frame 17; LVDT 21 vs. Beam CL deflection

6.3 Relative-Frame Displacement Comparisons

Figures 6.27 through 6.42 illustrate plots for the four loops studied of the load-relative displacement hysteresis curves overlaid with the load-displacement loops of the frame at the same elevation as the relative LVDT. With the exception of a few characteristics, such as the relative displacement being offset from the frame displacement, all of these plots behave similarly. Therefore, only a few representative plots will be discussed.

Figures 6.27 and 6.28 illustrate the comparison plots for LVDT's 9 and 12 for frame 2. Loops one and two are shown in figure 6.27. Both the frame load-displacement hysteresis and the relative displacement hysteresis exhibit a flat-line portion of approximately the same length in loop one. During testing, this pinching phenomenon was thought to be a sliding effect after the beam-panel interface had deteriorated to an extent. As the system was loaded, the beam would slide along the panel until the panel-column gap had closed and the panel was engaged. At this point, the load would begin to increase with increasing deflection. Loop one exhibits the above described behavior.

Loops two, three, and four negate the possibility that this entire pinching behavior, which was observed in all frame LVDT's during testing, was due to a sliding effect. The effect can be seen in loop two, but it becomes much more pronounced in loop four in figure 6.28. From the hysteresis

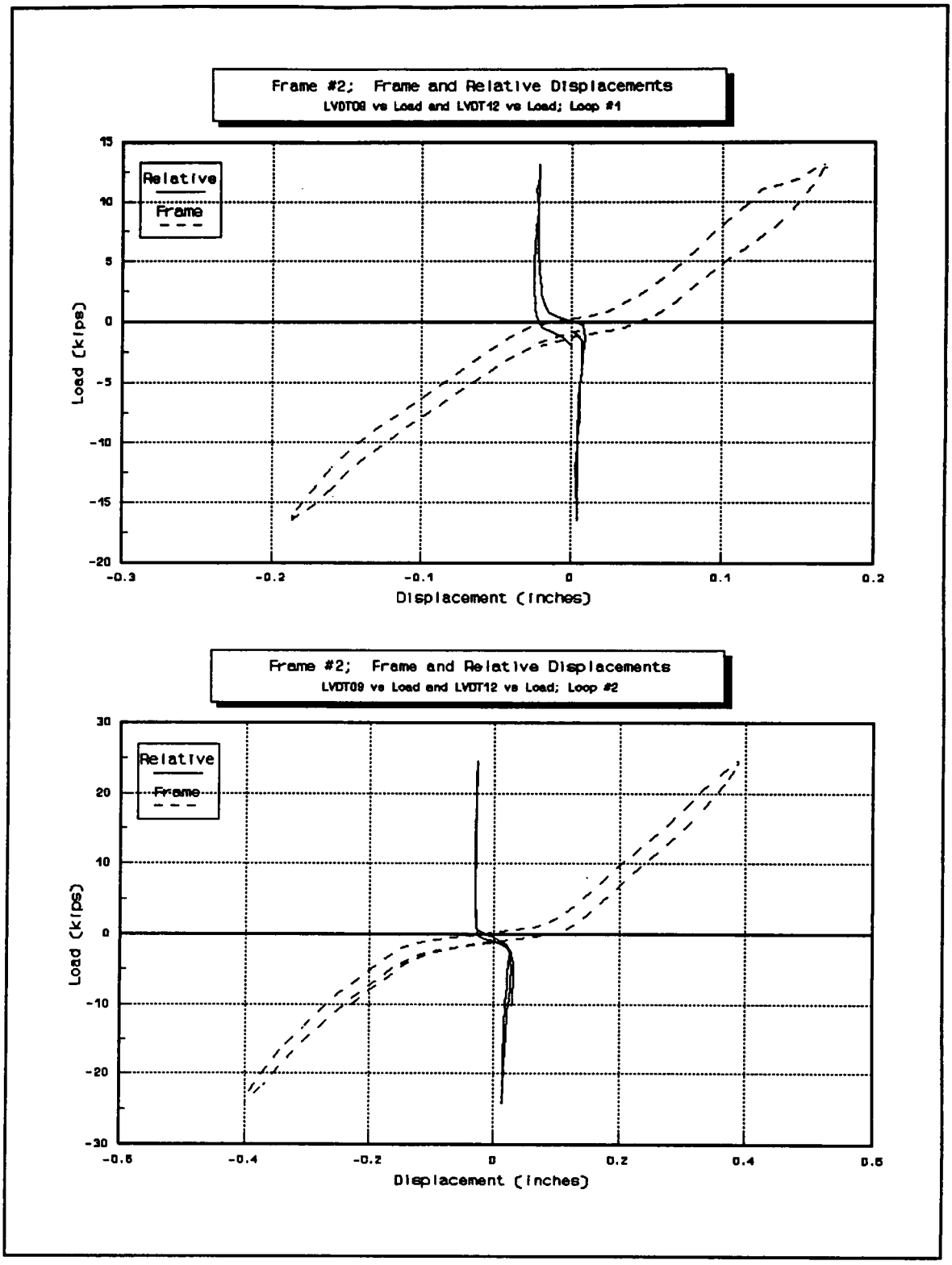


Figure 6.27: Frame 2; Relative & frame displacement vs. load (LVDT 12 & 9; Loops 1 & 2)

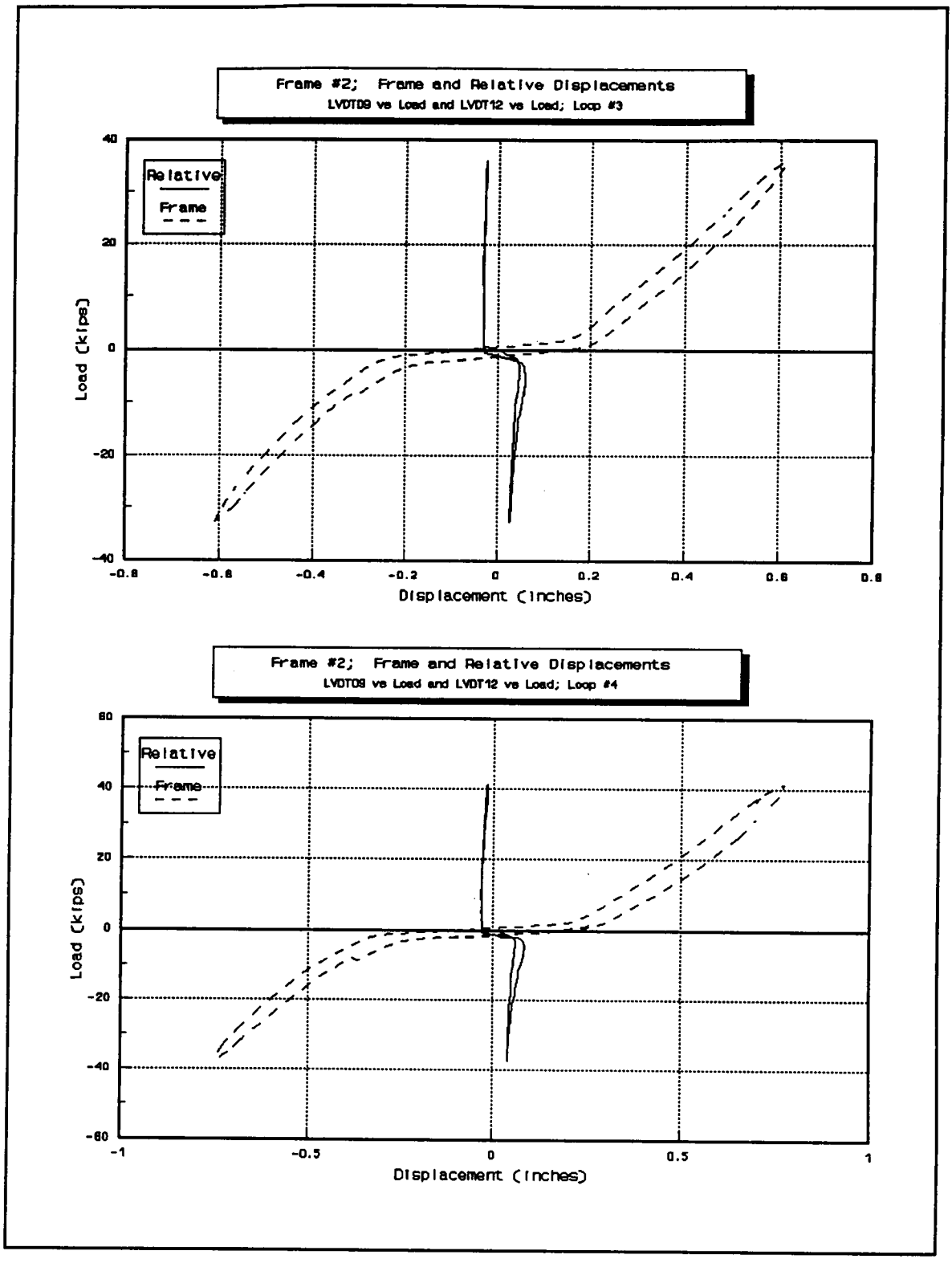


Figure 6.28: Frame 2; Relative & frame displacement vs. load (LVDT 12 & 9; Loops 3 & 4)

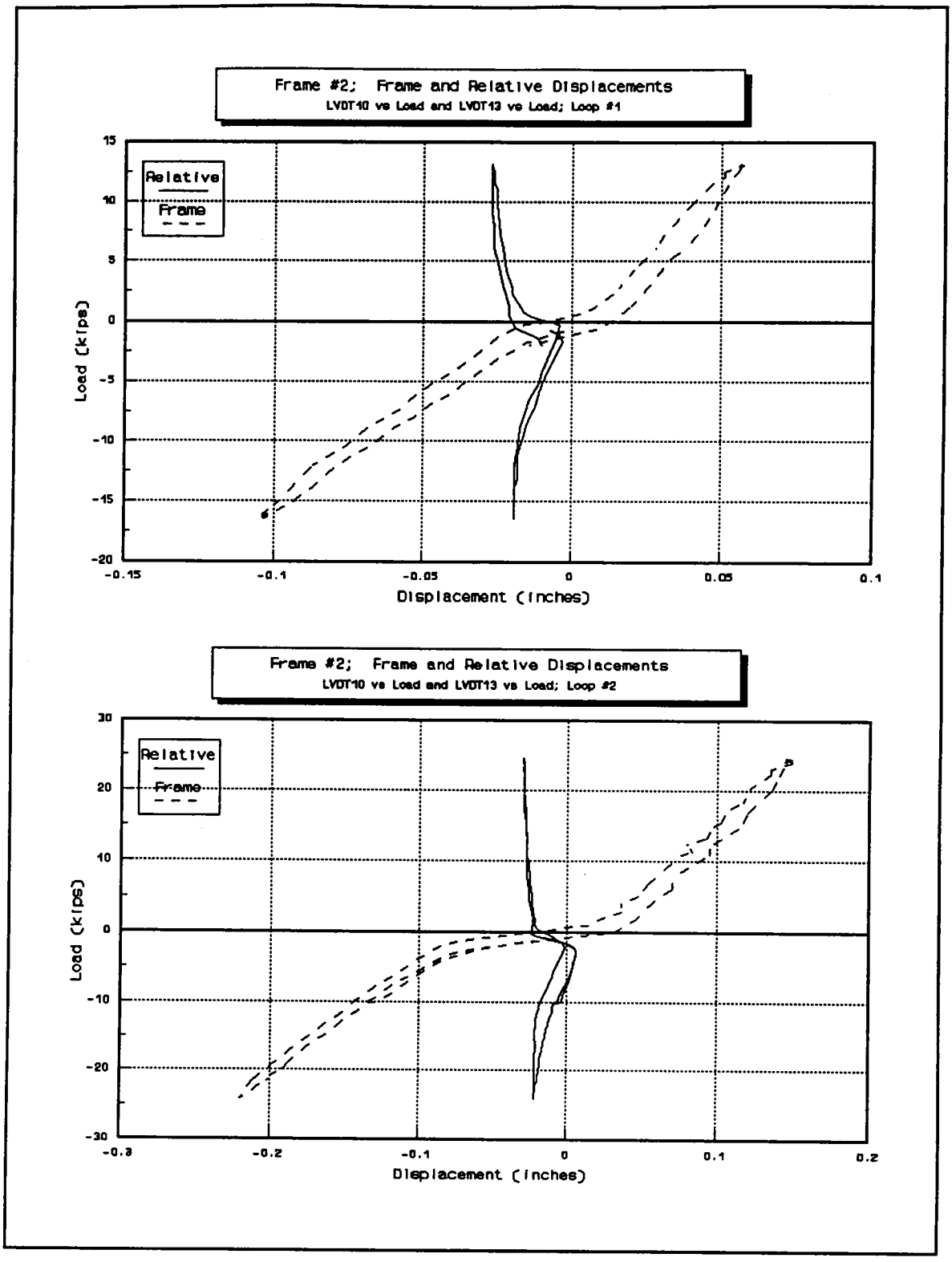


Figure 6.29: Frame 2; Relative & frame displacement vs. load (LVDT 13 & 10; Loops 1 & 2)

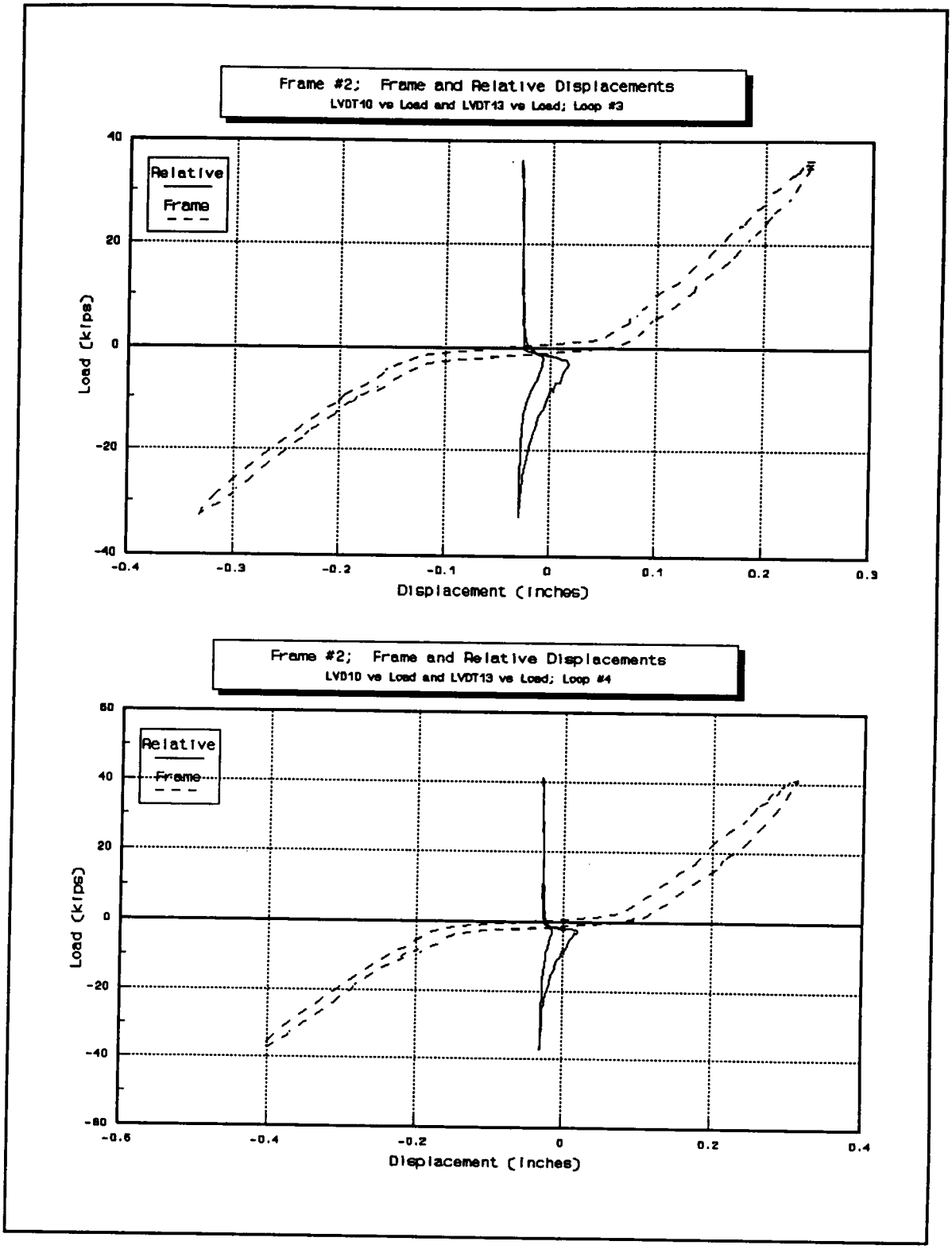


Figure 6.30: Frame 2; Relative & frame displacement vs. load (LVDT 13 & 10; Loops 3 & 4)

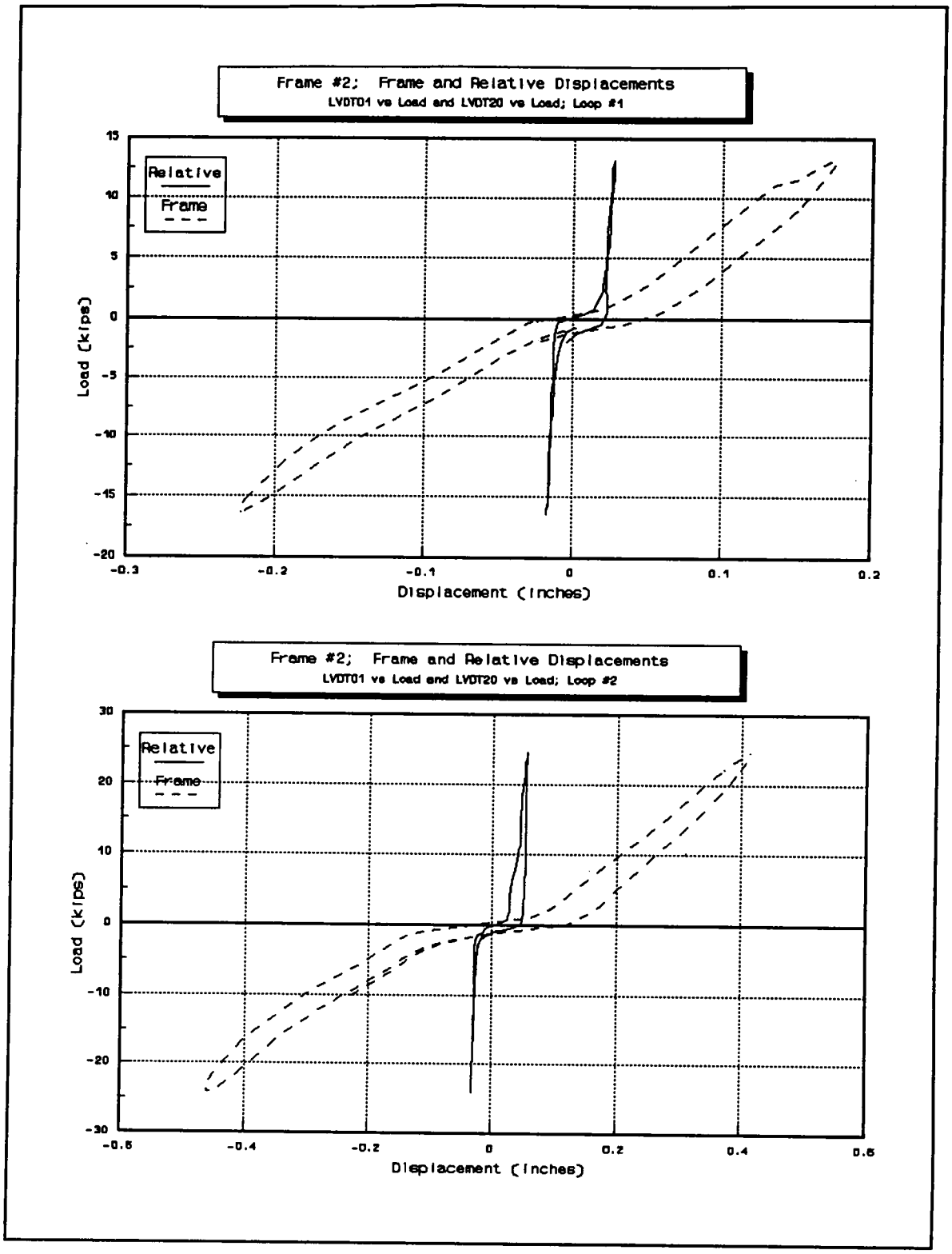


Figure 6.31: Frame 2; Relative & frame displacement vs. load (LVDT 20 & 1; Loops 1 & 2)

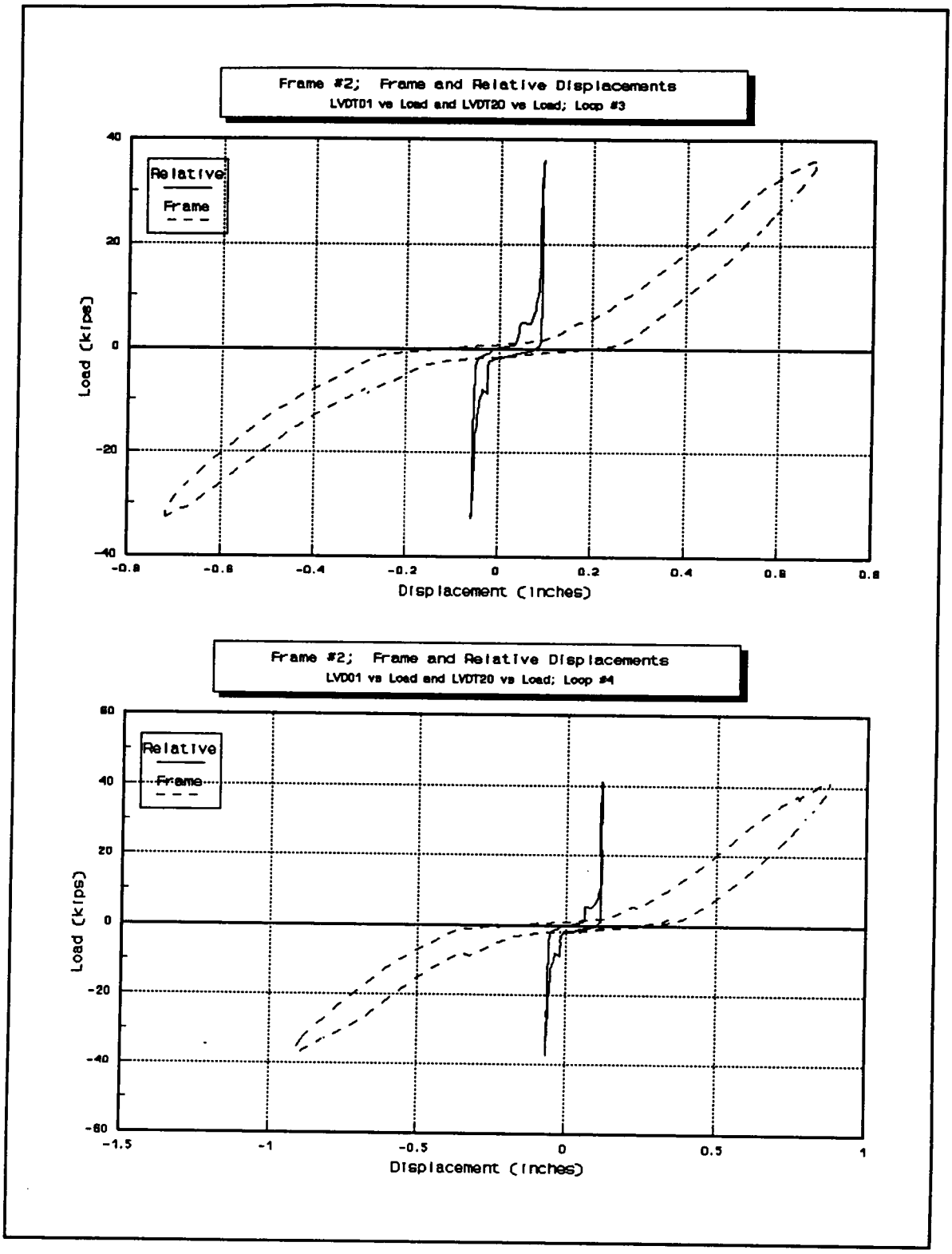


Figure 6.32: Frame 2; Relative & frame displacement vs. load (LVDT 20 & 1; Loops 3 & 4)

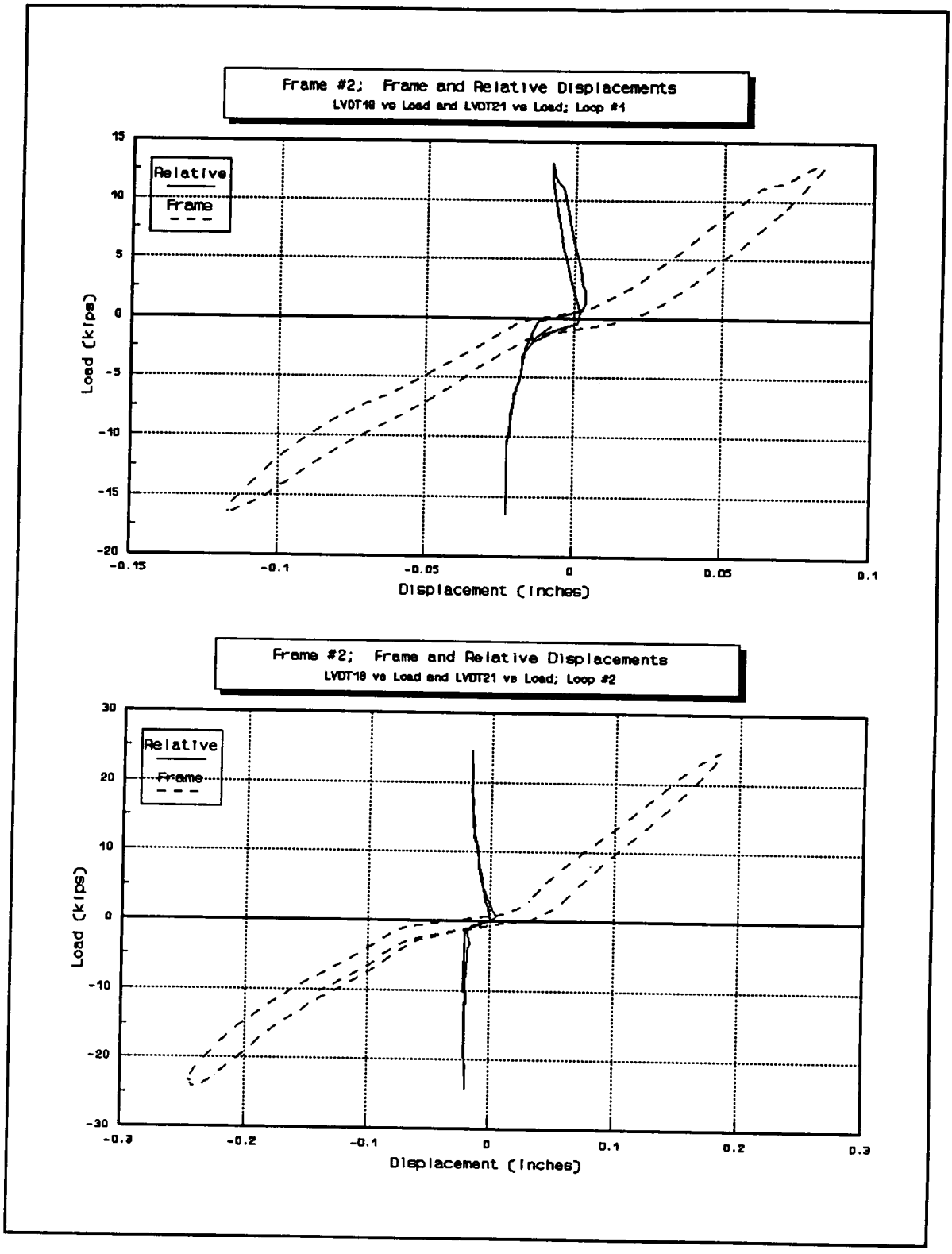


Figure 6.33: Frame 2; Relative & frame displacement vs. load (LVDT 21 & 18; Loops 1 & 2)

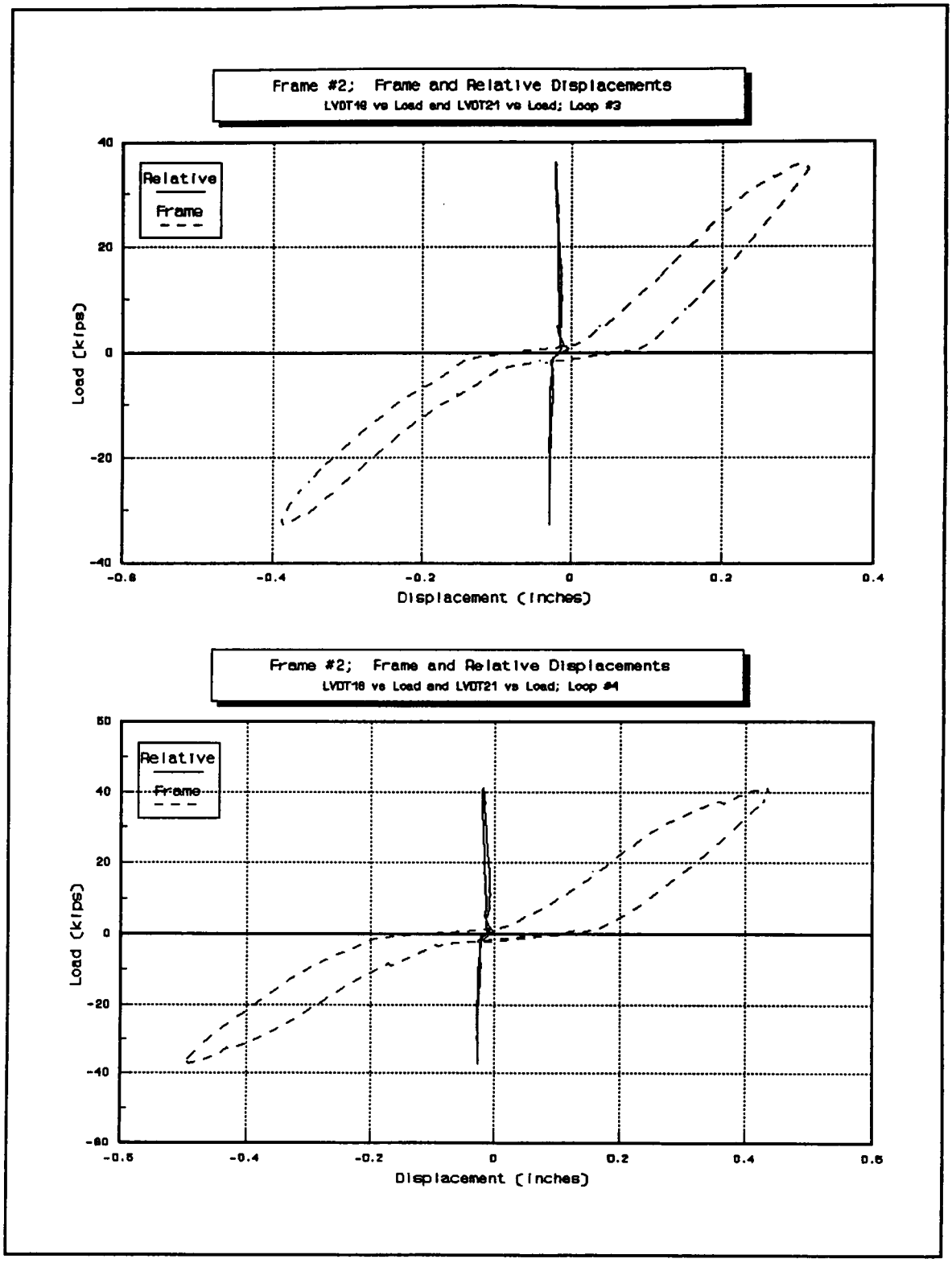


Figure 6.34: Frame 2; Relative & frame displacement vs. load (LVDT 21 & 18; Loops 3 & 4)

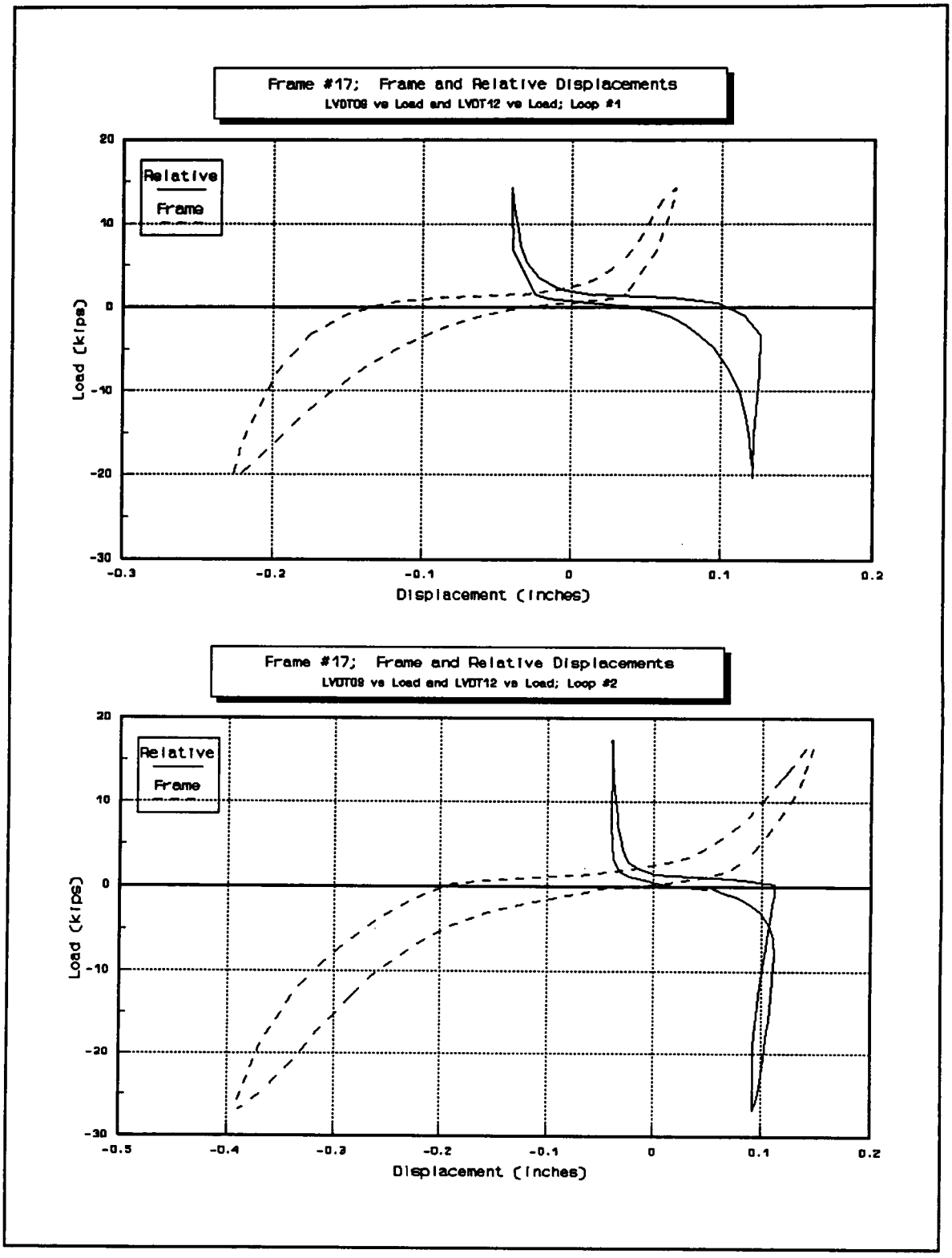


Figure 6.35: Frame 17; Relative & frame displacement vs load (LVDT 12 & 9; Loops 1 & 2)

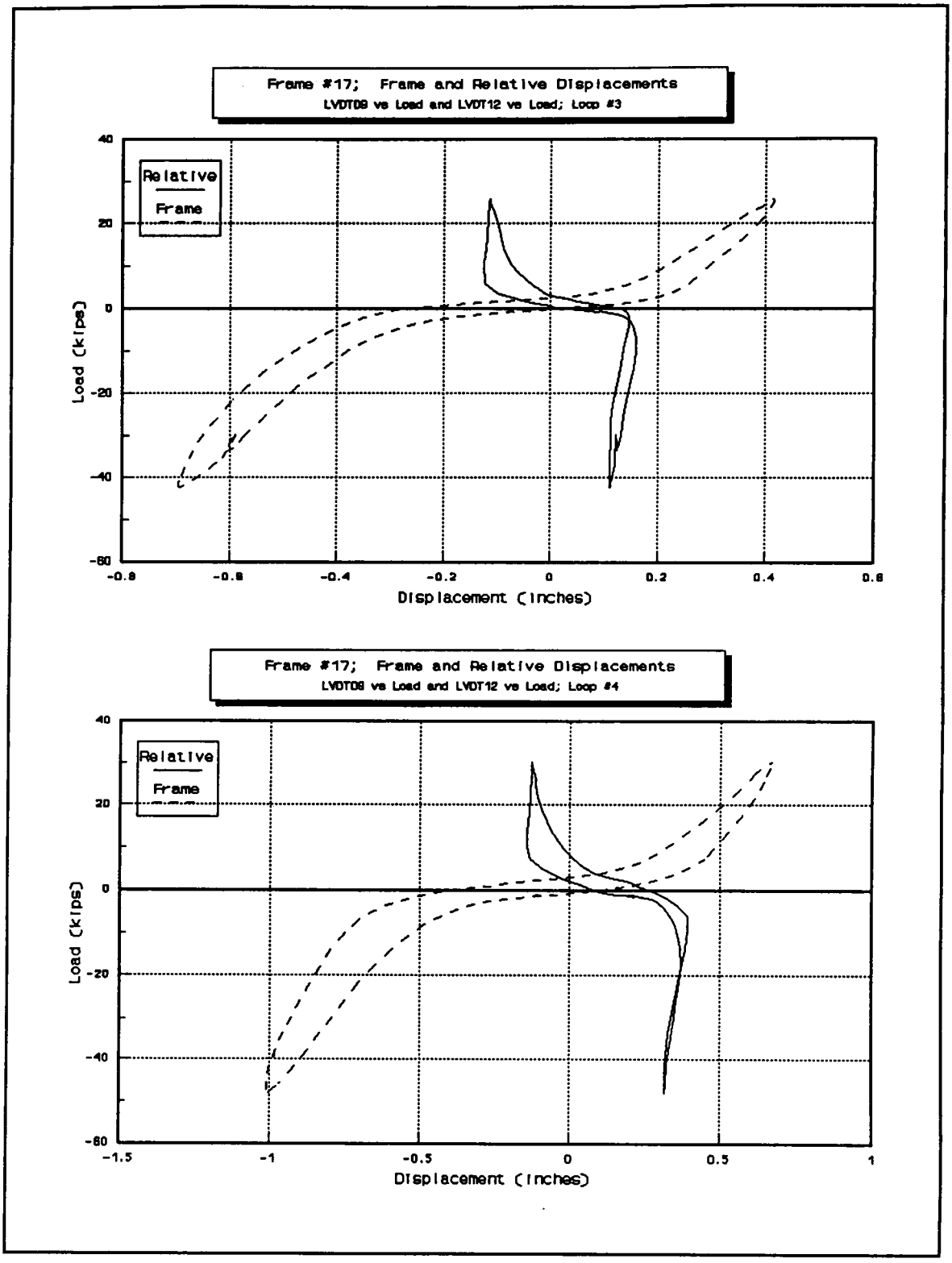


Figure 6.36: Frame 17; Relative & frame displacement vs load (LVDT 12 & 9; Loops 3 & 4)

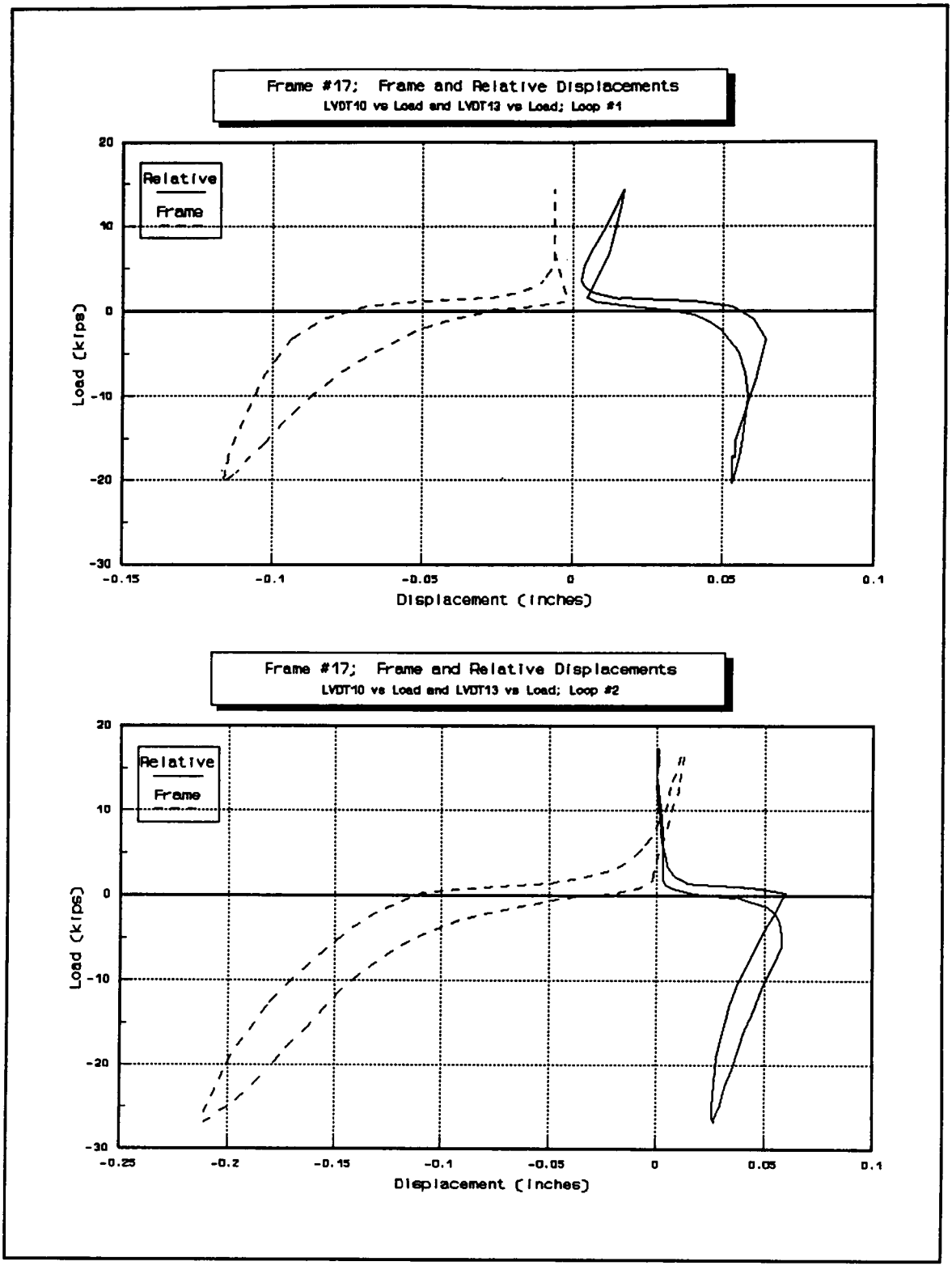


Figure 6.37: Frame 17; Relative & frame displacement vs load (LVDT 13 & 10; Loops 1 & 2)

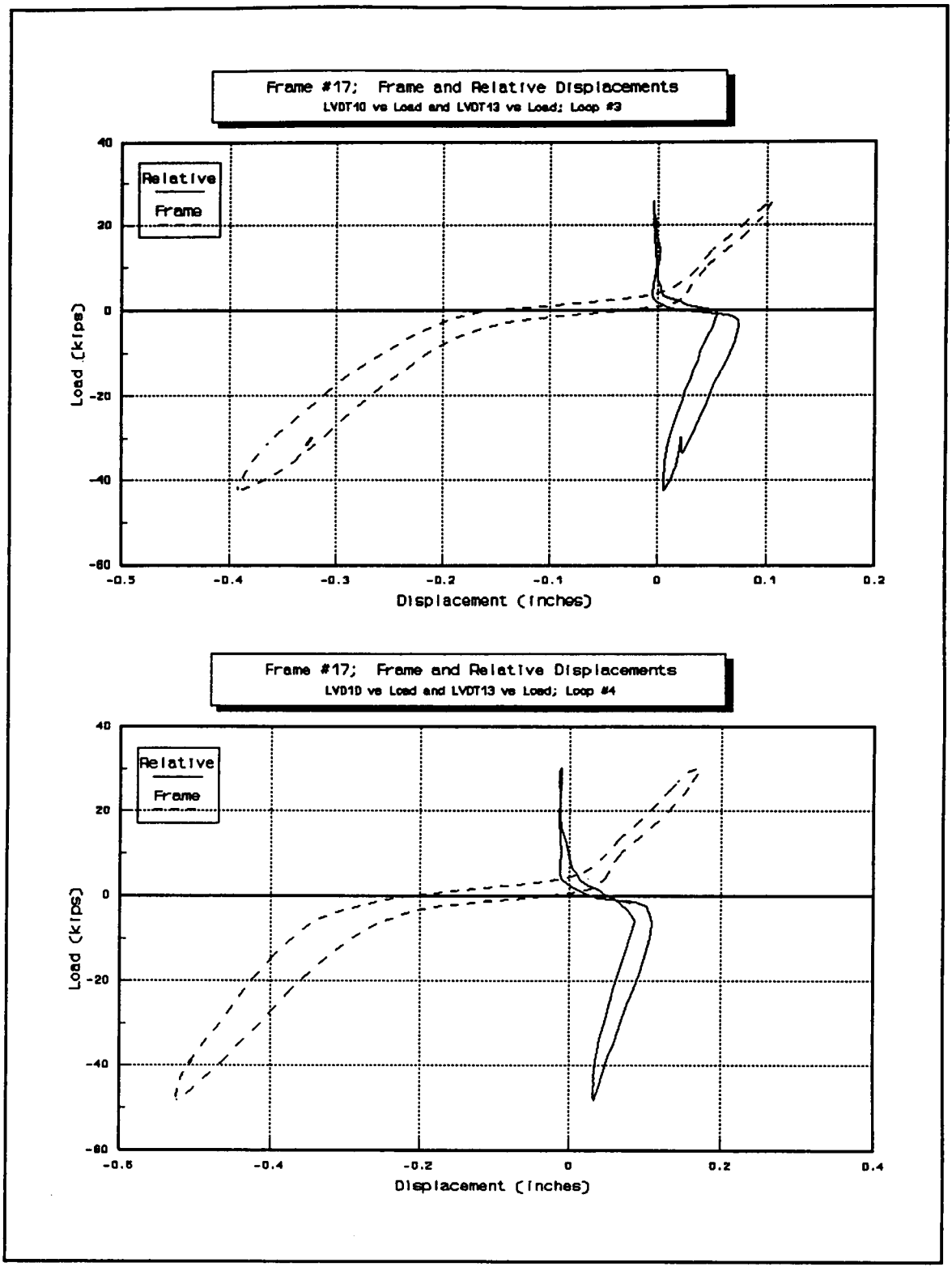


Figure 6.38: Frame 17; Relative & frame displacement vs load (LVDT 13 & 10; Loops 3 & 4)

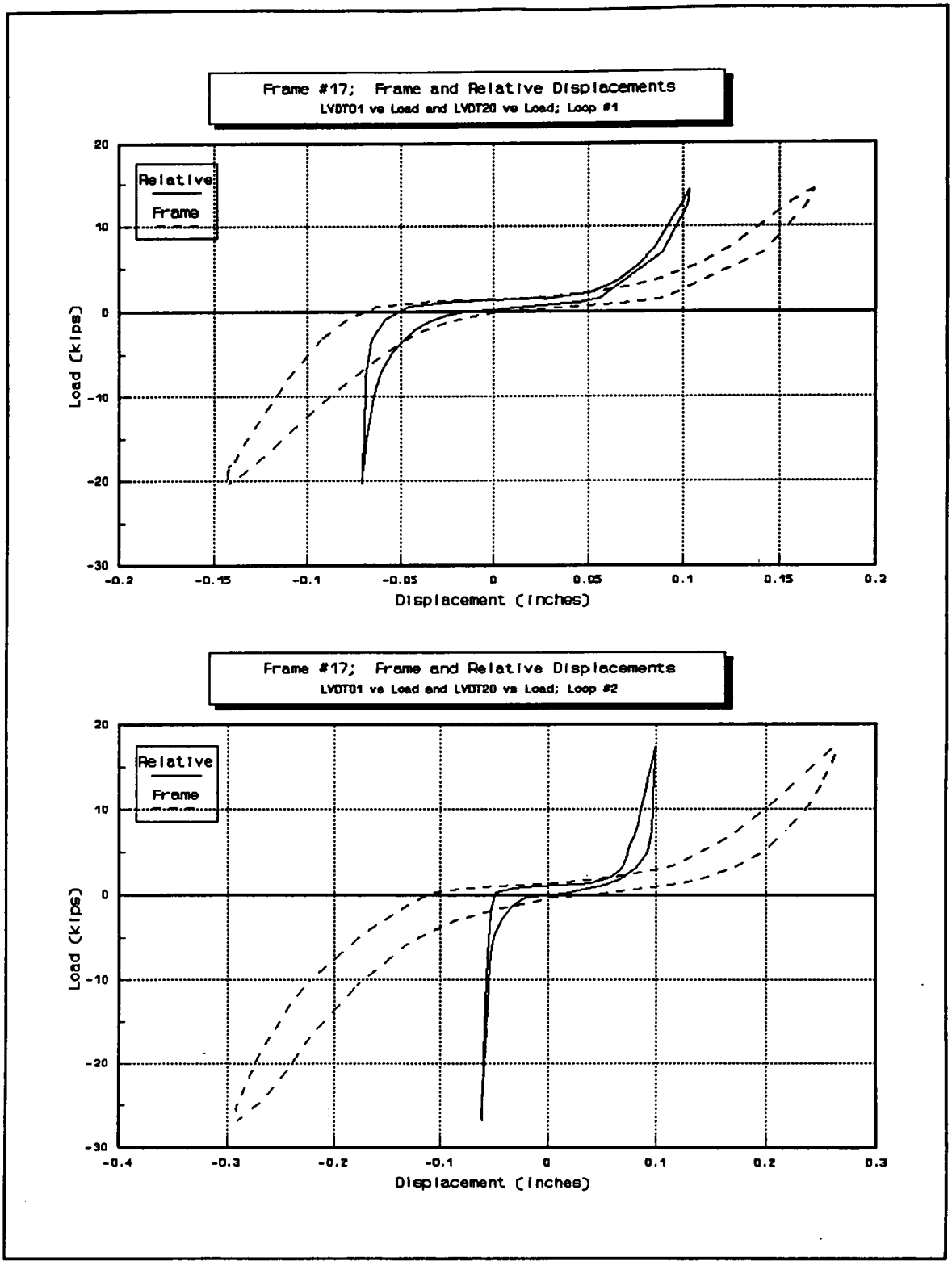


Figure 6.39: Frame 17; Relative & frame displacement vs load (LVDT 20 & 1; Loops 1 & 2)

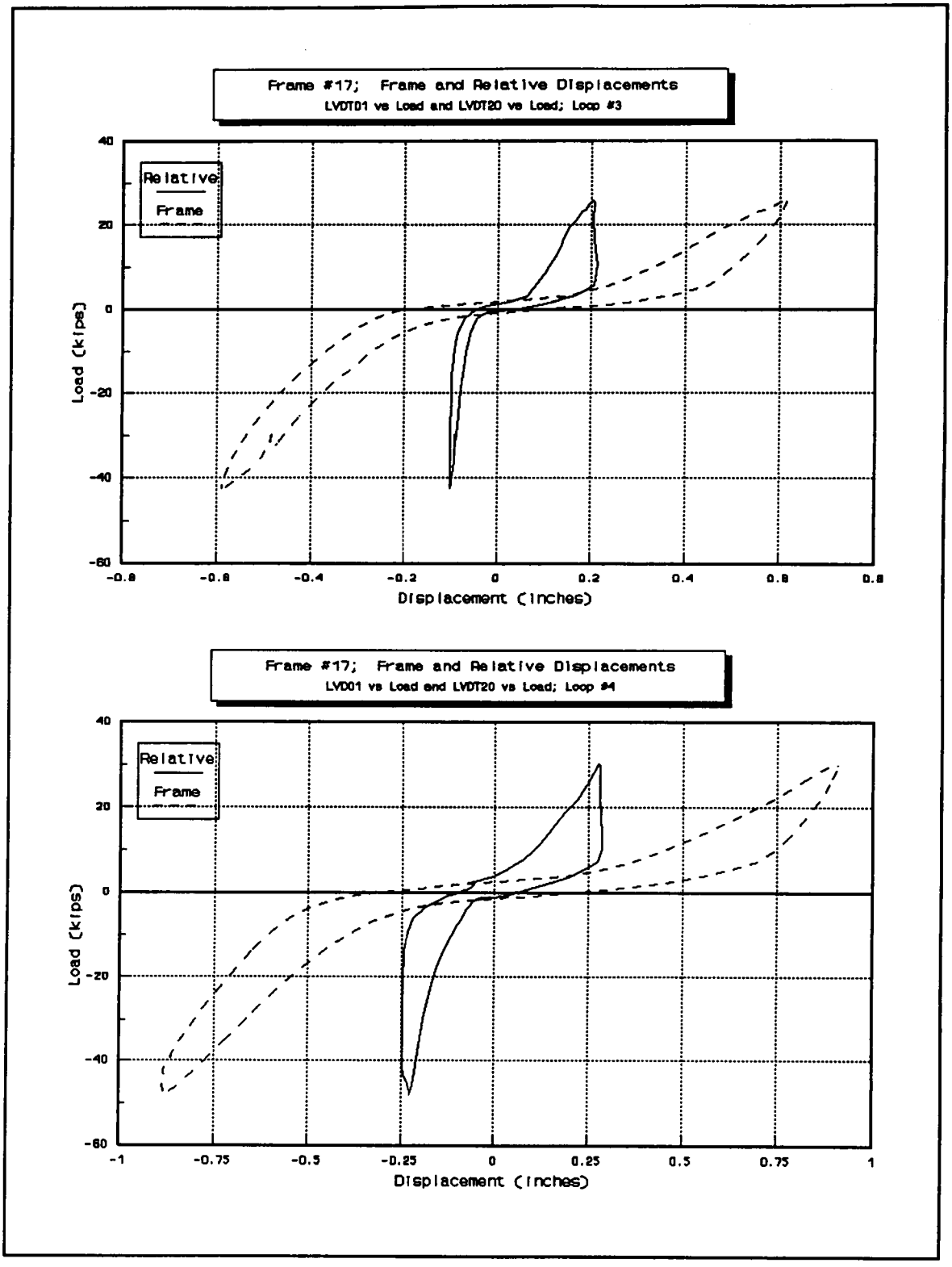


Figure 6.40: Frame 17; Relative & frame displacement vs load (LVDT 20 & 1; Loops 3 & 4)

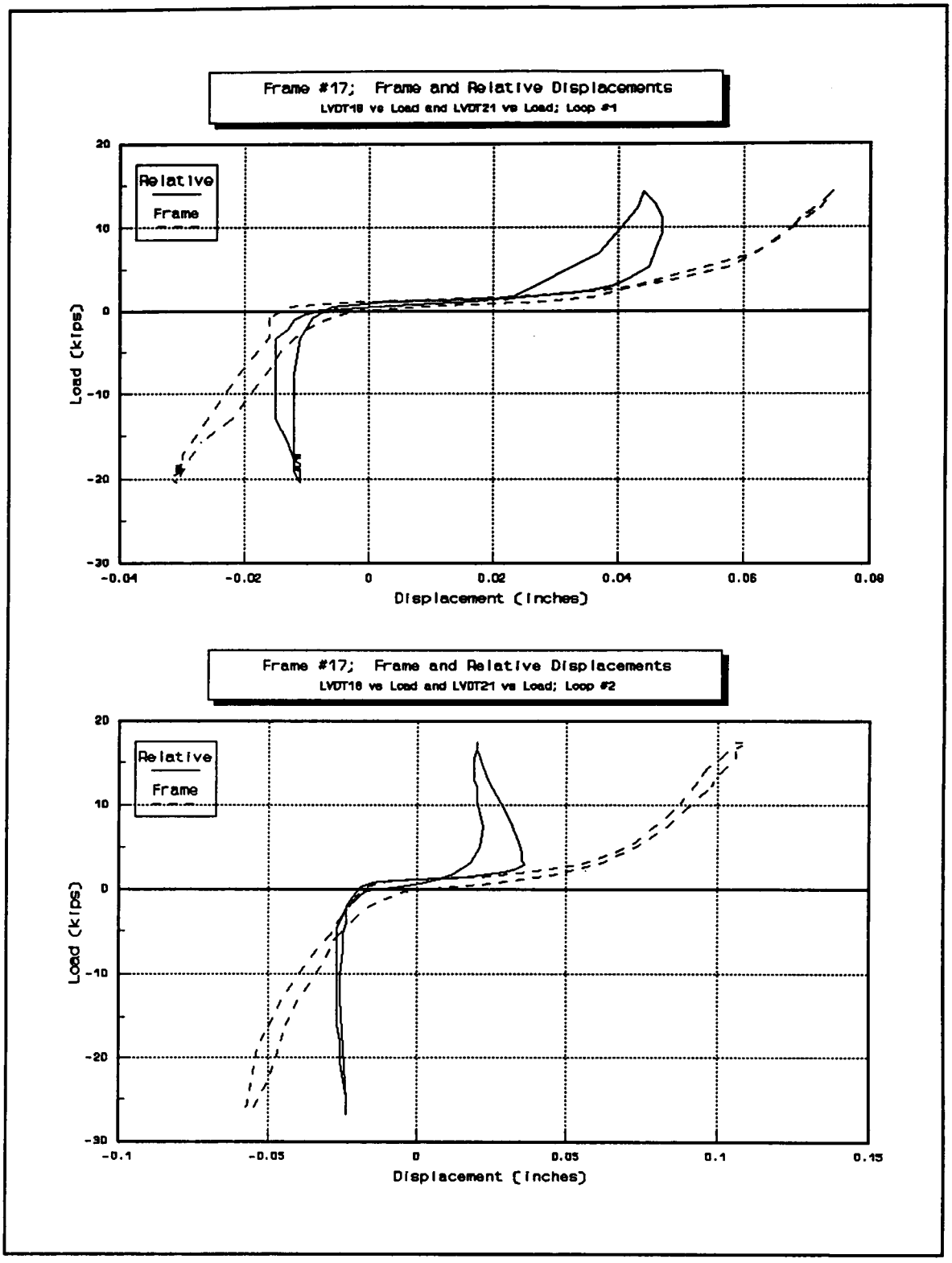


Figure 6.41: Frame 17; Relative & frame displacement vs load (LVDT 21 & 18; Loops 1 & 2)

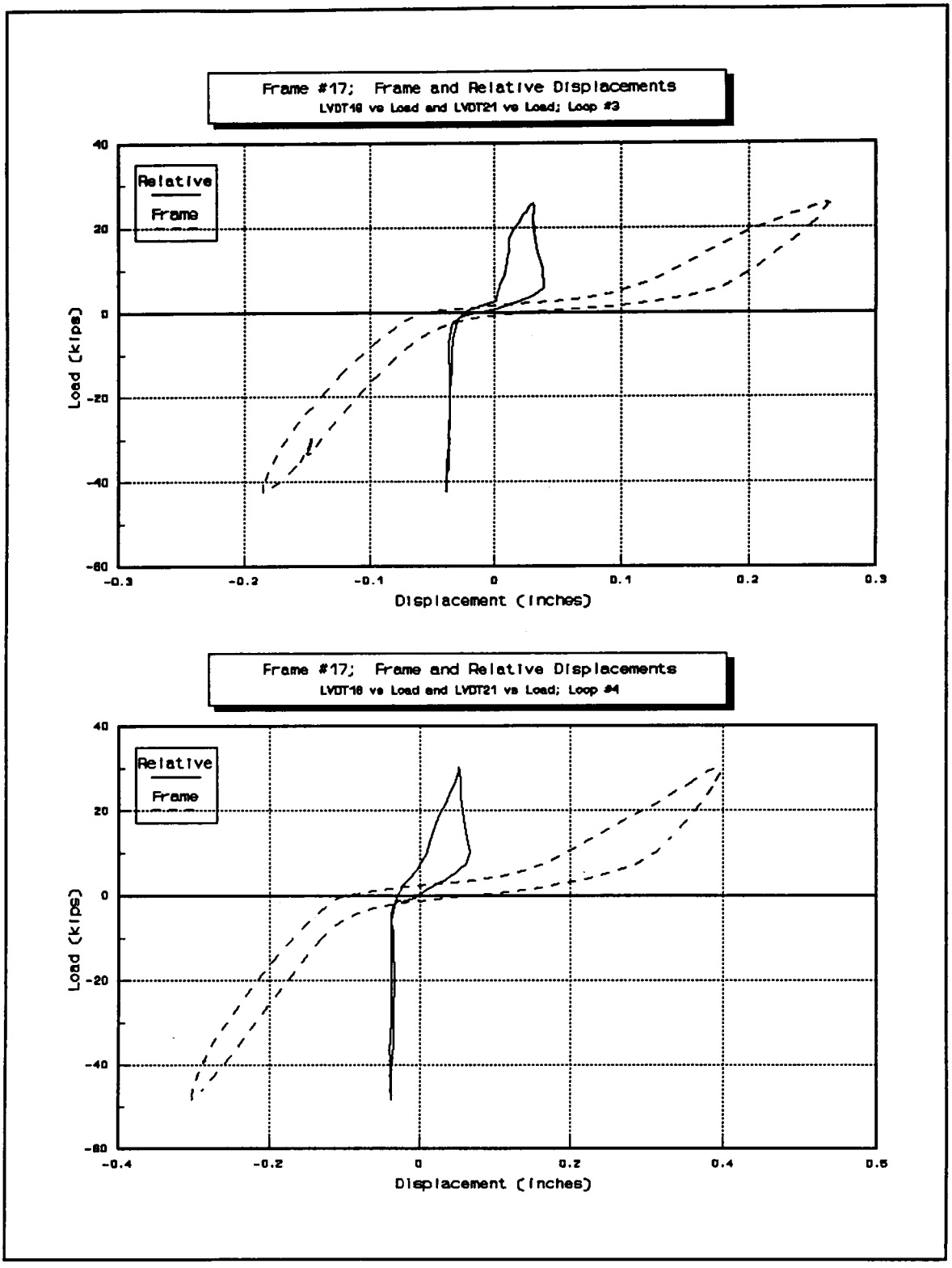


Figure 6.42: Frame 17; Relative & frame displacement vs load (LVDT 21 & 18; Loops 3 & 4)

curve of LVDT 9, the frame LVDT, it is observed that there was slightly more that 0.25 inches of "sliding" in either the beginning of the compressive or tensile loading. However, there was approximately 80% more flat-line deflection in the frame LVDT than the relative LVDT. This supports the theory that this sliding effect was due, at least in part, to the non-linear properties of the clay tile. The sliding effect was partially due to some plastic deformation of the tile. During the testing of the prisms (Boyd, 1993), it was shown that there was plastic straining of the tile at levels significantly below the ultimate load. If there were no non-linear deformation of the tile, the flat-line portions of the relative LVDT hysteresis and the frame LVDT hysteresis at the same location, would coincide for the most part. Some head joint mortar crushing and crushing of the tile also accounted for part of this phenomenon.

All of these comparison plots behaved identically for frame 2. Also, the relative displacement, as compared to the frame displacement, was on the order of 10 to 20% of the frame displacement for frame 2. The comparison plots for frame 17 behaved in a similar manner in that there was a "sliding" phenomenon in the frame and relative displacement hysteresis curves. However, in the comparison plots for the LVDT's on the leeward side of frame 17, there was a shifting anomaly between the frame LVDT hysteresis and the relative hysteresis.

Figures 6.43 and 6.44 illustrate the leeward column and panel deflections. These deflections were taken at various points during the ultimate cycle for frame 2. This illustrates the given the deflection behavior and the reason for the closing of the gaps on the leeward column. As the load increases, there is more force in the strut, causing it to experience larger deformations. In particular, it deforms in shear and the effective width of the strut increases. Therefore, there is more contact area with the column after parallel diagonal cracking has occurred, which causes the mid-height gap to close. During this time, the gap at the top remains fairly constant as the top corner of the panel and the frame moves in unison. At the maximum compressive load for the cycle, the gap at the top closes slightly, as illustrated in figure 6.44. This is also verified in the hysteresis curves of figures 6.1 through 6.3.

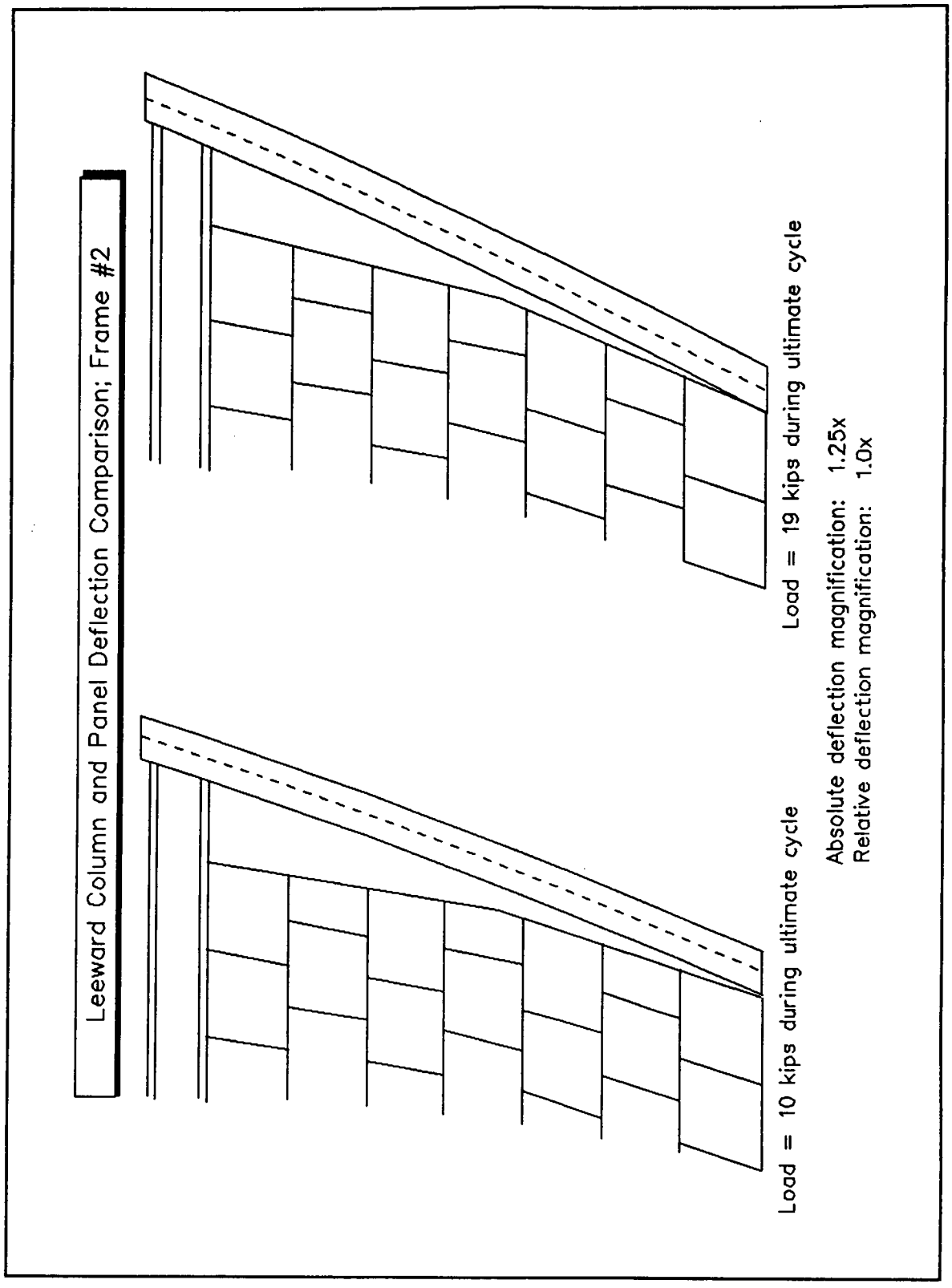


Figure 6.43: Leeward column-panel displacements

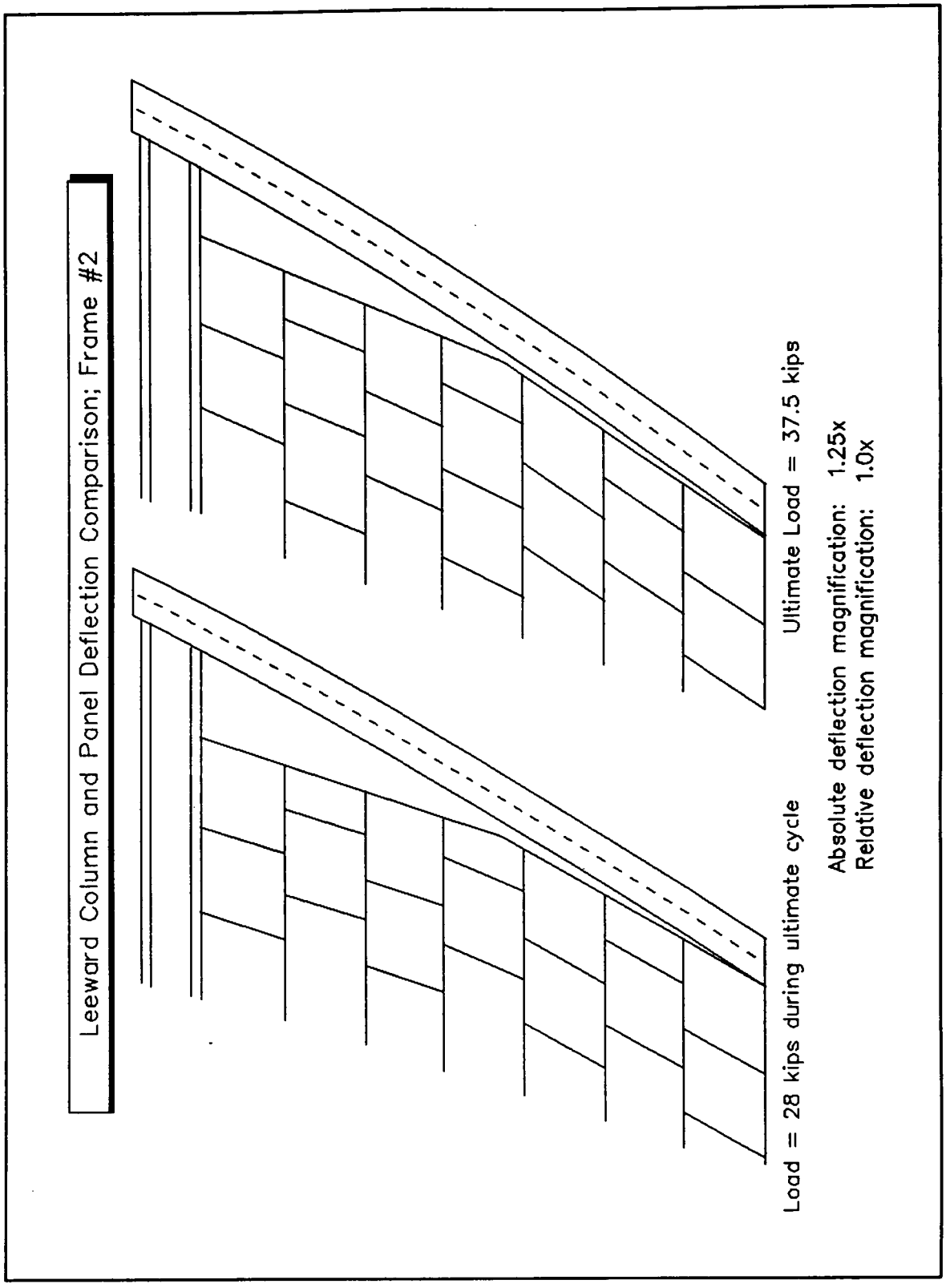


Figure 6.44: Leeward column-panel displacements

Chapter 7: SUMMARY, CONCLUSIONS, AND RECOMMENDATIONS

7.1 Research Summary

The behavior of two one-bay, one-story structural clay tile infilled structural steel frames subjected to in-plane loading was investigated to determine their in-plane stiffness, hysteretic behavior, and ultimate strength. The primary aim of this study was to examine the load-deflection relationships and the general system behavior. The two frames, numbers 2 and 17, were constructed with identical confining frames with the columns being bent about the weak axis; however, the aspect ratio was varied. Frame 2 was constructed with an aspect ratio of 1:1 and frame 17 with a 1.5:1 aspect ratio. No other parameters or boundary conditions were varied.

A literature survey presented past experimental results on similar frames with masonry infills. Analytical techniques presented by this past research were used in the prediction of the initial stiffness and ultimate loads of the systems.

7.2 Conclusions

The following conclusions are based on the observation of the clay tile infilled steel frames. All conclusions are based upon only two tests; therefore, the statistical validity of any conclusions should be taken into account.

7.2.1 General System Behavior

Although the ultimate strength and the initial stiffnesses were different, both frames exhibited similar behavior. Both tests proceeded as follows: within the first few cycles, peripheral cracks were formed at the panel-frame interface. This had a significant impact on the reduction of stiffness of both systems. Next, the panels experienced a tensile failure that resulted in a cracking along the compressive diagonal. The cracking loads were 24.17 kips for frame 2 and 25.45 kips for frame 17. These values were roughly 65% and 53% of the ultimate loads for frames 2 and 17, respectively. This was followed by face shell cracking and eventual spalling of the face shells.

Frame 2 experienced an ultimate load of 37.5 kips and frame 17 experienced 48.2 kips. Using analytical methods from previous research, ultimate loads for both frames were predicted within 11% for frame 2 and 6% for frame 17. Both of these predictions were unconservative ones. Frame 2 exhibited a post-ultimate strength of about 30% of it's ultimate load. Frame 17 maintained load of roughly 75% of the ultimate load to the conclusion of the test. The hysteretic response, and thus the stiffness of frame 2 degraded to that of the bare frame response, while frame 17 maintained a stiffness that was approximately five times greater than the bare frame stiffness.

Several conclusions may be drawn from these observations. The larger aspect ratio is certainly a positive attribute to this type of system. Although the greater aspect ratio does not appear to increase the cracking load significantly, it does increase the system stiffness, ultimate load, post-ultimate load and post-ultimate stiffness.

7.2.2 Panel Behavior

Envelope behavior for the panel vertical, horizontal and diagonal LVDT's was investigated. The load-strain envelopes for both frames exhibited a softening point that roughly coincided with the occurrence of diagonal cracking in the panel. Using the equivalent strut area, a stress-strain envelope was developed for the panel compressive strut of both frames. Although frame 17 experienced an ultimate compressive load of roughly 11 kips more than frame 2, the stress at ultimate was somewhat less than that of frame 2. This exhibits another benefit of the larger aspect ratio. The larger aspect ratio reduces the angle that the strut forms with the horizontal, thus reducing the force in the strut. The larger aspect ratio also results in a larger equivalent strut area, which reduces the stress in the strut.

7.2.3 Frame-Panel Relative Displacements

The relative movements of the columns and panel and the beam and panel were also examined. The load-deflection

hysteresis of each individual frame-panel relative LVDT conveyed information about the gapping that occurred at the frame-panel interface. Of particular interest were the relative movements at the leeward column. The gapping at the top leeward column ranges from 0.01 inches during the first loop studied to 0.08 inches for frame 2. At the mid-height, the gapping was approximately 25% of these values. Frame 17 experienced larger gapping, but the ratio between the top and mid-height positions remained roughly the same. As suggested in chapter 6, the panel deforms in shear and the column deforms with a curvature; therefore, there is less gapping at the mid-height. This results in the top corners of the panel experiencing more abuse from the frame as a result of the constant opening and closing of the gap. Perhaps the use of partially restrained connections at the base of the frame would partially alleviate this phenomenon. Of course, this would mean that bracing would have to be constructed in several bays of the structure.

Perhaps the most informative plots from chapter 6 are the relative-absolute displacement comparison plots. The pinching effect, seen in figures 6.27 through 6.42 are partially due to a sliding and gapping effect of the frame relative to the panel. However, as can be seen in most of these plots, approximately 70% to 80% is due to plastic strains in the panel.

7.3 Recommendations For Further Study

The following recommendations are suggested for further research into this area:

1) Ultimate load prediction analysis from previous research is based upon the loading of the system being monotonic to failure. Although the predictions for the ultimate loads were very close, they were slightly high. They were also derived for use with a concrete masonry infill and the clay tile are slightly more brittle. One or two specimens, loaded monotonically to failure could be used to verify these analytical techniques with this infill material.

2) The use of the larger aspect ratio reveals some definite advantages, such as increased stiffness and ultimate strength. It is believed that there is probably a limit as to how large the aspect ratio can be made and still have beneficial effects on the system. The use of even larger aspect ratios might reveal the limit.

3) The use of fully restrained beam to column connection and perhaps a partially restrained column-floor connection is suggested to gage their effects on the system.

4) The effects of vertical loading has been shown to have an advantageous effect on infilled systems subjected to racking loads. This type of testing is suggested since it more closely models an in-situ condition.

5) One of the primary reasons for this research is the effects of seismic loading on infilled frames. Thus far, this research has consisted of statically loaded frames. Some dynamic testing is recommended. Although it is understood that this is a relatively expensive process, this type of testing would result in a better understanding of the effects of seismic loading.

LIST OF REFERENCES

LIST OF REFERENCES

American Institute of Steel Construction, Inc., "Allowable Stress Design." 9th ed., Chicago, Illinois

Amos, Kenneth Andrew. 1985. "The Shear Strength of Masonry Infilled Steel Frames." Thesis submitted in partial fulfillment of the requirements for the degree of Master of Science. University of New Brunswick, Canada.

American Society for the Testing of Materials. 1983 Annual Book of ASTM Standards. Section 4, Vol. 04.01 Philadelphia, Penn.

Baura, H.K., and Mallick, S.K. 1977. "Behavior of Mortar Infilled Steel Frames Under Lateral Loading." Building and Environment. Vol. 12, pp. 263-272.

Bennett, Richard M., and Flanagan, Roger D. 1991. "Laboratory Procedure for the Testing of Hollow Clay Tile Infilled Steel Frames." University of Tennessee; Knoxville, Tennessee.

Bertero, V., and Brokken, S. 1984. "Infills in Seismic Resistant Buildings." Journal of Structural Engineering. ASCE, 109(6), pp. 1337-1361.

Boyd, Kurt A. 1993. "Compressive Strength and Constitutive Behavior of Clay tile Prisms." Thesis submitted in partial fulfillment of the requirements for the degree of Master of Science. University of Tennessee, Knoxville, Tennessee.

Dawe, J.L., Seah, C.K. 1988. "Behavior of Masonry Infilled Steel Frames." Canadian Journal of Civil Engineering, Vol. 16, pp. 865-876.

Holmes, Malcom. 1961. "Steel Frames with Brickwork and Concrete Infilling." Proceedings of the Institution of Civil Engineers. Vol. 19, pp. 473-478

Holmes, Malcom. 1963. "Combined Loading on Infilled Frames." Proceedings of the Institution of Civil Engineers. Vol. 25, pp 31-38.

Jamal, Bassam. 1993. "Plastic and Elastic Behavior of Infilled Frames Subjected to In-Plane Loading." Dissertation presented for the degree of Doctor of Philosophy. University of Tennessee; Knoxville, Tennessee.

Klingner, R.E., and Bertero, V.V. 1987. "Earthquake Resistance of Infilled Frames." Journal of the Structural Division, ASCE. 104(ST6), pp.973-989.

Liauw, T.C., and Kwan, K.H. 1982. "Non-linear Analysis of Multistory Infilled Frames." Proceedings of the Institution of Civil Engineers. Vol. 73, Part 2, pp. 441-454.

Liauw, T.C., and Kwan, K.H. 1983. "Plastic Theory of Non-integral Infilled Frames." Proceedings of the Institution of Civil Engineers. Vol. 75, pp.379-396.

McBride, Roy T. 1984. "The Behavior of Masonry Infilled Steel Frames Subjected to Racking." Thesis submitted in partial fulfillment of the requirements for the degree of Master of Science. University of New Brunswick, Canada.

Moghaddam, Hassan A., and Dowling, Patrick J. 1988. "Earthquake Resistant Design of Brick Infilled Frames." Brick and Block Masonry. (??)

Polyakov, S.V. 1956. "Masonry in Framed Buildings." Gosudarstvennoe izdatel'stvo Literatury po stroitel'sstvu i architecture, Moscow, 1956. Translated by G.L. Crairns, 1963.

Ployakov, S.V. 1960. "On the Interaction Between Masonry Filler Walls and Enclosing Frame When Loaded in the Plane of the Wall." Translations in Earthquake Engineering, Earthquake Engineering Research Institute. San Francisco, California, pp. 36-42.

Richardson, John. 1986. "The Behavior of Masonry Infilled Steel Frames." Thesis submitted in partial fulfillment of the requirements for the degree of Master of Science. University of New Brunswick, Canada.

Stafford-Smith, Bryan. 1962. "Lateral Stiffness of Infilled Frames." Journal of the Structural Division, ASCE. 88(ST6), pp. 183-199.

Stafford-Smith, Bryan. 1966. "Behavior of Square Infilled Frames." Journal of the Structural Division, ASCE. 92(ST1), pp. 381-403.

Stafford-Smith, Bryan. 1968. "Model Test Results of Vertical and Horizontal Loading of Infilled Frames." Journal of the Structural Division, ASCE. 65(8), pp. 618-624.

Stafford-Smith, Bryan, and Carter, C. 1969. "A Method for the Analysis of Infilled Frames." Proceedings of the Institution of Civil Engineers. Vol. 44, pp. 31-48.

Stafford-Smith, Bryan, and Riddington, J.R. 1978, "The Design of Masonry Infilled Steel Frames for Bracing Structures." The Structural Engineer. 58B(1), pp. 1-8.

Yong, Teck Chin. 1983. "Shear Strength of Masonry Infilled Panels in Steel Frames." Thesis submitted in partial Fulfillment for the degree of Master of Science. University of New Brunswick, Canada.

APPENDIX

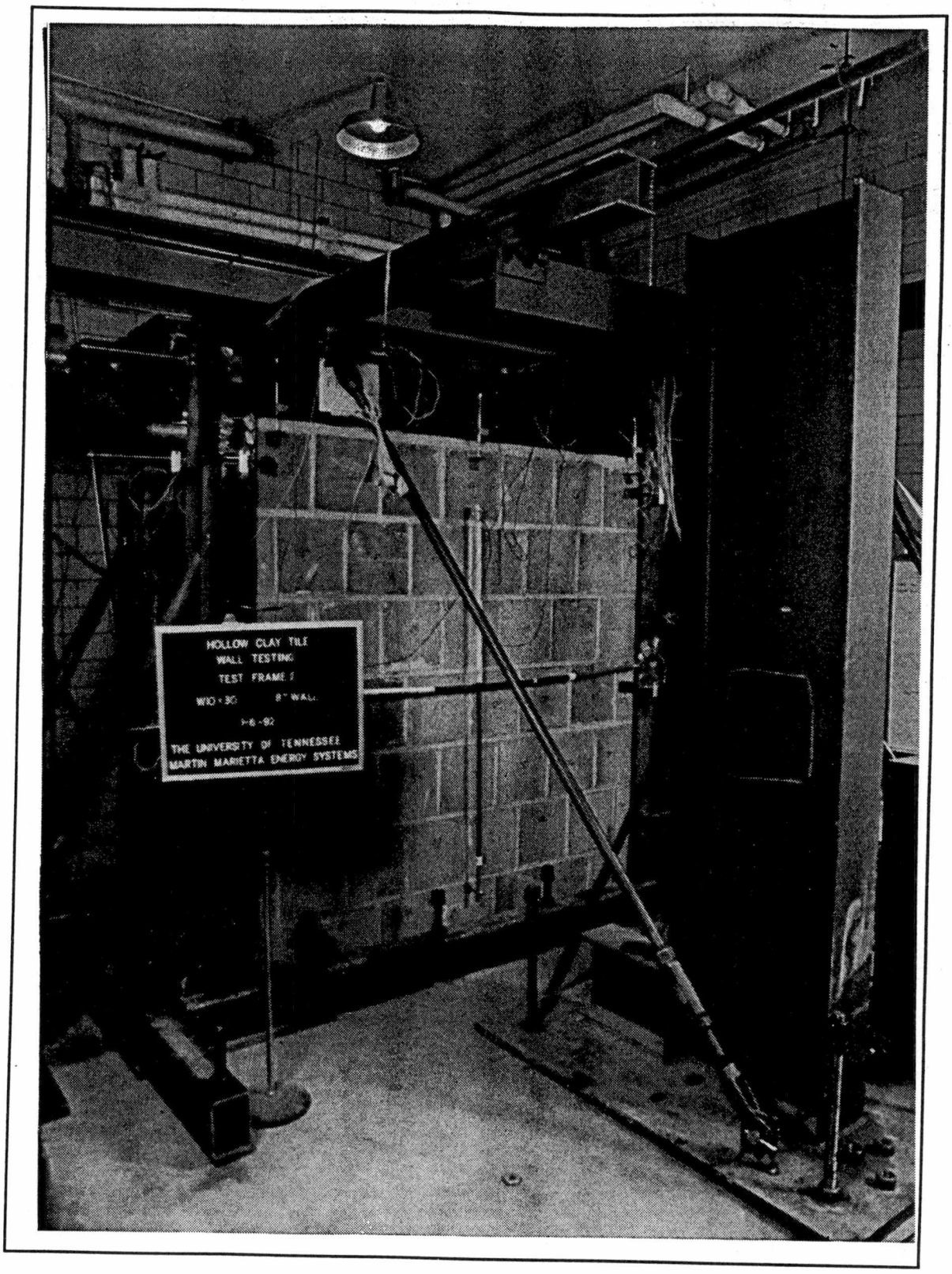


Figure A.1: Frame 2 prior to testing

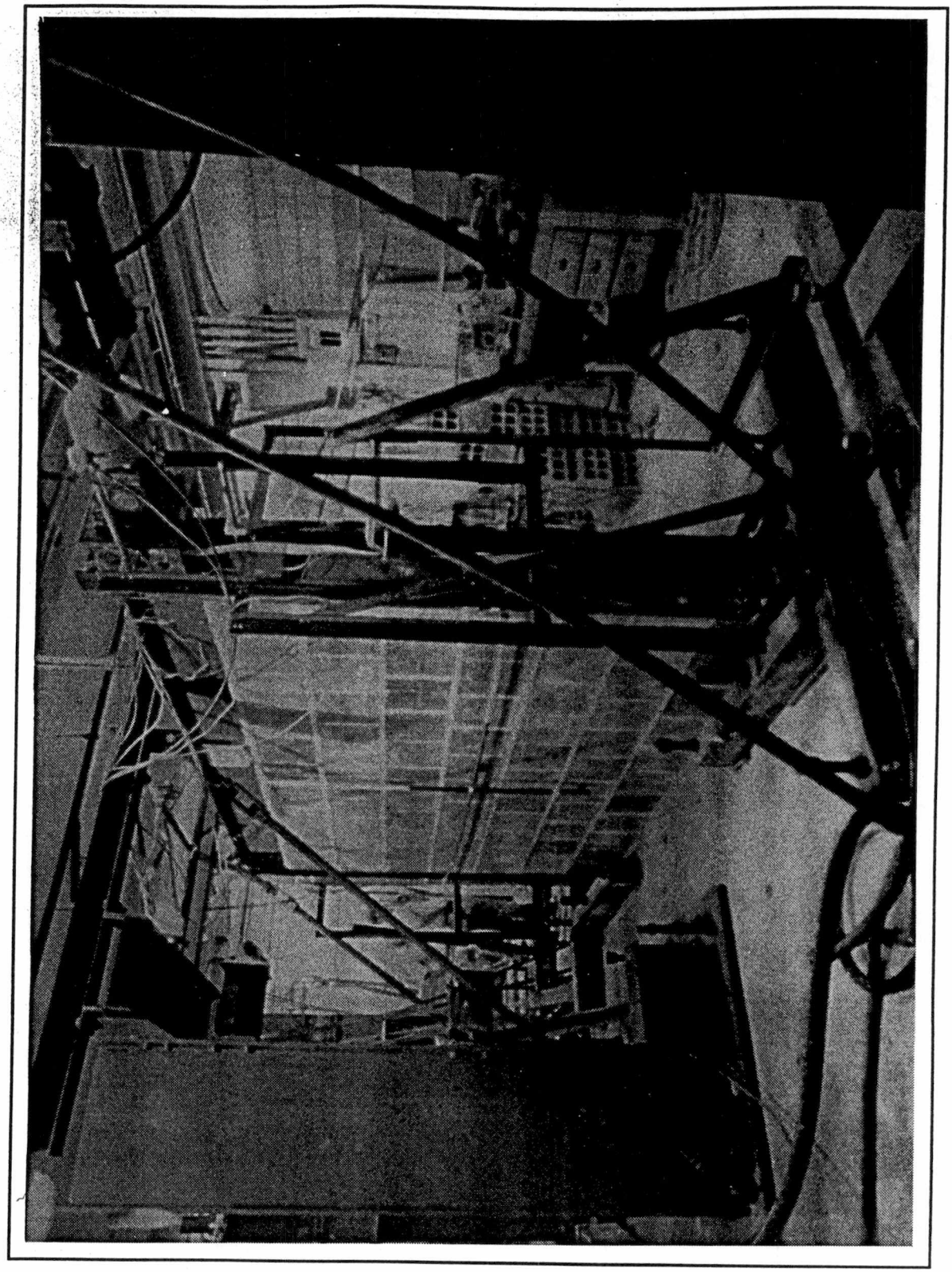


Figure A.2: Frame 17 prior to testing

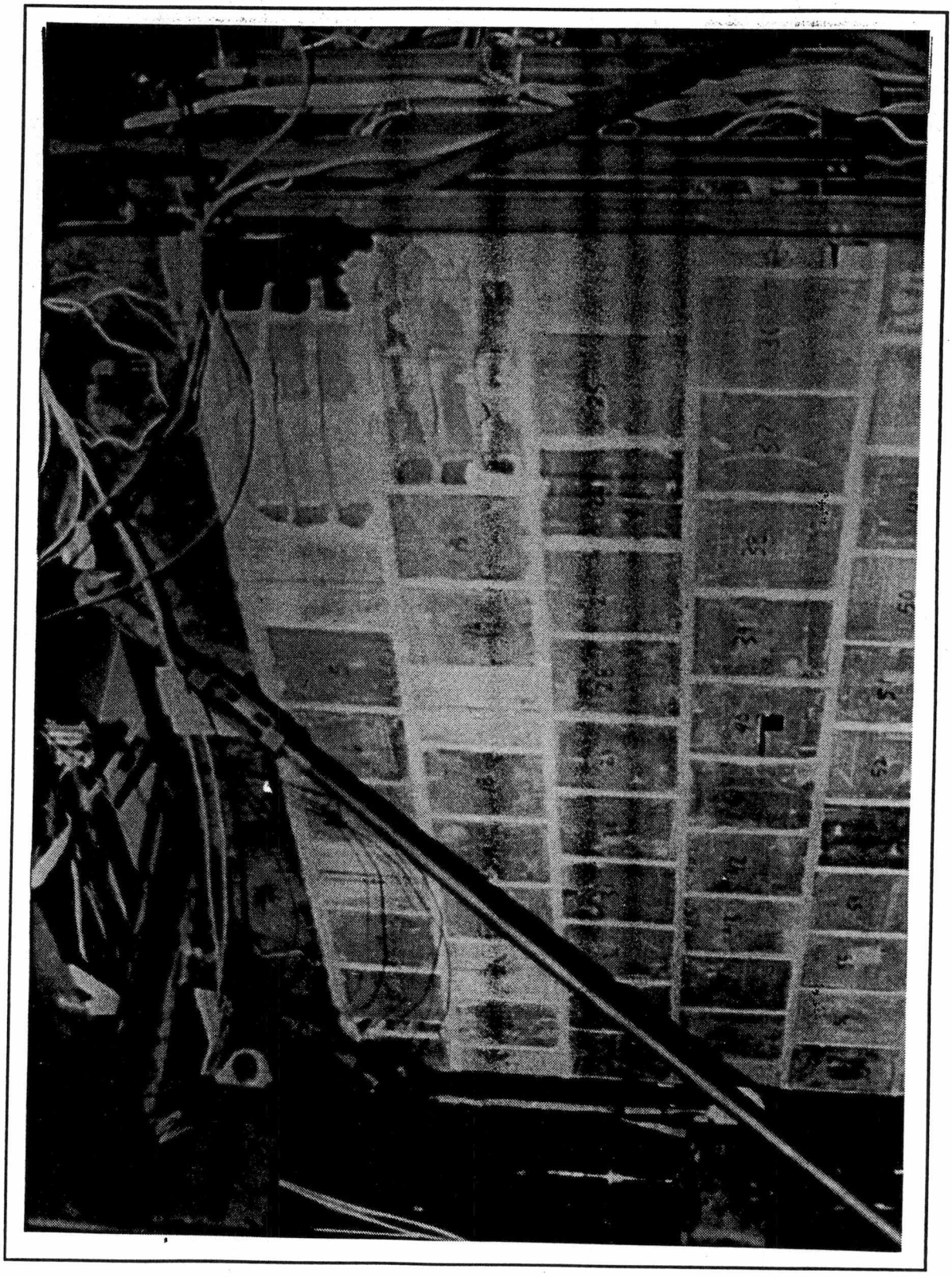


Figure A.3: Frame 2; Corner crushing

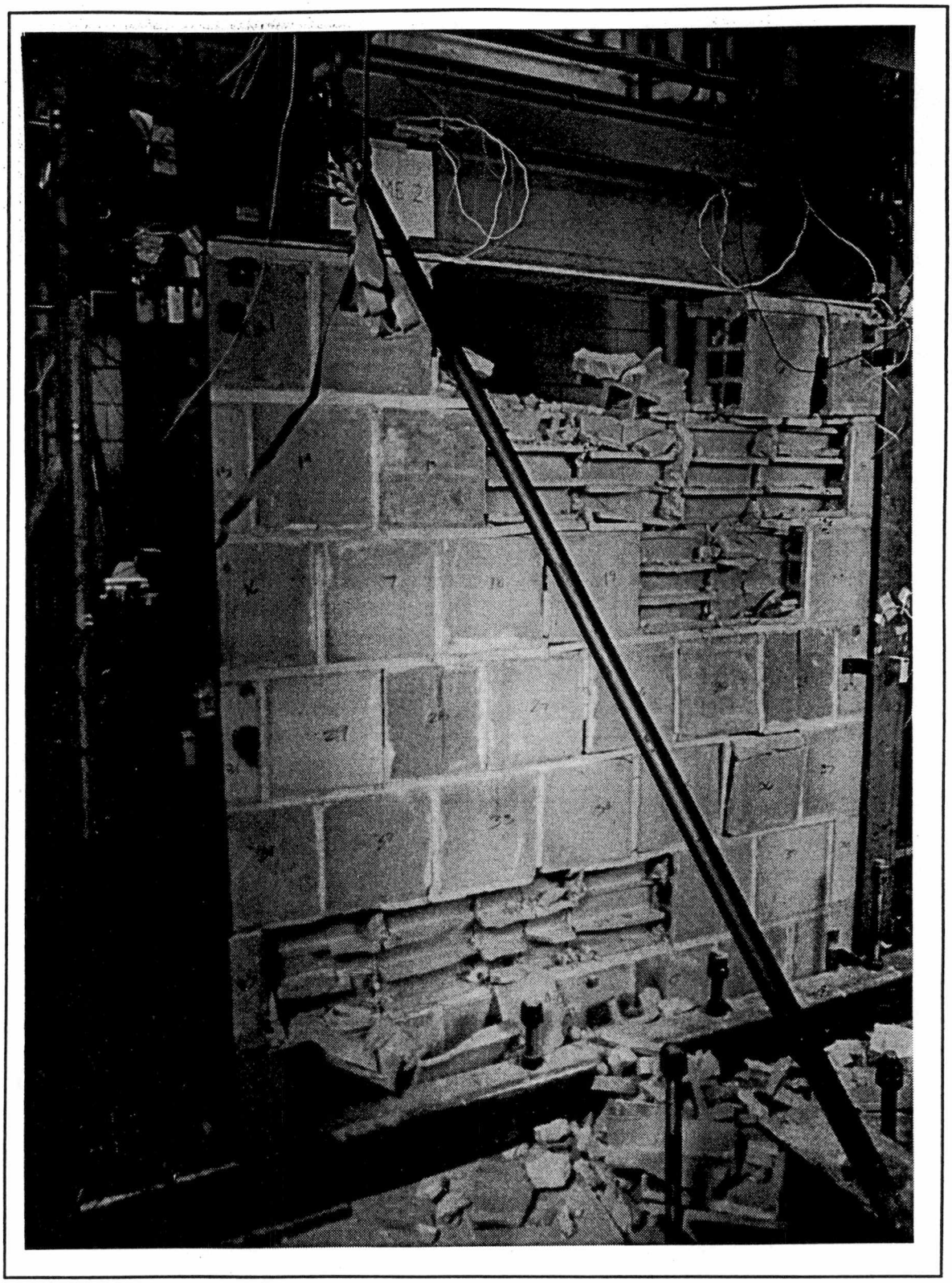


Figure A.4: Frame 2 after testing

VITA

George Alexander Barclay was born in Morristown, Tennessee on December 4, 1960. He attended both primary and secondary schools there and graduated from Morristown-Hamblen High School East in June of 1979. The following September, he enrolled in the University of Tennessee in the School of Architecture. He left school in the spring of 1983 and worked for several years. He returned to the University of Tennessee in January of 1989 and received a Bachelor of Science in Civil Engineering in December of 1991. In May of 1993, he received a Master of Science degree in Civil Engineering, with a concentration in structures.